Dissertation

submitted to the

Combined Faculty of Natural Sciences and Mathematics

of Heidelberg University, Germany

for the degree of

Doctor of Natural Sciences

Put forward by

Marc Schiffer

born in Cologne

Oral examination: October 13th, 2021

Probing Quantum Gravity:

Theoretical and phenomenological consistency tests of asymptotically safe quantum gravity

Referees:

Prof. Dr. Astrid Eichhorn

Prof. Dr. Razvan Gurau

I have contributed to the following publications, the results of which have been used in this thesis. The material in these publications will be used in the following, without further reference. For the convenience of the reader, I list the publications in reverse chronological order, and indicate in which section of this thesis the publications are discussed in detail.

- [1] **Non-perturbative propagators in quantum gravity**,
  Benjamin Knorr, and Marc Schiffer, Universe 7 (2021) 7, 216; See Sec. 3.2.

- [2] **The de Sitter Instanton from Euclidean Dynamical Triangulations**, Scott Bassler, Jack Laiho, Marc Schiffer, and Judah Unmuth-Yockey, Phys.Rev.D 103 (2021) 114504; See Subsec. 3.3.2.

- [3] **Newtonian binding from lattice quantum gravity**,
  Mingwei Dai, Jack Laiho, Marc Schiffer, and Judah Unmuth-Yockey, Phys.Rev.D 103 (2021) 11, 114511; See Subsec. 3.3.1.

- [4] **Light charged fermions in quantum gravity**,
  Gustavo P. de Brito, Astrid Eichhorn, and Marc Schiffer, Phys.Lett.B 815 (2021) 136128; See Sec. 4.5.

- [5] **Lorentz invariance violations in the interplay of quantum gravity with matter**,
  Astrid Eichhorn, Alessia Platania, and Marc Schiffer, Phys.Rev.D 102 (2020) 2, 026007; See Sec. 4.6.

- [6] **Asymptotic safety, string theory and the weak gravity conjecture**,
  Senarath de Alwis, Astrid Eichhorn, Aaron Held, Jan M. Pawlowski, Marc Schiffer, and Fleur Versteegen, Phys.Lett.B 798 (2019) 134991; See Subsec. 4.3.2.

- [7] $d = 4$ **as the critical dimensionality of asymptotically safe interactions**,
  Astrid Eichhorn, and Marc Schiffer, Phys.Lett.B 793 (2019) 383-389; See Sec. 4.4.

Furthermore, the following sections contain work from ongoing collaborations, which will be published in the future:

- **The weak-gravity bound in Abelian gauge systems**,
  in collaboration with Astrid Eichhorn, and Jan Kwapisz; See Subsec. 4.2.2

- **Rejection-free algorithm for euclidean dynamical triangulations**,
  in collaboration with Mingwei Dai, Walter Freeman, Jack Laiho, Aaron Trowbridge and Judah Unmuth-Yockey; See Subsec. 3.3.3.

The following publications are not discussed in detail in this thesis:

- **How perturbative is quantum gravity?**,
  Astrid Eichhorn, Stefan Lippoldt, Jan M. Pawlowski, Manuel Reichert, and Marc Schiffer, Phys.Lett.B 792 (2019) 310-314;

- **Zooming in on fermions and quantum gravity**,
  Astrid Eichhorn, Stefan Lippoldt, and Marc Schiffer, Phys.Rev.D 99 (2019) 8, 086002;

Probing Quantum Gravity:
Theoretical and phenomenological consistency tests of asymptotically safe quantum gravity

Marc Schiffer

Abstract Asymptotically safe quantum gravity might provide a unified description of the fundamental dynamics of quantum gravity and matter. Asymptotic safety is the quantum realization of scale symmetry. In general, symmetries constrain the possible interactions and dynamics of a system. Scale symmetry is no exception and imposes constraints on the dynamics and interactions of quantum gravity and matter. In this thesis, we will investigate aspects of asymptotically safe quantum gravity, and present indications that it passes several theoretical and phenomenological consistency tests.

We will find indications that a lattice formulation of asymptotically safe quantum gravity features an appropriate classical regime. Furthermore, we will investigate under which conditions a scale invariant regime at high energies is consistent with the low-energy matter degrees of freedom and their interactions. We will see that the interplay of quantum gravity and matter might put lower bounds on the number of fermions in our universe, and even constrain fundamental parameters of our universe, such as its dimensionality.

Even if not realized at arbitrarily high energies, approximate scale invariance at intermediate energies could still govern the dynamics of nature. We will find indications that also in such scenarios, much of the predictive power of the asymptotically safe fixed point persists. It might allow translating bounds on symmetry violations in the matter sector into indirect bounds on violations of this symmetry in the gravitational sector.

Zusammenfassung Asymptotisch sichere Quantengravitation könnte eine gemeinsame Beschreibung der fundamentalen Dynamik von Quantengravitation und Materie ermöglichen. Asymptotische Sicherheit ist die Quantenrealisation von Skalensymmetrie. Symmetrien schränken im Allgemeinen die möglichen Wechselwirkung und die Dynamik von Systemen ein. Auf die gleiche Art schränkt auch Skalensymmetrie die Wechselwirkung von Quantengravitation und Materie ein. In dieser Arbeit werden wir verschiedene Aspekte asymptotisch sicherer Quantengravitation erkunden, und Hinweise herausarbeiten, dass dieses Szenario verschiedene theoretische und phenomenologische Konsistenztests besteht.

Wir werden Hinweise finden, dass eine Formulierung asymptotisch sicherer Quantengravitation auf dem Gitter ein entsprechendes klassisches Regime besitzt. Außerdem werden wir erforschen, unter welchen Bedingungen ein Skalen-invariantes Regime bei hohen Energien mit den Materiefreiheitsgraden und Wechselwirkungen bei niedrigen Energien kompatibel ist. Wir werden sehen, dass das Zusammenspiel von Quantengravitation und Materie untere Schranken für die Anzahl an Fermionen in unserem Universum setzt, und sogar fundamentale Parameter unseres Universums, wie seine Dimensionalität einschänken könnte.

Selbst wenn sie nicht bis zu beliebig hohen Energien realisiert ist, könnte Skaleninvarianz bei endlichen Energien die Dynamik der Natur bestimmen. Wir werden Hinweise finden, dass des asymptotisch sichere Fixpunkte auch in solchen Szenarien einen großer Teil seiner prediktiven Kraft behält. Er könnte es erlauben, zwischen Einschränkungen auf Verletzungen von Symmetrien im Materiesektor und indirekte Einschränkungen auf Verletzungen der gleichen Symmetrie im gravitativen Sektor, zu übersetzen.

Contents

1. Introduction

The current understanding of our universe is built on two main pillars: General Relativity (GR), and the Standard Model of particle physics (SM). The SM is formulated as a quantum field theory of matter fields, while GR is a classical field theory of geometry.

The first main pillar for the understanding of our universe, GR, accurately describes the gravitational interaction of massive objects at a large range of distance-scales. The first picture of the supermassive object in the center of a neighboring galaxy [8–10] provides strong evidence for a crucial prediction of GR: the existence of black holes. This observation resonates with the detection of gravitational waves, which can be attributed to the collision of two black holes [11–13]. These observations indicate that the validity of GR extends into the strong curvature regime.

Yet, the same objects that provide the first experimental tests of GR beyond the weak-curvature regime, also predict the failure of GR in physical regimes: for example, in their center, black holes feature singularities where their curvature diverges. Therefore, GR can only be an effective, not a fundamental, description of the gravitational interaction in our universe. However, the regime where the onset of singularities would become important is also the regime where the quantum nature of spacetime is expected to play a key role, the Planckian regime.

The second main pillar for the understanding of our universe, the SM, accurately describes visible matter and their interactions via three fundamental interactions. The discovery of the Higgs boson [14, 15] is one of the most recent test of the SM. Intriguingly, the measured value of the Higgs mass allows the SM to be consistent up to Planckian energies, without major modifications [16, 17]. However, if the SM was extrapolated beyond Planckian energies, it also predicts singularities: Several sectors of the SM feature singularities, where couplings are predicted to diverge. These divergences indicate that the SM is only an effective description of the visible matter in our universe.

Since both GR and the SM are only effective descriptions of our universe, we are left with the following, so-far unanswered questions: What are the fundamental building blocks of nature? What determines their dynamics? And, how can we test theories in the Planckian regime?

There are different directions towards answering these questions on the fundamental structures of our universe. These directions are usually referred to as theories of quantum gravity. The reason for a variety of proposals is related to the enormous amount of energy it would take to observe quantum fluctuations of spacetime, for example, in particle collisions. Therefore, it is questionable, whether there are direct observational windows into the quantum-gravity regime. Nevertheless, theories of quantum gravity have to be tested and validated. All of them have to pass several consistency tests: First, they should be internally consistent and not feature instabilities. Second, and most importantly, the properties of the universe that we can observe and experimentally test at low energies should be emergent.

In this thesis we will focus on a minimalistic approach to quantum gravity, called asymptotically safe quantum gravity [18], which is based on the conjectured realization of scale symmetry. The goal of this thesis is to present several theoretical and phenomenological consistency tests of asymptotically safe quantum gravity.

This thesis is structured as follows: In Chapter 2, we will lay out the basic concepts that underlie the thesis. For this purpose, Section 2.1 motivates asymptotically safe quantum gravity as a UV-complete and predictive candidate for a quantum-field theoretic description of spacetime and matter.

In Section 2.2, we will introduce the functional renormalization group (FRG) as one suitable method to search for asymptotic safety. The FRG is a functional tool that allows to extract the scale dependence of couplings and operators in terms of partial differential equations. The search for asymptotic safety with the FRG translates into the search for fixed-points, at which the scale dependence of all couplings vanishes.

In Section 2.3, we will introduce Euclidean dynamical triangulations (EDT) as a complementary tool to search for asymptotic safety. EDT is a lattice formulation of quantum gravity and extracts quantum fluctuations of spacetime via Monte-Carlo simulations of random geometries. The search for asymptotic safety in EDT translates into the search for a continuous phase transition of the lattice theory.

In Chapter 3, we will first review indications for the asymptotically safe fixed point in pure gravity and in gravity-matter systems. In Section 3.2, we will study the momentum dependence of non-perturbative propagators as one way to test the theoretical consistency of asymptotically safe quantum gravity, since propagators encode important information on the causality and unitarity of a theory. We find indications that disentangling the different modes of the graviton propagator is crucial to accurately resolve its momentum dependence. Furthermore, we find indications that the momentum dependence only mildly depends on the choice of gauge fixing, signaling the robustness of the FRG computation. In Section 3.3 we will present two independent indications that EDT features a semi-classical regime that is consistent with what we would expect in a four-dimensional Euclidean universe: In Subsection 3.3.1 we will show indications that EDT can reproduce the Newtonian potential for scalar particles in a four-dimensional Euclidean world. Further, in Subsection 3.3.2 we will present indications that EDT is consistent with semi-classical fluctuations around a de Sitter background.

We will turn to phenomenological consistency tests of asymptotically safe quantum gravity in Chapter 4. We will review phenomenological consequences of the asymptotically safe fixed point on the matter sector in Section 4.1. In Section 4.2 we will first review indications for the *weak gravity bound* in asymptotic safety. This bound indicates that metric fluctuations must be weak enough to allow for a UV complete matter sector. We will then extend the investigation of the weak gravity bound in the Abelian gauge sector, by considering the full set of lowest-dimensional induced operators. In Subsection 4.3.1 we will introduce the concept of effective asymptotic safety, where the scale invariant regime is not fundamental, but emerges above the Planck scale from a fundamental theory. We will investigate conditions for the explicit example where the fundamental description of nature is given in terms of string theory. We will confront asymptotically safe quantum gravity with observational consistency tests i) based on the observed dimensionality of our universe in Section 4.4, ii) based on the observation of light fermions in our universe in Section 4.5, and iii) based on the non-observation of Lorentz-invariance violations at low energies in Section 4.6.

In Chapter 5 we will conclude and give an outlook on possible future directions to perform consistency tests on asymptotically safe quantum gravity.

2. Asymptotic safety: Methodological setup

In the following, we will motivate and introduce asymptotically safe quantum gravity. In Section 2.2 and Section 2.3 we will introduce the two main tools used in this thesis to investigate asymptotic safety: the functional renormalization group, and Euclidean dynamical triangulations.

2.1. Short introduction to asymptotically safe quantum gravity

Asymptotic safety is the quantum realization of scale symmetry. Symmetries in general play a key role in our current understanding of nature. On the one hand, diffeomorphism symmetry is key to describe the dynamics of spacetime, and is a cornerstone of the theory of GR. Diffeomorphism symmetry states that physical laws, for example the motion of particles, are independent of the choice of coordinates. GR is a classical field theory of the metric.

Global and local symmetries are key to understand the interactions of the visible matter of our universe. These symmetries determine the type of matter fields in the SM and constrain their interactions. The SM is therefore a gauge theory and is formulated in the framework of quantum field theory.

Both discussed theories, GR and the SM, have to emerge in the low energy limit of a fundamental theory that describes nature. One common path to attempt this, is to quantize GR and to formulate quantum gravity as a quantum field theory of the metric. However, the same prescription to quantize a classical theory, which is successfully used in the matter sector, fails for gravity. The problem is caused by infinitely many terms that have to be added in the quantization procedure, which spoil predictivity.

In the following, we will discuss this perturbative breakdown of quantum gravity, which indicates that a predictive quantum field theory of the metric is missing an important ingredient. We will then introduce one proposal for this missing ingredient: the quantum realization of scale symmetry at high energies. This realization of scale symmetry is called asymptotic safety. As we will discuss in the following the symmetry principle would restore predictivity, if it applies to quantum gravity. In particular, we will discuss how asymptotic safety might provide a predictive quantum-field theoretic description of quantum gravity and matter.

2.1.1. Perturbative quantum gravity

A standard argument for the perturbative non-renormalizability of quantum gravity is the negative mass dimension of the Newton coupling $[G_{\mathrm{N}}] = -2$. We will now briefly demonstrate that indeed each loop order introduces new power-law divergences, which have to be absorbed by counter-terms. We will also show that these counter-terms actually vanish for pure gravity at 1-loop order [19]. However, including matter [19–21], or going beyond the 1-loop approximation, non-vanishing counter-terms have to be added [22].

The starting point for the standard procedure of perturbative quantization is the classical

action in Euclidean space. For gravity this is given by

$$S_{\rm EH} = \frac{1}{16\pi G_{\rm N}} \int \mathrm{d}^d x \sqrt{g} \, \left(R - 2\bar{\Lambda} \right) \,, \tag{2.1}$$

where d is the dimension of spacetime, R is the Ricci scalar, and $g = \det(g_{\mu\nu})$. We will neglect the cosmological constant in the following, i.e., $\bar{\Lambda} = 0$. This action is then expanded in perturbatively small metric fluctuations $h_{\mu\nu}$ about a flat background $\delta_{\mu\nu}$ according to,

$$g_{\mu\nu} = \delta_{\mu\nu} + \epsilon \, h_{\mu\nu} \,, \qquad \text{with} \qquad \epsilon = \sqrt{8\pi G_{\rm N}} \,. \tag{2.2}$$

In this expansion, the coefficient ϵ^2 is the perturbative expansion parameter.

For an expectation for the counter-terms that can arise in such an expansion, let us investigate the superficial degree of divergence. It is based on dimensional analysis and gives an expectation of which divergences are expected to occur at a given loop level. If no cancellations between different loop orders happen, these divergences have to be absorbed by the introduction of counter-terms.

The expansion around a flat background allows to transform to Fourier space. It follows that $R \sim p^2$, due to the two derivatives acting on the metric in real space. Therefore, for the propagator P and any vertex V it follows that $P \sim 1/p^2$ and $V \sim p^2$. Each closed loop introduces the integration over the loop momentum. Therefore, a diagram with L closed loops, P internal graviton-lines and V vertices diverges as p^D, when $p \to \infty$. The superficial degree of divergence D is given by

$$D = dL - 2(P - V) = 2 + (d-2)L \,, \qquad \text{with} \qquad L = P - V + 1 \,, \tag{2.3}$$

where the relation between L, P and V can be checked explicitly by adding an additional loop to a given diagram. Therefore, in $d = 4$ and at 1-loop order, we expect p^4 divergences of the Feynman diagrams. Since the original action only contains the Ricci scalar, which is $\sim p^2$, we might already anticipate, that the p^4 divergence cannot be absorbed into the original action.

We can limit the counter-terms to diffeomorphism invariant operators, which can be shown using the background field method [23–25]. Therefore, at the one-loop order, there are three possible counter-terms, namely [19]

$$\Delta S_1 = \int \mathrm{d}^4 x \sqrt{g} \left(\alpha \, R^2 + \beta \, R_{\mu\nu} R^{\mu\nu} + \gamma \, R_{\mu\nu\rho\sigma} R^{\mu\nu\rho\sigma} \right) \,, \tag{2.4}$$

where $R_{\mu\nu}$ and $R_{\mu\nu\rho\sigma}$ are the Ricci- and Riemann tensor, respectively. At this level in curvature, the topological Gauss-Bonnet invariant

$$E = R^2 - 4 R_{\mu\nu} R^{\mu\nu} + R_{\mu\nu\rho\sigma} R^{\mu\nu\rho\sigma} \,, \tag{2.5}$$

allows to express the squared Riemann tensor in terms of the squared Ricci scalar and the squared Ricci tensor.

However, counter-terms that vanish on-shell can be transformed away by a field transformation, see [19, 25]. Therefore, counter-terms that vanish on-shell do not contribute to physical processes and can be neglected. Indeed, in vacuum $R = 0$ and $R_{\mu\nu} = 0$ are solutions to the equations of motion encoded in the Einstein-Hilbert action (2.1) for $\bar{\Lambda} = 0$. Consequently, at 1-loop and in vacuum, there are no counter-terms [19]. In the presence of matter, the two independent counter-terms no longer vanish on shell [19–21].

Furthermore, since the superficial degree of divergence (2.3) depends on the number of loops, new counter-terms will arise at higher loops. Specifically at 2-loop order, one counter-term, the so-called Goroff-Sagnotti counter-term, does not vanish on-shell [22, 26]. It reads

$$\Delta S_2 \sim \int \mathrm{d}^4x\sqrt{g}\, R_{\mu\nu}{}^{\rho\sigma} R_{\rho\sigma}{}^{\kappa\lambda} R_{\kappa\lambda}{}^{\mu\nu} \,. \tag{2.6}$$

Higher derivative theories and unitarity

One way to circumvent the appearance of new counter-terms at each loop level, is to add all independent curvature squared operators, namely

$$S_{R^2} = \int \mathrm{d}^4x\sqrt{g}\left(a\, R^2 + b\, R_{\mu\nu}R^{\mu\nu}\right) \,, \tag{2.7}$$

to the classical action $S_{\rm EH}$ [27]. Explicit computations confirm that the theory can be renormalized with a finite number of counter-terms [27], and even asymptotically free for specific values of the couplings a and b [28, 29].

However, the presence of higher curvature operators gives rise to a massive spin-0 and a massive spin-2 mode, which propagate in addition to the massless spin-2 graviton [27]. Expanding the quadratic action in these modes, reveals that the massive spin-2 mode and the graviton have the opposite sign in the kinetic term. This results in the so-called Ostrogradsky instability [30], where the Hamiltonian is not bounded from below.

At the quantum level, the massive spin-2 mode becomes a ghost-like term with negative norm, see [31]. If the ghost is stable and coupled to other modes in the theory, it could spoil unitarity at high energies, see also [32]. For quadratic gravity, this question remains open, see [33–36], and we will comment on this question in more general higher-derivative theories in Section 3.1.

Effective field theory description of quantum gravity

In the previous paragraphs, we have discussed that a perturbative quantization either leads to new counter-terms at each loop order, or to a renormalizable theory that might be unstable. This however is only problematic when extending the theory to arbitrarily high scales.

Already the 2-loop counter-term of the perturbative expansion is a dimension six operator. Therefore, on dimensional grounds it has to be suppressed by $1/M^2$, where M is some mass scale. Since the superficial degree of divergence increases with each loop order, the corresponding counter-terms will be even higher dimensional, and therefore more strongly suppressed. In the context of quantum gravity, the most natural mass scale is the Planck mass $M_{\rm Pl}$, such that $M \simeq M_{\rm Pl}$. Therefore, below the Planck scale, the perturbative counter-terms will be very strongly suppressed, which allows for an effective description of quantum gravity [37], see [38, 39] for reviews. At the Planck scale, this description breaks down, since infinitely many counter-terms, whose couplings are free parameters of the theory, become relevant.

If the scale associated with the potential instability of quadratic gravity lies above the Planck scale, the theory is consistent at least up to the Planck scale. Therefore, both theories that we have described above can be treated as an effective field theory below the Planck scale. In both cases the Planck scale serves as a cutoff, where either infinitely many counter-terms become large, or where instabilities spoil unitarity.

This effective description of quantum gravity [37, 40], allows computing the leading quantum gravity contribution to the two-particle potential. The potential of two particles with masses m_1

and m_2 at a distance r reads [37]

$$V(r) = -\frac{G_{\rm N}\, m_1\, m_2}{r}\left(1 - \frac{G_{\rm N}(m_1+m_2)}{r\, c^2} - \frac{127}{30\pi^2}\frac{G_{\rm N}\hbar}{r^2\, c^3}\right), \tag{2.8}$$

where we have explicitly reinstated factors of $\hbar$ and c. Here, the first term is the classical Newton potential, the second term corresponds to post-Newtonian corrections, and the third term is the quantum gravitational contribution.

While the leading quantum-gravity contribution is tiny at low energies (and correspondingly large distances r), the computation shows that quantum gravity and matter can be described in a consistent framework. Since this framework looses predictivity at high energies, the challenge is to find a predictive UV completion for quantum gravity and matter.

2.1.2. Asymptotic safety: Quantum scale symmetry

As we have discussed above, the key problem of quantum gravity is the loss of predictivity, or of unitarity at the Planck scale. There are several approaches to overcome this problem. While some approaches, for example string theory [41, 42] or causal sets [43] abandon the framework of a local quantum field theory, other approaches aim for a non-perturbative quantization of gravity, for example Loop Quantum Gravity [44].

In the following, we will discuss a third option, namely the realization of scale symmetry at high energies. Just like any other symmetry, scale symmetry might impose conditions on the theory. If its realization provides infinitely many conditions on higher-order operators, then predictivity within a local QFT framework might be restored.

Classical scale invariance is broken by quantum fluctuations, since they turn the vacuum into a screening or anti-screening medium. Accordingly, in the presence of quantum fluctuations, the theory depends on the scale. If these quantum fluctuations vanish asymptotically at high energies, classical scale invariance will be recovered. This is known as asymptotic freedom, and realized in Yang-Mills theories [45, 46].

Asymptotic safety is a generalization of asymptotic freedom: instead of vanishing, the effects of quantum fluctuations balance at non-vanishing values of the couplings. The scenario is realized if the dimensionless counterparts of all couplings approach non-vanishing constant values at high energies [18]. The high-energy regime is interacting and scale invariant. Asymptotic safety is the quantum realization of scale symmetry. If it is realized, the observables of the theory remain finite, and the theory is valid at arbitrary energy scales [18]. For reviews on asymptotic safety, see, e.g., [47–53], and for a general discussion on quantum scale symmetry see [54].

Predictivity in asymptotic safety

We will now discuss in more detail how the scale-invariant regime might be realized, and how scale invariance might impose infinitely many conditions on the couplings that parametrize the system. We will in the following always consider the dimensionless versions of all couplings, since the finiteness of these couplings implies the finiteness of observables [18].

The beta functions of a set of couplings g_i encode their scale dependence. Therefore, at a point in the space of couplings, where all beta functions vanish, the theory does not depend on the scale and is therefore scale invariant. These points are called fixed points $\mathbf{g}_*$, defined by the condition

$$\beta_{g_i}\big|_{g_i=g_{i,*}} \equiv k\,\partial_k\, g_i(k)\big|_{g_i=g_{i,*}} = 0\,, \tag{2.9}$$

where $g_{i,*}$ are the components of the vector $\mathbf{g}_*$, where k is a momentum scale, and where

$$g_i(k) = \bar{g}_i(k) k^{-d_{\bar{g}_i}} \tag{2.10}$$

are the dimensionless counterparts of dimensionfull couplings $\bar{g}_i$ which have a canonical mass dimension $d_{\bar{g}_i}$.

The set of beta functions β_{g_i} linearized around a fixed point $\mathbf{g}_*$, reads

$$\beta_{g_i} = \sum_j M_{ij}(g_j - g_{j,*}) + \mathcal{O}\left((g_j - g_{j,*})^2\right) , \qquad \text{with} \qquad M_{ij} = \frac{\partial \beta_{g_i}}{\partial g_j}\Big|_{g_i = g_{i,*}} , \tag{2.11}$$

where the zeroth order vanishes by definition of a fixed point. The so-called stability matrix M_{ij} is not necessarily diagonal, since in general each beta function β_{g_i} can depend on any other coupling g_j.

We will now transform to a system of couplings $\hat{g}_j$, which is centered around the fixed point $\mathbf{g}_*$, and where M_{ij} is diagonal. In this system, the set of beta functions simplifies to

$$\beta_{\hat{g}_i} = k\,\partial_k\,\hat{g}_i = -\Theta_i\,\hat{g}_i\,, \qquad \text{with} \qquad \Theta_i = -\text{eig}(M)\,, \tag{2.12}$$

where we have introduced the critical exponents Θ_i. This set of partial differential equations for the scale dependent couplings is solved by

$$\hat{g}_i(k) = c_i \left(\frac{k}{k_0}\right)^{-\Theta_i} , \tag{2.13}$$

where c_i are constants of integration, which can be understood as initial conditions at the scale k_0. We can now transform back to the system spanned by the couplings g_i, where the scale dependent couplings read

$$g_i(k) = g_{i,*} + \sum_j c_j\ (V_j)_i \left(\frac{k}{k_0}\right)^{-\Theta_j} . \tag{2.14}$$

Here, $(V_j)_i$ is the i-th component of the j-th eigenvector of the stability matrix, and k_0 is a scale of reference.

On the level of the scale dependent couplings $\hat{g}_i(k)$ (2.13), we can now study the predictivity of a fixed point in terms of the critical exponents Θ_i. For this, we consider a trajectory in the space spanned by the couplings $\hat{g}_i$, which enters the linearized regime around the fixed point $\hat{\mathbf{g}}_*$ at some scale k_0. In this regime (2.13), describes the trajectory in the space of couplings.

For $\text{Re}\,(\Theta_i) < 0$, the initial condition c_i becomes less and less important, when lowering the scale k/k_0. A direction in the space of couplings for which $\text{Re}\,(\Theta_i) < 0$ is called *irrelevant*, or IR-attractive: the fixed-point value $\hat{g}_{i,*} = 0$ is automatically approached when lowering the scale k/k_0, and the IR-value of $\hat{g}$ looses memory of the initial condition c_i. The residual dependence of $\hat{g}_i(k)$ on the initial condition c_i decreases, when decreasing k/k_0 further.

For $\text{Re}\,(\Theta_i) > 0$, the initial condition c_i becomes more and more important, when lowering the scale k/k_0. A direction in the space of couplings for which $\text{Re}\,(\Theta_i) > 0$ is called *relevant*, or IR-repulsive: along this direction the trajectory is pushed away from the fixed-point value $\hat{g}_{i,*} = 0$. By varying c_i at a fixed scale k_0, different IR values for $\hat{g}_i$ can be achieved. The residual dependence of $\hat{g}_i(k)$ on the initial condition c_i increases, when decreasing k/k_0 further.

For $\text{Re}\,(\Theta_i) = 0$, the so-called marginal directions, the first term in (2.11) vanishes. In this

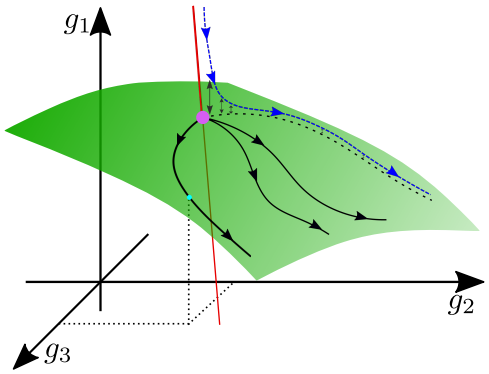

Fig. 2.1.: Illustration of a two-dimensional critical hypersurface in a three-dimensional theory space. The magenta point marks a fixed point with two relevant directions. The flow along trajectories emanating from this fixed point is confined to the critical hypersurface and therefore fully characterized by two couplings. The red line marks the IR critical hypersurface of the fixed point. Along this surface, trajectories are attracted towards the fixed point during their flow towards the IR.

case, sub-leading terms in the scale dependence of $\hat{g}_i$ are important. If the first contribution has positive (negative) sign, the direction is marginally relevant (irrelevant).

For an asymptotically safe fixed point, the scale where a trajectory enters the linearized regime is shifted towards $k_0 \to \infty$. Then, the trajectories become entirely independent of those initial conditions c_i that correspond to irrelevant directions. Accordingly, the IR values of the couplings are only determined by the relevant directions. In turn, the IR values of relevant directions have to be measured to determine the corresponding value of c_i.

In terms of the original system of couplings g_i, several relevant and irrelevant directions can contribute to the scale dependence of each coupling g_i. This is because the couplings g_i are not aligned with the eigendirections of the system. Nevertheless, only those coefficients c_j that correspond to relevant directions contribute and drive the flow of all couplings.

The relevant directions span the *UV critical hypersurface*, that contains all trajectories that can emanate from a fixed point. In Figure 2.1 we show an illustration of a two-dimensional critical hypersurface (green surface) in a three-dimensional space. The magenta point marks a fixed point with two relevant and one irrelevant direction. UV finite trajectories emanate from the fixed point and are confined to the critical hypersurface along their flow towards the IR (indicated by the arrows). For these trajectories it is sufficient to measure two couplings, for example g_2 and g_3 to fully determine the cyan point. Therefore, a finite-dimensional critical hypersurface implies the predictivity of a theory. A trajectory that is displaced off the critical hypersurface is not UV complete (blue line). The red line in Figure 2.1 shows the IR critical hypersurface of the magenta fixed point. Trajectories close to the IR critical hypersurface will be attracted towards the UV critical hypersurface along the irrelevant direction of the fixed point. The blue trajectory in Figure 2.1 will approximate the UV critical hypersurface when flowing towards the IR.

In summary, the scale dependence of a system is driven by the relevant directions. Each relevant direction contributes a free parameter, which has to be measured. After measuring all of these free parameters, the trajectory of a theory through the space of couplings is completely determined. The irrelevant directions are then a prediction of the theory. Therefore, any model that features a finite set of irrelevant directions is a predictive theory, since only finitely many experiments have to be performed to predict the other couplings.

In the following, we will call the space of couplings the theory-space, since each trajectory in

the space of couplings corresponds to a different theory.

We have seen that the number of positive critical exponents, i.e., the number of relevant directions, determines the predictivity of a theory. The less relevant directions a theory has, the more predictive it is. Therefore, even a theory that lives in an infinite-dimensional theory space is predictive, as long as it only features finitely many relevant directions. In this case, the asymptotically safe, or free, fixed point imposes infinitely many conditions on the couplings.

For an intuition on the critical exponents that we might expect, let us focus on the free, or Gaussian fixed point of a theory, where $g_{i,*} = 0$. Only contributions that are linear in any of the couplings enter the stability matrix.

At this fixed point, the stability matrix is diagonal, since only contributions linear in any coupling will enter the stability matrix. These linear contributions are the canonical mass dimensions of the couplings, cf. (2.10), such the critical exponents correspond to their canonical mass dimensions, $\Theta_i = d_{\bar{g}_i}$. At an interacting, or non-Gaussian fixed point (NGFP), the critical exponents receive an additional contribution due to quantum fluctuations, and

$$\Theta_i = d_{\bar{g}_i} + \kappa_i \,. \tag{2.15}$$

In a local QFT, there is only a finite number of couplings with $d_{\bar{g}_i} \geq 0$, i.e., there are only finitely many canonically relevant or marginal couplings. All other operators have increasingly negative canonical mass dimension. Unless the quantum contribution κ_i to infinitely many couplings becomes infinitely large, the number of relevant directions at a NGFP remains finite. Then the fixed point describes a predictive and UV-complete theory that lives in an infinite-dimensional theory space. Of course, a small number of relevant directions would be desirable in terms of predictivity. Indeed, in asymptotically safe quantum gravity, there are indications that the critical hypersurface is finite-dimensional, with only few relevant directions, see Section 3.1. From (2.15), we also see that quantum contributions to the critical exponent might turn a canonically relevant direction into an canonically irrelevant direction. In this case, the predictivity of the theory would be enhanced by quantum fluctuations. Indeed, in asymptotically safe quantum gravity, there are indications that the NGFP for gravity turns canonically marginal couplings into irrelevant directions, see Section 4.1.

While we have introduced and discussed asymptotic safety in the context of quantum gravity, the quantum realization of scale symmetry can also appear in non-gravitational models. Asymptotic safety has for example been investigated in Yang-Mills theories in $d = 4 + \epsilon$ dimensions [55], non-linear sigma models in $d = 2 + \epsilon$ [56–59] and the Gross-Neveu model in $d = 2 + \epsilon$ [60–63]. Furthermore, Gauge-Yukawa models in $d = 4$ can become asymptotically safe at weak coupling [64–68], see also [52] for a review.

2.2. Short introduction to the functional renormalization group

The functional renormalization group (FRG) is a tool which allows to extract the scale dependence of couplings and therefore to probe the scale dependence of classical and quantum field theories. It is a suitable method to search for NGFPs, and therefore allows probing the UV-behavior of theories. We will now motivate the flow equation which is at the heart of the FRG, and discuss some of its properties.

The flow equation

The key ingredient of the FRG is the scale dependent effective action Γ_k, which includes the effect of quantum fluctuations above the scale k^2. The scale k has the dimensions of a momentum, but does not directly correspond to a physical momentum scale. We will call it RG-scale in the following.

The scale dependent effective action Γ_k contains all field monomials $\mathcal{O}_i$, which are compatible with the symmetries of a theory. Furthermore, at finite scale k, Γ_k is restricted to field monomials that contain a positive integer number of derivatives. For detailed reviews, see, e.g., [69–73].

At fixed RG-scale k, Γ_k describes a point in theory space. When quantum fluctuations between k and $k-\delta k$ are integrated out, Γ_k moves along an RG trajectory. Therefore, the scale dependence of Γ_k contains the scale dependence of the entire theory, and can be used to extract the scale dependence of couplings g_i. The scale dependence of Γ_k is described by the flow equation [74–76].

To motivate and derive the flow equation, we start with the path integral for a QFT in Euclidean space. We will restrict the discussion to a simple scalar field φ with action $S[\varphi]$ for simplicity, but the following results generalize to fermions [77], gauge fields [78] and gravity [79]. The path integral for the scalar field theory is defined by the generating functional Z, or equivalently by the effective action Γ, given by

$$Z[J] = \int_\Lambda \mathcal{D}\varphi\, e^{-S[\varphi]+\int_x J\,\varphi}\,, \qquad \text{and} \qquad \Gamma[\phi] = \sup_J \left(\int_x J\,\phi - \ln Z[J]\right)\,, \tag{2.16}$$

where functional derivatives with respect to the source J generate n-point functions for φ, and where Λ is a UV cutoff to regularize the integration. We have introduced the expectation value of φ as $\langle\varphi\rangle = \phi$, and $\sup_J$ denotes the supremum in the Legendre transformation. Both $Z[J]$ and $\Gamma[\phi]$ define the path integral for the scalar field φ with action $S[\varphi]$, but $\Gamma[\phi]$ removes redundancies in terms of reducible correlation functions, which are contained in $Z[\varphi]$. The effective action $\Gamma[\phi]$ contains the quantum equation of motion for the field ϕ

$$\frac{\delta\Gamma[J]}{\delta\phi(x)} = J(x)\,, \tag{2.17}$$

which is in analogy to the classical equations of motion for the classical field φ. When solving the quantum equations of motion, one would integrate out all quantum fluctuations at once. The FRG follows the Wilsonian RG [80, 81] picture instead, and implements a momentum-shell wise integration of quantum fluctuations. This is achieved by introducing an artificial, scale dependent mass term $\Delta S_k[\varphi]$ into the generating functional, such that

$$Z_k[J] = \int_\Lambda \mathcal{D}\varphi\, e^{-S[\varphi]+\int_x J\,\varphi-\Delta S_k[\varphi]}\,, \quad \text{and} \quad \Gamma_k[\phi] = \sup\left(\int_x J\,\phi - \ln Z_k\right) - \Delta S_k[\phi]\,, \tag{2.18}$$

define the scale dependent generating function Z_k and the scale dependent effective action Γ_k, respectively. The mass-like term $\Delta S_k[\varphi]$ is defined as

$$\Delta S_k[\varphi] = \frac{1}{2}\int \frac{\mathrm{d}^d p}{(2\pi)^d}\,\varphi(-p)\,\mathfrak{R}_k(p^2)\,\varphi(p)\,, \tag{2.19}$$

where the field independent regulator $\mathfrak{R}_k$ suppresses modes with $p^2 < k^2$ such that only quan-

tum fluctuations above k^2 are included. In particular, the regulator has to satisfy

$$\mathfrak{R}_k(p^2) = \begin{cases} 0 & \text{for } p^2 > k^2\,, \\ > 0 & \text{for } p^2 < k^2\,, \end{cases} \qquad \text{and} \qquad \mathfrak{R}_k(p^2) \to \begin{cases} 0 & \text{for } k^2 \to 0\,, \\ \infty & \text{for } k^2 \to \Lambda \to \infty\,. \end{cases} \tag{2.20}$$

Since $\Delta S_k[\varphi]$ enters with a negative sign into the scale-dependent generating functional (2.18), modes with $p^2 < k^2$, i.e., IR modes, are suppressed. In particular, for $k \to \infty$, the regulator diverges and no quantum fluctuations are integrated out. Furthermore, the regulator vanishes for $k \to 0$, such that $\Gamma_k \to \Gamma$ as $k \to 0$, which ensures that the resulting effective action remains unchanged.

Starting from the definition of the scale dependent effective action Γ_k (2.18), which introduces the RG scale k, one can derive the flow equation for Γ_k [74–76], as

$$k\,\partial_k \Gamma_k = \frac{1}{2}\,\mathrm{STr}\left(\left(\Gamma_k^{(2)} + \mathfrak{R}_k\right)^{-1} k\,\partial_k \mathfrak{R}_k\right) = \frac{1}{2}$$

, \tag{2.21}

which describes the flow of the scale-dependent effective action from the classical action S, where no quantum fluctuations are integrated out, to the full quantum effective action Γ, where all quantum fluctuations are integrated out. In (2.21), we introduced the shorthand $\Gamma^{(2)}$ for the second functional derivative of Γ_k with respect to the fields, and the super-trace STr runs over all eigenvalues of the regularized propagator $\left(\Gamma_k^{(2)} + \mathfrak{R}_k\right)^{-1}$ and introduces an additional sign for Grassmann valued fields. Structurally, the flow equation (2.21) is a one-loop equation over the full non-perturbative propagator with regulator insertion. The latter is symbolized by the cross in (2.21). For a detailed derivation and discussion of the flow equation and its applications, see, e.g., [69, 71–73].

Expansion schemes

Since Γ_k contains all operators that are compatible with the symmetries of a theory, the flow equation (2.21) is an infinite-dimensional integro-differential equation. While the flow equation is formally exact, it is not exactly solvable. In practice, the infinite dimensional Γ_k is restricted to a, typically finite, set of operators by following systematic expansion schemes. The restricted set of operators is usually called a truncation of Γ_k. Within a truncation, the scale dependence of operators and couplings can be extracted by projecting the flow equation (2.21) onto the corresponding tensor structure by applying functional derivatives.

The use of a truncation introduces systematic uncertainties in the scale dependence of couplings. The truncated flow equation reduces the problem of solving the full path integral into technically more feasible bits. By enlarging the truncation systematically, and within a suitable scheme, the systematic uncertainties can be reduced, until the truncated set of flow equation converges to the full flow equation. The effective action consists of all combinations of the fields and their derivatives, which satisfy the underlying symmetry of the theory. Schematically, we can write Γ_k as

$$\Gamma_k[\phi] = \sum_{n \in \mathbb{N}} g_n\, \mathcal{O}_n[\phi]\,, \tag{2.22}$$

where g_n are coupling constants, or more generally expansion coefficients for the operator basis spanned by $\mathcal{O}_n[\phi]$.

One commonly used expansion scheme is the vertex expansion. There, the operators $\mathcal{O}_n$

would just be monomials of the field, such that

$$\Gamma_k[\phi;\, m] = \sum_{n=0}^{m} \int \mathrm{d}x_1 \dots \mathrm{d}x_n \, g_n(x_1, \dots, x_n) \prod_{i=1}^{n} \phi(x_i)\,, \quad \text{with} \quad g_n = \frac{1}{n!}\Gamma_k^{(n)}[\phi = 0]\,, \tag{2.23}$$

where $\Gamma_k^{(n)}$ is the n-th derivative of Γ_k with respect to the field. The flow equation for Γ_k then is written in terms of flow equations for the vertex functions $\Gamma_k^{(n)}[\phi = 0]$. More generally, in the presence of a background, the vertex functions would be $\Gamma_k^{(n)}[\phi = \phi_0]$, and the functional derivatives would be taken with respect to the fluctuation field. The vertex expansion reproduces the full Γ_k for $m \to \infty$, i.e.,

$$\lim_{m\to\infty} \Gamma_k[\phi;\, m] = \Gamma_k[\phi]\,. \tag{2.24}$$

In practice, the vertices $\Gamma_k^{(n)}$ are usually obtained from functional derivatives acting on a *seed action*, which is typically a classical action with gauge fixing and ghost contributions. We will employ a vertex expansion for gravity in Section 3.2, where we extract the scale dependence of the two-point functions.

Another well known expansion scheme is the derivative expansion, where Γ_k is organized in terms of the number of derivatives acting on fields. In each order of the expansion, the full field dependence is taken into account. The lowest order of the derivative expansion is the local-potential approximation, where Γ_k is just a kinetic term and the full field-dependent potential [69]. The next order of the expansion would then contain a field-dependent wavefunction renormalization, and so on.

The flow equation for gravity

The flow equation (2.21) relies on the notion of UV and IR modes, since the momentum-dependent regulator $\mathfrak{R}_k$ implements a momentum-shell wise integration of quantum fluctuations. In gravity, it is necessary to introduce an auxiliary background metric $\bar{g}_{\mu\nu}$, to consistently distinguish between UV and IR modes. The background metric then sets a scale against which energies are measured. Therefore, to employ the FRG for gravity, it is necessary to employ the *background field method* [82], where the full metric $g_{\mu\nu}$ is split into background metric $\bar{g}_{\mu\nu}$ and a fluctuation field $h_{\mu\nu}$. A common choice for such a split is the linear split

$$g_{\mu\nu} = \bar{g}_{\mu\nu} + h_{\mu\nu}\,, \tag{2.25}$$

which we will always employ in the following. Other parametrizations have been investigated for example in [83–99]. Unlike in a perturbative expansion, the amplitude of metric fluctuations $h_{\mu\nu}$ is unrestricted and can be arbitrarily large. Intuitively, one can think about the split (2.25) as introducing a field $h_{\mu\nu}$ that propagates on a background spacetime with metric $\bar{g}_{\mu\nu}$. The path integral of quantum gravity is then a path integral of metric fluctuations $h_{\mu\nu}$.

With a given split of the metric, the flow equation can be set up in terms of the background metric $\bar{g}_{\mu\nu}$ [79], by generalizing squared momenta p^2 to $-\bar{D}^2$, which is the covariant Laplacian with respect to $\bar{g}_{\mu\nu}$. On this background, modes with eig $\left(-\bar{D}^2\right) > k^2$ are UV modes.

While the introduction of the background is a technical necessity, the background in principle never has to be specified. Further, the full metric $g_{\mu\nu}$ in (2.25) is invariant under the shift $h_{\mu\nu} \to h_{\mu\nu} + \gamma_{\mu\nu}$, and at the same time $\bar{g}_{\mu\nu} \to \bar{g}_{\mu\nu} - \gamma_{\mu\nu}$. This encodes that the effective action and therefore physics, should only depend on one field, namely the physical metric.

However, for gravity, the field which enters the mass-like term ΔS_k (2.19) is the metric fluctuation $h_{\mu\nu}$. Therefore, ΔS_k depends on $h_{\mu\nu}$ and $\bar{g}_{\mu\nu}$ (via the background covariant derivatives) independently. Thus, the insertion of the regulator terms breaks shift-symmetry, and the scale-dependent effective action depends on $\bar{g}_{\mu\nu}$ and $h_{\mu\nu}$ individually, i.e., $\Gamma_k = \Gamma_k[\bar{g}_{\mu\nu}, h_{\mu\nu}]$. Background invariance is then encoded in so-called Nielsen, or split-Ward identities, see e.g., [100] and [53, 71, 101, 102], which encode the difference between correlation functions of the background field and the fluctuation field [97, 103–105]. Gauge-invariant formulations of the flow equation (2.21) have been proposed, e.g., in [106–112].

To introduce the notation and set conventions, let us come back to the expansion of Γ_k in the presence of a background. In the spirit of a vertex expansion, we can write

$$\Gamma_k[\bar{g}, h] = \Gamma_k[\bar{g}, 0] + \sum_{n=1}^{\infty} \left(\frac{\delta^n \Gamma_k[\bar{g}, h]}{\delta h_{\gamma_1\delta_1} \dots \delta h_{\gamma_n\delta_n}} \bigg|_{h_{\mu\nu}=0} \right) h_{\gamma_1\delta_1} \dots h_{\gamma_n\delta_n} \,, \tag{2.26}$$

where we have dropped the indices in the argument of Γ_k for a simpler notation. Here, the first term only depends on the background metric. The couplings appearing in this term will be called *background couplings* in the following. The second term in (2.26) gives the sum over n-point vertices. In general, the different n-point vertices will have different scale dependences, due to the presence of the regulator and the gauge fixing, but they are related by so-called Slavnov-Taylor identities, which encode diffeomorphism invariance, see, e.g., [53, 113] for a discussion. The couplings appearing in the different n-point vertices will be called *fluctuation couplings* in the following.

The physical couplings, i.e., those that we could in principle measure are the background couplings. From the flow equation (2.21), we can infer that their flow will be driven by the fluctuation couplings, specifically by the fluctuation propagator. The *background field approximation* [114] neglects the difference between the fluctuation propagator and the second derivative of Γ_k with respect to the background field. In this way, one replaces the fluctuation couplings by background couplings, specifically the fluctuation cosmological constant λ_2 by the background cosmological constant Λ. While this approximation allows employing large truncations, see the discussion in Section 3.1, it constitutes an additional approximation and leads to another source of systematic uncertainties. Specifically, the background field approximation has been found to suffer a strong regulator dependence, see, e.g.,[115], and [53], and references therein. Procedures to alleviate this dependence have been proposed and used, e.g., in [97, 102–105, 116].

In the following sections, we will extract the scale dependence of several couplings and n-point functions. In the computations based on the FRG, we employ the Mathematica packages *xAct* [117–121], *DoFun* [122, 123], as well as the *FormTracer* [124], for the evaluation of RG-flows.

2.3. Short introduction to Euclidean dynamical triangulations

In the last sections we have introduced asymptotic safety as the quantum realization of scale symmetry. We have argued that asymptotic safety in gravity might allow formulating a predictive, UV-complete theory of quantum gravity. Furthermore, we have introduced the FRG as one method to search for asymptotic safety.

We will now present another, complementary method to search for asymptotic safety in quantum gravity. Specifically, we will introduce *Euclidean dynamical triangulations* (EDT) as a lattice

method to search for asymptotic safety.

The idea of lattice theories is to discretize the d-dimensional space into a set of *lattice sites*. In the practical implementation, not the entire d-dimensional space is discretized, but a finite patch, such that the number of lattice sites is finite. These lattice sites are typically distributed equidistantly at a distance a across the entire patch. On the lattice, the lattice spacing itself serves as a UV-cutoff, since it marks the smallest possible scale that can be probed on the lattice.

The lattice is just a tool that regularizes the path integral via the UV-cutoff a. To recover continuum physics, the artificial discretization has to be removed, after integrating over quantum fluctuations. However, a straightforward limit $a \to 0$, leads to divergences in physical quantities. This is somehow expected, since, after regularizing the path integral with a cutoff, the theory has to be renormalized, to absorb the divergences that would appear when removing the cutoff.

On the lattice, the renormalization procedure consists in finding trajectories along which (the discretized analogues of) physical quantities remain finite as a function of a. These trajectories are then followed along, when decreasing $a \to 0$. If the trajectory then enters a regime, where the lattice parameters do not need to be adjusted anymore to keep the physical quantities constant, the lattice spacing a has dropped out. At this point, physics does not depend on the lattice spacing, and the $a \to 0$ limit can be taken. At this point, the lattice has lost the dependence on the length scale a, and has entered a scale-invariant regime. This point is a fixed-point on the lattice.

Typically, lattice theories loose the dependence on the lattice spacing a in the vicinity of continuous phase transitions. At these phase transitions, the correlation length diverges, indicating that the entire lattice is correlated and interacting. Since the correlation length diverges, the two-point correlation function is constant. If correlation functions are constant, there is no scale in the system, and it becomes scale invariant.

Therefore, the search for a continuum limit of lattice theories consists in the search for second- or higher-order phase transitions.

Most continuum theories are formulated on a non-dynamical gravitational background. Their lattice description is then described as dynamical degrees of freedom interacting on this discretized background. In gravity however, spacetime itself is dynamical, and is therefore the degree of freedom in lattice quantum gravity. The main goal of a lattice theory of quantum gravity is to discretize the Euclidean path integral

$$Z_{\mathrm{E}} = \int \mathcal{D}g_{\mu\nu}\, e^{-S_{\mathrm{E}}[g_{\mu\nu}]}\,. \tag{2.27}$$

One example for lattice theories of quantum gravity is known as *dynamical triangulations* (DT) [125, 126], see also [127]. In DT the d-dimensional space is discretized in terms of d-dimensional building blocks, the *d-simplices* t_d. The 0-, 1-, 2, and 3- simplices are points (vertices), lines (edges), triangles and tetrahedra, respectively. The path integral then is replaced by a sum over all different ways to triangulate the d-dimensional space, weighted by the Regge action [128]. The Regge action is a discretized version of the Einstein-Hilbert action and therefore encodes the curvature and cosmological constant of the lattices.

In the following, we will first motivate the Regge action and the partition function in terms of the fundamental building blocks of DT, in Subsection 2.3.1. Further, we will briefly discuss properties of the phase diagram of DT in the formulation proposed in [125, 126]. In Subsection 2.3.2 we will motivate the extension of DT by the inclusion of a non-trivial measure term.

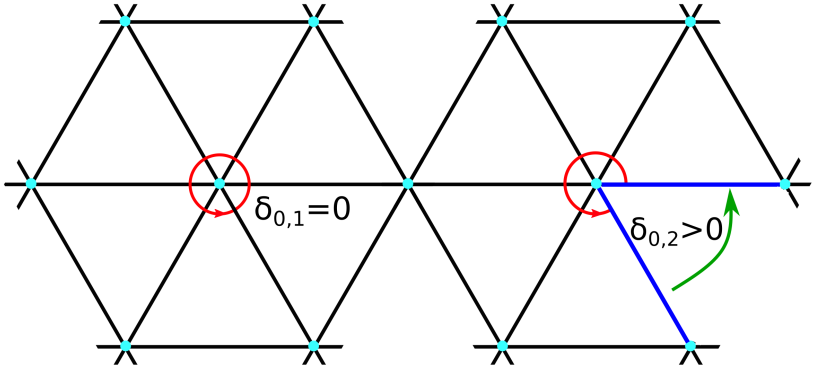

Fig. 2.2.: Illustration of a the deficit angle in a triangulation of the two-dimensional space. On the left, the central vertex is shared by six triangles, and the deficit angle vanishes. Therefore, the triangulated manifold is flat. On the right, the central vertex is only shared by five triangles. Gluing the blue edges together will result in a conical structure and a positive deficit angle. The manifold would have positive curvature.

We will discuss properties of the resulting phase diagram, and the status of this approach, which is called *Euclidean dynamical triangulations* (EDT).

2.3.1. The Regge action for dynamical triangulations

The main idea of the Regge action [128] is to provide a coordinate independent form of the classical Einstein-Hilbert action (3.16). For this, the formulation in terms of coordinates is replaced by a discretization in terms of triangulations. For the discretization of the d-dimensional manifold, we will assume equilateral simplices, such that there is only one parameter associated with the discretization: the edge length a.

There are two contributions to the Einstein-Hilbert action, namely the curvature term, and the volume term associated with the cosmological constant. The latter is discretized by summing over the volume of the highest-dimensional simplex, i.e.,

$$\int \mathrm{d}^d x \sqrt{g} \to \sum_{t_d} V_{t_d} \,. \tag{2.28}$$

For the discretization of the curvature term, let us first focus on $d = 2$ and then generalize to larger dimensions. In $d = 2$ the largest dimensional building blocks are triangles, such that a given manifold is discretized by gluing triangles along their edges. If the manifold is flat, each vertex belongs to six triangles (since the triangles are equilateral). The internal angle of each triangle is $\Theta_2 = \pi/3$, and the total angle covered by the triangles around each vertex is 2π, see Figure 2.2.

Removing one triangle and gluing together the free edges (blue lines in Figure 2.2), a conic structure forms, and the sum of angles around the vertex is smaller than 2π. The sum of angles around a vertex $t_{2,\,i}$ compared to the flat case is called the *deficit angle*, which in $d = 2$ reads [128, 129]

$$\delta_{t_{0,\,i}} = 2\pi - \mathcal{O}(t_{0,\,i}) \frac{\pi}{3} \,, \tag{2.29}$$

where $\mathcal{O}(t_{0,\,i})$ is the *vertex-order*, which gives the number of triangles that the vertex $t_{0,\,i}$ belongs to. For the example in Figure 2.2, the left panel corresponds to $\delta_{t_{0,\,1}} = 0$, while the right panel gives $\delta_{t_{0,\,2}} = \pi/3$. Therefore, we conclude that the deficit angle measures curvature and $\delta_{t_{0,\,i}} > 0$ corresponds to positive curvature, while $\delta_{t_{0,\,i}} < 0$ corresponds to negative curvature.

This can be generalized to d dimensions, where the deficit angle reads [128, 129]

$$\delta_{t_{d-2,\,i}} = 2\pi - \mathcal{O}(t_{d-2,\,i}) \arccos\left(\frac{1}{d}\right) , \tag{2.30}$$

where $\mathcal{O}(t_{d-2,\,i})$ is the order of the $d-2$ simplex, which gives the number of d simplices $t_{d-2,\,i}$ belongs to. In this way, on the discretized manifold, curvature is located on the $d-2$-simplices, so on triangles in $d=4$.

Therefore, the discretized version of the Einstein-Hilbert action reads [128]

$$S_{\text{ER}} = -\frac{1}{8\pi G_{\text{N}}}\left(\sum_{t_{d-2}} V_{t_{d-2}}\,\delta_{t_{d-2}} - \bar{\Lambda}\sum_{t_d} V_{t_d}\right) , \tag{2.31}$$

where the factor of $V_{t_{d-2}}$ in the curvature term can be understood by dimensional analysis.

We have motivated a discretized version of the gravitational action. For an evaluation of the partition function (2.27) we still have to replace the path integral over the metric by a suitable replacement on the lattice.

In quantum Regge calculus [130–134], the idea is to take one single possible triangulation, and then replace the integration over metrics by summing over all possible edge lengths a. Various possibilities of measure terms for the integration have been considered, e.g., in [131, 135, 136]. However, it is not clear if, keeping the triangulation fixed and only summing over different edge lengths is sufficient to sum over all possible geometries [125], and whether the formalism is actually gauge invariant [137, 138]. Furthermore, the question on a viable phase transition in any dimension is not entirely clarified yet and subject to current research [139–141].

2.3.2. The phase diagram of Euclidean dynamical triangulations

Instead of keeping the triangulation fixed and varying the edge length, the idea of DT is to keep the edge length fixed, but to sum over all possible triangulations. We will briefly discuss this in the following, and then focus on a special modification of DT, which introduces a non-trivial measure term.

Dynamical triangulations

In DT [125, 126, 142–145], the edge length is fixed, such that the volume of each d-simplex is fixed. Therefore the sum over the volume, as well as the sum over the curvature term can be performed explicitly. This yields the simplified version of the Regge action

$$S_{\text{ER}} = \kappa_d\, N_d - \kappa_{d-2} N_{d-2} , \tag{2.32}$$

where N_d and N_{d-2} are the total number of d- and $d-2$-simplices, respectively. The lattice parameters κ_d and κ_{d-2} are related to the Newton coupling and the cosmological constant by

$$\begin{aligned} \kappa_d &= \bar{\Lambda}\, V_{t_d} + \frac{d}{2}(d+1)\frac{\arccos(1/d)}{16\pi\, G_{\text{N}}} V_{t_{d-2}} , \\ \kappa_{d-2} &= \frac{V_{t_{d-2}}}{8\pi\, G_{\text{N}}} , \end{aligned} \tag{2.33}$$

with

$$V_{t_d} = \frac{\sqrt{d+1}}{d!\,\sqrt{2^d}} a^d \,. \tag{2.34}$$

Since the sums over simplices are performed explicitly, the action for DT only depends on global parameters of a given lattice, namely the number of d- simplices, and the couplings κ_d and κ_{d-2}.

In DT, the Euclidean path integral is replaced by the partition function

$$Z_{\mathrm{E}}(\kappa_d,\, \kappa_{d-2}) = \sum_T \frac{1}{C_T} e^{-S_{\mathrm{ER}}} \,, \tag{2.35}$$

where the sum goes over different triangulations T, and where $C(T)$ divides out equivalent ways of triangulating the same geometry, which might be present due to symmetries of the manifold. The sum over different triangulations can be understood as the sum over different geometries at fixed topology in the continuum.

In the large volume limit, and keeping the number of d-simplices constant, the partition function scales like [146–148]

$$Z_{\mathrm{E}}(\kappa_d,\, \kappa_{d-2}) \sim e^{N_d(\kappa_d^c - \kappa_d)} \,, \tag{2.36}$$

where we have introduced the *critical line* $\kappa_d^c = \kappa_d^c(\kappa_{d-2})$.

The critical line separates the phase diagram into two regions: for $\kappa_d < \kappa_d^c$, the partition function diverges in the limit of infinite building blocks. For $\kappa_d > \kappa_d^c$, the partition function is convergent in the $N_d \to \infty$ limit. Therefore, tuning to the critical line from $\kappa_d > \kappa_d^c$ allows extracting physical quantities. Approaching the critical line in this way, the partition function reads

$$Z_{\mathrm{E}}(\kappa_d \to \kappa_d^c,\, \kappa_{d-2}) \sim (\kappa_d - \kappa_d^c)^{2-\gamma} \,, \tag{2.37}$$

where $\gamma > 2$ is the *susceptibility exponent*.

From the Regge action for DT, (2.32), we see that the expectation value of d-simplices reads

$$\langle N_d \rangle = \frac{\partial \ln Z_E}{\partial \kappa_d} \sim \frac{\gamma - 2}{\kappa_d - \kappa_d^c} \,, \tag{2.38}$$

which diverges as $\kappa_d \to \kappa_d^c$. Keeping the physical volume $\langle V \rangle \sim a^d \langle N_d \rangle$ fixed while approaching the critical line *forces* the lattice spacing to decrease. This indicates that by approaching the critical line, a continuum limit might be recovered.

Indeed, in $d = 2$, the tuning $\kappa_d \to \kappa_d^c$ is sufficient to find a well-defined continuum limit [149–152], where DT reproduces the critical exponents of two-dimensional bosonic strings [153, 154]. DT in $d = 2$ can also be described in terms of $N \times N$ matrix models [154], where the continuum limit can be taken by taking $N \to \infty$, while approaching the critical line [155]. In this case, the path integral includes a sum over topologies, since it is topological fluctuations that render physical observables finite.

However, for $d = 4$ and in the presented formulation of DT, there is no indication for a suitable continuum limit. Instead, there are two different phases, the *collapsed* phase and the *branched polymer* phase. The latter features *baby universes* [156, 157], which render the observed dimensionality to below $d = 4$. Both of the phases do not resemble a physically viable regime, and the transition between the phases is first order [158–162].

One way to modify the formulation of DT, which might allow recovering a continuum description is *causal dynamical triangulations* (CDT) [163–165]. In CDT the summation over triangulations is restricted to those triangulations that have a proper causal structure and can be

obtained via a Wick-rotation from the Lorentzian theory, see [166] for a recent review. Causality is imposed on the triangulation by introducing two different types of edges, and allowing the gluing only between the same type of edge. Intriguingly, the inclusion of matter might induce a new phase transition in CDT [167].

Euclidean dynamical triangulations

An alternative way to modify the DT approach is by adding an ultra-local measure to the partition function [168–171], which then reads

$$Z_{\mathrm{E}} = \sum_{T} \frac{1}{C_T} \left[\prod_{j=1}^{N2} \mathcal{O}(t_{2\,,j})^{\beta} \right] e^{-S_{\mathrm{ER}}}\,, \tag{2.39}$$

where the triangle order $\mathcal{O}(t_{2\,,j})$ counts the number of four-simplices a given triangle belongs to, where S_{ER} is the Regge action (2.32), and where β is a new parameter of the theory. For $\beta = 0$ the original formulation of DT is recovered. We will refer to the partition function (2.39) with general β as the partition function of *Euclidean dynamical triangulations* (EDT), to distinguish it from DT without non-trivial measure term.

This measure can be motivated in two different ways: First, diffeomorphism invariance might be broken by the discretization procedure, such that a tuning of the exponent β is necessary to restore it in the continuum [172]. The argument is in analogy with the Wilson-fermion formulation of lattice QCD [173], where the lattice regulator breaks chiral symmetry. There a fine-tuning of the bare quark mass is necessary to restore the symmetry, which can only be fully recovered in the infinite volume, continuum limit, see [172, 174] for discussions. Similarly, a non-trivial measure term might be necessary to preserve diffeomorphism invariance on the lattice [175]. Tuning the measure term then might be required to restore the symmetry when approaching the continuum limit.

Second, the triangle order $\mathcal{O}(t_{2\,,j})$ is related to the deficit angle, see (2.30), which in turn is associated with the curvature of the geometry. Exponentiating the measure term and including it in the action, it might be interpreted as some combination of higher-order curvature operators [171]. If a fine-tuning of β allows approaching a continuum limit, this would indicate an additional relevant direction in asymptotically safe quantum gravity. Indications that at least one higher-order operator becomes relevant at the asymptotically safe fixed point have also been discovered using FRG methods, see the discussion in Section 3.1. An explicit inclusion of an R^2 operator in the original DT formulation [176] has however not lead to indications for a continuous phase transition. It would be interesting to revisit the explicit inclusion of R^2 on the lattice with modern computational methods.

The inclusion of a non-trivial measure term as in (2.39) has been studied in a special class of colored tensor models [177]. Tensor models are a natural way to obtain a statistical model for random geometries, and an expansion in terms of $1/N$ can be used to take approach the continuum limit, see [178–180] and [181] for a review. Indications for a higher-order phase transition were found analytically under the consideration of the non-trivial measure term [177]. This provides evidence for a continuum limit in DT with a non-trivial measure term via an analytical expansion in $1/\,N$. The limit $N \to \infty$ in this class of tensor models corresponds to $\kappa_{d-2} \to \infty$ in DT [177]. A direct link between the colored tensor model considered in [177] and the numerical simulations starting with the partition function (2.39) has not been established yet.

Details of the simulations

We will briefly discuss some details of the simulations performed in EDT. For a detailed discussion, see, e.g., [172].

The sum over triangulations is performed over a set of degenerate triangulations, where combinatorial manifold constraints are relaxed [182]. Distinct four simplices may share the same five vertices. However, each four-simplex is labeled by five distinct vertices, such that degenerate four-simplices are not allowed. Hence, the neighbors of a four-simplex are not necessarily unique. While this violates the commonly imposed combinatorial manifold constraints, degenerate triangulations feature reduced finite size effects, compared to combinatorial triangulations [182]. The difference of finite size effects was estimated to a factor of ~ 10 [182]. Furthermore, there are indications that combinatorial and degenerate triangulations share the same universality class, if a continuum limit exists [171, 172, 182].

The algorithm to perform the sum over triangulations consists of two main ingredients, see also [183]: First, there is a set of ergodic moves, the Pachner moves [126, 184–186], which preserve the topology of the triangulated manifold. Ergodicity ensures that any possible configuration can be realized starting from any other possible configuration, if the simulation runs for long enough. Therefore, these Pachner moves parametrize the fluctuations of the triangulation. There are five moves, and ergodicity requires that each move has a corresponding inverse move. The moves are given by adding or deleting a vertex, adding or deleting an edge, or exchanging the labels of two triangles [126, 185, 186], see also [187] for an illustration. The second ingredient is a Metropolis step, where one of the Pachner moves at a random simplex is proposed, and then either accepted or rejected.

The simulations are performed on a fixed global topology S^4. In principle, one would like to fix the bare cosmological constant in the simulations. However, then the volume of the lattice would be unconstrained, and the simulations would take excursions to lattices with a large number of four simplices N_4, which would take exponentially long. As an alternative, in practice the simulations are performed at a fixed lattice volume, which is achieved by adding a volume-preserving term into the action. This is common in DT, see also [171] and the action is supplemented with a term $\delta\lambda\left|N_4^{\text{fid}} - N_4\right|$. For $\delta\lambda > 0$ this term suppresses deviations from the target fiducial volume N_4^{fid}, such that the lattice volume is close to the target volume during the entire simulation. In practice, it is sufficient to make $\delta\lambda$ small enough, since the dependence on $\delta\lambda$ then is negligible. At a fixed volume, the value of κ_4 is then fixed, as it is tuned automatically to the pseudo-critical value κ_4^c, where the infinite lattice-volume limit $N_4 \to \infty$ could be taken. The tuning is adjusted such that an increase in N_4 is compensated by a change in κ_4. In the thermalized regime, N_4 fluctuates around the target volume, and κ_4 around the pseudo-critical value, see [172] for details. The phase diagram of EDT is then a two-dimensional plane spanned by β and κ_2.

The phase diagram

The phase diagram for EDT defined by the partition function (2.39) has been mapped out in [171, 188], and is shown in Figure 2.3. The solid line connecting the points A and B is a first order transition, which separates the branched polymer phase from the collapsed phase. It is the same transition that was discovered in the original DT formulation, corresponding to $\beta = 0$. Neither of the two phases resembles a semi-classical limit of gravity. While the branched polymer phase resembles a two-dimensional geometry, the collapsed phase is fractal-like with large dimension [188]. The line between C and D in Figure 2.3 is a cross-over, such that the crinkled region is

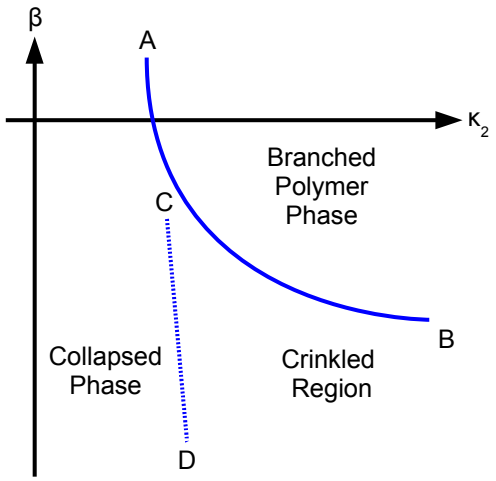

Fig. 2.3.: Illustration of the phase diagram of EDT as a function of κ_2 and β. The line AB is a first order phase transition, which separates the two phases already discovered in DT. The line CD is a cross-over line, such that the crinkled region is not a distinct phase, see [170–172, 188].

not physically different from the collapsed region [171, 172, 188]. Instead, the crinkled region appears to be part of the collapsed phase with large finite-size effects [171, 188].

Compared to the original DT proposal, EDT has one more free parameter, such that the phase-diagram might be richer. Indeed, there are indications that a fine-tuning of β, such that the first-order transition line AB is approached from $\kappa_2 < \kappa_2^c$, leads to semi-classical geometries with a dimension close to four [172]. It is postulated that a continuum limit exists for $\kappa_2 \to \infty$, and that it can be approached by following the first-order transition to large values of κ_2. The limit $\kappa_2 \to \infty$ also corresponds to the $N \to \infty$ limit in colored tensor models, where a higher order transition was found in a special model, including a non-trivial measure term [177].

We will now briefly review the evidence for the recovery of a semi-classical regime, when following the first-order line to large values of κ_2.

Using finite-volume scaling of the lattices, the Hausdorff dimension was measured in [172]. It was shown that it approaches $d_{\mathrm{H}} \approx 4$, when tuning towards the first-order line, thereby reproducing the expected dimensionality for a semi-classical regime of gravity.

A different estimator for the dimensionality is the spectral dimension, which is a fractal dimension defined by a diffusion process. On the EDT configurations, it varies with distance scale and approaches $d_{\mathrm{s}} \approx 4$ at long distances. This behavior is found in various approaches to quantum gravity [189–191].

Furthermore, the volume profile of the EDT geometries approaches the volume profile of Euclidean de Sitter space, when following the transition to larger κ_2, and increasing the volume [172]. Therefore, the agreement with the volume-profile of CDT [192] also improves in this limit. The agreement with the de Sitter volume is worst at long distances but improves for finer lattice spacings. This type of long-distance modifications is common, when a symmetry is broken by the lattice regulator. For example, in the Wilson fermion formulation of QCD, the lattice breaks chiral symmetry, but it can be restored in the continuum limit by fine-tuning. Nevertheless, for any finite lattice spacing, the breaking of chiral symmetry leads to modifications of the pion sector. The pions are the lightest states on the lattice, such that chiral-symmetry breaking on the lattice results in long-distance modifications of the theory [172–174].

Evidence for a semi-classical limit also is found in simulations including fermions in the

quenched approximation, where the back-reaction of the matter fields on the geometry is neglected. Specifically, Kähler-Dirac fermions [193] were investigated in [194]. They generalize the formulation of staggered fermions to random geometries, such that no notion of vielbeins or spin-connection is required. In flat space, and in the continuum theory, the Kähler-Dirac action reduces to four copies of the Dirac action. Similar to the behavior of staggered fermions, the degeneracy of Kähler-Dirac fermions on EDT geometries is lifted by the lattice discretization, but recovered in the continuum, infinite volume limit [194].

In the continuum, the Kähler-Dirac action features an exact $U(1)$-symmetry, which is related to chiral symmetry. The study of fermion bilinear condensates provides evidence that this $U(1)$ symmetry is not spontaneously broken by fluctuations of the geometry [194]. Therefore, the existence of light fermions, as we observe them in our universe, might be compatible with EDT.

We will discuss further consistency test for the EDT approach to asymptotically safe quantum gravity in Section 3.3.

3. Theoretical consistency tests

Despite the large separation of the Planck scale from experimentally accessible scales, it is crucial to test any theory of quantum gravity, since in the end any physically viable theory should describe nature in some regime. However, since direct experimental tests of quantum gravity are not easily available, we can only perform consistency tests to verify the viability of a given theory.

In this section, we will first review indications for the asymptotically safe fixed point in pure gravity, and in gravity matter systems. We will then discuss theoretical consistency tests for asymptotically safe quantum gravity. Specifically, in Section 3.2, we will investigate the momentum-dependence of the gravitational propagators, and discuss indications for the stability of the result based on mild gauge dependence. Furthermore, in Section 3.3 we will present evidence for asymptotic safety from the lattice. Specifically, we confront the EDT approach to asymptotic safety with theoretical consistency tests, and demand that it features a suitable classical regime in the appropriate limit.

3.1. Indications for the asymptotically safe fixed point for gravity and matter

Before presenting indications for the asymptotically safe fixed point, let us first review the mechanism that generates the fixed point: the balancing between canonical and quantum scaling. For this, consider a Yang-Mills theory on $d = 4 + \epsilon$, where the gauge coupling $\bar{g}_s$ is dimensionfull with canonical mass dimension $[\bar{g}_s] = -\frac{d-4}{2}$. For convenience we will continue the discussion in terms of the squared gauge coupling $\bar{\alpha}_s = \frac{\bar{g}_s{}^2}{(4\pi)^2}$. The corresponding dimensionless squared gauge coupling is given by $\alpha_s = \bar{\alpha}_s\, k^{d-4}$. Due to the canonical mass dimension of $\bar{\alpha}_s$, the scale dependence of α_s receives a dimensional contribution. To 1-loop order, it reads in $d = 4 + \epsilon$ dimensions

$$\beta_{\alpha_s} = \epsilon\, \alpha_s - a_0\, \alpha_s{}^2\,, \tag{3.1}$$

where the first term is the dimensional contribution, while the second term is the standard 1-loop coefficient. The coefficient a_0 has to be positive to be consistent with asymptotic freedom in $d = 4$. In $d = 4 + \epsilon$, there are two fixed points for α_s at

$$\begin{aligned} \alpha_{s*,1} &= 0\,, \qquad && \text{with} \qquad \Theta_1 = -\epsilon\,, \\ \alpha_{s*,1} &= \frac{a_0}{\epsilon}\,, \qquad && \text{with} \qquad \Theta_2 = \epsilon\,. \end{aligned} \tag{3.2}$$

The GFP is UV repulsive for $\epsilon > 0$, i.e., in $d > 4$. The NGFP is UV attractive for $\epsilon > 0$. Therefore, asymptotic freedom for the strong gauge coupling is replaced by asymptotic safety for $d > 4$. More generally speaking, models that are asymptotically free in the critical dimension d_{crit}, where the coupling is canonically marginal, might become asymptotically safe in $d = d_{\text{crit}} + \epsilon$.

Equation (3.1) shows one mechanism which can lead to asymptotic safety: the dimensional term linear in α_s is balanced by quantum fluctuations which enter at least quadratically into β_{α_s}.

This will be the mechanism at the heart of asymptotic safety in quantum gravity. For Yang-Mills theories, it is an open question, up to which value of ϵ asymptotic safety can be realized [195–197]. Other mechanisms leading to finite fixed-point values can be the balancing of different loop orders, or the balancing between bosonic and fermionic degrees of freedom, see [52] for a review.

The critical dimension in gravity is $d_{\text{crit}} = 2$, where the Newton coupling G_{N} is canonically marginal. Therefore, the scale dependence of the dimensionless version of the Newton coupling $G = G_{\text{N}}\, k^{d-2}$ in $d > 2$ has the same structure as β_{α_s} in $d > 4$. Specifically, it reads

$$\beta_G = \epsilon\, G - b_0\, G^2 + \mathcal{O}\left(G^3\right) , \tag{3.3}$$

where b_0 is a positive number. The numerical value of b_0 depends on the details of the computation, but the sign is positive in various approximations and schemes, see [198–200] and [85, 201] for FRG computations.

Asymptotic safety in quantum gravity might be realized as a consequence of the balancing between quantum contributions and the dimensional contribution [202]. The question whether the expansion in $d = 2 + \epsilon$ can be extended to $d = 4$ in a continuous way, is open.

We will review indications for the asymptotically safe fixed point in $d = 4$ in pure gravity, and in gravity-matter systems in the following section. We will focus on indications from FRG studies of quantum gravity and matter, and refer the reader to Section 2.3 and Section 3.3 for indications based on lattice studies.

3.1.1. The asymptotically safe fixed point for pure gravity

We start by assuming that the canonical mass dimension remains a suitable guiding principle at a NGFP, which allows to set up truncations that capture the relevant dynamics. This assumption can be tested a-posteriori, by extending the truncation and comparing the critical exponents with the canonical mass dimensions of the added operators.

For the leading-order truncation, the ansatz for the scale dependent effective action Γ_k is the Einstein-Hilbert action,

$$\Gamma_{k\,,\,\text{EH}} = -\frac{1}{16\pi G_{\text{N}}} \int \mathrm{d}^4x \sqrt{g} \left(R - 2\bar{\Lambda}\right) + S_{\text{gf}} + S_{\text{gh}} \,, \tag{3.4}$$

where $G = G_{\text{N}}\, k^2$ and $\Lambda = \bar{\Lambda}\, k^{-2}$ are the dimensionless counterparts of the Newton coupling and the cosmological constant. S_{gf} is the gauge-fixing action and S_{gh} is the action for the corresponding Fadeev-Popov ghost. These terms will be specified explicitly in Subsection 3.2.1, cf. (3.18), and (3.19). By the virtue of the background field method, the gauge fixing can be chosen such that background diffeomorphism invariance remains intact.

Within the background field approximation, the beta functions for G and Λ are schematically given up to second order in the couplings by

$$\beta_G = 2G - a_0\, G^2 \qquad \text{and} \qquad \beta_\Lambda = -2\Lambda + a_1\, G + a_2\, G\Lambda \,, \tag{3.5}$$

where the coefficients a_i are positive, see, e.g., [203]. The fixed point features two relevant directions, and is therefore fully UV-attractive in the subspace spanned by G and Λ. The schematic representation (3.5) highlights that indeed the balancing between canonical and quantum scaling might give rise to an asymptotically safe fixed point. This so-called *Reuter fixed point* exists for different choices of the gauge fixing and the regulator, see, e.g., [88, 203–207].

Starting from the Einstein-Hilbert action as a seed action, the Reuter fixed point has also been discovered in the bi-metric approach [100, 208, 209]. Furthermore, fluctuation computations up to the gravitational three [210–215] and four-point functions [216] provide evidence for the Reuter fixed point. The latter approaches carefully distinguish between background and fluctuation metric and are therefore key to obtain background independent results for the momentum dependence of physical quantities.

Despite quantitative differences, all these approximations indicate that a fixed point with two relevant directions exists. Furthermore, the system of flow equations for the Newton coupling and the cosmological constant admits trajectories that connect the asymptotically safe fixed point with a viable IR physics, where the dimensionless versions of the Newton coupling and cosmological constant are small and positive.

Approximations including curvature squared operators indicate the presence of at least one additional relevant direction [217, 218]. Including all independent curvature squared operators results in a fixed point with three relevant and one irrelevant direction [219–223]. The latter indicates the potential predictivity of the asymptotically safe fixed point, since the inclusion of a canonically marginal operator does not add another relevant direction. The presence of a only three relevant direction was also concluded from the analysis of the momentum structure of the gravitational four-point functions [216].

This also provides an a-posteriori justification for truncations based on canonical power counting. Since canonically marginal or irrelevant operators do not become relevant at the NGFP within a large body of approximations, a truncation based on canonical power counting might be suitable to describe dynamics of the system. Similarly, the canonically irrelevant Goroff-Sagnotti 2-loop counter-term adds an irrelevant direction [224]. However, [225] reported a stable fixed point, where a curvature cubed operator becomes relevant. While the same approximation features additional fixed points with less relevant directions, the nature of this fixed point deserves further exploration to investigate, whether it persists and is stable in extended truncations.

Truncations which extend the basis of operators to higher-dimensional operators in particular directions, include $f(R)$-type truncations. In polynomial expansions in the curvature scalar up to R^3, the fixed point can feature two or three relevant directions, depending on the technical details of the computations [226]. However, expansions including higher powers of the Ricci scalar show a near-canonical scaling of higher-order couplings [227–229]: the fixed-point values of higher order operators remain small, and their critical exponents are approximated by their canonical mass dimension. Specifically, for truncations including the Ricci scalar up to power 23, the critical exponent of the operator R^n are fitted by [229]

$$\Theta_n = b - a\, n \quad \text{with} \quad b = 2.91 \pm 0.05\,, \quad \text{and} \quad a = 2.042 \pm 0.002\,. \tag{3.6}$$

This highlights the near-canonical scaling, since for the slope a of the Θ_n is in quantitative agreement with the expected canonical slope of $a_c = 2$. Infinite-dimensional $f(R)$ truncations indicate the existence of a fixed-point which shares qualitative features of the fixed point in polynomial expansions, see, e.g., [93, 230–233].

A near-canonical scaling of the critical exponents of higher-order operators was also found in polynomial expansions including Ricci- [234] or Riemann [225] tensors. This provides evidence for the predictivity of the asymptotically safe fixed point, since the couplings of higher-order operators are predicted by the relevant directions, and are not free parameters. The near-canonical scaling also further justifies the suitability of canonical power counting as a guide to set up trun-

cations.

In summary, polynomial expansions of the scale dependent effective action in curvature operators indicate a finite-dimensional critical hypersurface. The exact number of relevant direction varies between two and four, depending on the chosen operators, the parametrization of metric fluctuations and the regulator. However, a fixed point with near-canonical scaling of higher-order operators is found in several different technical setups. This indicates that the Reuter fixed point features a finite number of relevant directions. It therefore might provide a predictive UV-completion of GR.

More recently, an expansion based on form factors was employed within the background field approximation [235, 236]. These computations on an expansion in curvature invariants, and aim at computing the scale dependence of the corresponding full momentum-dependent form factors. This is crucial to distinguish the dependence on the RG-scale k from the dependence on physical momenta, see also the discussions in [237] and [238]. The momentum dependence of couplings or form factors allows to investigate the high-energy behavior of the theory, for example related to the question of unitarity [239, 240], see also Subsection 3.2.1.

While computations in the form factor expansion rely on the background field approximation, the momentum dependence of couplings, more specifically of n-point correlators, can also be extracted in the vertex expansion. In the vertex expansion, it is crucial to extract the scale dependence of n-points at finite momenta, to capture their momentum dependence adequately at least on a qualitative level [113, 211–214, 216, 241–243]. This momentum dependence also allows reconstructing the spectral function of the graviton, and provides a first step towards addressing the question of unitarity beyond the background field approximation [244].

As a consequence of employing the FRG to investigate the Reuter fixed point, all evidence for the fixed point was discovered in Euclidean spaces. Evidence for the fixed-point has also been found on foliated spaces in terms of ADM variables [245–247], as well as in a covariant decomposition of the metric into spacial metric and normalized time-like vector [248]. Singling out a foliation structure is a first step towards the investigation of asymptotic safety in Lorentzian spacetimes, since the timelike vector might be used to perform a Wick rotation [245].

In summary, there is plenty of evidence for the existence of a NGFP for quantum gravity. This so-called Reuter fixed point has been found and investigated in various different approximations and truncations for the dynamics. They indicate that the critical hypersurface of the Reuter fixed point is finite dimensional, with two to four relevant parameters, depending on the exact technical details. Therefore, a predictive UV completion of GR in a quantum-field theoretic framework might be viable.

On unitarity in asymptotic safety

The presence of higher-curvature operators raises the question of unitarity in asymptotic safety. We will now briefly discuss this question on the example of a scalar field theory with a kinetic term containing higher derivatives. We will see that truncating the kinetic term can result in fake-instabilities of the truncated theory. Therefore, the presence of derivatives of arbitrary order might be crucial to retain unitarity in asymptotically safe quantum gravity.

Let us for simplicity consider a scalar theory in Euclidean space, whose dynamics can be described by the action

$$S_\phi \simeq \int \mathrm{d}^4x\sqrt{g}\left(\partial^\mu\phi\left(1+f_\phi(\Delta)\right)\partial_\mu\phi+\mathcal{O}(\phi^4)\right)\,, \tag{3.7}$$

where we introduced $\Delta = -\partial^\mu \partial_\mu$, and the form factor f_ϕ which summarizes all higher-derivative contributions to the kinetic term. Since we will focus on the propagator of the theory, the interactions summarized in the last term do not play a role.

On a flat Euclidean background, the propagator of this theory reads

$$G_\phi \sim \frac{1}{p^2 \left(1 + f_\phi(p^2)\right)} \,. \tag{3.8}$$

If $f_\phi(p^2) > -1$ for all $p^2 \in \mathbb{C}$, the propagator only features a single pole at $p^2 = 0$. Therefore, the resulting theory does not feature additional modes which could render the theory unstable.

To discuss the opposite case, let us expand the form factor f_ϕ as

$$f_\phi(p^2) = \sum_{n=1}^{\infty} a_n \left(p^2\right)^n \,. \tag{3.9}$$

For $n = 1$, the action S_ϕ for a scalar field is in analogy with the action for quadratic gravity $S_{\text{EH}} + S_{R^2}$, see (2.7). In this case, the propagator of the scalar field reads

$$G_\phi \sim \frac{1}{p^2 \left(1 + a_1 p^2\right)} = \frac{1}{p^2} - \frac{1}{\frac{1}{a_1} + p^2} \,, \tag{3.10}$$

where we have performed a partial fraction decomposition in the last step. The partial fraction decomposition shows that there are now two propagating modes with a standard, single-pole propagator. One of the modes is massless, while the propagator of the other one is massive, with $m^2 = -1/a_1$. Due to the relative negative sign between the two modes, the Euclidean propagator (3.10) violates reflection positivity [30], see also [249]. This instability already arises on the classical level. The additional particle is a ghost, and the corresponding Lorentzian propagator would violate unitarity.

If $a_1 > 0$, the propagator of the second mode is the propagator of a stable particle with mass $m^2 = 1/a_1$, indicating that the ghost is stable, and potentially part of the physical spectrum. If on the other hand $a_1 < 0$, the additional particle is a tachyonic ghost, leading to exponentially growing modes, resulting in instabilities of the theory. See also [32, 250] for detailed discussion on the different cases.

This analysis shows that, even if the full propagator does not feature additional poles, a truncation to finite order in momenta can create fake ghosts. An extensive analysis of general properties of these fake poles can be found in [251]. Therefore, in the FRG approach to asymptotically safe quantum gravity, the question of unitarity can only be addressed in computations that take the entire form factor f_ϕ into account.

In the context of asymptotically safe quantum gravity, specific form factors were constructed that satisfy unitarity bounds [239, 240], indicating that unitarity can be ensured under certain conditions. Furthermore, recently the graviton spectral function was reconstructed from the momentum-dependent evaluation of the anomalous dimension of the fluctuation fields [244]. The resulting spectral function is positive at vanishing RG scale, which also indicates that asymptotically safe quantum gravity might indeed be unitary.

The above argument and analysis of instabilities was performed on the level of a propagator on a flat background. However, instabilities on a given background do not necessarily indicate that the theory itself is unstable, see also [238]. It might also indicate that the chosen background is not suitable to characterize the theory. Therefore, even if a theory looks unstable on a flat background, expanding the theory on a non-trivial background can result in a stable

theory, see [252]. The question which background should be chosen to investigate instabilities of asymptotically safe quantum gravity is rather intricate, since the on-shell background is not known a-priori.

3.1.2. On the effect of matter on asymptotically safe quantum gravity

Besides the experimental observation of gravity in our universe, we also observe matter fields at low energies. These matter fields could in principle be emergent at low energies, resulting, for example from the compactification of higher-dimensional theories [253–255]. We will in the following assume that the observed matter degrees of freedom are fundamental. Therefore, a UV-completion of GR is neither necessary nor sufficient for a UV-complete description of our universe, which has to incorporate the observed matter degrees of freedom. We will now briefly summarize key aspects of the impact of matter fluctuations on gravity. For more detailed reviews, see, e.g., [51–53].

For a more intuitive understanding that matter degrees of freedom can substantially change the UV behavior of a theory, let us come back to the example of the Yang-Mills theories $d = 4$: For a pure gauge theory, the non-Abelian gauge coupling becomes asymptotically free and the GFP is UV attractive. Quantum fluctuations of charged matter result in an additional contribution to the one-loop scale dependence of the gauge coupling. In the presence of $N_{\rm F}$ fermions, the scale dependence reads

$$\beta_{\alpha_s} = {\alpha_s}^2 \, \frac{2}{16\pi^2} \left(\frac{2}{3} N_{\rm F} - 11 \right) , \tag{3.11}$$

where we explicitly inserted the coefficient $a_0 = \frac{22}{16\pi^2}$ in (3.1). In the pure gauge theory, the non-Abelian gauge coupling is asymptotically free. However, quantum fluctuations of charged fermions contribute with a positive sign to the scale dependence of α_s. Hence, for $N_{\rm F} > \frac{33}{2}$ the total one-loop contribution is positive. In this case, asymptotic freedom is lost, and the GFP for α_s becomes UV repulsive. This illustrates that the inclusion of matter can change the high-energy properties of a theory on a qualitative level, and even result in the UV-incompleteness of a theory.

Gravity couples to any type of matter degrees of freedom, such that scalars, fermions, and vector fields contribute to the scale dependence of gravitational couplings. To leading order, the contribution of minimally coupled matter, specifically $N_{\rm S}$ scalars, $N_{\rm F}$ Dirac-fermions, and $N_{\rm V}$ vector fields, to the scale dependence of the Newton coupling can be parametrized as

$$\beta_G\big|_{\rm matter} = G^2 \left(a_{\rm S} \, N_{\rm S} + a_{\rm F} \, N_{\rm F} + a_{\rm V} \, N_{\rm V} \right) , \tag{3.12}$$

where the coefficients $a_{\rm i}$ are real numbers. Therefore, matter degrees of freedom deform the gravitational fixed point. For small numbers of matter fields, the asymptotically safe fixed point of the gravity-matter system is therefore an extension of the Reuter fixed point of pure gravity. We will now discuss the different contributions $a_{\rm i}$ in more detail, focussing on their impact on the scale dependence of G first.

For scalar fields, $a_{\rm S} > 0$ was found in the background field approximation [87, 89, 94, 99, 256–258] and also in fluctuation computations [113, 241, 259]. The sign of scalar contributions to the scale dependence of the Newton coupling therefore agrees with perturbative studies using heat-kernel techniques [260, 261] and an ϵ expansion in $d = 2 + \epsilon$ dimensions [199].

The positive sign of $a_{\rm S}$ indicates an increasing fixed-point value $G_* > 0$. Technically, the fixed-point value diverges at a finite value for $N_{\rm S}$, and reappears at $G_* < 0$. However, this fixed point

is not connected with a phenomenologically viable regime with $G > 0$ at low energies, due to the IR attractive nature of the GFP. Therefore, the divergence of G_* might indicate a non-trivial bound on the number of scalar matter fields. However, in fluctuation computations, the possible divergence occurs in a regime, where large positive anomalous dimensions indicate that the truncation is not reliable anymore [113, 241]. An investigation of the curvature dependence of the scalar-gravity system indicates that a well-behaved fixed point for all values of $N_{\rm S}$ might exist at non-vanishing background curvature [259]. An expansion around a flat background might therefore require an increased truncation to resolve the large $N_{\rm S}$ behavior accurately.

For fermionic fields, a positive $a_{\rm F}$ was found in the background field approximation [243, 262–264], and also in fluctuation computations [241, 243, 265, 266], in agreement with perturbative studies [260, 261]. Within the background field approximation, different choices for the FRG-regulator $\mathfrak{R}_k^h$ can lead to a negative $a_{\rm F}$, see, e.g. [99, 262, 263]. However, as was argued in [262], these regulators might lead to unphysical results. This discussion and in particular the regulator-dependence of the sign of $a_{\rm F}$, highlights the limitations of the background field approximation.

In the background field approximation, and choosing a regulator such that $a_{\rm F} > 0$, the fixed-point value of the Newton coupling increases with increasing $N_{\rm F}$. Just as under the inclusion of scalar fields, the fixed-point value diverges for some value of $N_{\rm F}$, which is expected since the signs of $a_{\rm F}$ and $a_{\rm S}$ agree. Beyond that value of $N_{\rm F}$, the gravity-matter system lacks a viable fixed point.

The situation is different in the fluctuation computations, even though the sign of $a_{\rm F}$ agrees with the sign of $a_{\rm S}$. For increasing values of $N_{\rm F}$, G_* decreases, while λ_{2*} approaches the pole at $\lambda_2 = 1/2$. In this way, in the fluctuation computations, the gravity-matter system stabilizes itself dynamically under the inclusion of fermions. Hence, despite the positive sign of $a_{\rm F}$, G does not diverge, and, within the explored range of $N_{\rm F}$, and within small truncations, there is no indication for an upper bound on the number of fermions [241, 243, 265]. This conclusion persists in the presence of non-minimal fermion curvature couplings [243].

This difference between fermions and scalars in the fluctuation computations lies in the dynamics of the cosmological constant, which we have not taken into account until now, for simplicity. To understand this difference, we expand the scale dependence of the fluctuation cosmological constant λ_2 (mass parameter) in the presence of scalar and fermionic matter, evaluated at the pure-gravity fixed-point value for λ_2. It reads [113, 241, 266]:

$$\beta_{\lambda_2}\big|_{\lambda_2=\lambda_{2*}} \approx 1.1 + G\,(-1.8 + 0.02\,N_{\rm S} - 0.3\,N_{\rm F}) + \mathcal{O}(G^2)\,, \tag{3.13}$$

where the first term is the canonical contribution to β_{λ_2}, evaluated at the pure-gravity fixed point. We see that scalar and fermionic contributions to β_{λ_2} have the opposite sign. For increasing $N_{\rm S}$, the fixed-point value of G has to increase, when keeping λ_2 fixed. Conversely, for increasing $N_{\rm F}$, the fixed point value for G has to decrease, when keeping λ_2 fixed. Therefore, when combining the scale dependences for G and λ_2, G increases and eventually diverges when increasing $N_{\rm S}$, while G decreases, and λ_2 approaches the pole at $\lambda_2 = 1/2$, when increasing $N_{\rm F}$ [241, 243].

The inclusion of fermions seems to have a qualitatively different effect in the background field approximation, compared to the fluctuation computations. However, the effective gravitational coupling $G_{\rm eff}$, which parametrizes the gravitational effect on the matter system, is in qualitative agreement between background and fluctuation computation [243]. Therefore, despite the differences on the level of fixed-point values and the dynamics as a function of $N_{\rm F}$, the effect of quantum gravity on the matter sector might be qualitatively similar in both approximations,

see also the discussion in Section 4.1.

For vector fields, $a_{\rm V} < 0$ was found in the background field approximation [257, 258] and also in fluctuation computations [242], which is in agreement with perturbative studies [260, 261]. Due to the negative sign of $a_{\rm V}$, G_* decreases as a function of $N_{\rm V}$. However, since the fixed-point value for the cosmological constant remains finite, the studied truncations so far do not reveal a perturbative limit for $N_{\rm V} \to \infty$.

In summary, the asymptotically safe fixed point of pure gravity is suitably extendable for small enough numbers of minimally coupled matter fields. The sign of the matter contributions to the scale dependence of G is in agreement with perturbative studies. In the scalar matter sector, current truncations feature an upper bound on $N_{\rm S}$, where the fixed point diverges. A similar result holds for the fermionic sector in the background field approximation. In fluctuation computations, current truncations do not indicate the existence of an upper bound on the number of fermions.

More generally, [242] argues that a fixed point for gravity with minimally coupled and non self-interacting matter should always be present, since the matter degrees of freedom can be integrated out. According to this argument, any upper bound on the number of matter fields is just an artifact of the truncation. However, the asymptotically safe fixed point of gravity and matter also features non-minimal curvature-matter interactions [243, 267–269]. These might alter the fixed-point structure of the system, and eventually lead to non-trivial bounds on the matter content that is compatible with asymptotically safe quantum gravity.

In all approximations so far, the minimally coupled, and non-self interacting matter content of the SM is compatible with the asymptotic-safety paradigm for quantum gravity.

Let us briefly discuss an indication for the near-perturbative nature of the asymptotically safe fixed point for gravity matter systems, which has been called *effective universality* [113, 243, 266]. Effective universality refers to the approximate agreement of different avatars of the Newton coupling. Those avatars arise in the fluctuation computation, since each n-point function runs differently in the presence of a gauge fixing and the regulator. In a gravity-matter system, different n-point functions therefore allow to extract different *avatars* of the Newton coupling, for example from the graviton three-point vertex [213, 216, 242], the scalar-graviton vertex [94, 113, 267] or the fermion graviton vertex [243]. The different n-point vertices are related by modified Slavnov-Taylor identities, which encode how diffeomorphism invariance is broken, such that the different avatars do not correspond to independent free parameters of the theory.

Unlike in QCD, where the gauge coupling is dimensionless in $d = 4$, the beta function of the Newton coupling is not universal at one-loop. Therefore, the scale dependence of different gravity-matter vertices generally disagree from the pure-gravity vertex. In contrast, in the perturbative regime of QCD, where a one-loop approximation is valid, the gauge coupling is universal: it can be extracted from the three- or four-gluon vertex, or the quark-gluon vertex. In contrast to one-loop universality, *effective universality* refers to the semi-quantitative agreement of gravity-matter vertices and pure gravity vertices [113, 216, 243, 266]. Indeed, at the asymptotically safe fixed point, the beta functions of all different gravity and gravity-matter three-point vertices are effectively universal. In analogy to QCD, where universality only holds in the perturbative regime, effective universality was interpreted as an indication for the near-perturbative nature of quantum gravity [266].

This indication for the near-perturbative nature of gravity-matter systems is in line with the near-canonical scaling of higher curvature operators in pure gravity, see [225, 227–229, 234] and Subsection 3.1.1. The feature of effective universality has several important implications: first, it

indicates that the Slavnov-Taylor identities that relate the different vertex correlation functions are simple close to the fixed-point. As emphasized above, this might indicate that the asymptotically safe fixed point lies in a near-perturbative regime. Second, effective universality requires non-trivial cancellations between different diagrams contributing to the scale dependence of the vertex correlators. These cancellations, which do not happen away from the fixed-point, might indicate the physical nature of the fixed point, instead of being a truncation artifact. For the latter, delicate cancellations leading to the conclusion that physics might be near-perturbative appears to be unlikely.

The near-perturbative nature of gravity-matter systems is also indicated by the inclusion of non-minimal curvature matter couplings. Canonically irrelevant non-minimal couplings remain irrelevant at the asymptotically fixed point [243, 263, 264, 267], and do not significantly alter the dynamics of the minimally coupled system. The latter statement is also true for marginal non-minimal couplings in the scalar sector [268, 269].

Overall, there is plenty of evidence for the asymptotically safe fixed point for pure gravity and for gravity-matter systems, explored with FRG methods. This puts us in the position to perform additional consistency tests, to further investigate, if asymptotically safe quantum gravity might be a viable candidate for a UV-complete description of our universe.

3.2. Non-perturbative propagators in quantum gravity

The physical RG running is one key object to study within a QFT. It translates into the momentum dependence of correlation functions and therefore characterizes the high-energy behavior of the theory. These momentum-dependent correlation functions are the basic building blocks of physical observables like scattering cross-sections.

The propagator, i.e., the inverse two-point function, is the simplest non-trivial correlation function. The propagator carries information on the causality and unitarity of the theory. Furthermore, if a spectral function exists [244], it is related to the propagator. An accurate description of the propagator is therefore crucial to determine, whether asymptotically safe quantum gravity is a viable candidate for a theory of quantum gravity.

In this work, we will compute the full momentum dependence of the graviton propagator, and the propagator of the corresponding Fadeev-Popov ghost. We will employ FRG techniques, as introduced in Section 2.2. We will distinguish between all modes of the graviton and the ghost propagators. The ghost is a vector field and therefore decomposes into a transverse and a longitudinal mode. The graviton splits into a gauge invariant spin two mode (the transverse-traceless mode), a gauge invariant spin zero mode, and a gauge vector mode. The physical information on the system is stored in the two gauge-invariant modes of the graviton propagator. The other modes can however contribute to the scale and momentum dependence of these two modes.

The central results that are presented in this section are:

1. The spin two and spin zero modes of the graviton feature qualitative and quantitative differences in their momentum dependence, see Figure 3.3.

2. The gauge dependence is small, see Figure 3.3.

3. At the investigated point in the gravitational parameter space, the fixed-point propagators do not feature additional poles, see Figure 3.4.

This section is structured as follows: We will present the fluctuation setup in Subsection 3.2.1, and discuss general properties of the RG flows in Subsection 3.2.2. In Subsection 3.2.3 we will discuss the relation between form factors, anomalous dimensions and wavefunction renormalizations. In Subsection 3.2.4 we will discuss the numerical strategy, and present the numerical results. We summarize and conclude in Subsection 3.2.5

3.2.1. Momentum dependence in quantum gravity: The fluctuation approach

For simplicity, we will employ a flat background in the following, i.e., decompose the full metric according to

$$g_{\mu\nu} = \delta_{\mu\nu} + h_{\mu\nu}\,, \tag{3.14}$$

see also (2.25). In a diffeomorphism invariant theory, each diffeomorphism invariant operator would be labelled by one single coupling. However, in the context of the FRG, the regulator as well as gauge fixing breaks diffeomorphism invariance. Hence, the scale dependences of different n-point functions originating from the same diffeomorphism invariant operator do in general not agree [113, 216, 242, 243, 266]. To account for this difference, we will introduce separate couplings for each operator in the vertex expansion. In order to thoroughly investigate the propagators of the system, we will distinguish the transverse-traceless and the gauge independent scalar mode on the level of the 2-point function. We approximate the seed action generating the n-point vertices by

$$S = S_{\rm EH} + S_{\rm gh} + S_{\rm gf}\,, \tag{3.15}$$

where the Einstein-Hilbert action describes the gravitational dynamics and is given by

$$S_{\rm EH} = -\frac{1}{16\pi\bar{G}}\int \mathrm{d}^d x\sqrt{g}\left(R - 2\bar{\Lambda}\right)\,. \tag{3.16}$$

Here, we have introduced the Newton coupling $\bar{G}$, as well as the cosmological constant $\bar{\Lambda}$. Computing the quantum effects of metric fluctuations requires to introduce a gauge-fixing condition $\mathcal{F}^\mu = 0$. We will choose

$$\mathcal{F}^\mu = \left(\bar{g}^{\mu\kappa}\bar{D}^\lambda - \frac{1+\beta_h}{d}\,\bar{g}^{\kappa\lambda}\bar{D}^\mu + \frac{\gamma_h}{d}\bar{D}^\mu\bar{D}^\kappa\frac{1}{\bar{D}^2}\bar{D}^\lambda\right)h_{\kappa\lambda}\,, \tag{3.17}$$

where $\bar{D}^\mu$ is the background covariant derivative, and β_h and γ_h are gauge parameters. Including the tensor structure associated with γ_h allows to extract the scale dependence of all independent tensor structures on the level of the graviton two-point function. We implement the gauge fixing condition by including a gauge fixing action

$$S_{\rm gf} = \frac{1}{32\pi\,\alpha_h\,\bar{G}}\int \mathrm{d}^d x\sqrt{\bar{g}}\,\mathcal{F}^\mu\bar{g}_{\mu\nu}\mathcal{F}^\nu\,, \tag{3.18}$$

where the parameter α_h controls how strongly the gauge fixing condition is implemented on the level of the path integral. The Landau limit, i.e., $\alpha_h \to 0$ corresponds to a strict implementation. The gauge fixing action gives rise to Fadeev-Popov ghosts, whose dynamics are given by

$$S_{\rm gh} = \frac{1}{16\,\bar{G}}\int \mathrm{d}^d x\sqrt{\bar{g}}\,\bar{c}_\mu\,\frac{\delta\,F^\mu}{\delta h_{\sigma\kappa}}\,\mathcal{L}_c g_{\sigma\kappa}\,, \tag{3.19}$$

where $\mathcal{L}_c g_{\sigma\kappa}$ is the Lie derivative of the full metric in the direction of the ghost field, and reads

$$\mathcal{L}_c g_{\sigma\kappa} = 2\bar{g}_{\rho(\sigma}\bar{D}_{\kappa)}c^\rho + c^\rho \bar{D}_\rho h_{\sigma\kappa} + 2h_{\rho(\sigma}\bar{D}_{\kappa)}c^\rho \,, \tag{3.20}$$

where the round brackets indicate normalized symmetrization. Starting from the specified seed action, and using the linear parametrization of metric perturbations, we expand the scale dependent effective action Γ_k via the vertex expansion [211, 212] in powers of the fluctuation fields, i.e.,

$$\Gamma_k[\Phi, \bar{g}] = \sum_{n=0}^{\infty} \frac{1}{n!} \Gamma^{(n)}_{k\, A_1 \dots A_n}[0, \bar{g}]\, \Phi^{A_n} \dots \Phi^{A_1} \,. \tag{3.21}$$

Here, we have introduced the superfield Φ, containing all fluctuation fields in the system, which reads

$$\Phi^A = (h_{\mu\nu}(x), c^\mu(x), \bar{c}_\mu(x)) \,, \tag{3.22}$$

the summation over repeated superfield-indices entails a summation over discrete indices, and an integration over the coordinates. Starting from the seed action, in our setup the vertices $\Gamma^{(n)}_k$ are approximated as the n-th functional derivative of the seed action (3.15) with respect to the superfield Φ. They satisfy flow equations similar to (2.21), see, e.g., [216]. We introduce individual dimensionless couplings g_n and λ_n that label the vertices by a rescaling which reads

$$\Gamma^{(n)}_{k\, A_1 \dots A_n}\big[0, \bar{g}, \bar{G}, \bar{\Lambda}\big] \to \Big(k^{2-d} g_n\Big)^{n/2} \Gamma^{(n)}_{k\, A_1 \dots A_n}\Big[0, \bar{g}, k^{2-d} g_n, k^2 \lambda_n\Big] \,. \tag{3.23}$$

In the presence of a gauge fixing condition, as well as a regulator, the scale dependence of the individual couplings g_n and λ_n does not necessarily agree. Additionally, also the couplings labeling pure gravity, ghost-gravity, or gravity-matter vertices do in general not agree and should therefore be distinguished. In the present context, we will however assume that regulator and gauge fixing only mildly break diffeomorphism invariance, and therefore assume that $g_n = g_c = g_3$, and $\lambda_n = \lambda_3$ for $n \geq 3$. Accordingly, we will only distinguish the couplings labeling the two-point vertices from higher order vertices. Indications that diffeomorphism invariance is indeed only mildly broken, justifying this approximation was found in the context of *effective universality* [113, 216, 243, 266], see also Subsection 3.1.2.

Since we are interested in the momentum dependence of the propagator, we will focus on the two-point functions in the following. In the pure gravity sector, there are five independent tensor structures, three of them labeled by the gauge parameters α_h, β_h and γ_h, and two of them are unaffected by the gauge choice. Those two tensor structures are related to the transverse traceless mode $h^{\mathrm{TT}}_{\mu\nu}$ defined as

$$\bar{D}^\mu h^{\mathrm{TT}}_{\mu\nu} = 0 \,, \qquad \bar{g}^{\mu\nu} h^{\mathrm{TT}}_{\mu\nu} = 0 \,, \tag{3.24}$$

and to the physical scalar mode $h^0_{\mu\nu}$, which satisfies

$$h^0_{\mu\nu} = \Pi^0{}_{\mu\nu}{}^{\alpha\beta}\, h_{\alpha\beta} \,. \tag{3.25}$$

Here, we have used the scalar projector Π^0, which is defined by demanding orthogonality to the transverse-traceless tensor, and to the gauge-fixing action. Specifically, the scalar projector satisfies

$$\Pi^0 \cdot S^{(2)}_{\mathrm{gf}} = S^{(2)}_{\mathrm{gf}} \cdot \Pi^0 = 0 \,, \qquad \Pi^0 \cdot \Pi^{\mathrm{TT}} = \Pi^{\mathrm{TT}} \cdot \Pi^0 = 0 \,. \tag{3.26}$$

The explicit forms of the projectors Π^{TT} and Π^0 on a flat background are given in Section A.1, their generalization to general backgrounds can be found in [223].

We will now discuss the procedure to resolve the scale dependence of the different tensor structures on the level of the two-point function. We will start with the momentum independent parts of the correlators. To distinguish the different tensor structures, we introduce two graviton mass parameters, namely μ_{TL} and μ_0, which correspond to the traceless and trace sector, respectively. Explicitly, μ_{TL} and μ_0 are introduced on the level of the two-point function via [215]

$$\begin{aligned}\Gamma_h^{(2)\,\mu\nu\rho\sigma} =& S_{\text{EH}}^{(2)\,\mu\nu\rho\sigma}\big|_{\bar{\Lambda}=0} + S_{\text{gf}}^{(2)\,\mu\nu\rho\sigma} \\ &+ \frac{k^2}{32\pi}\left(\Pi^{\text{TL}\,\mu\nu\rho\sigma}\,\mu_{\text{TL}} - \frac{\Pi^{\text{Tr}\,\mu\nu\rho\sigma}}{(d-1)(d+\gamma_h)^2}\left(A^2\mu_{\text{TL}} + d(d-2)B^2\mu_0\right)\right),\end{aligned} \tag{3.27}$$

where A and B are gauge-dependent coefficients specified in (A.3) and (A.4), and where the traceless projector Π^{TL} and the trace projector Π^{Tr} are given explicitly in (A.6).

We introduce the dimensionless parameters μ_{TL} and μ_0 as in (3.27) to ensure that the two propagating modes feature standard propagators with graviton mass parameters μ_{TL} and μ_0 respectively. Equation (3.27) is only a rewriting of the two-point function to allow for the convenient introduction of the two individual mass parameters. Specifically, it holds that

$$\Gamma_h^{(2)\,\mu\nu\rho\sigma}\big|_{\mu_{\text{TL}}\to -2k^{-2}\bar{\Lambda},\,\mu_0\to -2k^{-2}\alpha\bar{\Lambda}} = S_{\text{EH}}^{(2)\,\mu\nu\rho\sigma} + S_{\text{gf}}^{(2)\,\mu\nu\rho\sigma}\,, \tag{3.28}$$

where the coefficient α depends on the dimensionality d, and on the gauge-fixing parameters α_h, β_h, and γ_h, and is given in (A.8).

To extract the full momentum dependence of the propagator, we introduce independent and momentum dependent wavefunction renormalizations for the transverse-traceless and the gauge-invariant scalar mode. These are introduced via the rescaling

$$h_{\mu\nu} \to \mathcal{Z}_{h\,\mu\nu}{}^{\rho\sigma}\, h_{\rho\sigma}\,, \tag{3.29}$$

with the wavefunction renormalization tensor $\mathcal{Z}_h$ defined as

$$\mathcal{Z}_{h\,\mu\nu}{}^{\rho\sigma} = \delta_{(\mu}{}^{\rho}\,\delta_{\nu)}{}^{\sigma} + \left(\sqrt{Z_{h^{\text{TT}}}(p^2)} - 1\right)\Pi^{\text{TT}}{}_{\mu\nu}{}^{\rho\sigma} + \left(\sqrt{Z_{h^0}(p^2)} - 1\right)\Pi^{0}{}_{\mu\nu}{}^{\rho\sigma}\,, \tag{3.30}$$

which ensures that the transverse-traceless and the gauge-invariant scalar modes are rescaled individually, while the rest remains constant. For the two-point function (3.27) the rescaling (3.30) is achieved by

$$\Gamma_h^{(2)} \to \mathcal{Z}_h \cdot \Gamma_h^{(2)} \cdot \mathcal{Z}_h\,. \tag{3.31}$$

The scale dependence of the graviton wavefunction renormalization is captured by the anomalous dimension

$$\eta_{h^{\text{x}}}(p^2) = -\partial_t \ln Z_{h^{\text{x}}}(p^2)\,, \tag{3.32}$$

where the subscript x labels the respective mode. For the regulator in the flow equation (2.21) we choose a spectrally adjusted one, i.e.

$$\mathfrak{R}_k^{h\,\mu\nu\rho\sigma} = \Gamma_h^{(2)\mu\nu\rho\sigma}\big|_{\mu_{\text{TL}}=\mu_0=0}\,\mathcal{R}_k(p^2)\,, \tag{3.33}$$

which ensures that no mass-like contributions are regularized, such that the regulator properties (2.20) are satisfied [71, 88, 270, 271]. Here, we have introduced the regulator function $\mathcal{R}_k$, which ensures the momentum-shell wise integration of quantum fluctuations.

We will employ the Landau gauge, i.e., $\alpha_h \to 0$, which is a fixed point for all gauge parameters

[102, 215]. Then, the graviton propagator reads

$$\begin{aligned} G_h =& \frac{32\pi}{Z_{h^{\mathrm{TT}}}(p^2)} \frac{1}{p^2 + \mathcal{R}_k(p^2) + \mu_{\mathrm{TL}}\, k^2} \Pi^{\mathrm{TT}} \\ & - \frac{32\pi}{Z_{h^0}(p^2)} \frac{1}{(d-2)(d-1)} \frac{C}{B^2} \frac{1}{p^2 + \mathcal{R}_k(p^2) + \mu_0\, k^2} \Pi^0 \,, \end{aligned} \tag{3.34}$$

with the coefficients C and B given in (A.4) and (A.4), respectively.

We proceed similarly in the ghost sector, where we distinguish the transverse mode and the longitudinal mode. To capture their individual momentum dependence, we rescale the modes with momentum-dependent wavefunction renormalizations $Z_{c^{\mathrm{L}}}$ and $Z_{c^{\mathrm{T}}}$, respectively. They are introduced via the rescaling

$$c_\mu \to \mathcal{Z}_{c\,\mu}{}^{\nu}\, c_\nu \,, \qquad \bar{c}_\mu \to \mathcal{Z}_{c\,\mu}{}^{\nu}\, \bar{c}_\nu \,, \tag{3.35}$$

with the wavefunction renormalization tensor

$$\mathcal{Z}_{c\,\mu}{}^{\nu} = \sqrt{Z_{c^{\mathrm{T}}}}\, \Pi^{\mathrm{T}}{}_{\mu}^{\ \nu} + \sqrt{Z_{c^{\mathrm{L}}}}\, \Pi^{\mathrm{L}}{}_{\mu}^{\ \nu} \,, \tag{3.36}$$

where the longitudinal and transverse projectors Π^{L} and Π^{T} are explicitly given in (A.9). As for the gravitons, the scale dependence of the wavefunction renormalization of the ghost modes is captured by their anomalous dimension defined as

$$\eta_{c^{\mathrm{x}}} = -\partial_t \ln Z_{c^{\mathrm{x}}} \,, \tag{3.37}$$

where the superscript x labels the two different ghost modes.

In summary, in the Landau gauge, i.e., $\alpha_h \to 0$, there are four momentum-dependent anomalous dimensions, and two graviton mass parameters. On the level of the two-point function and when distinguishing the different modes, these six scale dependences completely parametrize the scale dependence of the two-point correlation function. The Landau limit is crucial in the sense that it provides a simplified basis. Since $\alpha_h \to 0$ is a fixed point for all gauge parameters α_h, β_h and γ_h [102, 215], their scale dependence does not contribute to the flow of the above mentioned correlation functions.

3.2.2. General properties of the RG flows

In the following, we will discuss some general properties of the RG flow of the different n-point correlators that we aim to investigate. In the graviton sector, and in the Landau limit, the full gauge dependence is encoded in the projector on the scalar mode Π^0. For this projector we observe that

$$\Pi^0[\beta_h,\, \gamma_h] = \Pi^0 \left[\frac{d\beta_h - \gamma_h}{d + \gamma_h}, 0 \right] \,. \tag{3.38}$$

Additionally, in the Landau limit, the tensor-structure of the graviton propagator is parametrized solely by the projectors on the two physical modes, cf. (3.34). Therefore, when projecting the external legs of n-point functions on the two physical modes, the parameter γ_h is redundant and can be removed by a rescaling of β_h.

In the ghost sector, non-trivial cancellations between gauge dependent contributions from vertices and propagators lead to the same observation: the rescaling of β_h as in (3.38) completely removes γ_h from the scale dependence of all n-point functions we aim to investigate. Therefore, in the following we will choose $\gamma_h = 0$ for simplicity of notation. However, the re-

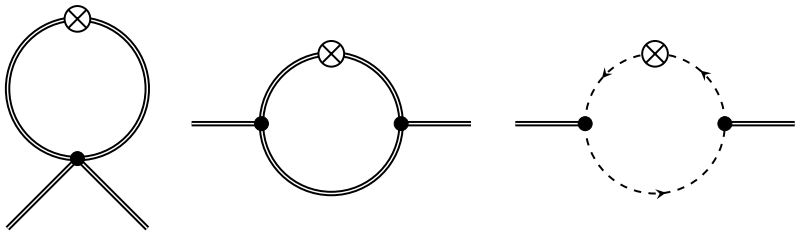

Fig. 3.1.: We show the diagrams which contribute to the scale dependence of the graviton two-point function. Double lines indicate gravitons, dashed lines stand for the Faddeev-Popov ghosts, and the circled cross denotes the regulator insertion $\partial_t \mathcal{R}_k$.

dundancy of γ_h on the level of the scale dependence of n-point functions is not equivalent with the redundancy of the tensor structure labeled by γ_h which appears in (3.17). This tensor structure is nevertheless the fifth linearly independent tensor-structure in the graviton sector on the level of the two-point function.

One crucial building block of all diagrams contributing to the scale dependence of n-point functions is the product of a regulator insertion and two propagators. With the regulator specified in (3.33), and the graviton propagator (3.34), this product reads for the graviton sector

$$\begin{aligned} G_h \cdot \left(\partial_t \mathfrak{R}_k^h\right) \cdot G_h = & \frac{32\pi}{Z_{h^{\mathrm{TT}}}(p^2)} \frac{\partial_t \mathcal{R}_k(p^2) - \eta_{h^{\mathrm{TT}}} \mathcal{R}_k(p^2)}{\left(p^2 + \mathcal{R}_k(p^2) + \mu_{\mathrm{TL}}\, k^2\right)^2} \Pi^{\mathrm{TT}} \\ & - \frac{32\pi}{Z_{h^0}(p^2)} \frac{1}{(d-2)(d-1)} \frac{C}{B^2} \frac{\partial_t \mathcal{R}_k(p^2) - \eta_{h^0} \mathcal{R}_k(p^2)}{\left(p^2 + \mathcal{R}_k(p^2) + \mu_0\, k^2\right)^2} \Pi^0 \,. \end{aligned} \tag{3.39}$$

Importantly, this product decays into the projectors on the transverse-traceless and the gauge-independent scalar mode. This feature holds in the Landau limit and is a consequence of a cancellation of contributions of gauge modes in the propagator with contributions in the regulator. These cancellations entail that the flow of n-point functions projected on the gauge-invariant modes is only driven by those gauge-invariant modes itself. Accordingly, no gauge modes drive the scale dependence of the gauge-invariant components of n-point functions. This observation significantly reduces the number of relevant tensor structures of higher-order n-point functions, since vertices with one or more gauge mode will not contribute to the scale dependence of any physical n-point correlator [53].

In the following we will discuss how to extract the scale dependence of the different couplings and wavefunction renormalizations by projection on respective modes of the diagrams contributing to the RG-flow, which are shown in Figure 3.1. The scale dependence of the graviton two-point function, when projected on the transverse-traceless part structurally reads [212, 241]

$$-(y + \mu_{\mathrm{TL}})\, \eta_{h^{\mathrm{TT}}}(y) + \partial_t \mu_{\mathrm{TL}} + 2\mu_{\mathrm{TL}} = \frac{1}{k^2\, Z_{h^{\mathrm{TT}}}(p^2)} \Pi^{\mathrm{TT}}{}_{\mu\nu}{}^{\rho\sigma}\, \dot{\Gamma}^{(2)}_{h\ \rho\sigma}{}^{\mu\nu} \equiv \mathrm{flow}_{\mathrm{TT}}(y)\,, \tag{3.40}$$

where we have introduced the shorthand $y = \frac{p^2}{k^2}$. Here, the last term on the left-hand sides comes from the scale derivative acting on the explicit factor k^2 appearing in (3.27). In complete analogy, the flow of the scalar part of the graviton two point function reads

$$-(y + \mu_0)\, \eta_{h^0}(y) + \partial_t \mu_0 + 2\mu_0 = \frac{1}{k^2\, Z_{h^0}(p^2)} \Pi^0{}_{\mu\nu}{}^{\rho\sigma}\, \dot{\Gamma}^{(2)}_{h\ \rho\sigma}{}^{\mu\nu} \equiv \mathrm{flow}_0(y)\,. \tag{3.41}$$

We disentangle the momentum dependent and momentum independent parts of (3.40) and

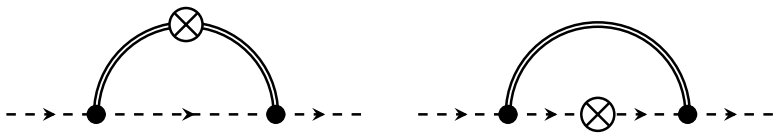

Fig. 3.2.: We show the diagrams which contribute to the scale dependence of the ghost two-point function. Double lines indicate gravitons, dashed lines stand for the Faddeev-Popov ghosts, and the circled cross denotes the regulator insertion $\partial_t \mathcal{R}_k$.

(3.41) by evaluating both equations at $y = -\mu_{\text{TL}}$, and $y = -\mu_0$, respectively [212], which results in

$$\partial_t \mu_{\text{TL}} = -2\mu_{\text{TL}} + \text{flow}_{\text{TT}}(-\mu_{\text{TL}})\,, \qquad \partial_t \mu_0 = -2\mu_0 + \text{flow}_0(-\mu_0)\,, \tag{3.42}$$

and

$$\eta_{h^{\text{TT}}}(y) = -\frac{\text{flow}_{\text{TT}}(y) - \text{flow}_{\text{TT}}(-\mu_{\text{TL}})}{y + \mu_{\text{TL}}}\,, \qquad \eta_{h^0}(y) = -\frac{\text{flow}_0(y) - \text{flow}_0(-\mu_0)}{y + \mu_0}\,. \tag{3.43}$$

Analogously, the equations for the anomalous dimensions in the ghost sector read

$$y\,\eta_{c^{\text{T}}}(y) = \frac{1}{k^2\, Z_{c^{\text{T}}}(p^2)} \Pi^{\text{T}}{}_{\mu}{}^{\nu}\, \dot{\Gamma}^{(2)}_{c\ \nu}{}^{\mu} \equiv \text{flow}_{c^{\text{T}}}(y)\,, \quad y\,\eta_{c^{\text{L}}}(y) = \frac{1}{k^2\, Z_{c^{\text{L}}}(p^2)} \Pi^{\text{L}}{}_{\mu}{}^{\nu}\, \dot{\Gamma}^{(2)}_{c\ \nu}{}^{\mu} \equiv \text{flow}_{c^{\text{L}}}(y)\,, \tag{3.44}$$

where the diagrammatic representation of $\text{flow}_c(y)$ is shown in Figure 3.2.

3.2.3. Form factors and wavefunction renormalizations

To make a connection with the question of unitarity, we will now briefly discuss the relation of the momentum-dependent wavefunction renormalization and the form factors that enter the propagators of the theory, cf. [235, 236]. On a flat background, the full information on the graviton propagator is captured by the action

$$\Gamma \simeq \frac{1}{16\pi \bar{G}} \int \mathrm{d}^d x \sqrt{g} \left(2\bar{\Lambda} - R - \frac{1}{4}\frac{d-2}{d-1} R\, f_R(\Delta)\, R + \frac{1}{4}\frac{d-2}{d-3} C^{\mu\nu\rho\sigma} f_C\,(\Delta)\, C_{\mu\nu\rho\sigma} \right)\,, \tag{3.45}$$

where $C^{\mu\nu\rho\sigma}$ is the Weyl tensor, and where f_R and f_C are form factors. The normalization of the form factors in (3.45) is chosen such that they enter the propagators of the theory in the form of (3.8). The action (3.45) is based on a curvature expansion of the full effective action, such that f_R and f_C capture the full momentum dependence of the graviton propagator, assuming a diffeomorphism invariant theory. As we have discussed in Subsection 3.1.1, the presence of non-trivial form factors does not necessarily introduce new poles into the propagator, cf. (3.8). However, to extract the scale dependence of operators starting from a curvature expansion, one usually has to employ the background field approximation. This approximation neglects the difference between background and fluctuation propagator. Due to the breaking of diffeomorphism invariance by the gauge condition and the regulator, this approximation potentially suffers from background dependence. Additionally, since diffeomorphism invariance is only restored in the $k \to 0$ limit, the expansion in terms of curvature operators (3.45) does in general not agree with the expansion in terms of vertex correlators.

In the following, we will investigate, whether it is possible to extract the diffeomorphism invariant part of the propagator, the form factors, from the vertex correlation functions, without explicitly computing Ward identities. To this end, we will compare the propagators neglecting

their difference due to the breaking of diffeomorphism invariance. This is motivated by the feature of effective universality [113, 216, 243, 266] discovered at the UV-fixed point, which indicates that diffeomorphism invariance might only be mildly broken. To establish a mapping between the background form factors and the vertex correlation functions, let us briefly indicate the schematic form of the unregularized propagator on a flat background arising from (3.45), where we additionally set the cosmological constant to zero:

$$\bar{G}_h^{\mathrm{TT}}(p^2) \sim \frac{1}{p^2\,(1+p^2\,f_C(p^2))}\,, \qquad \bar{G}_h^{0}(p^2) \sim \frac{1}{p^2\,(1+p^2\,f_R(p^2))}\,. \tag{3.46}$$

Comparing this with the unregularized fluctuation propagator (3.34) at $\mu_{\mathrm{TL}} = \mu_0 = 0$, suggests that

$$\frac{Z_{h^{\mathrm{TT}}}(p^2)}{Z_{h^{\mathrm{TT}}}(0)} = 1 + p^2 f_C(p^2)\,, \qquad \frac{Z_{h^{0}}(p^2)}{Z_{h^{0}}(0)} = 1 + p^2 f_R(p^2)\,, \tag{3.47}$$

allows to map the momentum dependent wavefunction renormalizations to the form factors. Generalizing this to non-vanishing values of $\bar{\Lambda}$, and accordingly μ_{TL} and μ_0 is not straightforward, since $\bar{\Lambda}$ enters $\bar{G}_h^{\mathrm{TT}}$ and $\bar{G}_h^{0}$ in a gauge-dependent ratio. Since this is in general not required for the fluctuation propagators, it is in general not possible to map the background propagators in a one-to-one way to the fluctuation propagators. We will not discuss this issue in more detail here, since a general mapping between background and fluctuation quantities involves the solution of the modified Ward identities.

Usually, in the context of asymptotically safe quantum gravity, the wavefunction renormalizations Z_Φ are not discussed in detail, since they cancel by construction. Hence, one uses momentum-dependent anomalous dimensions to characterize the momentum dependence of the two-point function. Those are obtained by the logarithmic scale derivative of the wavefunction renormalization, cf. (3.32) and (3.37). For the anomalous dimension, no fixed point condition is imposed.

Here, we will translate to a formulation in terms of a dimensionless, momentum dependent wavefunction renormalization $z(y)$, which is constant with respect to the RG-scale at a fixed point of the system, cf. [243]. It is related to the wavefunction renormalization introduced in (3.30) and (3.36) by

$$z_x(y) = k^{\eta_x(0)} Z_x(y)\,, \tag{3.48}$$

where the subscript refers to the different wavefunction renormalizations, which we will drop in the following. We refer to $z(y)$ as dimensionless, since at a fixed point of the system, the anomalous scaling dimension cancels with the canonical scaling dimension. With this definition, we find the relation between anomalous dimension and dimensionless wavefunction renormalization as

$$\eta(y) = \eta(0) - \frac{\dot{z}(y)}{z(y)} + 2y\frac{z'(y)}{z(y)}\,, \tag{3.49}$$

where the overdot indicates the logarithmic scale derivative with respect to the intrinsic k-dependence, excluding the scaling of the argument. The last term takes this scaling of y into account. At a fixed point, by construction $\dot{z}_* = 0$, such that

$$\eta_*(y) = \eta_*(0) + 2y\frac{z_*'(y)}{z_*(y)}\,. \tag{3.50}$$

This differential equation for the wavefunction renormalization can be solved to

$$z_*(y) = z_*(0)\,\mathrm{e}^{\int_0^y \mathrm{d}s\,\frac{\eta_*(s)-\eta_*(0)}{2s}}\,. \tag{3.51}$$

With this direct access to the wavefunction renormalization at the fixed point, we can calculate the fixed-point form factor from the corresponding momentum dependent anomalous dimension by inverting (3.47), leading to

$$f_*(y) = \frac{\mathrm{e}^{\int_0^y \mathrm{d}s\, \frac{\eta_*(s)-\eta_*(0)}{2s}} - 1}{y}\,, \tag{3.52}$$

see Section A.2 for details on the derivation. In this way, we can extract the full momentum dependence of the propagator from the anomalous dimension of the fluctuation field, and investigate the presence of instabilities or ghosts in the system.

3.2.4. Numerical strategy and results

Before presenting and discussing the results for the form factors f_C and f_R constructed via (3.52), we will now briefly discuss the numerical strategy to compute the momentum dependent RG-flows. First, the projection procedure for the anomalous dimensions, cf. (3.43), requires the evaluation of the flow at $p^2 = -\mu_{\mathrm{x}}$. Allowing for positive values of the two graviton mass parameters μ_{x} gives rise to additional challenges in performing the loop integration.

A first challenge is related to the presence of terms of the form

$$\frac{1}{(p^2 + 2pqx + q^2)}\,, \qquad \frac{1}{(p^2 + 2pqx + q^2)^2}\,, \tag{3.53}$$

where x is the cosine of the angle between the external momentum p and the loop momentum q. These terms have the form of unregularized, massless propagators, and arise due to the projectors appearing in the propagators, see (3.34). Therefore, they are a feature of gravity, and occur in a similar fashion in the spin-one sector of the theory. Allowing for values $p^2 < 0$, those terms feature a pole at $x = 0$ and $q^2 = -p^2 = \mu_{\mathrm{x}}$. To perform the integrals over these poles, we split the integration into a disk centered around the poles, and the rest. Inside the disk, we choose radial coordinates. One can show that the Jacobian of the coordinate transform and the angular integration remove all poles. The resulting integrals are then finite and well defined.

A second challenge is related to the definition of the regulator for, in general complex, momenta. To avoid this, we choose the regulator as a function of the real part of the argument. Additionally, we have to choose a regulator that reproduces the desired behavior of the regularized propagator at $p^2 = -\mu_{\mathrm{x}}$, such that

$$\left.\frac{1}{p^2 + \mathcal{R}_k(p^2) + \mu_{\mathrm{x}}}\right|_{p^2=-\mu_{\mathrm{x}}} = \frac{1}{\mathcal{R}_k(-\mu_{\mathrm{x}})}\,. \tag{3.54}$$

Additionally, the regularized propagator for large masses should behave like a standard regularized propagator, implying that

$$\mathcal{R}_k(-\mu_{\mathrm{x}}) \sim 1 + \mu_{\mathrm{x}}, \qquad \text{as } \mu_{\mathrm{x}} \to -\infty\,. \tag{3.55}$$

Furthermore, the regulator should not introduce any additional poles into the integration region. One choice that satisfies all these criteria is

$$\mathcal{R}_k(y) = \frac{\mathrm{e}^{-\tilde{y}}}{1 + \mathrm{e}^{-2\tilde{y}}} + \frac{1 - \tilde{y}}{1 + \mathrm{e}^{2\tilde{y}}}\,, \qquad \tilde{y} = \mathrm{Re}\, y\,, \tag{3.56}$$

which for large positive arguments approaches the exponential regulator.

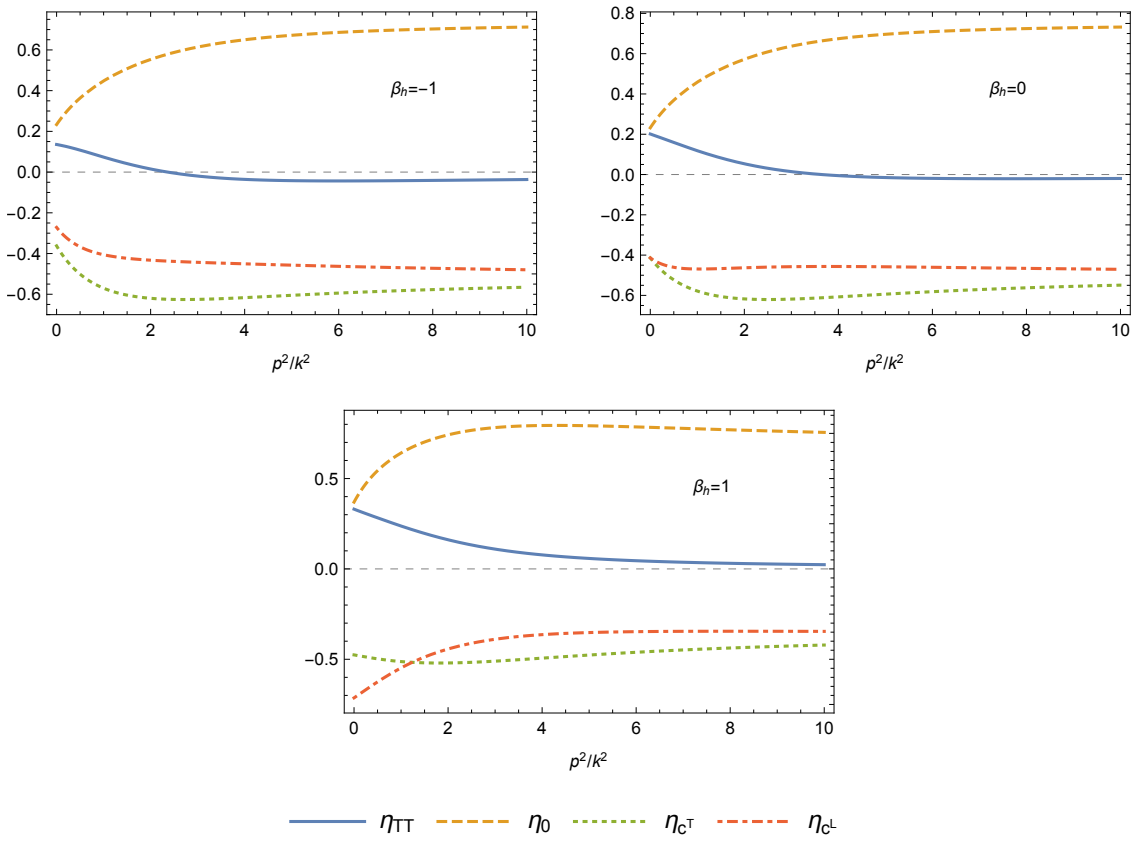

Fig. 3.3.: We show the gauge dependence of the momentum-dependent anomalous dimensions for $d = 4$, $g = 1$, $\mu_{\mathrm{TL}} = \mu_0 = 0$, and the regulator (3.56).

Let us now briefly discuss the numerical strategy to evaluate the integration over loop momenta. For this, we observe that the anomalous dimensions are bounded at $p^2 = 0$, and $p^2 = \infty$, which we can show analytically, see Section A.3. Additionally, we assume that the anomalous dimensions are bounded on the entire real line. Under these conditions, we can expand the anomalous dimension in terms of rational Chebyshev functions [272]

$$\eta(y) = \sum_{n \geq 0} \eta_n \, T_n \left(\frac{y-1}{y+1} \right) , \tag{3.57}$$

which is equivalent to compactifying the integration region, and using a standard expansion of η in terms of Chebyshev functions. This expansion shows desirable convergence properties, if the represented function is smooth, cf. [273]. In the context of functional RG flows, they have been discussed in [274–276], and specifically for the case of gravity in [98, 235, 236].

In practice, we truncate the expansion (3.57) at some finite order n, and evaluate the equations at a finite set of collocation points. Then, the set of integral equations for the anomalous dimensions reduces to a set of algebraic equations for the expansion coefficients η_n. This can be solved using standard linear algebra. We test the accuracy of the truncation of (3.57) by verifying, whether the numerical results satisfy the analytical properties of the anomalous dimensions that we derive in Section A.3.

Gauge dependence

We will now discuss the gauge dependence of the momentum-dependent anomalous dimensions. For simplicity, we will choose vanishing mass parameters, i.e., $\mu_{\text{x}} = 0$, and $d = 4$. The anomalous dimension for choices of the gauge-fixing parameter $\beta_h \in \{-1, 0, 1\}$ are shown in Figure 3.3. The dependence on β_h is mild, and only on the qualitative level. The mild gauge dependence of all four anomalous dimensions is a promising indication that, even though beta functions are inherently gauge-dependent, this dependence is small and controlled. We see that for all choices of β_h, only the spin-two mode of the graviton $\eta_{h^{\text{TT}}}(p^2)$ approaches zero at large momenta, indicating the feature of momentum locality [212, 213, 216], see also Section A.3. The two graviton anomalous dimensions feature qualitative and quantitative differences in their momentum dependence. This highlights the importance of disentangling these tensor structures, at least on the level of the two-point functions.

Conversely, the two anomalous dimensions of the ghost agree at $p = 0$, which is expected from the analytical analysis, see (A.19). This provides a cross check for the numerical setup. Furthermore, the value of each ghost anomalous dimension at large p is close to their value at $p = 0$. As a consequence, $\eta_{c^{\text{L}}}$ and $\eta_{c^{\text{T}}}$ are in qualitative agreement across all the displayed choices of the gauge-parameter β_h. Therefore, in the shown gauge-choices, one single, constant ghost anomalous dimension is an accurate approximation.

Form factors and the derivative expansion

Let us finally discuss the structure of the form factors reconstructed via (3.52). As a specific point in the gravitational parameter space, we choose $d = 4$, $g = 1$, $\beta_h = 1$, as well as $\mu_{\text{TL}} = \mu_0 = 0$. This point is in general no fixed point of the theory, but serves as an example to illustrate the general features of the reconstructed form factors. Furthermore, the investigation of the changes of the anomalous dimensions as functions of β_h, μ_{TL} and μ_0, indicates, that the main qualitative features generalize to a larger region of the gravitational parameter space, see [1] for the dependence on the mass parameters.

The reconstructed form factors at the specified point are shown in Figure 3.4. At this point, f_R^{fluc} is positive for all momenta, while f_C^{fluc} is negative. Since the R^2 form factor is positive, there is no additional pole in the propagator for the gauge-invariant scalar mode. Similarly, since the absolute value of the C^2 form factor is small enough, there is no additional pole for the transverse-traceless propagator. The absence of new poles in the fluctuation propagator indicates that asymptotically safe quantum gravity might be unitary [239, 240, 251, 277].

Both form factors go to constant values for vanishing momenta, and show a power-law fall-off towards large momenta. The typical logarithmic behavior of f_R and f_C, which can be obtained perturbatively, is expected to come out correctly, once the flow equation is integrated to $k \to 0$, at least in a parameter-region where the effective-field-theoretic setup around a flat background is valid, cf. [244]. Notably, f_C^{fluc} qualitatively agrees with that obtained in a background approximation of conformally reduced gravity [235].

Let us close this discussion by re-connecting the reconstructed form factors with the derivative expansion discussed in Subsection 3.1.1. For this, we perform a derivative expansion of the reconstructed form factors, which reads

$$\begin{aligned} f_R^{\text{fluc}}(y) &\approx -0.46 + 0.43y - 6.49y^2 + \mathcal{O}(y^3)\,, \\ f_C^{\text{fluc}}(y) &\approx -0.094 - 0.21y + 3.2y^2 + \mathcal{O}(y^3)\,. \end{aligned} \tag{3.58}$$

We see that, at the investigated point, the derivative expansion of both form factors features

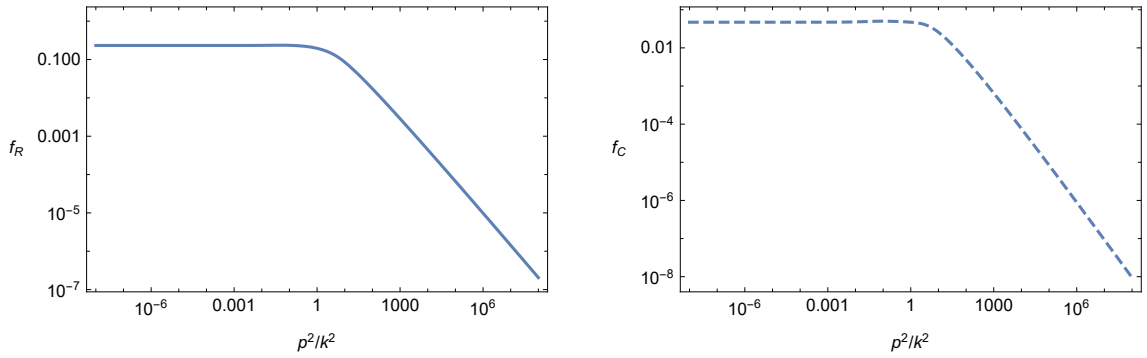

Fig. 3.4.: We show the fluctuation form factors reconstructed via (3.52) using the momentum-dependent anomalous dimensions. We show the form factors at the point $d = 4$, $g = 1$, $\beta_h = 1$, as well as $\mu_{\text{TL}} = \mu_0 = 0$, and the regulator (3.56). Solid lines indicate positive values of the form factors, while dashed lines indicate negative values.

iterating signs. This means that, depending on which order the derivative expansion is stopped at, the propagators of the theory might feature fake-ghosts [251]. This highlights the importance of extracting the full momentum dependence of the propagators, in order to investigate the unitarity of a given theory.

3.2.5. Summary and conclusion

We have investigated the full non-perturbative momentum dependence of the graviton and ghost propagator in quantum gravity. This includes the spin two and spin zero modes of the graviton, and the spin one and spin zero mode of the ghost. We employed the FRG to extract the scale dependence of the propagators in a momentum-dependent fashion, and resolved the gauge-dependence of the results.

A key result is that the propagators of the two graviton modes behave qualitatively different. While the anomalous dimension of the spin two mode vanishes at large momenta, the anomalous dimension of the spin zero mode approaches a non-vanishing value. This qualitative feature is independent of the gauge choice. It might therefore have physical significance in the context of *momentum locality*, which is discussed in [212, 213, 216]. The two ghost modes agree qualitatively, and their anomalous dimensions are approximately momentum independent.

The weak dependence of the anomalous dimensions of the gauge choice, cf. Figure 3.3 is a promising hint that the FRG might give rise to stable and reliable results, even in small truncations.

In this section, we have discussed a major step towards the complete and systematic computation of correlation functions in quantum gravity. Based on the presented results, we expect that disentangling the different modes plays a crucial role in the discussion of spectral functions [244], since both modes will feature individual spectral functions. In this context, the presented work provides a step towards investigating the fate of unitarity in asymptotically safe quantum gravity, and therefore lays a basis for future tests of internal consistency.

3.3. Evidence for asymptotic safety from the lattice

In a lattice approach to asymptotic safety the UV fixed point would appear as continuous phase transition with finite values for the renormalized Newton coupling and cosmological constant.

This is one of the most important tests that EDT must pass. As a second test, the theory must reproduce GR in the appropriate limit, and reproduce low-energy observations.

Together with indications for a fixed point from functional methods, EDT could then establish the scenario of asymptotic safety as a viable candidate for an UV-complete description of four-dimensional gravity.

In the following, we will confront EDT with two distinct consistency tests: First, we will investigate, if EDT admits a semi-classical and non-relativistic limit, which is consistent with Newtonian binding in $d = 4$ dimensions. Second, we will investigate, if EDT geometries admit a semi-classical regime, by making contact with the Hawking-Moss instanton. We will find that EDT passes both of these consistency tests. Further, in both studies we will extract a value of the renormalized Newton coupling $G_{\rm N}$ in units of the lattice spacing. Intriguingly, the values for $G_{\rm N}$ from both studies are in agreement with each other within 1σ.

3.3.1. Newtonian binding from Euclidean dynamical triangulations

In this work we will use matter as a probe to test the fundamental properties of EDT. Specifically, we will investigate scalar fields propagating on EDT geometries, and extract the binding energy of two-particle bound states.

Previous studies of scalar bound states in EDT [278] did not include the local measure term, see Section 2.3. In this case, the Newton coupling is positive such that gravitational binding is possible. However, it is not possible to recover a Newtonian limit, where the relation between the binding energy and the renormalized mass agrees with the ground state of a two-particle bound state in four dimensions.

In the following, we will follow the steps outlined in [278], and complement them with the strategy of taking the continuum limit with the use of the non-trivial measure term and the associated parameter β. We confirm that there is an attractive force between scalar particles. Furthermore, after taking the infinite volume, continuum limit, we find a dependence of the binding energy on the renormalized mass, which is in agreement with Newtonian binding in the non-relativistic limit and in $d = 4$.

We can then use the Newton law to extract the value of the Newton coupling $G_{\rm N}$ in units of the lattice spacing. This is not known a-priori on the lattice and translates the lattice units into physical units. We find that the lattice spacing of our finest lattices are smaller than the Planck scale. This provides evidence that EDT can reproduce the correct long-distance physics, and that EDT lattices can probe length scales below the Planck scale, such that the continuum limit might be taken.

Scalar fields and dynamical triangulations

To test the low-energy theory that emerges from EDT, we will use scalar fields as a probe for spacetime. For the gravitational part of the action, we choose the Einstein-Hilbert action $S_{\rm EH}$ (3.16) as the starting point. For the matter sector, we consider real, non-interacting massive scalar fields that are minimally coupled to gravity. Their dynamics is described by

$$S_{\rm M} = \int \mathrm{d}^4x\sqrt{g}\left(\frac{1}{2}g^{\mu\nu}\partial_\mu\phi\partial_\nu\phi + \frac{1}{2}m_0^2\phi^2\right) , \tag{3.59}$$

where m_0 is the bare mass.

To simulate the gravity-matter system on the lattice, we discretize both actions. For the

Einstein-Hilbert action, the discretization is given in terms of the Regge action [128] S_{ER}, cf. (2.32). For the scalar action, we choose the most simple discretization, where each scalar field $\phi(x)$ at spacetime coordinate x is associated with a four-simplex. Therefore, in the employed triangulation, each scalar field will always have five neighbors through the five surrounding tetrahedra. In this simple discretization, the lattice action for a scalar field reads

$$S_{\mathrm{M}}^{\mathrm{lattice}} = \frac{1}{2}\sum_{\langle xy\rangle}(\phi_x - \phi_y)^2 + \frac{m_0^2}{2}\sum_x \phi_x^2\,, \tag{3.60}$$

where the summation over $\langle xy\rangle$ refers to the summation over a nearest-neighbor pairs of two four simplices.

We do not include the matter interaction into the Boltzmann weight when generating the ensembles. This is the so-called quenched approximation. In this approximation, we neglect the back-reaction of the scalar fields onto the geometry. We only consider the effect of the geometry on the propagation of scalar particles.

Although the quenched approximation is an uncontrolled approximation, we expect the qualitative features of the full theory to be present in this approximation. The main advantage of this approximation is that we can reuse the ensembles generated and analyzed in previous works [172]. The ensembles that we will use for the investigation of scalar fields on a fluctuating geometry are summarized in Table B.1.

In the absence of a mass term, the lattice action for the scalar field (3.60) preserves the shift symmetry of the continuum action of a free, massless scalar field (3.59), see [194, 279, 280]. The shift symmetry ensures that the renormalized mass goes to zero when the bare mass vanishes, without fine-tuning. This property serves as a non-trivial test of the lattice simulations.

To bring the lattice action for the scalar field into a more convenient form, we expand the terms in the action (3.60). Since we are working on a compact topology, parts of the sum can be performed explicitly. After normalizing the coefficient of the kinetic term to one, we can write

$$S_{\mathrm{M}}^{\mathrm{lattice}} = \sum_{x,y}\phi_x\, L_{xy}\,\phi_y\,, \tag{3.61}$$

where the summation over lattice sites x and y is unrestricted, and where the matrix L_{xy} reads

$$L_{xy} = (D_x + m_0^2)\delta_{xy} - A_{xy}\,. \tag{3.62}$$

Here, D_x is the number of neighboring four-simplices of a given four-simplex at position x, and where δ_{xy} is the Kronecker delta. With our choice for the discretization of the Euclidean four-space, $D_x = 5$ holds, and A_{xy} is the adjacency matrix, which encodes whether the lattice sites x and y share a tetrahedra:

$$A_{xy} = \begin{cases} 1, & \text{if } x \text{ and } y \text{ share a tetrahedra,} \\ 0, & \text{else}\,. \end{cases} \tag{3.63}$$

The continuum limit of the matrix L_{xy} is the Klein-Gordon operator, and the inverse is the scalar propagator. Therefore, the matrix elements of L_{xy}^{-1} contain the propagators between two four-simplices. We will use the propagator of scalar fields in the following to extract the gravitational binding energy between two scalar particles.

Gravitational binding energy: Lattice formulation

We will now review the form of the binding energy between scalar particles in the presence of gravity, both on the lattice, and in the continuum.

The binding energy between two particles is defined as the mass difference between two individual particles, and the two-particle bound state, i.e.,

$$E_b = 2m - M\,, \tag{3.64}$$

where m is the mass of a single particle, and M the mass of the two-particle bound state. If $E_b > 0$, the two-body bound state has a lower energy than the two unbounded particles. Therefore, it is energetically favorable to form a bound state, indicating the attractive nature of gravity. If $E_b < 0$, it is energetically favorable to remain unbounded, indicating a repulsive nature of gravity.

Since the mass of a particle or bound state is encoded in the propagator, we need the one- and -two particle propagators, (L_{xy}^{-1}) and $(L_{xy}^{-1})^2$, respectively, to extract the binding energy on the lattice. Here $(L_{xy}^{-1})^2$ is the two-particle propagator between x and y.

With the one- and two-particle propagators, we can compute the average two-point correlation functions of one particle and two particles, as a function of geodesic distance on the lattice. As a function of the geodesic distance r between two four-simplices, they read [278]

$$G_s(r) = \left\langle \frac{\sum_{x,y} L_{xy}^{-1}\delta_{|x-y|,r}}{\sum_{x,y}\delta_{|x-y|,r}} \right\rangle\,, \quad \text{and} \quad G_s^{(2)}(r) = \left\langle \frac{\sum_{x,y} (L_{xy}^{-1})^2\delta_{|x-y|,r}}{\sum_{x,y}\delta_{|x-y|,r}} \right\rangle\,. \tag{3.65}$$

The definition of the one-particle two-point correlator $G_s(r)$, and the two-particle two-point correlator $G_s^{(2)}(r)$ involve two different averages. The first average is indicated by the explicit sums, and averages over all possible distances with a separation of $|x-y| = r$. In practice this average is not performed to full extent. Instead, a fixed number of source points x are chosen, from which the propagator and distances to all other points are computed. The second average is the ensemble average, indicated by the angled brackets. In practice this is implemented via an average over configurations.

From the two-point correlators G_s and $G_s^{(2)}$, we can compute the binding energy between two scalar particles. For this, we use the asymptotic forms of G_s and $G_s^{(2)}$ for large distances r, which are expected to fall off exponentially,

$$G_s(r) \sim \frac{e^{-mr}}{r^p}\,, \qquad \text{and} \qquad G_s^{(2)} \sim \frac{e^{-Mr}}{r^q}\,, \tag{3.66}$$

where m and M are the renormalized one- and two-particle masses. With this asymptotic behavior, the ratio of both correlators for large distances r reads

$$F(r) = \frac{G_s^{(2)}(r)}{G_s^2(r)} \sim \frac{e^{-(M-2m)r}}{r^{q-2p}}\,. \tag{3.67}$$

In this ratio, we can identify the binding energy E_b with the exponent, and the power-law exponent γ as

$$E_b \equiv 2m - M\,, \qquad \text{and} \qquad \gamma \equiv q - 2p\,. \tag{3.68}$$

The binding energy E_b and the renormalized mass are related to the logarithm of the ratio of F

and the two-point correlator G, respectively:

$$\log F(r) \simeq E_b\, r + Z_E - \gamma \log r\,, \qquad \text{and} \qquad \log G_s(r) \simeq -m\, r + Z_G - p \log r\,, \tag{3.69}$$

where Z_E and Z_G are constants. The binding energy and the renormalized mass appear as linear contributions to $\log F(r)$ and $\log G_s(r)$, respectively. They can therefore be extracted from the lattice by measuring the two-point correlators $G_s(r)$ and $G_s^{(2)}(r)$ for a range of distances r.

Gravitational binding energy: Non-relativistic limit

We have seen how to extract the binding energy from the scalar field propagating on the four-dimensional lattice. We will now consider the energy levels associated with gravitational bound states.

We follow [278] and work under the assumption that the mass of a single scalar field is much lighter than the Planck mass. The particles are therefore gravitationally weakly coupled, and the binding energy is well below the mass scale of the single scalar particle.

Under these assumptions, we can work in the non-relativistic limit, where the Schrödinger equation with a gravitational potential effectively describes two-particle bound states. The bound-state solution is then analogous to the solution for positronium. The only difference is that the Coulomb potential is replaced by the gravitational potential.

We can therefore consider the Schrödinger equation

$$\left(-\nabla^2 + 2\mu\, U(r)\right)\, \psi(r,\theta,\varphi) = E\, \psi(r,\theta,\varphi)\,, \tag{3.70}$$

with gravitational potential

$$U(r) = -\frac{G_{\mathrm{N}}\, m^2}{r}\,, \tag{3.71}$$

with the particle mass m, the reduced mass μ of the two-particle system, and the dimensionfull Newton coupling G_{N}. The solution to the Schrödinger equation with general $1/r$ potentials is well known, which leads to energy eigenvalues

$$E_n = \frac{G_{\mathrm{N}}^2 m^5}{4\, n^2}\,, \qquad \text{with} \qquad E_1 = \frac{G_{\mathrm{N}}^2 m^5}{4}\,, \tag{3.72}$$

where n is the principal quantum number labeling the energy levels, E_1 is the ground state, and where we have chosen natural units, i.e. $\hbar = c = 1$. The energy eigenvalues give a prediction for the dependence of the binding energy of the mass of the scalar field in the non-relativistic limit.

To make contact between the binding energy obtained using lattice methods and the ground-state energy of the bound state, we first have to take the continuum, infinite volume limit in the lattice results.

On the lattice, at finite lattice spacing and volume, the fractal dimension of the geometry varies as a function of distance scales, see Section 2.3. Even at the largest scales that we can probe on the lattice, the measured spectral dimension is approximately three. Only in the continuum, infinite volume limit, the spectral dimension is extrapolated to four, which is consistent with experimental observations in our universe. Therefore, at finite lattice spacing and volume, we might not be able to observe the appropriate dependence of the binding energy on the mass of the scalar particle.

To get a better intuition on the differences we might expect from our lattices that feature a

spectral dimension below four, consider that in a $d = 2+1$ dimensional world, the same derivation as above would lead to $E_1 \sim m^2$. Therefore, if the scalar fields on our small and coarse lattices see a long distance effective dimension of around three, we might expect an exponent in the power law below 5. Further, we might expect a large extrapolation of that exponent from ~ 2 on our lattices to ~ 5 in the continuum, infinite volume limit.

For a more suitable interpretation of the scaling of the binding energy as a function of the mass, let us model the power-law as a function of the dimension d. In $d = 1 + 1$ dimension, $E_1 \sim m$. Together with the scaling in $d = 2+1$ and $d = 3+1$, we can perform a simple quadratic fit to

$$E_1 \sim m^{\epsilon}\,, \qquad \text{with} \qquad \epsilon = d^2 - 4d + 5\,. \tag{3.73}$$

This interpolation is valid for the effective long distance dimensions that were found on the EDT lattices [172] previously. Therefore, this simple relation between the scaling exponent α and the dimension d should be reliable to determine which value of the dimension d corresponds to the scaling α that we find on the lattice [172].

To compare the lattice results with the ground-state energy of the bound state E_1, we have to take the non-relativistic limit as well [278]. For a first estimate on the relativistic corrections to the ground-state energy E_1, consider an effective Hamiltonian including relativistic corrections, with

$$H = 2\sqrt{m^2 + p^2} - \frac{G_{\mathrm{N}}\, m^2}{r}\,. \tag{3.74}$$

By replacing $p \to 1/r$, and minimizing the energy, we obtain [278]

$$E_b = 2m - 2m\sqrt{1 - \frac{G_{\mathrm{N}}^2\, m^4}{4}}\,. \tag{3.75}$$

Therefore, relativistic corrections are negligible if $G_{\mathrm{N}}\, m^2/2 \ll 1$. Under this condition, we can compare our lattice results with the ground state energy E_1. We will later see that the region which is suitable to extract the binding energy satisfies this condition.

Numerical results: Lattice correlation functions and mass dependence

To extract the two-point correlators $G_s(r)$ and $G_s^{(2)}(r)$ (3.65), we use exact inversion of the matrix L_{xy} on a given lattice for various values of the bare mass m_0. As an approximation, we do not use every simplex as a possible source for the average over simplices with distance r. Instead, we vary the number of sources on each configuration, and assess the effect of the number of sources on the statistical error for the correlators. We give more detail on the exact construction and on the error estimate for the correlators in Subsection B.1.1.

We compute $G_s(r)$ and $G_s^{(2)}(r)$ for all ensembles in Table B.1, and for different values of the bare mass m_0. On each of these ensembles, and for each value of m_0, we use a fit function

$$f(r) = X\, r + Y + Z \log[r]\,, \tag{3.76}$$

for both $\log[F]$ and $\log[G_s]$, where X, Y and Z are fit parameters. By fitting the data for $\log[F]$ and $\log[G_s]$ with an ansatz $f(r)$, we extract the binding energy E_b, the renormalized mass m and the scaling exponents β and γ, as a function of m_0, see (3.69). We give details on the fitting procedure and on how to choose a suitable fit-range for the fit of the form $f(r)$ (3.76) on the data for $\log[F]$ and $\log[G_s]$ in Subsection B.1.1.

As an example, we show the data and fit for $\log[F]$ and $\log[G_s]$ for the $N_4 = 16000$ simplex

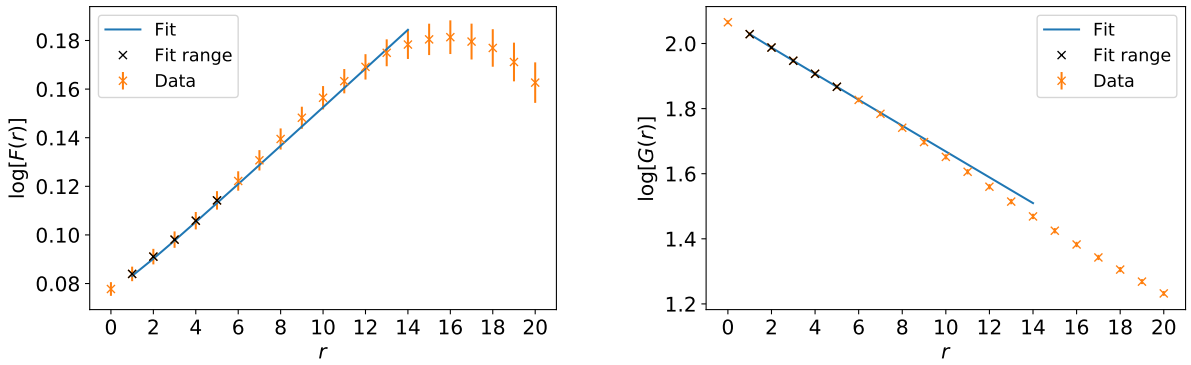

Fig. 3.5.: We show the data for $\log[F(r)]$ (left panel) and for $\log[G_s(r)]$ (right panel), see (3.65) and (3.69), for the $N_4 = 16000$ simplex ensemble at $\beta = -0.776$, and for $m_0 = 0.004$. The chosen fit range is shown in black, and the fit with an ansatz $f(r)$ (3.76) is shown as blue solid line. For the fit of $\log[F(r)]$, we obtain $\chi^2/\text{d.o.f.} \approx 0.77$ and a p-value of 0.46. For the fit of $\log[G_s(r)]$, we obtain $\chi^2/\text{d.o.f.} \approx 0.19$ and a p-value of 0.83. We refer to Subsection B.1.1 for details on how the fit range is determined.

ensemble at $\beta = -0.776$ in Figure 3.5. In a similar way, we obtain the values of the binding energy E_b and the renormalized mass from the respective fit functions $f(r)$, for a wide range of bare masses m_0 on each of the ensembles in Table B.1.

We show the dependence of the renormalized mass m on the bare mass m_0 in the left panel of Figure 3.6 for different volumes of the $\beta = 0$ ensembles. The renormalized mass approaches zero, as the bare mass decreases. This is a consequence of the shift-symmetry of the lattice action. This behavior provides a check of the computation, and of the fitting procedure that was used to extract the renormalized mass m.

In the right panel of Figure 3.6, we show one example for the dependence of the binding energy E_b on the renormalized mass. To make contact with a Newtonian limit of gravity, there must be a power-law dependence of E_b on m, see (3.73).

Further, to compare the results between different lattice spacings, we put the values for the binding energy and the renormalized mass in the same units. This is necessary, since the masses and binding energies are dimensionfull quantities. Therefore, before performing any fit, we re-express all values for E_b and m in units of the lattice spacing of the fiducial lattice at $\beta = 0$. We do this by rescaling with the relative lattice spacings in Table B.1.

After the re-scaling, we use an ansatz of the form

$$E_b = A\, m^{\alpha}\,, \tag{3.77}$$

where A and α are fit parameters. In the continuum, non-relativistic and infinite volume, we expect $A = G_{\text{N}}^2/4$, and $\alpha = 5$, see (3.72). This ansatz provides a good description of our data for all ensembles, except for the two coarsest ensembles at $\beta = 1.5$ and $\beta = 0.8$. For these ensembles, we find indications for a negative binding energy at small masses, indicating a repulsive gravitational interaction. We refer to Subsection B.1.2 on how we interpret this feature, and how we treat the data points for the two coarsest ensembles. In Subsection B.1.2 we also give details on the choice of a suitable fit range for the renormalized masses m.

In the following, we will use the fit function

$$E_b = A|x - B|^{\alpha} + C\,, \tag{3.78}$$

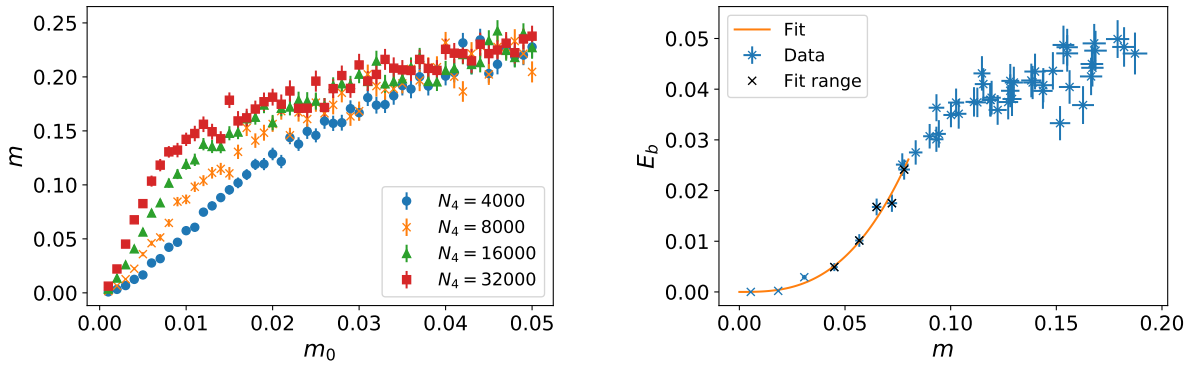

Fig. 3.6.: Left panel: We show the renormalized mass m as a function of the bare mass m_0 for different lattice volumes of the $\beta = 0$ ensemble. We see that the renormalized mass approaches zero for sufficiently small bare masses.
Right panel: We show the binding energy E_b as a function of the renormalized mass m for the $\beta = -0.776$ ensemble with $N_4 = 16000$. The fit range is indicated in black, and the blue solid line shows the power-law fit with the ansatz (3.77).

for the two coarsest lattice spacings, where A, B C, and α are fit parameters, see Subsection B.1.2 for a justification. As a cross-check, we will in the following also drop these two ensembles from future fits. The stability of the final result under the inclusion of these data points provides an a-posteriori justification for the modified fit ansatz (3.78).

We perform the power-law fit (3.77) and (3.78), respectively, for all our ensembles listed in Table B.1. For each ensemble, we extract the coefficients α and A. In analogy to the continuum limit, where $G_{\mathrm{N}} = \sqrt{4A}$, we associate a value of G_{N} at finite lattice spacing and volume with each fit coefficient A. This interpretation might suffer systematic uncertainties due to the finite volume and lattice spacing. These systematic uncertainties are expected to vanish in the continuum limit, where $G_{\mathrm{N}} = \sqrt{4A}$ should hold, cf. (3.72).

With the values for α and G_{N} for each ensemble, we can now perform the infinite volume, continuum limit extrapolation. We perform independent extrapolations for α and G_{N}.

Continuum, infinite volume extrapolation

We will now introduce the dimensionless version of the Newton coupling G_{N} by normalizing with respect to the fiducial lattice spacing ℓ_{fid} as $G = G_{\mathrm{N}}/\ell_{\mathrm{fid}}^2$, where ℓ_{fid} is the lattice spacing of the $\beta = 0$ ensembles. For the infinite volume, continuum limit extrapolation, we choose the simplest ansatz suggested in terms of the relative lattice spacing ℓ_{rel} and the inverse physical volume $1/V$, and inspired by diffeomorphism invariance in the continuum theory (which excludes odd powers in ℓ_{rel}). Therefore, we choose the fit ansatz

$$\alpha = \frac{H_\alpha}{V} + I_\alpha\, \ell_{\mathrm{rel}}^2 + \frac{J_\alpha}{V^2} + K_\alpha\, \ell_{\mathrm{rel}}^4 + L_\alpha\,, \tag{3.79}$$

and

$$G = \frac{H_G}{V} + I_G\, \ell_{\mathrm{rel}}^2 + \frac{J_G}{V^2} + K_G\, \ell_{\mathrm{rel}}^4 + L_G\,. \tag{3.80}$$

Here, H_i, I_i, J_i, K_i and L_i are fit parameters. We include corrections which are quadratic in the inverse volume, and quadratic in the squared lattice spacing, since we see curvature in our data for the smallest volumes and coarsest lattice spacings.

We also perform a cross-check dropping the coefficients K_i, and at the same time neglecting

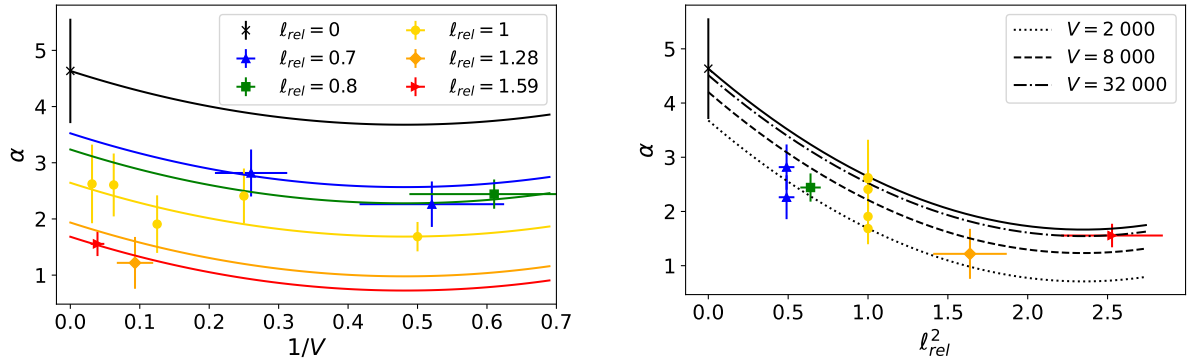

Fig. 3.7.: We show the data for the power-law exponent α that relates the renormalized mass m to the binding energy E_b, see (3.77). The data points correspond to the scaling extracted on different ensembles, see Table B.1. The black data point is the value of α in the infinite volume, continuum limit extrapolation. We find $\alpha = 4.6 \pm 0.9$. For the fit we find $\chi^2/\text{d.o.f.} = 0.56$ and a p-value of 0.73.
Left panel: The power-law exponent α as a function of the inverse physical volume expressed in units of 1000 simplices. The colored lines show the best fit of the ansatz (3.79) for the relative lattice spacings of the used ensembles. The black line indicates the continuum limit extrapolation.
Right panel: The power-law exponent α as a function of the squared relative lattice spacing. The dotted (dashed, dashdotted) line shows the best fit of the ansatz (3.79) for different physical volumes V. The black solid line indicates the infinite volume limit.

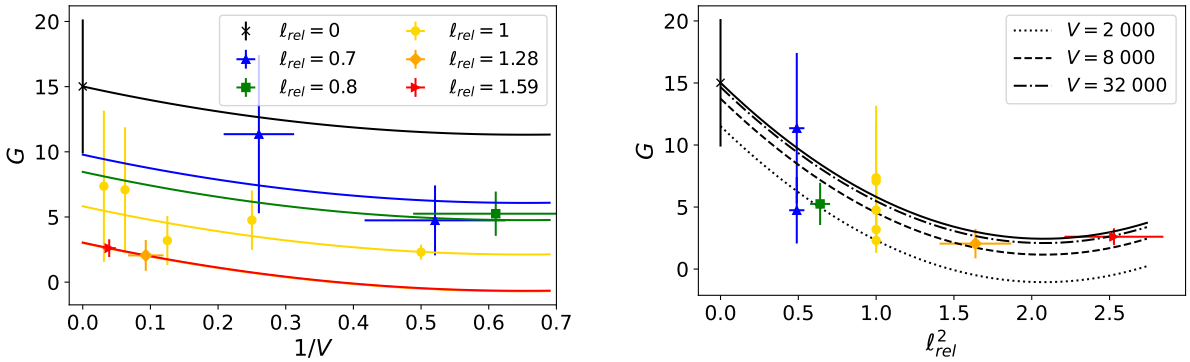

Fig. 3.8.: We show the data for the Newton coupling G, as extracted from (3.77) with $G_\text{N} = \sqrt{4\,A}$, and $G = G_\text{N}/\ell^2_\text{fid}$. The data points correspond to the scaling extracted on different ensembles, see Table B.1. The black data point is the value of G in the infinite volume, continuum limit extrapolation. We find $G = 15 \pm 5$. For the fit we find $\chi^2/\text{d.o.f.} = 0.37$ and a p-value of 0.87.
Left panel: The Newton coupling G as a function of the inverse physical volume expressed in units of 1000 simplices. The colored lines show the best fit of the ansatz (3.80) for the relative lattice spacings of the used ensembles. The black line indicates the continuum limit extrapolation.
Right panel: The Newton coupling G as a function of the squared relative lattice spacing. The dotted (dashed, dashdotted) line shows the best fit of the ansatz (3.80) for different physical volumes V. The black solid line indicates the infinite volume limit.

the two coarsest ensembles. The result from this fit are consistent within one-sigma to the result to the full set of data using the full fit functions (3.79) and (3.80).

The data points, as well as the extrapolations for α and G are shown in Figure 3.7 and Figure 3.8, respectively. There, we show the extrapolation as a function of the inverse volume, and of the squared relative lattice spacing. The left and right panel of Figure 3.7 and Figure 3.8 show therefore different slices through the two-dimensional parameter space spanned by $1/V$ and ℓ^2_{rel}. The fit of the data using the functions (3.79) and (3.80), and therefore the continuum, infinite volume extrapolation, is done separately for α and G.

Fitting the data against the ansatz (3.79) and (3.80), we assume that the data points are uncorrelated. Since the different data points are extracted from different ensembles, this assumption is reasonable. For the fit of the power-law coefficient α, we find $\chi^2/\text{d.o.f.} = 0.56$ and a p-value of 0.73. For the fit of the Newton coupling G we find $\chi^2/\text{d.o.f.} = 0.37$ and a p-value of 0.87. The extrapolated infinite volume, continuum limit values are $\alpha = 4.6 \pm 0.9$ and $G = 15 \pm 5$.

The value of the power-law exponent α agrees with the exponent in $d = 4$, where $\alpha = 5$ is expected, within the error bars. This agreement indicates that the Newtonian limit can be recovered from EDT. If we take the dependence of α on the dimension into account, cf. (3.73), we find that our value for α corresponds to $d = 3.9 \pm 0.2$. Therefore, our result is consistent with Newtonian binding in four dimensions at long distances and in the continuum limit.

There is no a-priori expectation for the value of the Newton coupling G which is obtained from the lattice, since it sets the lattice spacing in physical units. However, it should satisfy certain consistency checks, as discussed previously. First, for the non-relativistic limit we require that $G_{\text{N}}\, m^2/2 \ll 1$, cf. (3.75). With the extrapolated value for G_{N} in the units of our fiducial lattice, this translates into $m^2 \ll 0.13$ in those units. Since the fit window for the renormalized mass closes at $m^2 \approx 0.02$, cf. Figure 3.6 and Subsection B.1.2, this condition is satisfied. Furthermore, the Newtonian limit also requires an attractive gravitational coupling, i.e., $G_{\text{N}} > 0$, which is also satisfied in our extrapolation.

Since the dimensionfull Newton coupling G_{N} sets the lattice spacing in physical units, our value for G_{N} allows us to determine the lattice spacing in units of the Planck length for the first time. We find that

$$\sqrt{G_{\text{N}}} = \sqrt{G\,\ell^2_{\text{fid}}} = \ell_{\text{Pl}} = (3.9 \pm 0.7)\ell_{\text{fid}}\,, \qquad \text{hence} \qquad \ell_{\text{fid}} \approx (0.26 \pm 0.05)\ell_{\text{Pl}}\,. \tag{3.81}$$

Accordingly, our finest lattice spacing is around $1/6$ the Planck length. Therefore, the analyzed lattice spacings might be smaller than the Planck length, indicating that the investigated EDT simulations are indeed sensitive to quantum gravitational fluctuations.

3.3.2. The de Sitter instanton from Euclidean dynamical triangulations

We will now perform an additional and independent consistency test for asymptotic safety in a lattice formulation. For this, we will investigate the finite-volume scaling of the bare cosmological constant κ_4. We will argue that recovering a semi-classical regime of gravity implies a linear scaling of κ_4 as a function of $1/\sqrt{V}$. We will furthermore present indications that for large volumes, our lattice simulation is consistent with this expectation.

We will study the saddle-point approximation of the Euclidean partition function about de Sitter space. A similar analysis has been performed for CDT [281] to characterize the phase diagram of CDT. We will show how the parameters in the effective action of the lattice theory can be related to the continuum Hawking-Moss instanton solution [282] on a de Sitter space.

This relation allows us to extract the renormalized Newton coupling G_{N} from the finite-volume scaling of the bare cosmological constant. Our result agrees with the Newton coupling extracted from the observation of Newtonian binding within 1σ, see Subsection 3.3.1 and [3].

In the following, we will first discuss the de Sitter instanton, and point out how it might allow to extract the Newton coupling in our setup. We will then present the numerical results for the finite-size scaling of the bare cosmological constant, and for the conversion of different lattice units. Finally, we will present the determination of the Newton coupling.

The de Sitter instanton

Previous studies of EDT including the local measure term show indications that the lattice geometries resemble the overall shape of a Euclidean de Sitter space [172]. The agreement of the lattice geometry with a Euclidean de Sitter space improves, when following the first-order phase transition towards the postulated continuum limit [172].

We will now go one step further and investigate the semi-classical approximation of the EDT partition function about the classical de Sitter space.

Consider the partition function of EDT (2.39). We assume that the sum over triangulations of fixed four-volume has already been performed. Then, the partition function reduces to a sum over N_4. The leading behavior of the partition function is exponential in N_4, and reads [281]

$$Z(\kappa_4,\, \kappa_2) = \sum_{N_4} e^{-(\kappa_4 - \kappa_4^c) N_4}\, f(N_4,\, \kappa_2)\,, \tag{3.82}$$

where $f(N_4,\, \kappa_2)$ is a sub-exponential in N_4, and where κ_4^c is the pseudo-critical value of the coupling κ_4. Tuning κ_4 to the pseudo-critical value κ_4^c allows to take the infinite lattice-volume limit $N_4 \to \infty$. This procedure is also possible in the unphysical phase of the EDT phase-diagram. Therefore, the limit $\kappa_4 \to \kappa_4^c$ and $N_4 \to \infty$ is not necessarily equivalent to the limit of infinite physical volume.

The pseudo-critical value κ_4^c is not known a-priori, but emerges during the simulation. On the practical level, it is determined by adjusting the value of κ_4, such that for a given configuration, the volume fluctuates around the target volume. In this situation, the next metropolis step is equally likely to increase or decrease the lattice volume.

The continuum limit extrapolation of κ_4^c corresponds to the renormalized cosmological constant. Therefore, we can identify [281], see also [126]

$$(\kappa_4 - \kappa_4^c)\, N_4 = \frac{\Lambda}{8\pi G_{\mathrm{N}}} V\,, \tag{3.83}$$

with $V = V_4\, N_4$, where V_4 is the volume of a four-simplex in link units.

Once the bare parameters for the Newton coupling κ_2 and the non-trivial measure β are chosen such that the simulations are in the physical region of the phase diagram, the volume of the semi-classical universe is determined by specifying a target volume N_4. Therefore, the size of the de Sitter universe uniquely fixes κ_4 for given κ_2 and β. Therefore, also the renormalized cosmological Λ at a fixed and finite volume constants uniquely determined.

If the partition function of EDT (2.39) reproduces gravity in the semi-classical limit, the sub-leading exponential behavior in (3.82) is given by the Einstein-Hilbert term. Based on power

counting, we can infer the 4-volume dependence of this term as

$$\frac{1}{16\pi G_{\mathrm{N}}}\int \mathrm{d}^4x\sqrt{g}\,R \sim \frac{\sqrt{V}}{G_{\mathrm{N}}}\,. \tag{3.84}$$

This consideration determines the function $f(N_4,\,\kappa_2)$ in (3.82), such that the partition function should have the form [281]

$$Z(\kappa_4,\,\kappa_2) = \sum_{N_4} e^{-(\kappa_4-\kappa_4^c)N_4+g(\kappa_2)}\,, \tag{3.85}$$

after all degrees of freedom except the four-volume have been integrated out. We expect the scaling of g to be

$$g(\kappa_2) \sim \frac{a^2}{G_{\mathrm{N}}}\,, \tag{3.86}$$

where a is the edge length of the simplices. When approaching the continuum limit, the edge length a decreases, such that g approaches zero. If this limit exists, N_4 diverges at the same time as a vanishes, such that the volume in physical units remains fixed. For a given lattice spacing, the value of g has to be determined in the simulations. For this, we consider the expectation value of the number of four-simplices $\langle N_4\rangle$. In a saddle-point expansion, this expectation value is given by [281]

$$\langle N_4\rangle = \frac{\sum_{N_4} N_4 e^{-(\kappa_4-\kappa_4^c)N_4+g(\kappa_2)\sqrt{N_4}}}{\sum_{N_4} e^{-(\kappa_4-\kappa_4^c)N_4+g(\kappa_2)\sqrt{N_4}}} \approx \frac{g^2(\kappa_2)}{4(\kappa_4-\kappa_4^c)^2}\,. \tag{3.87}$$

In our simulations, N_4 fluctuates around the target volume such that $\langle N_4\rangle = N_4$ is an input parameter of each ensemble. We can solve the saddle-point expansion (3.87) for g, which gives

$$g = 2|\kappa_4-\kappa_4^c|\sqrt{N_4}\,. \tag{3.88}$$

Therefore, a semi-classical limit is realized in the simulations, if κ_4 scales linearly as a function of $1/\sqrt{N_4}$. We will use this condition later to verify that our simulations indeed feature a semi-classical limit.

We can determine the slope of the linear dependence by studying the finite-volume scaling of κ_4 in the simulations. This study then determines the value of g on a given ensemble. With the value of g, we can determine the ratio G_{N}/a^2 up to a proportionality constant due to (3.86).

To determine the proportionality constant that relates g with G_{N}/a^2, we go back to the saddle-point expansion which we used in (3.87). Employing the same expansion for the partition function (3.85), gives

$$Z(\kappa_2,\,\kappa_4) \approx \exp\left(\frac{g^2(\kappa_2)}{4(\kappa_4-\kappa_4^c)}\right) = \exp\left(\frac{3\pi}{G_{\mathrm{N}}\bar{\Lambda}}\right). \tag{3.89}$$

For the last equality, we assumed that the continuum partition function is dominated by the de Sitter instanton. Under this assumption, the continuum expression it the known production amplitude of the Hawking-Moss instanton [282]. For the last equality in (3.89) we also assumed that the lattice geometries approximate the continuum de Sitter solution better and better, when approaching the continuum limit. Then, the de Sitter instanton also dominates the partition function of the lattice geometries when approaching the continuum limit.

This assumption can be tested in two ways: First, we can plot κ_4 as a function of $1/\sqrt{N_4}$, and verify the linear relation (3.88). Second, we can extract the renormalized Newton coupling G_{N}

and compare it with the determination based on Newtonian binding of scalar particles [3], see also Subsection 3.3.1. To obtain the Newton coupling from the semi-classical partition function, we combine (3.83) with (3.88) and (3.89), which leads to

$$G_{\mathrm{N}} = \frac{5^{\frac{1}{4}}\, a^2}{16\sqrt{N_4}|\kappa_4 - \kappa_4^c|}\,. \tag{3.90}$$

Therefore, the Newton coupling in link units reads

$$\frac{G_{\mathrm{N}}}{a^2} = \frac{5^{\frac{1}{4}}}{16|s|}\,, \tag{3.91}$$

where s is the slope determined by a fit to κ_4 as a function of $1/\sqrt{N_4}$.

In practice, the slope s has to be determined for each ensemble characterized by the bare values of β and κ_2. Even different values of N_4 at fixed lattice spacing require additional simulations at the same values for β and κ_2, but at larger values of N_4, to extract the finite-volume scaling of κ_4. This is necessary, since the transition line in the $\kappa_2 - \beta$ plane also moves as a function of N_4. Therefore, for each ensemble along the first-order transition line, summarized in Table B.1, we extract the slope s from the finite-volume scaling of κ_4. We can then use (3.91) to compute a value for the Newton coupling G_{N} for each of the ensembles. These values of G_{N} must then be extrapolated to the continuum, infinite volume limit.

However, the described analysis involves one subtlety: for the extrapolation to the continuum, infinite volume limit, we need the value of G_{N} in the same physical units across ensembles. The relative lattice spacing, which allows the comparison between ensembles is however given in simplex units ℓ, not in link units a, normalized to the fiducial lattice spacing ℓ_{fid} at $\beta = 0$. The value of the Newton coupling from (3.91) is however given in link units a. Therefore, we need to translate the values of G_{N} into simplex units. We will use the conversion

$$G = \frac{G_{\mathrm{N}}}{\ell_{\mathrm{fid}}^2} = \frac{G_{\mathrm{N}}}{a^2}\left(\frac{a}{\ell}\right)^2 \ell_{\mathrm{rel}}^2 = \frac{5^{\frac{1}{4}}}{16|s|}\left(\frac{a}{\ell}\right)^2 \ell_{\mathrm{rel}}^2\,, \tag{3.92}$$

where the lattice conversion factors a/ℓ are given in the second column of Table B.1, and where $\ell_{\mathrm{rel}} = \ell/\ell_{\mathrm{fid}}$. Here, we have re-introduced the Newton coupling in lattice units as $G = G_{\mathrm{N}}/\ell_{\mathrm{fid}}^2$. We discuss the determination of the conversion factors in detail in Subsection B.2.1. Intuitively, the lattice spacing ℓ measures the separation of the center of four-simplices, while the link unit a is the edge length of the simplices. In a flat space, there is a fixed relation between these two quantities. When introducing curvature, this ratio changes, such that we have to measure it on each of the ensembles.

Numerical results: Finite-volume scaling and continuum, infinite volume extrapolation

Table B.1 summarizes the ensembles which will be used in the following. They have been generated and studied in previous works [3, 172, 188], and include ensembles at several different physical volumes and lattice spacings. The relative lattice spacings were obtained by studying the return probability of a diffusion process on the lattices. The return probability is dimensionless, but depends on the diffusion time step. The latter is a dimensionfull quantity. The relative lattice spacings are then obtained by rescaling the diffusion time step on various ensembles, such that the return probability lies on a universal curve [188]. The relative lattice spacing is just the rescaling factor, and the rescaling is performed such that the universal curve

corresponds to the return probabilities for the ensembles at $\beta = 0$. The errors on the relative lattice spacing resemble the uncertainties in the matching procedure.

The lattice conversion factors a/ℓ are obtained in a similar way, by comparing the return probability on the direct lattice (on the edges) with the one on the dual lattice (on the four-simplices): for a given ensemble, the diffusion time step on the direct lattice is rescaled such that both return probabilities agree. The lattice conversion factor for this ensemble is then a function of the rescaling factor. To correct for finite volume effects, the conversion factors are extrapolated to the infinite volume limit. For more detail on the conversion factors, as well as on the error estimates, see Subsection B.2.1.

To investigate the finite-volume scaling of κ_4, we generated new lattices at fixed values of κ_2 and β, and for increasing volumes. The new ensembles are summarized in Table B.4. As the lattice-volume is increased while keeping the lattice spacing fixed, one of the parameters κ_2 or β has to be re-adjusted in order to compensate for the shift of the phase transition line, which moves as a function of the volume.

For each ensemble close to the transition line, we therefore generated new ensembles at larger volumes, but the same values for β and κ_2. We use these configurations at larger volumes to extract the finite-volume scaling of κ_4 for the corresponding tuned ensemble.

Since the phase transition line shifts to larger values of κ_2 for increasing volumes, it is necessary to generate the new ensembles at larger volumes. This ensures that the new ensembles are in the correct phase.

To compute the Newton coupling according to (3.92), we need to extract the slope s from the finite-volume scaling of κ_4. For fixed values of κ_2 and β, and for increasing values of N_4 we measure the tuned value of κ_4 at each of the volumes. We assume that the errors on κ_4 are purely statistical. They are estimated after blocking the data to account for autocorrelation errors, see Subsection B.1.1 for details. The measured values of κ_4 are summarized in Table B.4, where the smallest volumes for given values of κ_2 and β corresponds to the tuned ensemble, which is located close to the first order phase transition.

The slope s is then extracted via a linear fit

$$\kappa_4(N_4) = A_{\kappa_4} + s\,\frac{1}{\sqrt{N_4}}\,, \tag{3.93}$$

where A_{κ_4} and s are fit parameters.

In Figure 3.9 we show two examples of these fits at different relative lattice spacings ℓ_{rel}. In some of the fits, see, e.g., the right panel in Figure 3.9, the smallest volume was discarded, since it was not well described by a linear fit on the other data points. This might be due to finite-volume effects. Another reason might be the closeness to the first-order phase transition, which might result in contamination from occasional tunneling into the unphysical phase, where the values for κ_4 are significantly larger [188].

We find evidence for a linear scaling of κ_4 as a function of $1/\sqrt{N_4}$ for all investigated lattice spacings and volumes. This provides numerical evidence for the validity of the semi-classical approximation (3.88). We summarize the slope s for each of the ensembles in Table B.5. We also list the $\chi^2/\text{d.o.f.}$ and the p-value of each fit. These parameters confirm the quantitative agreement of our data with a linear relation between κ_4 and $1/\sqrt{N_4}$.

With the finite-volume scaling of κ_4, the conversion factors a/ℓ between link and simplex units, and the relative lattice spacing in simplex units, we can now use (3.92) to compute a value for the Newton coupling G at each of the ensembles. As in Subsection 3.3.1, this data has

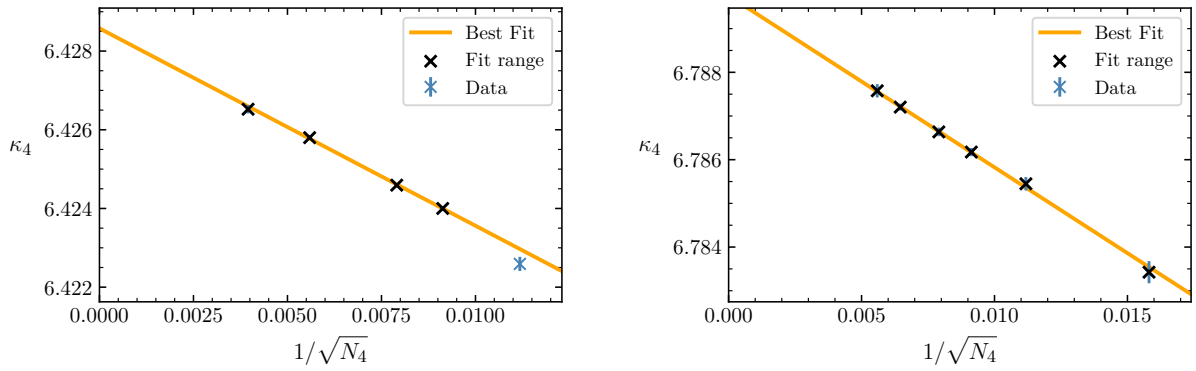

Fig. 3.9.: Examples for the finite-volume scaling of κ_4 as a function of $1/\sqrt{N_4}$.
Left panel: For our fiducial lattice spacing, $\beta = 0$, and for $\kappa_2 = 0.5886$, the line shows a linear fit according to (3.93). The fit results in a slope $s = -0.724 \pm 0.032$, and in $\chi^2/\text{d.o.f} = 1.4$, and a p-value of 0.24.
Right panel: For the lattice at $\beta = -0.6$ and $\kappa_2 = 2.245$, the line shows a linear fit according to (3.93). The fit results in a slope $s = -0.393 \pm 0.022$, and in $\chi^2/\text{d.o.f} = 0.15$, and a p-value of 0.96.

to be extrapolated to the continuum, infinite volume limit, to obtain the renormalized Newton coupling. We use the fit function (3.80), which we used for the extrapolation of the Newton coupling obtained from Newtonian binding. We will set $J_G = 0$ in the ansatz (3.80), since the inclusion of $1/V^2$ corrections does not improve the quality of the fit. As a cross-check for the extrapolation, we also perform a fit with $K_G = 0$, and simultaneously neglecting the data points with $\ell_{\text{rel}} > 1$. The resulting value for G in the continuum, infinite volume limit for this fit agrees within 1σ with that of the extrapolation including the coefficient K_G and all data points.

The extrapolation of G is shown in Figure 3.10 against the inverse volume (left panel) and the squared relative lattice spacing (right panel). The colored lines in the left panel of Figure 3.10 indicate lines of constant relative lattice spacing. The black line shows the continuum extrapolation. The right panel shows a different cut through the space spanned by $1/V$ and ℓ^2_{rel}. The dotted, dashed, and dashdotted lines show lines of fixed volume at the fiducial lattice spacing. The black cross in both panels of Figure 3.10 shows the continuum, infinite volume extrapolation of the Newton coupling $G = 14.3 \pm 3.6$. The fit results in $\chi^2/\text{d.o.f} = 0.87$, which corresponds to a p-value of 0.46. This value is in excellent agreement with the Newton coupling obtained from Newtonian binding, see Subsection 3.3.1, which lead to $G = 15 \pm 5$.

3.3.3. Towards a rejection-free algorithm for Euclidean dynamical triangulations

One of the limitations of numerical simulations in EDT is the low acceptance rate r of the Monte-Carlo simulations, when following the first order phase transition towards larger values of κ_2. This coincides with the regime, where the postulated continuous phase transition might be located [172, 177], and where the lattice spacing become smaller. As a rough estimate, the finest lattices generated for the investigation of Newtonian binding energy [3], cf. Subsection 3.3.1 is about $q \approx 10^{-6}$.

To understand why this low acceptance rate is problematic, let us first review the key steps of the Metropolis algorithm[1], which is used in the current implementation of the EDT simulations.

[1]This algorithm was developed and implemented by Nicholas Metropolis, Arianna Rosenbluth, Marshall Rosenbluth, Augusta Teller, and Edward Teller in [283]. We will however stick to the commonly used naming convention, and just refer to it as *Metropolis* algorithm.

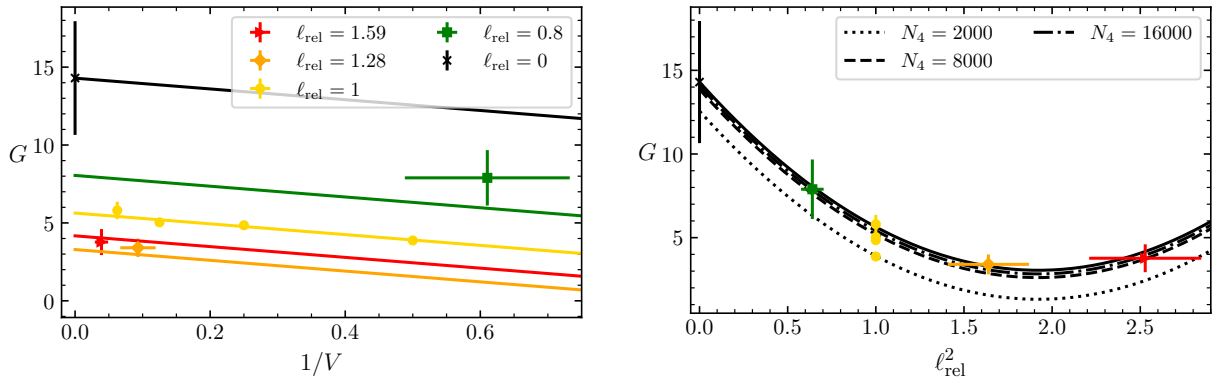

Fig. 3.10.: We show the data for the Newton coupling G, as extracted from (3.77). The data points correspond to the scaling extracted on different ensembles, see Table B.1. The black data point is the value of G in the infinite volume, continuum limit extrapolation. We find $G = 14.3 \pm 3.6$. For the fit we find $\chi^2/\text{d.o.f.} = 0.87$, corresponding to a p-value of 0.46.
Left panel: The Newton coupling G as a function of the inverse physical volume expressed in units of 1000 simplices. The colored lines show the best fit of the ansatz (3.80) for the relative lattice spacings of the used ensembles. The black line indicates the continuum limit extrapolation.
Right panel: The Newton coupling G as a function of the squared relative lattice spacing. The dotted (dashed, dashdotted) line shows the best fit of the ansatz (3.80) for different physical volumes V. The black solid line indicates the infinite volume limit.

For a system described by an action $\mathcal{S}$, the probability $p_{A\to B}$ to transition from a state A to another state B is assigned as

$$p_{A\to B} = \begin{cases} 1\,, & \text{if } \mathcal{S}_B \leq \mathcal{S}_A\,, \\ e^{\mathcal{S}_A - \mathcal{S}_B}\,, & \text{if } \mathcal{S}_B > \mathcal{S}_A\,. \end{cases} \tag{3.94}$$

In addition to the assignment of probabilities, one has to specify a set of allowed changes on the system, which we will refer to as *moves* in the following. In the EDT simulations, the allowed moves are the Pachner moves discussed in Subsection 2.3.2, for the Ising model it would just be a single spin-flip that can occur on each lattice site.

The algorithm then performs the following steps:

1. Pick a lattice site j by random.
2. Compute the probability $p_{A\to B}(j)$ (3.94) of the move at lattice site j.
3. Generate a random number $r \in (0, 1)$.
   a) If $r < p_{A\to B}$: do nothing.
   b) Else: perform proposed move at lattice site j.
4. Repeat from 1.

If a move is accepted, the lattice changes, until it eventually reaches a thermalized state, where it fluctuates around an equilibrium, which is the state one is usually interested in.

We can see that a low acceptance rate q is undesired, since many moves will be proposed, without the lattice changing at all. For the EDT simulations, the second step in the above list is numerically costly, since the local lattice geometry has to be reconstructed to compute $p_{A\to B}$.

Rejection-free algorithms

To avoid computing many probabilities $p_{A\to B}$ for moves that will be rejected, we aim at employing a so-called *rejection-free* (RF) algorithm [284–290], where each proposed move is accepted. This type of algorithms is commonly used in dynamical systems, for example to simulate the growth of crystals, see [291] for an overview.

The idea of the RF algorithm is the following [291]:

1. Initialize:
   a) Compute probability $p_{A\to B}$ at each lattice site i, save them in a list $p_i = p_{A\to B}(i)$.
   b) Save a list of summed probabilities $P_i = \sum_{i\leq l} p_l$.
2. Generate a random number $r \in (0, \mathrm{Max}(P_i))$.
3. Find the lattice site j such that $P_{j-1} < r \leq P_j$ (with $P_0 = 0$).
4. Perform the move at lattice site j.
5. Update the entries of p_i and P_i.
6. Repeat from 2.

Compared to the Metropolis algorithm, we need an initialization, where the probability for a move at each lattice site has to be computed. We can intuitively understand the third step in such way that the RF algorithm chooses the move, which would have been eventually accepted by the Metropolis algorithm. The difference between the entries P_{j-1} and P_j is exactly the probability p_j of the site j. Therefore, larger p_j are more likely to be picked by the RF algorithm. This is exactly the same as in the Metropolis algorithm.

Another difference to the Metropolis algorithm is the fifth step, where the entries of the lists p_i and P_i have to be updated. If a move at lattice site j only affects the probabilities of a limited number n of neighboring lattice sites, only those probabilities p_i have to be evaluated.

We can now see the potential speedup: For the Metropolis algorithm at acceptance rate q, one has to evaluate on average $1/q$ probabilities until one move is accepted. For the RF algorithm, and after the initialization procedure, one has to evaluate n probabilities for each accepted move. Therefore, for sufficiently low acceptance rates q, where $1/q > n$, the rejection free algorithm is expected to perform better.

Rejection-free algorithm for EDT and the use of ponderances

There are still two issues with the proposed RF algorithm: The first issue is related to the number of moves n that would have to be updated after each accepted move in EDT simulations, and the second issue is related to the Monte-Carlo "time" evolution of the system. We will address both points.

The partition function for EDT (2.39) actually depends on global parameters of the configuration, namely the number of four-simplices N_4, and the number of two-simplices N_2, see (2.32). Since the Pachner moves for EDT can change these numbers after each accepted move (the moves consist of adding or deleting simplices), the probability $p_{A\to B}(j)$ for each lattice site j changes after each move. Therefore, the fifth step of the RF algorithm entails recomputing *all* probabilities.

Exponentiating the local measure term in the partition function (2.39), we can understand it as part of the action, and write

$$S_{EDT} = S_{\text{loc}} + S_{\text{glob}} \,, \tag{3.95}$$

where S_{glob} is the Regge action, and S_{loc} is the exponentiated measure term. However, the definition of the probability $p_{A\to B}$ in (3.94) does not separate into a global and a local part, due to its piece-wise definition, specifically

$$p_{A\to B} \neq (p_{A\to B})_{\text{loc}}\,(p_{A\to B})_{\text{glob}} \,. \tag{3.96}$$

Therefore, we cannot factor out the global part, and indeed need to update the entire list of probabilities.

However, the assignment of probabilities (3.94) is only one way to ensure *detailed balance*. Detailed balance states that in equilibrium, each elementary process (the moves on the lattice) is in equilibrium with its reverse process, see, e.g.[292]. Detailed balance is fulfilled, if

$$\frac{p_{A\to B}}{p_{B\to A}} = e^{\mathcal{S}_A - \mathcal{S}_B} \,, \tag{3.97}$$

and we can see that the definition (3.94) satisfies detailed balance. A different way to maintain detailed balance is via the definition

$$\mathcal{P}_{A\to B} = \sqrt{e^{\mathcal{S}_A - \mathcal{S}_B}} \,, \tag{3.98}$$

which is not piecewise defined and therefore factorizes into

$$\mathcal{P}_{A\to B} = (\mathcal{P}_{A\to B})_{\text{loc}}\,(\mathcal{P}_{A\to B})_{\text{glob}} \,, \quad \text{with} \quad (\mathcal{P}_{A\to B})_{\text{i}} = \sqrt{e^{\mathcal{S}_{A,\text{i}} - \mathcal{S}_{B,\text{i}}}} \,, \tag{3.99}$$

where i labels the local and global part, respectively. We will call the quantity defined in (3.98) *ponderances*, since $\mathcal{P}_{A\to B}$ is not bounded and therefore cannot be interpreted as a probability. Exchanging probabilities by ponderances now allows us to separate the local from the global information, and to only store and update the local part. We can then apply the RF algorithm discussed above for EDT, in such way that we only have to recompute few ponderances after each accepted move.

Let us now come to the last issue we have to address, before we can use the rejection free algorithm: Monte-Carlo "time". The time that passed in a simulation is measured in terms of attempted moves. This is intuitive, when thinking about dynamical systems, where each time step δt_{att} a move is attempted. If the acceptance rate q is low, the system will stay in the same state for a long time. The RF algorithm however counts accepted moves. If we would perform a step in the RF algorithm each time step δt_{att}, the time evolution of the system would look very different.

To compensate for this discrepancy, we associate an average dwell time t_{d} to each accepted move. We define it as

$$t_{\text{d}} = \frac{N}{\sum_{i=1}^{N} \mathcal{P}_{A\to B}(i)} \,, \tag{3.100}$$

which is just the inverse, average ponderance, where N is the total number of lattice sites. We can understand the dwell time again from dynamical systems: low ponderances would in a Metropolis algorithm translate into low acceptance rates. Therefore, the smaller the average ponderance, the longer (in terms of attempted moves) a system will remain in the same state. In this way, we can reproduce the same time-evolution with the RF algorithm.

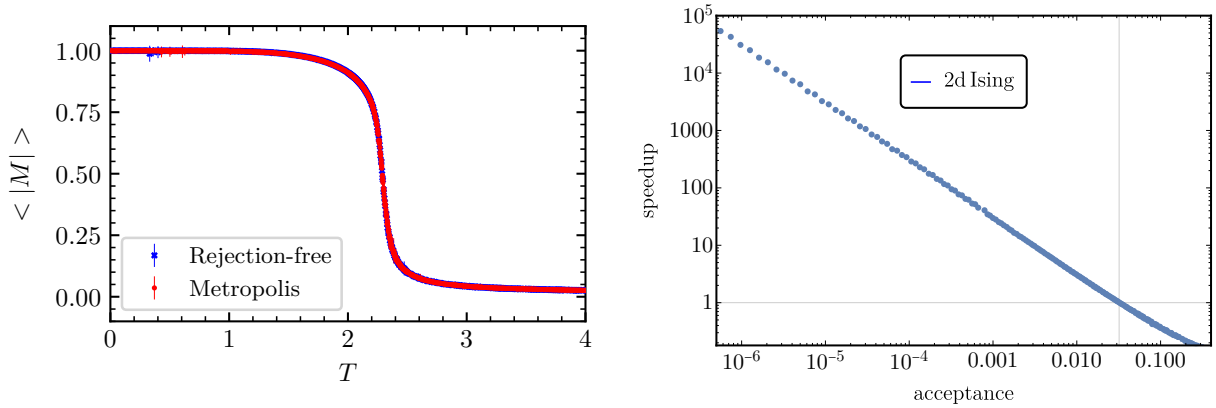

Fig. 3.11.: Left panel: The average magnetization of the two-dimensional Ising model as a function of the temperature T. The red data points and error-bars show the magnetization obtained with the Metropolis algorithm, the blue data points and error-bars show the magnetization obtained with the RF algorithm.
Right panel: We show the speedup as a function of the temperature for the two-dimensional Ising model, when employing the RF algorithm, compared to the Metropolis algorithm.

Proof of principle: The Ising model in two dimensions

To test the accuracy of the proposal of ponderances, and the associated dwell-time, we use the Ising model in $d = 2$ for a proof of principle. The use of ponderances would not be necessary in the Ising model, since we will assume nearest-neighbor interactions only. However, the Ising model is well-studied and therefore provides a solid starting point to compare. Furthermore, the Ising model features a regime of low acceptance at low temperatures, such that we can also test whether the RF algorithm provides the expected speedup.

The partition function of the Ising model in $d = 2$ reads

$$Z_{\mathrm{I}} = \sum_{\{\sigma\}} e^{-\frac{1}{T}\sum_{\langle ij\rangle}\sigma_i\,\sigma_j}\,, \tag{3.101}$$

where $\sigma_i = \pm 1$ labels a single lattice site, where the sum over $\langle ij\rangle$ indicates the sum over nearest neighbors j for a spin at lattice site j, and where T is the temperature of the system.

For a given temperature, we start the simulation from a randomized lattice. After a time to allow the lattice to thermalize, we start measuring the magnetization of the lattice,

$$M = \frac{1}{N}\sum_{i=1}^{N}\sigma_i\,. \tag{3.102}$$

For each temperature, we perform one simulation with the RF algorithm, where we measure M after a fixed dwell time t_{d}. For comparison, we perform another simulation with the standard Metropolis algorithm, where we measure M after a fixed number of attempted moves.

The resulting average of $|M|$ on a 32×32 lattice is shown in the left panel of Figure 3.11. We can see good agreement between both algorithms, and indeed the average magnetization in both algorithms at each temperature agrees within 1σ.

Even though the partition function of the Ising model is less complex than the partition function of EDT, we interpret this excellent agreement as a proof of principle for the RF algorithm, and for the use of ponderances.

The right panel of Figure 3.11 shows the speedup of the RF algorithm as a function of the acceptance q. We can see that the speedup increases one order of magnitude, when decreasing the acceptance rate by one order of magnitude.

Performance estimate for EDT

While the implementation and verification of the RF algorithm for EDT is still ongoing, let us briefly comment on expected performance gains. As mentioned above, the acceptance rate for the finest lattices that were simulated and analyzed so far, is about $q \approx 10^{-6}$, and decreases further, when following the first-order transition to larger values of κ_2.

At the same time, we find that the ponderance of about $n \sim 10^3$ simplices need to be updated after each accepted move. This results in the very promising expectation of a performance gain by roughly three orders of magnitude, at the current ensembles.

This speedup might be an important stepping stone when further investigating the phase diagram of EDT. It will allow us to simulate larger volumes at finer lattice spacings, and might allow us to find further evidence for the existence, or the absence of a continuum limit of EDT.

3.3.4. Summary and conclusion

Any theory of quantum gravity must feature the observed or expected classical physics in the appropriate limit. This especially applies to a lattice theory for quantum gravity, where the emergence of a classical limit can be used as a test for the existence of a continuum limit of the lattice formulation.

In this spirit, we have confronted the asymptotic safety scenario in terms of EDT with two independent tests for the emergence of a classical limit. On the one hand, we have studied scalar particles that propagate on the lattice geometries. We have found that their interaction is well described by the Newtonian potential, in the appropriate non-relativistic and classical limit. On the other hand we have studied the emergence of the de Sitter space in EDT. We have found that the lattice geometries are compatible with the semi-classical de Sitter solution in the continuum, infinite volume limit.

In Subsection 3.3.1 we have studied the binding energy of the two-particle bound state of two identical scalar particles, as a function of the renormalized mass of the scalar particle. Here, we have used scalar matter as a probe to test the properties of EDT geometries. The computation passes several non-trivial consistency tests. First, the renormalized mass of the scalar field vanishes, in the limit where the bare mass vanishes. This shows that shift symmetry is not broken by the lattice discretization. Second, the binding energy of the two-particle bound state shows a power-law dependence on the renormalized scalar mass, in the non-relativistic limit. At finite lattice spacing and finite lattice volume, the scaling exponent is close to the expected behavior, based on the measured spectral dimensions on these geometries [172].

In the continuum limit, infinite volume extrapolations, the power law dependence resembles a Newtonian potential in $d = 4$ dimensions. Indeed, from the scaling exponents on our lattices we find that the scaling in the continuum limit, infinite volume extrapolation corresponds to $d = 3.9 \pm 0.2$. Furthermore, we can extract the Newton coupling in lattice units from the binding energy. We find $G = 15 \pm 5$, which allows us to translate the lattice spacing into the physical Planck-scale as $\ell_{\mathrm{Pl}} = \sqrt{G_{\mathrm{N}}} = (3.9 \pm 0.7)\ell_{\mathrm{fid}}$. This indicates that the lattice spacings of the EDT simulations are smaller than the Planck scale, suggesting that there is no barrier to taking a continuum limit.

In Subsection 3.3.2 we have studied the saddle point approximation of the Euclidean partition function about the de Sitter space. In the semi-classical approximation, the bare cosmological constant is expected to be linear in $1/\sqrt{V}$, where V is a finite lattice volume. Our data is in agreement with this linear dependence across all ensembles, see Figure 3.9.

With this agreement, we can extract the Newton coupling in link units by a comparison of the saddle-point approximation to the Hawking-Moss instanton solution, which is expected to dominate the partition function in the continuum. We extract a value for the Newton coupling in link units for each ensemble, and translate those values into the dimensionless Newton coupling G in terms of simplex units. In the continuum limit, infinite volume extrapolation we find $G = 14.3 \pm 3.6$, which leads to $\ell_{\text{Pl}} = \sqrt{G_{\text{N}}} = (3.8 \pm 0.5)\ell_{\text{fid}}$.

The uncertainties in both studies are dominated by the determination of the relative lattice spacing ℓ_{rel}. The uncertainties in this quantity also determine the uncertainties on the physical volume, see Figure 3.8, and Figure 3.10. We expect to reduce the uncertainties on ℓ_{rel} by studying larger volumes and finer lattice spacings in the future.

The result for the Newton coupling from the analysis of Newtonian binding of scalar particles is in excellent agreement with the Newton coupling extracted from a saddle-point approximation. The agreement is non-trivial, since both studies are independent and probe different directions towards a classical limit of quantum gravity. In the first study, we measure the gravitational interaction between scalar particles. In the second study we investigate the semi-classical expansion of the Euclidean partition function. Both features emerging from EDT, governed by the same Newton coupling provides evidence that EDT is not just a theory of random geometry, but a theory of gravity.

Intriguingly, the agreement of the Newton coupling from pure gravity and gravity-interactions was also found in FRG studies of gravity-matter systems [113, 216, 243, 266], see Subsection 3.1.2. While this feature of *effective universality* refers to the UV values of different avatars of the Newton coupling, while the Newton coupling extracted from EDT corresponds to the classical Newton coupling. Nevertheless, this similarity encourages us to explore similarities between EDT and the FRG approach to asymptotically safe quantum gravity in the future.

4. Phenomenological Consistency Tests

On the classical level, gravity and matter are intertwined via the Einstein equations. They encode how gravity governs the movement of matter, and in turn how matter forces spacetime to curve. This connection between the dynamics of spacetime and matter is expected to persist on the quantum level, and in a theory describing the fundamental interactions of our universe. Therefore matter fields can be used as a probe for gravity: investigating carefully and understanding the dynamics of matter, we can learn about the underlying dynamics of gravity.

In our universe, we have observational access to both gravity, and matter at low energies. In this regime, the matter sector is accurately described by the SM, while gravity is described by GR. The SM is formulated as a quantum theory of matter fields. GR is a classical field theory of the metric. The quest of asymptotically safe quantum gravity is to formulate a predictive quantum theory of matter and the metric. The regime where quantum effects of the metric are expected to be dominant, the Planck-scale, is however far beyond the reach of direct experimental tests. Therefore, any model of quantum gravity can only and has to be confronted with consistency tests.

Due to the interaction between gravity and matter, there are two directions in which we can use our knowledge about matter to learn about the fundamental properties of spacetime, and to test models of quantum gravity and matter. For both of these consistency tests, we will assume that the matter degrees of freedom that we observe at low energies are fundamental fields and also present at high energies. Intriguingly, for the SM this is a consistent assumption [16, 17].

First, we can explore under which conditions the gravitational sector is UV complete, in the presence of the observed matter degrees of freedom. For asymptotically safe quantum gravity, we have reviewed the status of this question in Subsection 3.1.2.

Second, we can investigate how asymptotically safe quantum gravity affects the matter sector. The matter sector features dimensionless couplings, which, in contrast to gravitational couplings, are not Planck-scale suppressed. These matter couplings are measured directly at low energies. At these experimentally accessible scales, direct signatures from quantum gravity will be very tiny. However, the interaction between quantum gravity and matter at high energies can leave structural imprints on the matter sector, for example in terms of symmetries. Therefore, dimensionless matter couplings could be used as a bridge from the high-energy regime, where the quantum properties of spacetime are important, down to experimentally accessible scales.

In the following we will first review the status of the effect of asymptotically safe quantum gravity on the matter sector. We will focus on the effect of gravity on marginal couplings in Section 4.1, and we will discuss the gravitational effect on higher-order matter interactions in Section 4.2. In Section 4.3, we will introduce the scenario of *effective asymptotic safety*, where a fundamental description of the universe is connected to the IR via an intermediate asymptotically safe scaling regime. In particular, we will discuss conditions on the asymptotically safe fixed point, such that string theory might be the fundamental theory, in Subsection 4.3.2. In Section 4.4 we will study the gravitational effect on marginal and on higher-order couplings in the Abelian gauge sector in a combined way. We investigate the question, which dimen-

sions of spacetime are compatible with the existence of a UV complete Abelian gauge sector. In Section 4.5 we study the gravitational effect on four-fermion interactions in the presence of a non-vanishing gauge coupling. We will see that the observation of light fermions at low energies puts constraints on the dynamics at high energies. Finally, in Section 4.6, we will exploit the interaction between gravity and matter, and investigate how the breaking of Lorentz invariance in the gravitational sector affects the matter sector. We will see that the matter sector can in general not be protected from the breaking of Lorentz invariance. Together with observational constraints on Lorentz-invariance violations in the matter sector, the gravity-matter interplay might allow to put indirect constraints on violations of Lorentz invariance in the gravitational sector.

Let us remind the reader that we work in a Euclidean space. The continuation of the presented results to a Lorentzian signature is an open question, and is part of the systematic uncertainties of our investigations, see also [238] for a discussion.

4.1. Phenomenological consequences of the Reuter fixed point in the matter sector

We will now focus on the effect of quantum gravity on marginal couplings. In the SM, there are three sectors featuring marginal couplings, namely the gauge sector, the scalar sector and the Yukawa sector. The scale dependence of any marginal coupling g_i can be schematically written as

$$\beta_{g_i} = -f_{g_i}\, g_i + \#_{\text{matter}}\, g_i^{n_i} + \mathcal{O}(g_i^{n_i+1})\,, \tag{4.1}$$

where $n_i = 2$ for scalar ϕ^4 couplings, and $n_i = 3$ for gauge and Yukawa couplings. Here, f_{g_i} refers to the leading-order gravitational contribution, and $\#_{\text{matter}}$ is the one-loop matter contribution. Different sectors of the SM realize different sign combinations of f_{g_i} and $\#_{\text{matter}}$. These sign combinations lead to different phenomenological implications, which can be used to confront the underlying theory of quantum gravity with phenomenological consistency tests.

4.1.1. Gauge sector

The Abelian gauge sector of the SM features a scale-dependent hypercharge coupling $g_Y(k)$. Quantum fluctuations of charged matter turn the vacuum into a screening medium [293]. This means that the measured charge grows larger and larger when probing smaller length scales. The screening nature of the vacuum is encoded in $\#_{\text{matter}} > 0$. Before discussing the effect of metric fluctuations on the Abelian coupling, let us first review the high-energy properties of the Abelian gauge coupling in the SM. Specifically, the beta function for g_Y, and the resulting scale-dependent gauge coupling read

$$\beta_{g_Y}|_{\text{SM}} = \frac{1}{16\pi^2}\frac{41}{6}{g_Y}^3 + \mathcal{O}({g_Y}^5)\,, \quad \text{and} \quad {g_Y}^2(k) = \frac{{g_Y}^2(k_0)}{1 - \frac{1}{8\pi^2}\frac{41}{6}{g_Y}^2(k_0)\ln\left(\frac{k}{k_0}\right)}\,, \tag{4.2}$$

where k_0 is a reference scale.

The positivity of the one-loop coefficient encodes the screening nature of the vacuum. Due to the positive sign, the gauge coupling diverges at a finite scale. This divergence, the so-called Landau pole, can only be avoided by setting $g_Y(k_0) = 0$. However, in this case, the Abelian hypercharge vanishes at all scales, which is in contradiction with experimental observations of an interacting Abelian gauge sector at low energies. Therefore, the presence of the Landau pole

signals the breakdown of the SM at finite, trans-Planckian scales [293].

The argument above was exemplified based on a one-loop approximation to the scale dependence of g_Y. This approximation is only valid, as long as the coupling is small, and hence breaks down long before the Landau-pole in (4.2) is reached. However, non-perturbative studies using lattice [294, 295] and functional [296] methods suggest that the divergence of the gauge coupling persists beyond perturbation theory.

Due to the Landau pole, a UV-completion of the SM requires the presence of new physics. Asymptotically safe quantum gravity might provide a minimalistic extension of the SM, which induces a UV-completion in the gauge sector [297–299]. This extension is minimalistic, since it does not require any new degrees of freedom beyond the known ones: the SM matter fields, and gravity.

Under the inclusion of asymptotically safe quantum gravity, the scale dependence of the Abelian hypercharge reads

$$\beta_{g_Y} = -f_g\, g_Y + \frac{1}{16\pi^2}\frac{41}{6}\, {g_Y}^3 + \mathcal{O}({g_Y}^4)\,, \tag{4.3}$$

where the gravitational contribution is summarized in the coefficient f_g. This contribution enters linearly in the scale dependence of the Abelian hypercharge and therefore dominates at small values for g_Y. Explicit computations using the FRG yield $f_g \geq 0$ [242, 297, 298, 300–302], which would indicate an antiscreening effect of metric fluctuations.

Before discussing implications of this antiscreening effect, let us first comment on the scheme dependence of f_g. Since the gravitational coupling is dimensionfull, the gravitational contribution f_g is non-universal and scheme-dependent. Perturbative studies using dimensional regularization indicate that $f_g = 0$ [303–307]. In this case the direct effect of metric fluctuations on the Abelian gauge coupling vanishes, and the Landau-pole behavior of the pure-matter system is not altered. However, perturbative studies do not account for the contribution from higher-order couplings, which would additionally contribute to f_g [302], see also Section 4.4. Perturbative studies using a cutoff regularization were shown to lead to $f_g > 0$ [308], which is in qualitative agreement with FRG studies.

Even though the gravitational contribution f_g is scheme dependent, the resulting scheme dependent beta-function β_{g_Y} also contains scheme independent information. Specifically, f_g corresponds to the critical exponent of the Gaussian fixed point $g_{Y*} = 0$. Critical exponents are expected to be scheme independent, and can be measured, at least in non-gravitational systems. Within truncations, critical exponents might still acquire a scheme dependence. Furthermore, the sign of f_g also encodes the existence of a NGFP $g_{Y*} > 0$, which is also expected to be a scheme independent bit of information.

In the following, we will therefore aim to extract parts of this scheme-independent information by fixing a scheme, i.e., by choosing a specific FRG regulator $\mathcal{R}_k$, and within a truncation. While a quantitatively accurate extraction of critical exponents might not be possible in small truncations, the systematic enlargement of the truncation is expected to eventually show apparent convergence on scheme-independent information. Qualitative features of the system, such as the sign of critical exponents, are expected to already be robust within small truncations.

We will now work in a scheme where $f_g > 0$ holds, such that metric fluctuations have an anti-screening effect on the vacuum. Intuitively, f_g acts akin to a dimensional contribution to the gauge coupling, due to the linearity in g_Y. For $f_g > 0$, a similar contribution of the scale dependence of g_Y would be present in $d < 4$, where the Abelian hypercharge is canonically rel-

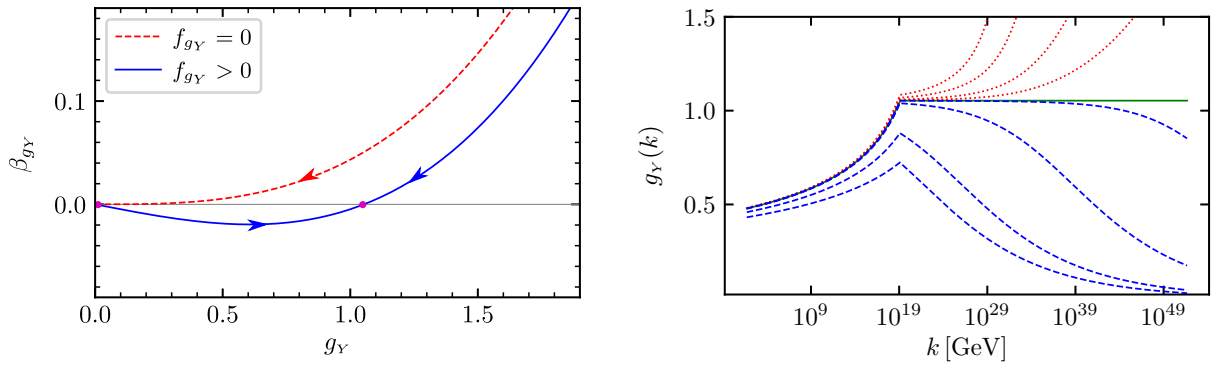

Fig. 4.1.: Left panel: The beta function for the Abelian hypercharge g_Y, see (4.3). In the absence of gravity (red dashed line) the GFP is IR-attractive, resulting in the presence of a Landau pole, cf. (4.2). Under the inclusion of asymptotically safe quantum gravity (blue, solid line), and with $f_{g_Y} > 0$, the GFP becomes UV-attractive, resulting in asymptotic freedom for g_Y. The presence of $f_{g_Y} > 0$ also gives rise to a NGFP.
Right panel: The scale dependent Abelian gauge coupling $g_Y(k)$ in the presence of $f_{g_Y} > 0$. The dashed blue trajectories emanate from the GFP and flow towards the IR attractive NGFP. The green solid line is the predictive trajectory, starting from the NGFP $g_{Y*} > 0$. Any trajectory that is above the predictive trajectory for any k is UV unsafe.

evant. Therefore, the gravitational contribution acts as an effective dimensional reduction. The GFP becomes UV attractive, and the Abelian gauge sector would be UV-complete, see Figure 4.1. Therefore, there are indications that the gauge coupling sees an effectively reduced dimension and becomes asymptotically free, in asymptotically safe quantum gravity [242, 297, 298, 300–302].

The gravitational contribution f_g is a function of the gravitational couplings. Below the Planck scale, gravity behaves classically, such that the dimensionless version of the Newton coupling G is approximately zero, such that $f_g \approx 0$ in this regime. Conversely, $f_g \approx$ const beyond the Planck scale, where the gravitational couplings assume their fixed-point values.

In summary, for sufficiently small values of g_Y, the gravitational contribution to β_{g_Y} dominates over the screening contribution from charged matter. Due to the anti-screening nature of metric fluctuations, any value of $f_g > 0$ is sufficient to reduce the effective dimensionality of g_Y to below four. Then, g_Y becomes asymptotically free, and quantum-gravitational contributions induce a UV-completion of the Abelian gauge sector.

If $f_g > 0$ holds, a second, NGFP $g_{Y*} > 0$ arises. At this NGFP the Abelian hypercharge becomes asymptotically safe and an irrelevant direction, see Figure 4.1. The IR value of the Abelian gauge coupling is then a prediction of the underlying UV complete theory, since irrelevant directions do not introduce free parameters into the system. The trajectory which leads to the predicted IR value of g_Y serves as an upper bound for UV-complete trajectories [298]: since g_Y is irrelevant at the NGFP, it attracts RG trajectories towards the IR. Trajectories with $g_Y(k) < g_{Y*}$ at some scale k, will lead to IR values for g_Y which are strictly smaller than the predicted IR value. Trajectories with $g_Y(k) > g_{Y*}$ at some scale k, will lead to IR values for g_Y which are strictly larger than the predicted IR value. Since those trajectories approach the NGFP from above, they cannot emanate from UV-complete theory, unless a third fixed point at larger values for g_Y exists, see Figure 4.1.

Intriguingly, the NGFP for g_Y predicts an IR value of the hypercharge, which is above the measured value, but might be compatible with it within estimated error bars of the predicted value [297, 298]. Therefore, asymptotically safe quantum gravity could induce a UV-completion of

the Abelian gauge sector, see also [302], which might even predict the IR value of the Abelian hypercharge. This predictive scenario has been investigated in [297–299, 309], and we study further consequences of the NGFP in Subsection 4.3.2 and Section 4.6.

For non-Abelian gauge couplings, the matter contribution $\#_{\text{matter}}$ is negative, which leads to asymptotic freedom for the strong coupling. Since the minimal coupling of gravity to matter does not distinguish between Abelian and non-Abelian gauge theories, the gravitational contribution f_g is the same for both theories. Hence, it leaves asymptotic freedom for non-Abelian gauge theories intact [301]. If $f_g > 0$, the logarithmic running of the non-Abelian gauge coupling is replaced by a power-law running at high energies.

4.1.2. Yukawa sector

In the Yukawa sector of the SM, the situation is similar to the Abelian gauge system. For the scale dependence of the Yukawa coupling y, it holds that $\#_{\text{matter}} > 0$, which leads to the presence of a Landau pole at finite scales.

The sign of the gravitational contribution to the Yukawa coupling depends on the fixed-point values of the gravitational couplings. There is a critical value Λ_{crit} of the cosmological constant, such that $f_y < 0$ for $\Lambda < \Lambda_{\text{crit}}$ [310–315]. Then, the GFP for the Yukawa coupling becomes relevant, inducing asymptotic freedom in the Yukawa sector. As for the Abelian gauge coupling, an anti-screening gravitational contribution, $f_y < 0$ gives rise to a NGFP, where the Yukawa coupling becomes irrelevant. Focussing on the Yukawa coupling of the top quark, this NGFP puts an upper bound on the mass of the top quark, which can be reached from the GFP $y_* = 0$. If the NGFP is realized, the IR value of the top mass would become a prediction of the UV-complete theory. Using gravitational beta functions obtained via the background field approximation [257, 316], $\Lambda < \Lambda_{\text{crit}}$ is indeed realized [310–315]. The predicted mass of the top quark agrees with the experimentally observed value, within an estimated lower bound on the error bars of the predicted value [317].

Combining this scenario with the realization of the predictive fixed point for the Abelian gauge coupling allows to predict the mass difference between the top and the bottom quark [299]. Taking more than one generation of Yukawa couplings into account, allows accommodating non-vanishing masses for the strange quark and the down quark, however, increasing the predicted value for the top mass [318].

For $\Lambda > \Lambda_{\text{crit}}$, the sign of f_y is positive, which enhances the Landau-pole problem, since the divergence of the Yukawa coupling is shifted to lower scales. The only possibility to make the Yukawa-sector UV-complete is to set $y = 0$ at all scales. This however would lead to vanishing quark-masses, which is incompatible with observations. Therefore, the parameter-region where $\Lambda > \Lambda_{\text{crit}}$ is excluded from the viable gravitational parameter space [315, 317]. The gravitational fixed points obtained in fluctuation computations lie in the regime where $\Lambda > \Lambda_{\text{crit}}$ [241]. It is an open question how non-vanishing quark masses can be obtained in fluctuation computations.

4.1.3. Scalar sector

The scalar sector of the SM features the scale dependent Higgs-quartic coupling λ_4. The matter contribution to the scale dependence of λ_4 is positive, i.e., $\#_{\text{matter}} > 0$. Therefore, also in the scalar sector the Gaussian fixed point is IR attractive.

Quantum fluctuations of the metric have an additional screening effect on the scalar coupling, i.e., $f_{\lambda_4} > 0$ [87, 89, 256, 312, 313, 319]. Additionally, if all other couplings in the SM

become asymptotically free, the scalar sector features a fixed-point, which is compatible with shift symmetry [315]. Therefore, quantum fluctuations of the metric flatten the scalar potential.

Since $f_{\lambda_4} > 0$, the scalar coupling λ_4 only features the Gaussian fixed point, which is IR attractive. Therefore, the only possibility to UV-complete the scalar sector, is to set $\lambda_{4*} = 0$. If the Yukawa and the Abelian gauge coupling also realize their Gaussian fixed points, $\lambda_4(k) \approx 0$ will hold until the Planck scale. There, non-vanishing contributions from matter-fluctuations induce a finite value for λ_4. Below the Planck scale, matter fluctuations will drive the scalar coupling towards larger positive values [320]. For Planck-scale values of the SM couplings that lead to their observed values in the IR, a Higgs mass in the vicinity of the observed value is reached [320]. Since the Gaussian fixed point for the scalar coupling is IR-repulsive, this value for the Higgs mass is a prediction of the theory. The exact value of the predicted Higgs mass strongly depends on the top mass.

When coupling the scalar sector of the SM to gravity, there is also a canonically marginal scalar curvature coupling $\xi\phi^2 R$. At its Gaussian fixed point, the non-minimal coupling can either be relevant or irrelevant, depending on the gravitational fixed-point values [87, 89, 256, 321, 322]. The non-minimal coupling ξ does not lead to qualitative changes of the fixed-point structure of the scalar-gravity theory. Specifically, the NGFP for the Yukawa coupling, which is necessary to accommodate massive fermions in the IR [317], remains intact in the presence of ξ [269].

The non-minimal scalar curvature coupling ξ is of phenomenological interest, since it could provide a mechanism for inflation. This mechanism, the so called Higgs-inflation, requires a particular ratio of the non-minimal coupling and the scalar quartic coupling. However, this ratio seems to be unachievable in an asymptotically safe scenario, at least in small truncations, see [269]. Hence, further mechanisms for inflation need to be tested for their compatibility with asymptotic safety.

4.1.4. Dark matter

There is plenty of experimental evidence that matter degrees of freedom exist, which are not included in the SM, see, e.g., [323–326]. Up to date, no viable candidate for these so-called dark matter degrees of freedom has been directly detected, see, e.g., [327] for an overview.

Within asymptotically safe quantum gravity, several models for dark matter have been tested for their compatibility with a fixed point for the gravity-matter system. In particular, models where the dark sector is coupled to the visible sector via a marginal Higgs-portal coupling between two visible and two dark scalars have been investigated, e.g., in [268, 319, 328–330]. However, unless shift symmetry for both scalar fields is broken, the portal coupling only features a Gaussian fixed point [269, 319]. A non-vanishing Higgs portal coupling is then generated along the flow towards the IR, where it modifies the flow of the quartic coupling of the visible scalar. If shift symmetry is broken in both scalar sectors, a non-vanishing fixed-point value for the Higgs-portal coupling is available. In this case the flow of the quartic coupling is modified more strongly. This modification results in a reduction of the prediction for the Higgs mass on the level of few percent [330].

The Higgs-portal coupling has been used to construct dark-matter models that are compatible with asymptotic safety in [268, 269, 328, 329]. Intriguingly, the predictive power of the fixed point also carries over to the dark-scalar sector, where all canonically marginal couplings become a prediction of the theory [268, 269].

Conclusion

Overall, the asymptotic-safety paradigm for quantum gravity and matter has passed several non-trivial consistency tests. The presented tests exploit our knowledge about matter at low energies. The fundamental theory is then constrained by demanding that the low-energy observables of the fundamental theory are in agreement with the measured values.

Furthermore, we have seen some examples, where the UV-complete theory actually fixes couplings in the matter sector to unique values. The corresponding low-energy values of those couplings would then be a prediction of the theory. If the experimentally determined value of the coupling disagrees with the prediction, the corresponding fixed-point is ruled out by observational consistency.

If the experimentally determined value agrees with the prediction, then the interplay of quantum gravity and matter predict parameters, which are free in the SM. Therefore, the gravity-matter interplay enhances the predictive power, even in the matter sector.

The gravity-matter interplay therefore provides a very powerful testing ground for asymptotically safe quantum gravity. We will present further consistency tests in the following.

4.2. The weak gravity regime of asymptotically safe quantum gravity

In the context of asymptotically safe quantum gravity, there are several arguments and observations in favor of a weakly coupled nature of quantum gravity.

Firstly, the SM is perturbative at the Planck scale. This allows for the possibility that the underlying UV-completion generating these values is at least near-perturbative. Indications that this scenario could indeed be realized in $d = 4$ have been discovered in [298, 299, 317, 319, 320], see also Section 4.1.

Secondly, from a conceptual point of view, a near-perturbative nature of asymptotically safe quantum gravity is preferred due to the controllability. In a near-perturbative setup, canonical power-counting remains a suitable guiding principle, which allows to set up approximations that capture the relevant physics. Indications for such a near-perturbative behavior have been found in $d = 4$ on the basis of the near-canonical scaling of higher-curvature operators [225, 227–229, 234], as well as due to the semi-quantitative agreement of vertex correlation functions [113, 229, 243, 266], see also Section 3.1.

Thirdly, the gravitational fixed point in asymptotically safe quantum gravity arises due to a balancing between canonical and quantum scaling. In non-gravitational systems featuring this mechanism, the NGFP can be traced back to a GFP in the critical dimension. This might allow recovering the asymptotically safe fixed point from a Padé-resummation of the ϵ-expansion around the critical dimension, which can be computed perturbatively. Fourthly, there are explicit indications for the asymptotically safe fixed point from one-loop perturbation theory [331, 332].

Specifically in asymptotically safe quantum gravity, there is another reason in favor of a weakly coupled regime of quantum gravity: there are indications that metric fluctuations have to remain small enough to allow for a UV complete theory [333]. Beyond the weak-gravity regime, they can trigger new divergences in higher-order matter interactions. This happens, since the interacting nature of quantum gravity percolates into the matter sector and induces all matter-interactions which are allowed by the symmetries of the system [302, 314, 315, 333, 334], see also [335].

The fixed-point values of these induced interactions remain small in the weak-gravity regime.

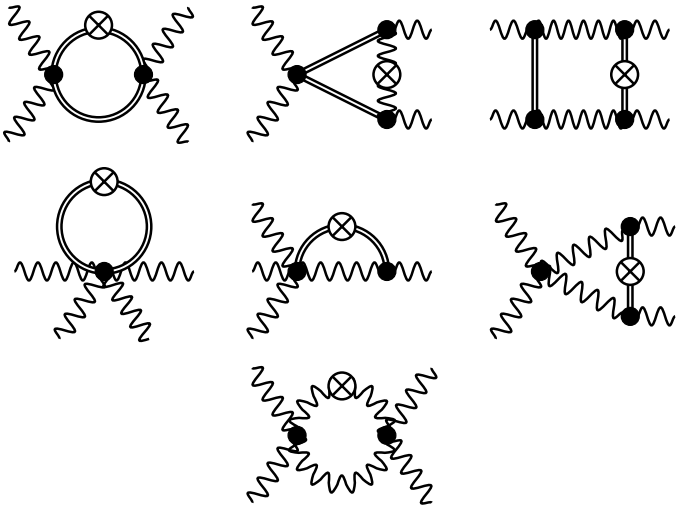

Fig. 4.2.: Diagrams that contribute to the scale dependence of four-gauge-field couplings κ_2 and w_2. Double lines indicate metric fluctuations, wavey lines indicate Abelian gauge fields. The regulator insertion, which is indicated by the cross, is understood to appear on each of the different internal lines. The first line shows inducing contributions, i.e., contributions to A_0 in (4.4).

This is a consequence of gravity shifting the GFP into a NGFP. The critical exponents of these gravitationally shifted Gaussian fixed points (sGFP) are close to the canonical mass dimension.

Beyond the weak gravity regime, however, the induced fixed-point values grow, and the critical exponents deviate strongly from the canonical dimension. Eventually gravity can shift the NGFP into the complex plane. The regime, where the would-be fixed point is complex valued, is phenomenologically not viable, since the theory is not UV complete there. The so-called *weak gravity bound* (WGB) [302, 314, 315, 333, 334] separates the phenomenologically viable from the excluded region.

We will now focus on the Abelian gauge sector and review the mechanism giving rise to the WGB in a simple toy model in more detail, see Subsection 4.2.1. In Subsection 4.2.2, we will extend the system and discuss the complete basis of linearly independent self-interactions of the Abelian gauge field, at the level of dimension 8-operators. In Subsection 4.2.3, we will compare the WGB of different systems, indicating that the excluded strong-gravity regime is in qualitative agreement in each of the investigated sectors.

4.2.1. Example: the Abelian gauge sector

Starting with a standard kinetic term of the gauge field, metric fluctuations will for example induce interactions of the form $w_2(F^2)^2$. In the presence of gravitational interactions, a graviton loop generates a non-vanishing flow, even at $w_2 = 0$, indicating that the coupling w_2 is induced and cannot be consistently turned off.

Schematically, the scale dependence of w_2 is given as [302]

$$\beta_{w_2} = A_{0,w_2}(G) + w_2\, A_{1,w_2}(G) + w_2^2\, A_{2,w_2}\,, \tag{4.4}$$

where the coefficients A_{0,w_2} and A_{1,w_2} depend on the gravitational couplings. The w_2-independent contribution vanishes without gravity, such that $A_{0,w_2} \to 0$ as $G \to 0$. This can be intuitively understood from the diagrammatic representation of β_{w_2}, which is shown in Figure 4.2.

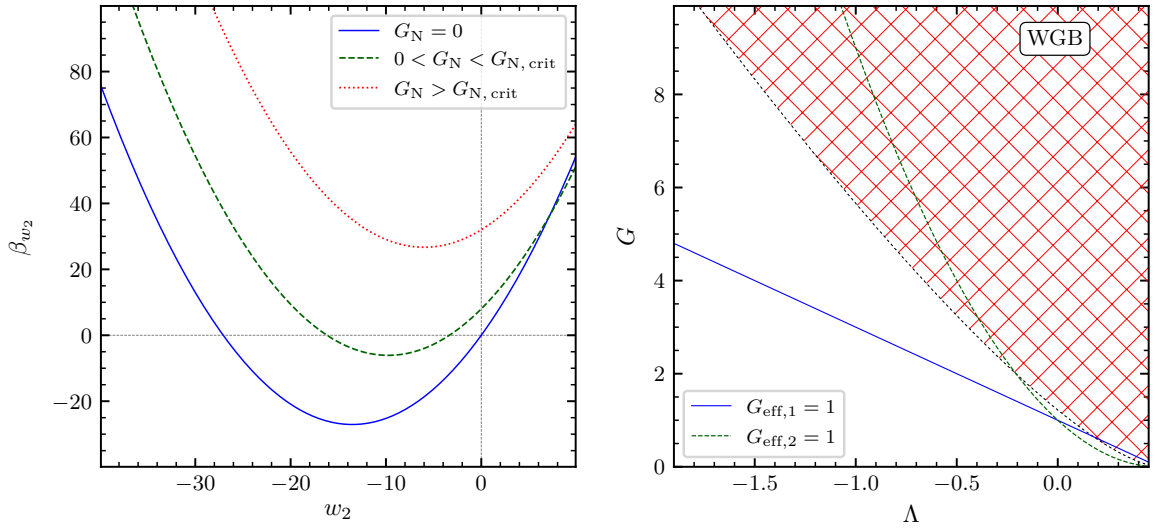

Fig. 4.3.: Left panel: Scale dependence of the induced interaction w_2. In the absence of gravity (blue solid line), it features a GFP and can be consistently set to zero. Small enough metric fluctuations (green dashed line) induce a non-vanishing interaction w_2, until they become too strong and induce new divergences in the gauge sector (red dotted line). Right panel: the red hatched region marks the excluded strong gravity regime in the gravitational parameter-space, see also [302]. We indicate the lines of constant effective gravitational coupling $G_{\mathrm{eff},n}$, see (4.7), towards which direction in the G-Λ plane gravity becomes stronger.

The diagrams in the first line encode the w_2-independent contribution A_{0,w_2}. Since all those diagrams contain a graviton propagator, their contribution vanishes, if gravity is decoupled.

Therefore, if gravity is absent, i.e., if $G = 0$, then $w_{2*} = 0$ is a fixed point of the system, such that it can consistently be turned off, cf. the blue line in Figure 4.3. If however $G \neq 0$, the diagrams shown in the first line of Figure 4.2 are in general non-vanishing and induce a coefficient $A_{0,w_2} \neq 0$. Then, the GFP for $G = 0$ is shifted away from zero (green line in Figure 4.3), due to the presence of gravitational interactions. In this case, both fixed points become interacting and are given by

$$w_{2*} = \frac{-A_{1,w_2} \pm \sqrt{A_{1,w_2}^2 - 4A_{0,w_2}\,A_{2,w_2}}}{2A_{2,w_2}}\,, \tag{4.5}$$

which has only real solutions if [302]

$$A_{0,w_2}\,A_{2,w_2} \leq \frac{A_{1,w_2}^2}{4}\,. \tag{4.6}$$

This condition can be re-expressed as a bound on the gravitational coupling G. Beyond the bound (red line in Figure 4.3), the induced interaction does not feature a real fixed-point. Therefore the theory becomes UV incomplete, which excludes this region from the viable gravitational parameter space.

In the right panel of Figure 4.3, we schematically show this excluded region beyond the WGB for the case of the induced coupling w_2, as red region, see also [302]. The WGB separates the viable gravitational parameter space from the excluded strong-gravity regime.

To get an intuition for the WGB and its shape in the plane of gravitational couplings, it is

convenient to parametrize the effect of quantum gravity via effective gravitational couplings

$$G_{\text{eff},\,n} = \frac{G}{(1-2\Lambda)^n}\,. \tag{4.7}$$

In our approximation, these effective couplings determine how strongly gravity affects the matter system. The effective gravitational couplings can increase in two ways: i) increasing the Newton coupling G, while keeping Λ fixed, or ii) shifting $\Lambda \to \frac{1}{2}$ pole, while keeping G fixed. The coefficients A_{0,w_2} and A_{1,w_2} are functions of $G_{\text{eff},\,1}$ and $G_{\text{eff},\,2}$, while A_{2,w_2} is independent of gravitational contributions, which can be understood from the diagrammatic representation Figure 4.2. Depending on the combination of signs in the coefficients A_{0,w_2} and A_{1,w_2}, the condition (4.6) might be valid everywhere, or be violated in the strong gravity regime.

For the coupling w_2, the excluded region is shown in Figure 4.3. There, we also show the lines of $G_{\text{eff},\,1} = 1$ and $G_{\text{eff},\,2} = 1$. This shows that the excluded region indeed is a strong-gravity regime. It further shows that either of the two effective gravitational couplings is suitable to intuitively understand the gravitational effect on the matter sector.

We have introduced the WGB by focusing on the Abelian gauge sector as an explicit example [302]. The WGB arises, since gravity induces matter self-interactions, which are compatible with the symmetries of the system. Specifically, gravity only induces interactions which are compatible with all internal global and local symmetries, see [334]. Depending on the specifics of the scale dependence, i.e., on the coefficients A_i in (4.6), an excluded strong gravity regime might arise. Indeed, this excluded regime has also been discovered in the scalar sector [333, 334], and in the Yukawa sector [314, 315]. In the fermion sector, no indications for a WGB were found [336].

4.2.2. Induced interactions in the Abelian gauge sector

For simplicity, the previous argument was performed based on one single coupling. Let us now investigate the full tensor structure at this level in the canonical mass dimension in more detail. For this, we approximate the dynamics of the Abelian gauge sector by

$$\Gamma_k^{U(1)} = \Gamma_k^{U(1),\,\text{kin}} + \Gamma_k^{U(1),\,\text{int}}\,, \tag{4.8}$$

where $\Gamma_k^{U(1),\,\text{kin}}$ is the standard kinetic term of the gauge field including gauge-fixing,

$$\Gamma_k^{U(1),\,\text{kin}} = \frac{Z_A}{4}\int \mathrm{d}^4x\sqrt{g}\, g^{\mu\rho}\, g^{\nu\kappa}\, F_{\mu\nu}\, F_{\rho\kappa} + \frac{1}{\xi}\int \mathrm{d}^4x\sqrt{\bar{g}}\, \left(\bar{g}^{\mu\nu}\, \bar{D}_\mu\, A_\nu\right)\,, \tag{4.9}$$

and where $\Gamma_k^{U(1),\,\text{int}}$ contains

$$\Gamma_k^{U(1),\,\text{int}} = \frac{k^{-4}}{8}\int \mathrm{d}^4x\sqrt{g}\, \left(w_2\,(g^{\mu\rho}\, g^{\nu\kappa}\, F_{\mu\nu}\, F_{\rho\kappa})^2 + \kappa_2\,(g^{\mu\rho}\, g^{\nu\kappa}\, F_{\mu\nu}\, \tilde{F}_{\rho\kappa})^2\right)\,, \tag{4.10}$$

where Z_A is the gauge-field wavefunction-renormalization and ξ is the gauge-fixing parameter, which we will fix to $\xi \to 0$ in the following. Furthermore, w_2 and κ_2 are the dimensionless couplings corresponding to the only independent gauge-invariant interactions at this level in canonical mass dimension, and $F_{\mu\nu}\,\tilde{F}^{\mu\nu}$ are the field-strength tensor and the dual field-strength tensor, respectively, given by

$$F_{\mu\nu} = D_\mu A_\nu - D_\nu A_\mu\,, \qquad \tilde{F}^{\mu\nu} = \frac{1}{2}\epsilon^{\mu\nu\rho\sigma}F_{\rho\sigma}\,. \tag{4.11}$$

In the gravitational sector, we approximate the dynamics by the Einstein-Hilbert action $\Gamma_{k,\,\mathrm{EH}}$ (3.16), with scale-dependent counterparts and dimensionless counterparts G and Λ of the Newton coupling and the cosmological constant, respectively.

The general scale dependences of w_2 and κ_2 are rather complicated. For the present discussion, let us therefore focus on $\Lambda = 0$, and on the choice $\beta_h = 1$ for the graviton gauge fixing. In this case, the scale dependence for w_2 and κ_2 read

$$\beta_{w_2} = 8G^2 - G\frac{\kappa_2}{\pi} + \frac{\kappa_2^2}{6\pi^2} + w_2\left(\frac{5\kappa_2}{12\pi^2} - \frac{7G}{2\pi} + 4\right) + \frac{35w_2^2}{24\pi^2}\,, \tag{4.12}$$

$$\beta_{\kappa_2} = -8G^2 - G\frac{7w_2}{6\pi} - \frac{w_2^2}{24\pi^2} + \kappa_2\left(\frac{11w_2}{12\pi^2} - \frac{25G}{6\pi} + 4\right) + \frac{\kappa_2^2}{8\pi^2}\,, \tag{4.13}$$

where the first three contributions to β_{w_2} and β_{κ_2} are the inducing terms. Due to the first contribution in each beta function, both couplings are induced by gravity individually. Furthermore, both couplings induce each other, which is expected, since the operators share the same symmetries.

In the previous subsection, we have discussed the case where $\kappa_2 = 0$ was assumed. We have seen that in this case, there is a WGB, where the sGFP for w_{2*} vanishes into the complex plane, cf. Figure 4.3. We can indeed see from (4.12), and with $\kappa_2 = 0$, that the condition for the existence of a real fixed-point (4.6) is satisfied for small values of G. It will not be satisfied beyond $G \approx 1.2$.

Let us now focus on the opposite case, where we set $w_2 = 0$. From (4.13) we infer that the inducing coefficient, A_{0,κ_2}, is negative. Furthermore, the quadratic coefficient is positive, such that β_{κ_2} always features two real-valued fixed points, since the analogue of the condition (4.6) is satisfied for any value of G. Therefore, a truncation which only included the coupling κ_2 would not find a WGB in the system.

The situation is reversed, for a different choice of the gravity gauge-fixing parameter, for example for $\beta_h = -2$. In this case, A_{0,w_2} is negative. Since the quadratic coefficient A_{2,w_2} is the contribution from matter fluctuations, it is independent of β_h, and therefore always positive, cf. (4.12). Hence, for this choice for β_h, the coupling w_2 does not feature a WGB. In the same gauge, the coefficient A_{0,κ_2} has also changed the sign, and is now negative. Specifically, we find that $A_{0,\kappa_2}\big|_{w_2=0} = -A_{0,w_2}\big|_{\kappa_2=0}$ for all values of β_h. Hence, for $\beta_h = -2$ the coupling κ_2 features a WGB. The above argument neglected the back-coupling of w_2 into β_{κ_2} and vice-versa. As long as the fixed-point values for the induced interactions remain small, this approximation allows to analyse the qualitative features also of the coupled system.

This highlights that it might be crucial to consider the full set of operators at a given order in the canonical mass dimension. It is also encouraging that the qualitative features of the full system do not depend on the gauge: while each of the operators individually lead to β_h-dependent conclusions on the existence of a WGB, the full system always features a WGB. Therefore, the physical information, namely that a strongly coupled regime of quantum gravity appears to be incompatible with a UV-complete Abelian gauge sector might be gauge-independent.

We will now focus on $\beta_h = 1$ again. In the left panel of Figure 4.4 we show the values of the sGFP for the full system (4.10) as a function of G. The fixed-point values vanish at $G = 0$, and their absolute values increase when increasing the gravitational coupling. At $G \approx 1.4$, the fixed point collides with another fixed point and vanishes into the complex plane. After the collision, the absolute values of the imaginary parts increase monotonically, indicating that the fixed point is pushed further into the complex plane.

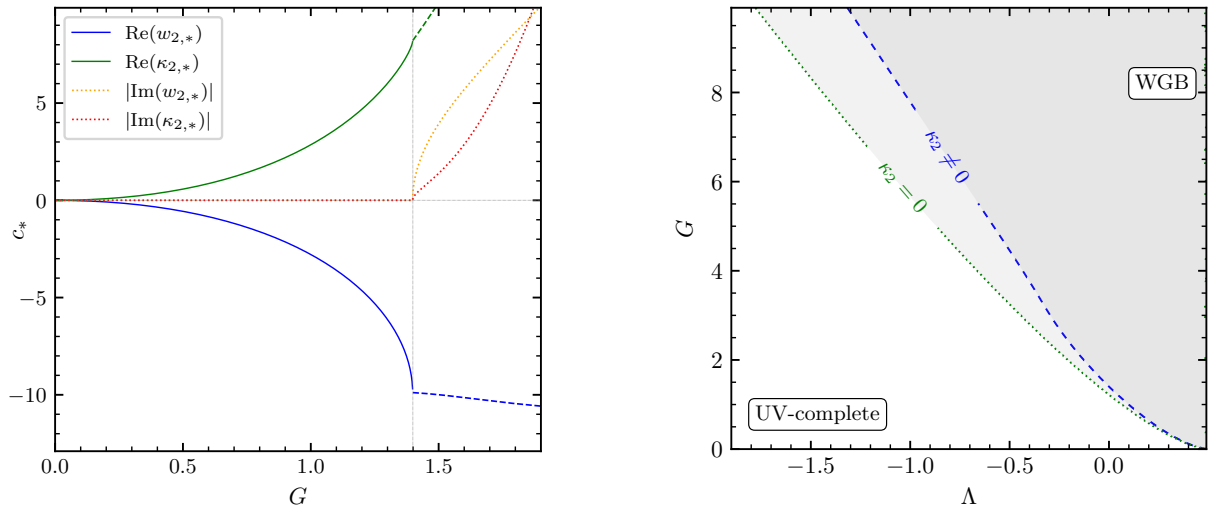

Fig. 4.4.: Left panel: We show the fixed-point values of the sGFP for the two induced interactions w_2 and κ_2 as a function of the Newton coupling G, and at $\Lambda = 0$, cf. (4.12) and (4.13). At the vertical line, the fixed point vanishes into the complex plane. Beyond that value of G, we show the real part of the would-be fixed point as dashed lines, and the imaginary part as dotted lines.
Right panel: We show the region where the sGFP lies in the complex plane. The grey regions indicate the excluded strong-gravity regime, where strong metric fluctuations induce new divergences in the matter sector. The blue dashed line indicates the WGB for the full system (4.10). For comparison, the green dotted line indicates the WGB for the system that only contains the F^4 operator.

In the right panel of Figure 4.4 we show the WGB in the plane spanned by Λ and G, which parametrize the gravitational dynamics in our approximation. The blue (dashed) line shows the WGB of the full system, including both induced couplings w_2 and κ_2. In the grey region, the sGFP is complex-valued. This indicates the presence of new divergences in the Abelian gauge sector, and excluded this region from the viable parameter space of asymptotically safe quantum gravity.

As a comparison, the green (dotted) line shows the WGB, if only the coupling w_2 is included in the truncation. Therefore the green line, and the corresponding grey region is the same region as shown in Figure 4.3, see also [302]. We see that the inclusion of the second linearly independent induced self-interaction of Abelian gauge fields changes the WGB on a quantitative level. The full system still features a WGB, but it has shifted towards larger values of the effective gravitation coupling $G_{\text{eff},n}$. Therefore, the inclusion of κ_2 stabilizes the system in the sense that, for fixed G and Λ, κ_2 drives the system away from a fixed-point collision.

In summary, the investigation of the full set of induced couplings might be crucial, since the presence of an excluded strong gravity regime for individual couplings is gauge-dependent. Within our approximation, the WGB does not exists for all choices of the gauge-fixing parameter β_h, if only one of the two independent couplings is considered. However, we find indications that the coupled system of both couplings features a WGB for a larger range of values for β_h.

In the Abelian gauge sector, and for $\beta_h = 1$, the inclusion of the second induced coupling κ_2 only changes the WGB on a quantitative level. The inclusion of κ_2 stabilizes the system and pushes the WGB into a more strongly coupled regime. Therefore, there is more parameter-room available for a UV-complete Abelian gauge sector, than one would estimate from a truncation that only included the F^4 operator.

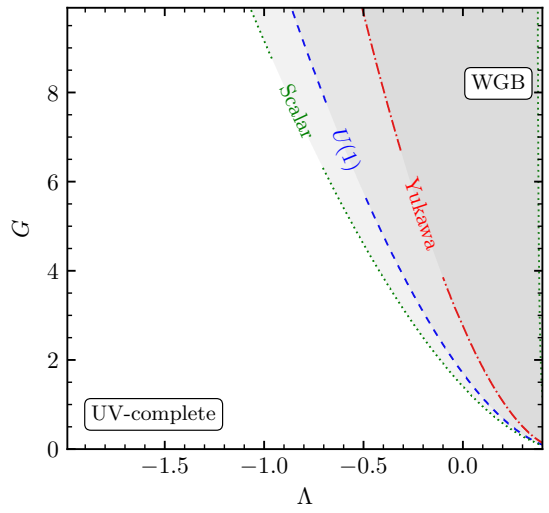

Fig. 4.5.: We show the individual WGB from different induced matter interactions, cf. (4.15). The red (dashdotted) line indicates the WGB of Yukawa-like interactions [315], the blue (dashed) line indicates the WGB of the Abelian F^4 interaction [302], and the green (dotted) line indicates the WGB for scalar self-interactions [333, 334]. We do not consider the back-reaction between the different sectors.

In the fermionic sector, the self-stabilization of the system is even stronger [336]: neglecting one of the two independent four-fermion operators would lead to a WGB for the coupling λ_+. However, if both induced four-fermion interactions are taken into account, the system does not feature a WGB [336], see also Section 4.5.

4.2.3. Comparison of different matter systems

Since different matter sectors feature a WGB independently, let us now compare its location in the gravitational parameter space. Specifically, we compare the WGB in the scalar [333, 334], the Yukawa [314, 315], and the gauge sector [302]. For completeness, the dynamics of the matter system is therefore approximated by

$$\Gamma_k^{\text{matter}} = \Gamma_k^{\text{Scalar}} + \Gamma_k^{\text{Yukawa}} + \Gamma_k^{U(1)}\,, \tag{4.14}$$

where we set $\kappa_2 = 0$ in $\Gamma_k^{U(1)}$, see (4.10), and where

$$\begin{aligned}\Gamma_k^{\text{Scalar}} =& \frac{Z_\phi}{2}\int \mathrm{d}^4x\sqrt{g}\, g^{\mu\nu}\partial_\mu\phi\partial_\nu\phi + \frac{k^{-4}g}{8}\int \mathrm{d}^4x\sqrt{g}\, g^{\mu\nu}g^{\kappa\lambda}\partial_\mu\phi\partial_\nu\partial_\kappa\phi\partial_\lambda\phi\,,\\ \Gamma_k^{\text{Yukawa}} =& iZ_\psi\int \mathrm{d}^4x\sqrt{g}\,\bar\psi\not{\nabla}\psi + i\,k^{-4}\int \mathrm{d}^4x\sqrt{g}\big[\chi_1\left(\bar\psi\gamma^\mu\nabla_\nu\psi - (\nabla_\nu\bar\psi)\gamma^\mu\psi\right)\left(\partial_\mu\phi\partial^\nu\phi\right)\\ &+\chi_2\left(\bar\psi\gamma^\mu\nabla_\mu\psi - (\nabla_\mu\bar\psi)\gamma^\mu\psi\right)\left(\partial_\nu\phi\partial^\nu\phi\right)\big]\,,\end{aligned} \tag{4.15}$$

with the dimensionless couplings g, χ_1, χ_2. The beta functions for g is taken from [334], and for χ_1 and χ_2 from [315]. The scale dependence for w_2 is given in Section C.1, where we chose $\beta_h = 0$ for consistency with the gauge choice in the other sectors.

In Figure 4.5, we show the individual WGB for each of the sectors. In each sector, we employ a perturbative approximation, where the anomalous dimensions coming from the regulator insertions are neglected. For this first comparison, we do not take the back-reaction between different sectors into account, i.e., we neglect for example the contribution from χ_1 and χ_2 to the scale dependence of g. We see that the excluded regions from all three individual systems are

in qualitative agreement. This indicates that gravity acts similarly on different matter sectors. The comparison suggests that the qualitative features of the excluded region of the fully coupled system might already be estimated from the individual systems. Furthermore, it suggests that potentially excluded regions, which arise due to canonically more irrelevant operators also behave qualitative similarly between different sectors.

4.3. Effective asymptotic safety and pseudo fixed-points

Until now, we have discussed the presence of NGFPs in the context of a UV-complete theory of quantum gravity and matter. In the following section, we will investigate the presence of fixed points as attractors of the RG-flow in a general theory space. For this purpose, we describe quantum gravity and matter beyond the Planck scale as a quantum field theory. However, this quantum field theory might break down at some scale in the far UV, where a more microscopic theory sets in.

Since the fundamental description of spacetime is unknown to date, it is intriguing to investigate, which UV-completions of the universe are compatible with one another. As a first step in that direction, we investigate which fundamental descriptions of spacetime can be connected to the IR via an intermediate asymptotically safe scaling regime. A second motivation for such a scenario is the question of unitarity in asymptotic safety: the asymptotically safe fixed-point regime only has to be free of unitarity violations below the cutoff scale in the far UV. Above that scale, the fundamental description of spacetime is expected to be unitary.

We will now introduce and discuss a generalization of the scenario of *effective asymptotic safety* in more detail. In effective asymptotic safety, the asymptotically safe fixed point serves as an IR-completion of a fundamental theory, since it attracts trajectories towards the IR, and connects them with a viable IR regime. Via this IR-completion, the fundamental theory could inherit the predictive power of the asymptotically safe fixed point. As one specific example for a more fundamental UV-completion, we investigate whether effective asymptotic safety and a fundamental theory described by string theory can be compatible with each other. For different scenarios where the idea of effective asymptotic safety is employed, see, e.g. [5, 269, 337, 338], as well as Section 4.6.

4.3.1. Main Idea

Instead of having a UV-completion given by an asymptotically safe fixed point, we will broaden our viewpoint and take the perspective of an effective-field theory with a finite, high-energy cutoff k_{UV}. At k_{UV} a quantum field description emerges from the fundamental theory, which sets the initial conditions for the RG-flow towards the IR. These initial conditions are given in terms of the values of the couplings at k_{UV}. In this context, if the fundamental theory was described by an asymptotically free or safe fixed point, the initial conditions would correspond to the values of the relevant couplings at the high energy scale k_{UV}.

If a quantum-field theoretic description features an instability at a physical scale M_{g}, this scale serves as a cutoff for the quantum field theory which indicates the need for a more microscopic description. The more microscopic theory is expected to be free from instabilities at M_{g}. The scale M_{g} can for example be related to the mass-scale of ghosts or kinetic instabilities. We will assume that the physical cutoff scale M_{g} can be translated into a RG cutoff scale k_{UV} of the same order. Only below this scale k_{UV} the RG flow in terms of the effective quantum-field theoretic degrees of freedom accurately describes the dynamics of the system.

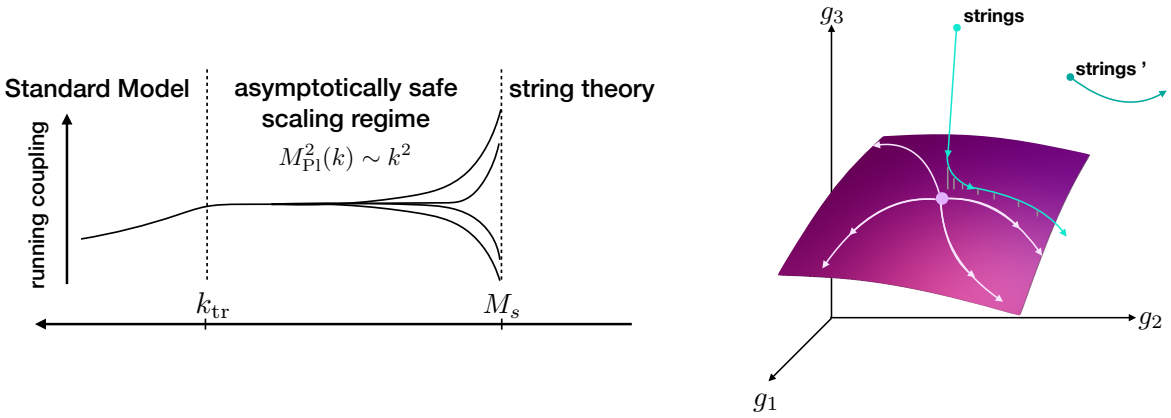

Fig. 4.6.: Left panel: Illustration of the scenario of effective asymptotic safety for the explicit example studied in Subsection 4.3.2, where the fundamental description is given in terms of string theory. Below the string scale M_s, a quantum-field theoretic description emerges, and the theory enters an intermediate asymptotically safe scaling regime. This scaling regime can result in universal predictions for couplings, for a large range of initial conditions at the string scale M_s. At the scale $k_{\rm tr}$, relevant operators drive the flow away from the scale-invariant point.
Right panel: Sketch of a three-dimensional theory-space with an asymptotically safe fixed point (light purple). The purple plane illustrates the UV critical surface of the fixed point. Its IR critical surface is a line that goes through the fixed point, and the cyan point. A string model that provides initial conditions on this line results in an effective QFT description that closely approaches the fixed point, until the RG trajectory leaves the fixed-point regime. At this scale, the effective QFT description of the string model is very close to the UV critical surface. A different model (strings') that sets the initial conditions for an effective QFT description away from the IR critical surface is not attracted to the UV critical surface.

An IR-attractive direction in theory space serves as an attractor towards the IR, if the initial condition for the coupling lies within its basin of attraction. Accordingly, those couplings will approach the fixed-point values of the IR-attractive directions as a function of $k < k_{\rm UV}$. At the Planck scale, the fixed-point values of irrelevant couplings are therefore approximately realized. From there, the effect of quantum gravity switches off dynamically, and the couplings flow according to their canonical mass dimension. The key idea of this scenario is summarized in Figure 4.6, where it is applied to an explicit candidate for a fundamental theory.

Let us now discuss the notion of IR attractors in terms of fixed points and pseudo fixed points in more detail. For this, let us consider some coupling ζ, whose scale dependence schematically reads

$$\beta_\zeta = b_0 + b_1\,\zeta + b_2\,\zeta^2\,, \tag{4.16}$$

where the coefficients b_i are functions of other, including relevant couplings. Let us first assume that the coefficients b_i are real and constant as a function of the RG-scale k. Clearly, ζ features two fixed points, at

$$\zeta_{*,\,1/2} = \frac{-b_1 \pm \sqrt{b_1^2 - 4b_0b_2}}{2b_2}\,, \qquad \text{with} \qquad \Theta_{1/2} = \mp\sqrt{b_1^2 - 4b_0b_2}\,, \tag{4.17}$$

where $\Theta_{1/2}$ are the critical exponents of the fixed points. The sign of the critical exponent encodes whether a fixed point acts as an attractor or repulser of the flow towards the IR. A negative

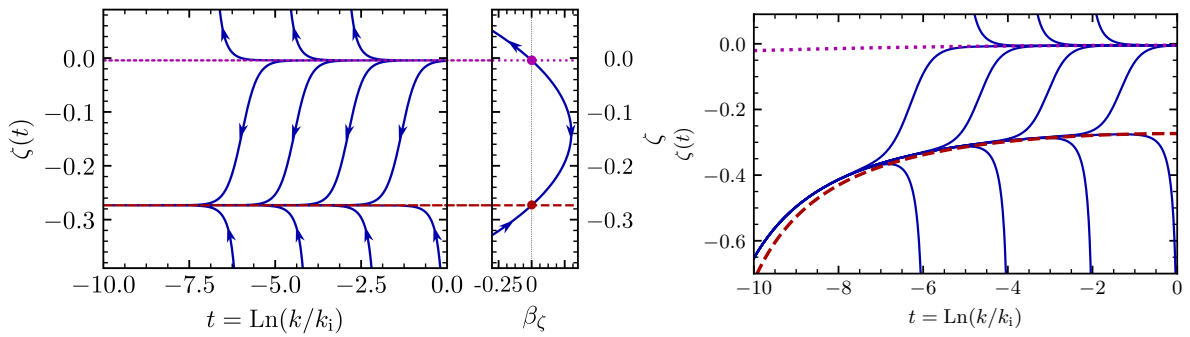

Fig. 4.7.: Left panel: We show the beta function and the RG-flow for the coupling ζ, for a specific values of the coefficients b_i in (4.16), see (4.61) for $G_{\rm N} = 1$, $a_1 = \Lambda = 0$, and $k_2 = k_0 = 1$. The magenta dotted line indicates the IR repulsive fixed point. The red dashed line indicates the IR attractive fixed point. The blue solid lines indicate sample RG trajectories obtained via a variation of the initial condition $\zeta(k_{\rm in})$, and the arrows indicate the flow towards the IR. RG-trajectories specified by initial conditions above the magenta line will be driven away from the IR -repulsive fixed point towards the IR, leading to large values of the coupling at low energies. RG-trajectories specified by initial conditions below the magenta line will be focused around the red dashed line towards the IR. Right panel: We show the flow for the case where the coefficients b_i are scale dependent, see (4.61), with $G_{\rm N} = 1$, $a_1 = \Lambda = 0$, and $k_0 = 1 - t^2/20$, and $k_2 = 1$. As a consequence, the zeros of β_ζ (magenta dotted and red dashed line) are scale dependent. These lines approximate the attractors/repulsers of the flow.

critical exponent indicates that the distance to the corresponding fixed point decreases towards the IR, such that the coupling is attracted by this fixed point. In contrast, if the critical exponent is positive, the distance of the coupling from the fixed point increases towards the IR. This behavior is summarized in the left panel of Figure 4.7: The fixed point with $\Theta < 0$ (red dashed line) acts as an IR attractor of RG trajectories shown as blue solid lines. The fixed point with $\Theta > 0$ (magenta dotted line) acts as an IR repulser of RG trajectories. As a consequence, there are two crucial observations based on the simplified example given by (4.16) and shown in Figure 4.7: First, the IR repulsive fixed point $\zeta_{*,2}$ separates all possible initial conditions into two regions. For the example shown in Figure 4.7, any initial condition with $\zeta(k_{\rm in}) \geq \zeta_{*,2}$ is disconnected from any value $\zeta(k) < \zeta_{*,2}$ along the RG-flow. Any initial condition with $\zeta(k_{\rm in}) < \zeta_{*,2}$ is connected to values at $\zeta(k) < \zeta_{*,2}$, and is within the basin of attraction of $\zeta_{*,1}$. In this sense, the IR repulsive fixed point shields a set of UV initial conditions from the second fixed point. Furthermore, trajectories starting at $\zeta(k_{\rm in}) > \zeta_{*,2}$ will be driven towards large values of ζ, when lowering the RG scale.

Second, the IR attractive fixed point $\zeta_{*,1}$ focuses trajectories. Therefore, except for initial conditions $\zeta(k_{\rm in}) \geq \zeta_{*,2}$, a large range of initial conditions for ζ at $k_{\rm in}$ will be focused around $\zeta_{*,1}$ at lower scales.

Let us now generalize to a scenario where the coefficients b_i in (4.16) are scale dependent. This can for example happen, when some couplings of the system are scale dependent themselves and did not reach a scale invariant regime yet. Then, the fixed points $\zeta_{*,1/2}$ become scale-dependent pseudo fixed-points $\zeta_{*,1/2}(k)$: they still solve $\beta_\zeta = 0$, but they are no longer related to a scale-invariant regime of the theory. $\zeta_{*,1/2}(k)$ are no longer the attractors or repulsers of the flow towards the IR. Instead, in the presence of a residual scale dependence of the system, a pair of related points $\tilde{\zeta}_{*,1/2}(k)$ are the attractors or repulsers of the flow. The expression for these points $\tilde{\zeta}_{*,1/2}(k)$ is rather involved, but they can be seen when plotting specific trajectories

for $\zeta(k)$: The red dashed line in the right panel of Figure 4.7 shows the IR-attractive pseudo fixed-point $\zeta_{*,1}(k)$. The blue solid line close to the pseudo fixed point is the actual attractor of RG-trajectories.

The effectiveness of the scale-dependent attractors depends on the speed of the flow, i.e., on the pseudo critical exponents $\Theta_{1/2}(k)$, compared to the residual scale dependence of $\zeta_{*,1/2}(k)$.

If the pseudo critical exponents are small compared to the residual scale dependence of $\zeta_{*,1/2}(k)$, the flow of $\zeta(k)$ will not follow the IR attractive fixed point. As a consequence, the value of $\zeta(M_{\rm Pl})$ will strongly depend on the scale dependence of the relevant couplings, and on the initial conditions.

If the pseudo critical exponents are sufficiently large, the flow of $\zeta(k)$ will easily follow the IR attractive fixed point, cf. Figure 4.7. Accordingly, a large range of initial conditions at high scales is focused around the IR attractive fixed point, and follows it towards lower energies. As a result, those trajectories will be mapped onto a small interval around the pseudo fixed point at the Planck scale. This is the solution to $\beta_\zeta = 0$ with all scale dependent couplings set to their Planck-scale values. As a consequence, the entire history, i.e., the scale dependence of the relevant couplings above the Planck scale is washed out.

In summary, the scenario described above allows to connect a more fundamental theory, which can be described by effective quantum-field-theoretic degrees of freedom below a trans-Planckian scale $k_{\rm UV}$, with the IR. Due to the approximate realization of the asymptotically safe fixed point, much of the predictive power of the latter carries over to this scenario. It is realizable under the following conditions:

1. A quantum field theoretic description of gravity and matter remains valid below $k_{\rm UV}$ and above the Planck scale.

2. The rate of change of the pseudo fixed point for the irrelevant couplings is smaller than the speed of the flow towards the pseudo fixed point. This criterion can be checked explicitly for a given system and has to hold for some scales k above $M_{\rm Pl}$.

3. The initial conditions for all couplings at the scale $k_{\rm UV}$ have to lie close to the instantaneous IR-critical hypersurface of the asymptotically safe pseudo fixed point at that scale.

The IR-critical hypersurface of a fixed point is defined as those initial conditions at high scales, that will approach the fixed point towards lower scales. As one explicit example, the IR-critical hypersurface of the fixed point shown in Figure 2.1 is the straight red line passing through the fixed point (magenta dot). An initial condition close to that line will be pulled towards the UV-critical hypersurface (green plane) towards lower scales. This feature persists in the generalized picture and in the presence of a pseudo fixed point, if condition 2. is satisfied. See also the right panel of Figure 4.6 for an explicit scenario. Therefore, the last condition ensures that the asymptotically safe (pseudo) fixed-point is approximated towards the IR.

In a more specific version of the described scenario, one assumes the presence of a fixed point, instead of a pseudo fixed-point. In this case, condition 2. is automatically satisfied. This specific case is called *effective asymptotic safety* in the literature [5, 6, 269, 337, 338].

In the context of the discussion of unitarity in asymptotically safe quantum gravity, the embedding of a regime of effective asymptotic safety into a more fundamental theory allows for a less strict interpretation of additional poles in the propagators of the theory: even if the graviton propagator features poles associated to the existence of ghost-states, the theory does not suffer from unitarity violations, if the associated mass scale lies beyond the cutoff $k_{\rm UV}$. Put differently, the presence of instabilities or unitarity-violating modes indicates the breakdown of

the description at the associated scale. In this way, the embedding of the asymptotically safe fixed point as an intermediate regime between a more fundamental theory and the IR, allows to take advantage of the predictive power of the IR -attractive directions of the fixed point, and at the same time circumvents the question of fundamental unitarity in the presence of potential fake-ghosts.

In the following, we will follow [6] and focus on this scenario and investigate the compatibility of string theory at high energies with an intermediate regime of effective asymptotic safety. We will first discuss some general prerequisites for both scenarios to be reconciled. More specifically, we will then investigate, whether the asymptotically safe fixed point lies in the swampland or the landscape of string theory [339], see also [340], and [341] for a review. As one criterion, we will focus on the weak-gravity conjecture [342] and study the constraints this conjecture imposes on asymptotically safe gravity-matter systems.

4.3.2. Example: The asymptotic-safety string-theory connection

To investigate the compatibility between string theory and an asymptotically safe scaling regime, we will first derive conditions on the relation between the string scale $M_{\rm s}$ and the transition scale $k_{\rm tr}$, which marks the end of the asymptotically safe scaling regime. In the present setup, the string scale plays the role of the scale $k_{\rm UV}$, where a quantum field-theoretic description emerges from string theory. Conversely, $k_{\rm tr}$ is the IR scale, where the fixed-point scaling ends, and from where the couplings scale according to their canonical mass dimension. In the previous discussion we have identified this scale with the Planck scale $M_{\rm Pl}$, but we will take a broader viewpoint in the following and keep $k_{\rm tr}$ general.

The dimensionless gravitational coupling at a scale k is given by

$$G(k) = \frac{k^2}{8\pi M_{\rm Pl}^2(k)}\,, \qquad \text{with} \qquad M_{\rm Pl}^2(k=0) = \frac{1}{8\pi G_{\rm N}}\,. \tag{4.18}$$

Here $M_{\rm Pl}(k)$ is the scale dependent Planck scale, and $G_{\rm N}$ the physical gravitational coupling measured in the deep IR. Within the lowest order truncation of the infinite-dimensional theory space, the scale dependence of the gravitational coupling is encoded in

$$k\partial_k G = 2\,G - 2\,\frac{G^2}{G_*}\,, \tag{4.19}$$

where G_* is the fixed-point value of G. This schematic representation of the scale dependence results from the balancing of canonical scaling and quantum scaling at the fixed point. We will demand that $G_* \geq 0$. This is necessary, since the regime with $G_* \leq 0$ is shielded from the physically viable regime where $G(k) \geq 0$ by the IR -attractive fixed point at $G_* = 0$, cf. the discussion in Subsection 4.3.1. Indications for an asymptotically safe fixed point with $G_* > 0$ have been found, see Section 3.1. This suggests that metric fluctuations have an anti-screening effect on the vacuum [202], which we will further discuss in Section 4.4. Clearly, also the quantum fluctuations of matter drive the scale dependence of the gravitational coupling. For the purpose of the present analysis, we will parametrize the effect of matter contributions by

$$G_*(N_{\rm eff}) \approx \frac{12\pi}{N_{\rm eff}}\,, \tag{4.20}$$

where $N_{\rm eff}$ is the sum of contributions from all matter fields, and metric fluctuations, weighted by some numerical prefactors. The precise fixed-point structure of general minimally coupled

gravity-matter systems is subject of current research and is discussed in more detail in Subsection 3.1.2. In the following we will assume that $N_{\text{eff}} > 0$, which is indeed supported by explicit computations for the matter content of the SM, see the discussion in Subsection 3.1.2.

We aim at deriving a relation between the asymptotically safe fixed-point value G_*, and the string coupling g_{s} and the volume of the compact space $\mathcal{V}$, which ensures that i) an intermediate asymptotically safe scaling regime is possible, and ii) a connection to viable IR physics is possible.

Let us first focus on the transition scale k_{tr} where the theory departs from the asymptotically safe scaling regime and flows towards the IR. For $N_{\text{eff}} > 0$, we can integrate the beta function for the gravitational coupling (4.19) to solve for the scale-dependent gravitational coupling, and solve (4.18) for the Planck mass, which results in

$$M_{\text{Pl}}^2(k) = M_{\text{Pl}}^2(0) + \frac{k^2}{8\pi\, G_*}\,. \tag{4.21}$$

Therefore, the dimensionfull Planck scale is constant $M_{\text{Pl}}^2(k) \approx M_{\text{Pl}}^2(0)$ in the IR, while it enters the asymptotically safe scaling regime if $k^2 > 8\pi\, M_{\text{Pl}}^2(0)\, G_*$. The transition scale between the classical and the asymptotically safe scaling regime is the scale where the second term in (4.21) starts to dominate. It can be estimated as

$$k_{\text{tr}}^2 \approx 8\pi\, M_{\text{Pl}}^2(0)\, G_*\,. \tag{4.22}$$

For sufficiently small fixed-point values G_*, the transition scale can therefore lie significantly below the classical Planck-scale. Specifically, matter fields might reduce G_* according to (4.20). This behavior has indeed been observed under the impact of minimally coupled matter fields see Section 4.1.

Let us now focus on the transition between string theory and the asymptotically safe scaling regime. If this regime exists, the matching relations of both regimes should use the scale dependent Planck scale at the matching scale $\bar{k}$. Then, the matching relations read

$$M_{\text{Pl}}^2(\bar{k}) = \frac{\bar{k}^2}{8\pi\, G(\bar{k})} = \frac{M_{\text{s}}^2 \mathcal{V}}{\sqrt{g_{\text{s}}}}\,, \tag{4.23}$$

where $\mathcal{V}$ is the volume of the compact space in string units, and where g_{s} is the string coupling. Equation (4.23) follows by demanding that the four-dimensional Planck-scale and the string scale are related at the matching scale $\bar{k}$. Furthermore, the matching scale $\bar{k}$ should be below the Kaluza-Klein (KK) scale, such that the intermediate scaling regime can be four-dimensional. The KK scale is related to the string scale by

$$\bar{k}^2 \lesssim M_{\text{KK}}^2 = \frac{M_{\text{s}}^2}{\mathcal{V}^{1/3}} = \frac{\sqrt{g_{\text{s}}}}{\mathcal{V}^{4/3}} \frac{\bar{k}^2}{8\pi G(\bar{k})}\,, \tag{4.24}$$

where we have used (4.23) to express the string scale in terms of the matching scale. To separate the information on the string-theoretic regime from the information on the effective quantum-field theoretic description, we rewrite the inequality (4.24) as

$$\frac{\mathcal{V}^{4/3}}{\sqrt{g_{\text{s}}}} \lesssim \frac{1}{8\pi\, G(\bar{k})} < \frac{M_{\text{Pl}}^2(\bar{k})}{k_{\text{tr}}^2} = \frac{1}{8\pi} \frac{1}{G_* - G(\bar{k})}\,, \tag{4.25}$$

where the second inequality follows from demanding that $\bar{k}^2 > k_{\text{tr}}^2$, which is necessary to re-

alize a scaling regime, together with (4.18). As emphasized in Subsection 4.3.1, the existence of the scaling regime depends on the initial condition for all couplings corresponding to IR repulsive directions of the asymptotically safe fixed point. Under the assumption that all relevant couplings are close to the asymptotically safe fixed point at the matching scale, the scale dependence of higher-order couplings in (4.25) is negligible. This assumption strengthens the inequality (4.25), and simplifies our considerations. The last equality in (4.25) follows from the expression for the scale dependent Planck scale (4.21), together with the scale dependent gravitational coupling (4.18), and with (4.22). This highlights that a long asymptotically safe scaling regime, i.e., $M_{\rm Pl}^2(\bar{k}) \gg k_{\rm tr}^2$, requires that the gravitational coupling at the matching scale is close to the fixed-point value.

Using the inequality (4.25) together with the requirement that $G_* > 0$ and $G(\bar{k}) > 0$, which are necessary conditions to connect the potential scaling regime with a viable IR regime, it follows that

$$1 < \frac{G_*}{G(\bar{k})} < 2\,. \tag{4.26}$$

We can express the first inequality in (4.25) for the volume of the compact space in terms of the fixed-point value of the dimensionless gravitational constant as

$$\frac{\mathcal{V}^{4/3}}{\sqrt{g_{\rm s}}} \lesssim \frac{2}{8\pi\, G_*}\,. \tag{4.27}$$

The two inequalities (4.26) and (4.27) ensure that an asymptotically safe scaling regime is possible, and that this might allow to connect to a viable IR regime. Clearly, there are in principle several possibilities to satisfy these inequalities:

1. a small volume of the compact space,

2. a small fixed-point value for the gravitational coupling G_*,

3. or a large string coupling $g_{\rm s}$.

If any of these conditions is satisfied, the scenario summarized in Figure 4.6 might be realized. We will now comment on each of these possibilities.

The first option cannot be realized due to T-duality considerations: due to this duality, the string scale acts akin to a minimal length scale. Length scales below the string scale have to be investigated in terms of the T-dual theory, see, e.g., [41, 42].

For the second option, i.e., when the fixed-point value is sufficiently small, the matching scale $\bar{k}^2$ might be as low as the IR Planck scale, $M_{\rm Pl}(0)$, while the latter is larger than $k_{\rm tr}$. Due to the small fixed-point value, this scenario would imply a weakly coupled regime of asymptotically safe quantum gravity. Indications for such a scenario, in the sense of near-Gaussian scaling of higher-order operators, have been found in pure gravity [225, 227–229, 234], and in gravity-matter systems [113, 243, 266], see also the discussion in Section 3.1. This scenario also allows for a near-perturbative UV-completion for the SM, and might actually be achievable under the impact of matter degrees of freedom, see Section 4.1.

The third option would imply that the string theory is sufficiently strongly coupled. This regime is computationally not easily accessible, but it might still be related to a weakly coupled asymptotically safe scaling regime. However, similar to the considerations regarding the compact volume, a strongly coupled string theory is often S-dual to a weakly coupled string theory. Therefore, if the asymptotically safe scaling regime was related to a strongly coupled string the-

ory, the latter should be replaced by its weakly coupled S-dual theory. The corresponding field theory should then be searched for an asymptotically safe scaling regime.

Indeed, a scenario where string theory at high energies is connected to the IR via an intermediate, asymptotically safe scaling regime, was explicitly constructed in [340].

The weak gravity conjecture and asymptotic safety

We will now consider more specific relations between the asymptotically safe scaling regime and the properties of the string theory. In particular, there are conjectured requirements an EFT has to satisfy to be a candidate low-energy limit of any string theory. In the proposed scenario, these requirements should also carry over to the asymptotically safe scaling regime. Some of these requirements are discussed in the context of global or gauged symmetries, and therefore apply beyond string theory, see, e.g., [342–346], and [341] for a recent review. It is a second and independent motivation to study some of the so-called swampland conjectures in the context of asymptotically safe quantum gravity. One prominent example is the weak gravity conjecture (WGC), see [342]. It states that a theory with a local $U(1)$ symmetry and corresponding gauge coupling e' should feature a charged particle with charge q and mass M_{WGC}, such that

$$eM_{\text{Pl}} \geq M_{\text{WGC}}\,, \tag{4.28}$$

where we have introduced $e = e'q$. As any coupling in the context of quantum field theories is scale dependent, also the inequality (4.28) should be rephrased in terms of scale-dependent couplings, as already emphasized in the original proposal [342]. It is however an open question, whether the inequality (4.28) should hold at any scale, or only at certain scales, e.g., the mass scale of the lightest particle. We will investigate the stronger statement in the following, and demand that the WGC holds for any scale below M_{s}. In terms of dimensionless and scale dependent quantities, the WGC can be rewritten as

$$e(k) \geq \frac{m_{\text{WGC}}(k)}{m_{\text{Pl}}(k)} \tag{4.29}$$

where m_{WGC} and m_{Pl} are the dimensionless counterparts of the two mass scales in (4.28).

In particular, in the asymptotically safe scaling regime, all dimensionless couplings are constant, which implies

$$e(k) = e_*\,, \qquad \text{and} \qquad \frac{m_{\text{WGC}}(k)}{m_{\text{Pl}}(k)} = \frac{m_{\text{WGC},*}}{m_{\text{WGC},*}}\,, \tag{4.30}$$

where $m_{\text{WGC},*}$, $m_{\text{WGC},*}$ and e_* are the fixed-point values of the dimensionless couplings. Therefore, the fixed-point properties of the asymptotically safe scaling regime determine whether the WGC is satisfied or not.

At the asymptotically safe fixed point of quantum gravity and matter, metric fluctuations induce higher-order interactions. These interactions do not feature a GFP and cannot be consistently set to zero, cf. Section 4.6 and Section 4.2. Canonically marginal couplings, as well as masses, can either be finite or vanishing, as their scale dependences features both Gaussian and non-Gaussian fixed-points. Therefore, in the current system with the two couplings $e(k)$ and $m_{\text{WGC}}(k)$, there are two viable fixed-points, namely

1. the maximally symmetric fixed point $e_* = m_{\text{WGC},*} = 0$,
2. and $e_* \neq 0$ and $m_{\text{WGC},*} \neq 0$.

Another logical possibility would be a fixed point at $e_* = 0$ and $m_{\text{WGC},*} \neq 0$, which clearly violates the WGC. However, in a system with a charged scalar particle and a gauge field, there are no indications that such a fixed point can be realized. Furthermore a fixed point at $e_* \neq 0$ and $m_{\text{WGC},*} = 0$ trivially satisfies the WGC. However, this latter fixed point does not exist, since a non-vanishing mass term for charged scalar particles is unavoidably induced by quantum fluctuations of the gauge field.

At the first fixed point, only higher-order interactions are present. Therefore, the scenario summarized in (4.29) does not apply, and one would have to derive similar constraints for the induced higher-order couplings.

At the second fixed point, a non-vanishing Abelian gauge coupling is realized [297–299, 302]. This fixed point arises when quantum fluctuations of charged matter and of the metric balance each other. Schematically, in the presence of quantum gravity, the scale dependence of the Abelian gauge coupling reads

$$\beta_e = -f_g\, e + \beta^{(1)}\, e^3 + \mathcal{O}(e^5)\,, \tag{4.31}$$

where the second term is the standard 1-loop contribution from charged matter, while the first term is the effect of metric fluctuations on the Abelian hypercharge. The gravitational contribution f_g is proportional to the gravitational coupling and therefore goes to zero below the Planck-scale. A similar contribution was discussed in a perturbative setup of quantum gravity in [306–308, 347, 348]. In the context of asymptotically safe quantum gravity, f_g is constant at the fixed point for the gravitational couplings. Functional methods yield $f_g \geq 0$ [242, 297–302], which highlights the anti-screening effect of metric fluctuations, see the discussion in Section 4.4 and Section 4.1. In this setup, an asymptotically safe fixed point with $e_* > 0$ indeed was found for various approximations of the gravitational dynamics [242, 297–302]. It arises because the anti-screening gravitational contribution balances the screening contribution of charged matter on the Abelian gauge coupling, see also Subsection 4.1.1. The NGFP is given by

$$e_* = \sqrt{\frac{f_g}{\beta^{(1)}}}\,. \tag{4.32}$$

The charged particle appearing in the WGC can be either bosonic, or fermionic. In the SM, chiral symmetry in the UV protects fermions from the generation of mass-terms. Results from the FRG indicate that this remains true, even in the presence of metric fluctuations [4, 265, 315, 316, 336, 349]. In contrast, an explicit breaking of chiral symmetry by non-vanishing Yukawa couplings is possible [299, 314, 315, 317], which leads to a non-vanishing vacuum-expectation value for a scalar. This ultimately leads to non-vanishing fermion masses. We will assume in the following that no spontaneous symmetry breaking occurs beyond the Planck scale. Indications that a spontaneously broken chiral symmetry can be avoided even in the presence of a non-vanishing value of the gauge coupling has been found in [4], cf. the discussion in Section 4.5. Then, fermions remain massless in the trans-Planckian regime. Therefore, the WGC is trivially satisfied for fermions, as $e_* > 0$. Accordingly, models of asymptotically safe quantum gravity, where chiral symmetry is not spontaneously broken at or beyond the Planck scale, appear to be compatible with the weak-gravity conjecture. They could therefore be part of the landscape of string theory.

Let us now focus on charged scalar fields as candidates for the lightest charged particles. In this case, a non-vanishing Abelian gauge coupling induces a mass term for the scalar field.

Schematically, the scale dependence of the mass reads

$$\beta_{m^2_{\text{WGC}}} = -2m^2_{\text{WGC}} + f_m\, m^2_{\text{WGC}} - \frac{3}{32\pi^2}e^2 + \dots\,, \tag{4.33}$$

where the first term encodes the canonical scaling, while f_m is the gravitational contribution. The last term indicates the contributions from gauge-field fluctuations. This term gives rise to a non-vanishing fixed-point value $m^2_{\text{WGC},*} \neq 0$, if the Abelian gauge coupling is non-vanishing in the UV, i.e. $e_* \neq 0$. More precisely, the fixed-point value for the scalar mass lies at

$$m^2_{\text{WGC},*} = \frac{-3e^2}{32\pi^2(2-f_m)}\,. \tag{4.34}$$

Clearly, the fixed-point value for the mass can have either sign, depending on the size of f_m. The explicit form of f_m has been obtained in various approximations for the gravitational dynamics, see, e.g. [256, 310, 311, 313, 319]. For $f_m < 2$, the fixed-point value for the squared mass would be negative, indicating the onset of spontaneous symmetry breaking.

We will now focus on the simpler case $f_m > 2$. Due to the positive sign of f_m, the gravitational contribution acts like an effective dimensional reduction for the mass parameter. If this dimensional reduction becomes larger than two, the Higgs mass-parameter becomes an irrelevant coupling, due to quantum-gravitational effects. Indications that this could indeed be realized were investigated in [256, 310, 311, 313, 319].

Specifically, the condition for the gravitational coupling reads

$$G_* \leq \frac{4\pi}{3}(f_m - 2)\,, \tag{4.35}$$

which we obtain by inserting the fixed-point value for the mass $m^2_{\text{WGC},*}$ (4.34) into the inequality describing the WGC (4.29), and by using the relation between the Newton coupling and the dimensionless Planck mass (4.18). Since f_m actually depends on the fixed-point value G_*, the condition (4.35) constraints the gravitational parameter-space for asymptotically safe quantum gravity. With this constraint, one can explicitly check whether an asymptotically safe fixed point could lie in the landscape of string theory.

Conclusion

We have investigated a specific case within the scenario of effective asymptotic safety. In this case, the spacetime is fundamentally described by string theory, on a fundamental level. First, we have derived conditions on the string theory, and on the asymptotically safe fixed point, such that an intermediate scaling regime might exist. Under these conditions, summarized in (4.26) and (4.27), the scenario illustrated in Figure 4.6 could in principle be realized. Second, we have investigated conditions that the weak-gravity conjecture imposes on the asymptotically safe scaling regime in such a scenario. We refer to [340] for a similar investigation, where the compatibility of the asymptotically safe fixed point, the WGC, and other swampland conjectures was discussed.

If the weak-gravity conjecture and other swampland conjectures are fulfilled, the asymptotically safe scaling regime is a potential candidate for the low energy effective description emerging from string theory. In this region of the landscape of string theories, the RG-flow might connect a compactification of string theory on a background with negative microscopic cosmological constant to an IR theory with positive cosmological constant.

We have not constructed a specific compactification that sets the coupling values at the matching scale $\bar{k}$ inside the basin of attraction of the asymptotically safe fixed point. We simply have studied more general conditions on this scenario, and investigated possible consequences. Therefore, this study only provides first steps towards investigating if an asymptotically safe scaling regime might exist in the string-theory landscape. In this region of the landscape, the low energy phenomenology of string theory is practically indistinguishable from the IR physics of asymptotic safety. Specifically, first-principle computations of SM couplings, which might be possible in asymptotic safety, would carry over to string theory.

In turn, the embedding of asymptotic safety puts the question of unitarity in a different light. In the embedded theory, unstable modes might be present, as long as their masses are at or beyond the string scale. These instabilities would then simply indicate that the description in terms of quantum-field theoretic degrees of freedom breaks down. Beyond the scale of instabilities, a formulation in terms of string theory has to be employed. Therefore, the class of possible fixed points that are compatible with string theory might be larger than the fixed points usually considered when searching for a fundamental scale invariant regime of quantum gravity and matter.

4.4. Critical dimensionality from asymptotically safe quantum gravity

All available experimental data confirms that our universe is four dimensional. Experiments reaching down to the micrometer scale and confirm the inverse-square law of gravity [350–353]. Conversely, searches for gravity-signatures in particle collisions do not find evidence for extra dimensions in energies up to several TeV at the LHC [354, 355], see also [326] for an overview. This missing evidence for higher dimensions naturally leads to the question: What is special about $d = 4$? And: Could other dimensions also be consistent with the phenomenology of the observed universe?

Different mathematical languages to describe the fundamental nature of spacetime tend to lead to different answers to these questions. In a string theoretic description of spacetime, $d = 10$ is special. This is the only dimensionality, where instabilities and inconsistencies are avoided. For the string theory, $d = 10$ is singled out based on mathematical consistency. In a quantum-field-theoretic language $d = 4$ is special. This is the dimensionality, where the interactions of the SM are perturbatively renormalizable. In gravity, perturbative renormalization of the Newton constant would be possible in $d = 2$ dimensions.

In the following section, we will focus on the interplay of asymptotically safe quantum gravity and matter. We will perform a step towards discovering, whether this interplay might also give rise to a preferred dimensionality. We will base our investigation on phenomenological consistency with the observation of an Abelian gauge sector in our universe.

The key results of our investigation can be summarized as:

1. A UV-completion of the Abelian gauge coupling shifts towards a more strongly coupled regime of quantum gravity for $d > 4$.

2. A strongly coupled regime of quantum gravity is excluded by demanding UV-complete induced interactions, see also Subsection 4.2.1.

3. In our approximations, the conditions 1) and 2) can only be reconciled in $d = 4$ and $d = 5$, which singles out these dimensions as special in asymptotically safe quantum gravity.

The following section is structured as follows: In Subsection 4.4.1, we will discuss how asymptotically safe quantum gravity might induce a UV-completion in the Abelian gauge coupling in $d = 4$. We will also show that this potential UV-completion is expected to shift towards a increasingly strongly coupled regime, when increasing the dimensionality. In Subsection 4.4.2 we will combine this observation with the existence of the WGB in the Abelian gauge sector. In a specific approximation, we will investigate in which regions of the gravitational parameter space both the Abelian hypercharge, as well as higher-order induced interactions can be simultaneously satisfied.

4.4.1. Asymptotically safe quantum gravity and the Abelian gauge sector in $d > 4$

We have discussed the high-energy properties of the Abelian hypercharge sector of the SM in Subsection 4.1.1. We discussed indications that asymptotically safe quantum gravity might induce a UV-completion in the Abelian gauge sector in $d = 4$: the gravitational contribution f_g acts akin to an effective dimensional reduction and therefore might induce asymptotic freedom for the Abelian hypercharge, see Figure 4.1.

We will now focus on the case where $d > 4$. We will assume that the extra dimensions are compactified such that observational bounds on the dimensionality of our universe are met. Furthermore, we will focus on the asymptotically safe fixed point in the far UV, at distances much smaller than the compactification scale.

The major difference to $d = 4$, cf. Subsection 4.1.1 is the canonical mass dimension of the Abelian hypercharge $[\bar{g}_Y] = 2 - \frac{d}{2}$, which is marginal in $d = 4$, but canonically irrelevant in $d > 4$. The canonical mass dimensions adds a contribution to the scale dependence of g_Y, which reads

$$\beta_{g_Y} = g_Y \left(\frac{d-4}{2} - f_g(d) \right) + \mathcal{O}({g_Y}^3) \,, \tag{4.36}$$

indicating that without gravity the Landau problem is more severe in $d > 4$. We will show that in the chosen scheme $f_g(d) > 0$ for all $d \geq 4$. Therefore, gravity always acts as an effectively decreased dimension. If gravitational fluctuations decrease the effective dimensionality to or below four, the Abelian gauge coupling becomes asymptotically free. Otherwise, the Abelian gauge coupling remains UV incomplete.

Specifically, in $d > 4$, the gravitational contribution f_g competes with a contribution from the canonical mass dimension of the gauge coupling. To reduce the effective dimensionality sufficiently, $f_g(d)$ has to be larger than the critical value

$$f_{g,\,\text{crit}}(d) = \frac{d-4}{2} \,. \tag{4.37}$$

In our setting, $f_g(d) > f_{g,\,\text{crit}}(d)$ is a necessary condition to avoid the Landau pole, and to render the Abelian hypercharge asymptotically free. Since $f_{g,\,\text{crit}}(d)$ increases with dimensionality, the gravitational contribution f_g has to increase accordingly to ensure $f_g(d) > f_{g,\,\text{crit}}(d)$. Unless $f_g(d)$ increases linearly with d, a gravitational solution to the Landau pole in the Abelian gauge sector might only be available in $d = 4$.

Before actually computing the gravitational contribution f_g in specific approximations, let us first note that there are two different contributions driving the dimensional dependence of f_g. On the one hand, the number of propagating gravitational degrees of freedom increases with $d(d-3)/2$. Accordingly, one might expect that the value of $f_g(d)$ increases in a similar way. On the other hand, however, the gravitational contribution $f_g(d)$ also depends on the integration over the momenta of virtual field configurations. The latter is related to the volume of a

Fig. 4.8.: Diagrams that contribute to the gauge field anomalous dimension. Double lines indicate metric fluctuations, wavey lines indicate Abelian gauge fields. The regulator insertion, which is indicated by the cross, is understood to appear on each of the different internal lines.

d-dimensional unit sphere, which decreases as $1/\Gamma[d/2]$, as $d \to \infty$. Therefore, keeping the gravitational fixed-point values constant, this is the opposite effect as needed for a gravitationally induced UV-completion of the Abelian gauge sector. However, structurally, the gravitational contribution f_g is proportional to the gravitational coupling G. Since the fixed-point value G_* will in general also depend on the dimensionality, $f_g(d)$ additionally depends indirectly on the number of dimensions. Therefore, an increasing gravitational contribution f_g can still be achieved by increasing the gravitational coupling G_*. This indicates that a possible gravitational solution to the Landau pole problem of the Abelian gauge coupling shifts into a more strongly coupled regime.

4.4.2. No asymptotically safe UV completion in $d > 5$

We will now first confirm the expectation that f_g decreases with increasing dimensionality. This shifts a possible UV completion of the Abelian gauge coupling into a more strongly coupled regime. We will then combine this observation with the considerations discusses in Section 4.2, where we have seen that the Abelian gauge sector features a WGB. This bound restricts the viable gravitational parameter space to the weakly coupled regime. Beyond this regime, strong metric fluctuations trigger new divergences in the Abelian gauge sector, which renders the theory UV incomplete, see Figure 4.3.

Specifically, we assume that the scale dependence for the Abelian gauge coupling can be extracted from the anomalous dimension. In this case, the gravitational contribution f_g is given by

$$f_g = -\frac{\eta_A|_{\text{grav}}}{2}\,, \tag{4.38}$$

and encoded in the diagrams shown in Figure 4.8. The assumption that the scale dependence of the Abelian gauge coupling can be extracted from the anomalous dimension holds exactly in $d = 4$, and in the perturbative regime. There, perturbative Ward identities are satisfied and encode the relation between η_A and β_{g_Y}. Beyond $d = 4$ and beyond the perturbative regime, the scale dependence of g_Y read off from the two-, three-, or four-point function might differ. However, these differences can be avoided in $d = 4$ for the gauge choice $\beta_h = 1$, as shown by explicit computations without higher-order interactions [298].

We work in a truncation of the dynamics of the system given by

$$\Gamma_k = \Gamma_{k,\,\text{EH}} + \Gamma_{k,\,U(1)}\,, \tag{4.39}$$

where $\Gamma_{k,\,\text{EH}}$ is the Einstein Hilbert action (3.16), complemented with the gauge fixing action (3.18), and where $\Gamma_{k,\,U(1)}$ is the action of the Abelian gauge field (4.9), with $\kappa_2 = 0$ and generalized for general dimension d. The choice of $\kappa_2 = 0$ is necessary, since the dual field strength $\tilde{F}$

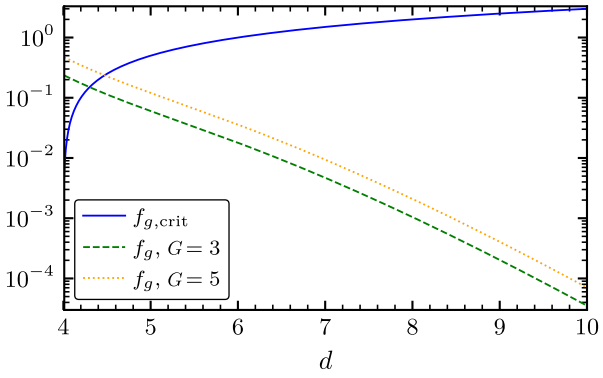

Fig. 4.9.: We show the value of the critical value $f_{g,\,\mathrm{crit}}(d)$, and the value of $f_g(d)$ in our approximation, cf. (4.40). Since $f_g(d)$ decreases rapidly, while $f_{g,\,\mathrm{crit}}(d)$ increases with d, the necessary condition $f_g(d) > f_{g,\,\mathrm{crit}}(d)$ is only satisfied for a limited values of d. The dimensionalities where this necessary condition is satisfied can be increased by increasing the value of the gravitational coupling G. The functions $f_g(d)$ are shown for $\Lambda = w_2 = 0$.

as defined in (4.11) is not a tensor in $d \neq 4$, and therefore breaks diffeomorphism invariance for $d > 4$. We will further introduce dimensionless versions of the Newton coupling $G = k^{d-2}\bar{G}$ and the cosmological constant $\Lambda = k^2\bar{\Lambda}$, respectively. We will employ the specific gauge choices $\alpha_h \to 0$, $\beta_h \to d/2 - 1$, and $\xi \to 0$.

For these choices, the gravitational contribution reads

$$\begin{aligned} f_g(d) =& G\,\frac{2^{1-d}\pi^{1-\frac{d}{2}}\left(16+(d-2)d\left(12+(d-9)d\right)\right)}{(d-2)d\,\Gamma\left[2+\frac{d}{2}\right](1-2\Lambda)^2}\,(2+d) \\ &+ G\,\frac{2^{3-d}((d-2)d-2)\pi^{1-\frac{d}{2}}}{(d-2)\Gamma\left[3+\frac{d}{2}\right](1-2\Lambda)}\left((4+d)+\frac{(4+d)}{1-2\Lambda}\right) \\ &- w_{2*}\,(4+d)\frac{4+d(d-1)}{2^{d+1}\pi^{\frac{d}{2}}\Gamma\left[3+\frac{d}{2}\right]}, \end{aligned} \tag{4.40}$$

where the contribution in the last line corresponds to the third diagram in Figure 4.8. It depends indirectly on the gravitational couplings via the fixed-point value w_{2*}.

As a first result, we can compare the gravitational contribution $f_g(d)$ at fixed value of the gravitational couplings to the critical value $f_{g,\,\mathrm{crit}}(d)$, which is shown in Figure 4.9. While $f_{g,\,\mathrm{crit}}(d)$ increases, the gravitational contribution $f_g(d)$ decreases with dimensionality. This is the opposite behavior which would be needed to induce a gravitational solution to the Landau-pole problem by satisfying $f_g(d) > f_{g,\,\mathrm{crit}}(d)$. This behavior agrees with the expectations discussed in Subsection 4.4.1. Therefore, a gravitational solution to the Landau-pole problem might become more difficult in larger dimensions. Since $f_g \sim G$, a strong increase of G is necessary to satisfy $f_g(d) > f_{g,\,\mathrm{crit}}(d)$ for a large range of d, cf. Figure 4.9. More precisely, $f_g(d)$ can be increased by increasing the effective gravitational couplings $G_{\mathrm{eff},\,1}$ and $G_{\mathrm{eff},\,2}$ defined in (4.7), which indicates that a UV completion of the Abelian gauge sector shifts into a more strongly coupled regime of quantum gravity.

To highlight that a strong increase of the effective gravitational couplings is not possible within a UV completion of the entire Abelian gauge sector, we study the scale dependence of the induced interaction w_2. For general dimension and gauge parameter $\beta_h = d/2 - 1$, it is given in Appendix C.

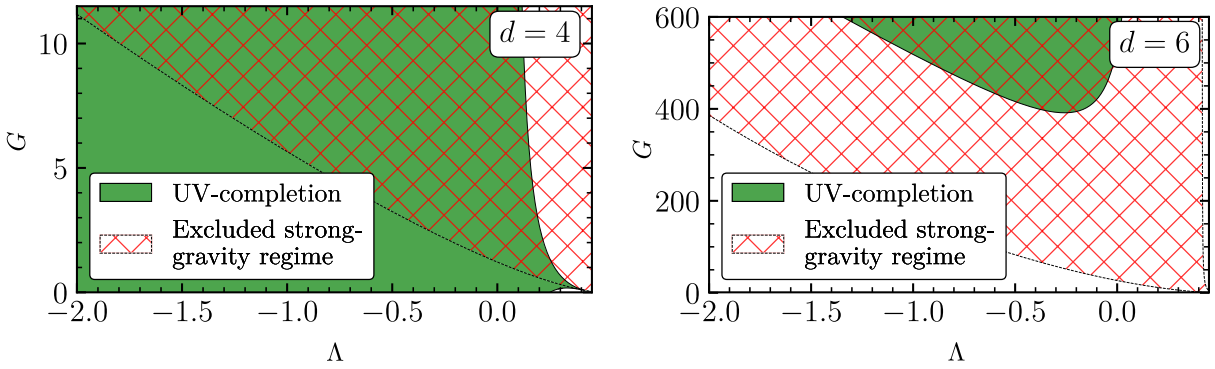

Fig. 4.10.: The green region indicates where $f_g(d) > f_{g,\,\mathrm{crit}}(d)$, inducing asymptotic freedom in the Abelian gauge sector. The red hatched region indicates where strong metric fluctuations induce new divergences in the matter sector. The left panel shows the situation for $d = 4$, while the right panel shows $d = 6$.

With the explicit result for $f_g(d)$ (4.40) and the scale dependence of the induced coupling w_2, we can explicitly check, in which region of the gravitational parameter space $f_g(d)$ is positive enough, within the weak-gravity regime.

The green region in the right panel of Figure 4.10 indicates the region where $f_g > 0$ holds in $d = 4$. In this region, the effective dimensionality of the Abelian hypercharge is lowered to below four, and asymptotic freedom is induced in the gauge sector. The red hatched area indicates the WGB for w_2, where strong metric fluctuations induce new divergences in higher-order interactions in the gauge sector, cf. Section 4.2. This region, which is also shown in Figure 4.3, is therefore removed from the viable parameter space. Therefore, in $d = 4$, there is a large region in the gravitational parameter space, where a UV complete Abelian gauge sector might be available. In $d = 4$, the fixed-point values of the minimally coupled, non-interacting, SM matter content, lies within the green region. This holds both for the gravitational fixed points obtained in the background approximation [99, 214, 257, 258], and also within the fluctuation approach [241, 242, 266] (assuming effective universality) [113, 243, 266], together with momentum-dependent anomalous dimension η_A [242]. This indicates that asymptotically safe quantum gravity could solve the Landau pole in $d = 4$ dimensions, as pointed out in [297, 302].

To investigate the situation for general dimension $d > 4$, we study the allowed region for values of the gravitational couplings $G \in [0, 1000]$ and $\Lambda \in [-1500, -0.5]$ as a function of d. The allowed region, normalized to $d = 4$ is shown as solid blue line in Figure 4.11. We see that the allowed region shrinks rapidly, and is already very small at $d = 5$. The allowed region shrinks entirely to zero at $d \approx 5.8$. Therefore, in $d \geq 6$, the region where metric fluctuations would lower the effective dimension of the gauge coupling sufficiently, has entirely shifted into the excluded strong gravity regime, see the right panel in Figure 4.10. In $d \geq 6$, the Abelian gauge sector remains UV incomplete, even in the presence of asymptotically safe quantum gravity. This is independent of possible fixed-point values G_* and Λ_*, since no value of these couplings leads to a UV-complete Abelian gauge sector, within the explored range.

Since we employed truncations and used the FRG, the computations leading to Figure 4.10 and Figure 4.11 are subject to systematic errors. Extensions of the truncation will likely change the excluded and the allowed regions, as well as the fixed-point values for G and Λ. Only very large deformations of the regions could change the conclusion that there is no viable region in the gravitational parameter space in $d = 6$ and beyond.

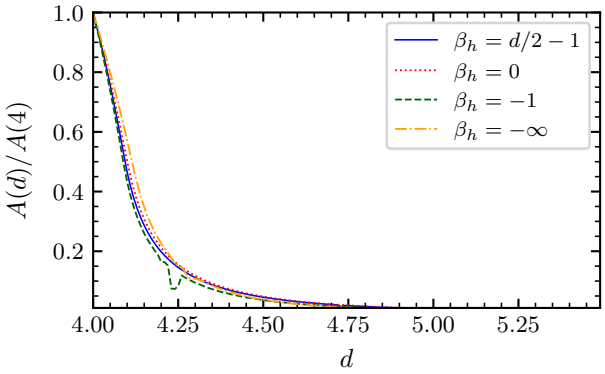

Fig. 4.11.: We show the area where a UV-completion of the Abelian gauge sector is possible for $G \in [0, 1000]$ and $\Lambda \in [-1500, 0.5]$. The solid blue line shows the behavior of $A(d)$ for the gauge choice $\beta_h = d/2 - 1$, used for (4.40), Figure 4.9, and Figure 4.10. The other lines serve as a comparison of $A(d)$ for different choices of the gauge-fixing parameter β_h.

While physical quantities are, in principle, independent of the gauge choice, they will generically be gauge dependent when computed within truncations. The amount of gauge dependence of physical quantities, like critical exponents or scattering amplitudes, can be used to estimate whether the truncation has converged. Strong gauge-dependences indicate the need for extended truncations. Mild gauge-dependences indicate apparent convergence in physical quantities.

To estimate the systematic uncertainty introduced by the truncation, we study the gauge dependence of the main result, namely the behavior of the allowed region $A(d)$. This is expected to be related to physical quantities, since it encodes the existence of a real fixed-point, where the Abelian gauge coupling is relevant. The curve $A(d)$ normalized to $d = 4$ for different choices of the gauge parameter β_h is shown in Figure 4.11. The qualitative agreement of all three curves might be interpreted as an indication that the main result of this section, namely the absence of a gravity-induced UV completion for the Abelian gauge sector in $d \geq 6$ is actually physical and might hold independent of the employed approximations.

4.4.3. Summary and conclusion

A UV completion of the SM in terms of Asymptotically safe quantum gravity might be able to restrict free parameters of the SM, such as the low-energy values of several couplings, cf. Section 4.1. Even in the best possible scenario, free parameters related to the quantum nature of spacetime remain free. In this section we have addressed one of them, namely the dimensionality of spacetime. We have found indications that $d = 4$ and $d = 5$ are the only dimensionalities where a UV-complete Abelian gauge sector can be accommodated.

This conclusion is based on the presence of two competing effects: On the one hand, quantum fluctuations of the metric have to be strong enough to induce a UV-completion for the Abelian gauge coupling g_Y. Only if the effective dimensionality of g_Y is lowered to below four, g_Y becomes asymptotically free. However, the canonical dimension increases with d, such that the gravitational contribution also needs to increase. As a first result, we have shown that in fact the gravitational contribution decreases as a function of d, cf. Figure 4.9. This effect can be compensated by increasing the effective gravitational coupling. This indicates that a gravitationally induced UV-completion of the Abelian gauge coupling shifts into a more strongly coupled regime of quantum gravity. On the other hand, the Abelian gauge sector admits a WGB for in-

duced higher-order interactions. Beyond the weak gravity regime, strong metric fluctuations induce new divergences in the Abelian gauge sector. These divergences prevent the viability of a gravity-induced UV-completion. The WGB excludes a region from the viable gravitational parameter space.

In $d = 4$, it is possible to remain in the allowed region, while simultaneously reducing the effective dimensionality of g_Y to below four, cf. Figure 4.10. When increasing d, the region where this is possible decreases quickly, cf. Figure 4.11.

An embedding into a grand-unified theory (GUT) might prevent this conclusion to some extent. Depending on the matter content, GUTs can be asymptotically free or feature Landau poles in $d = 4$, see, e.g. [356]. The former become asymptotically safe in $d = 4 + \epsilon$ dimensions, even in the absence of gravity [55, 195, 196]. Without gravity, there is an upper critical dimension, where asymptotic safety for non-Abelian $SU(N)$ theories is lost [195]. Beyond this upper critical dimension, these theories are no longer UV-complete on their own. Since gravity couples universally to the Abelian and non-Abelian gauge fields, the gravitational contribution f_g would also lower the effective dimensionality of non-Abelian gauge couplings. Therefore, we expect that gravity shifts the upper critical dimension to larger values of d. However, this shift only becomes large, for large values of the effective gravitational couplings. The existence of an excluded strong-gravity regime is also expected for non-Abelian gauge theories. In summary, we expect that embedding the SM into a GUT could provide a way to accommodate a UV-complete matter sector in larger dimensions, but presumably not far beyond $d \approx 6$.

This study indicates that the predictive power of the asymptotically safe fixed point for quantum gravity and matter might extend to parameters that fix the geometry of spacetime. It is remarkable that a UV-complete, quantum field theoretic description of the fundamental building blocks of nature, with no additional degrees of freedom beyond the observed ones, might single out $d = 4$ as the only dimensionality, which is compatible with the observation of an Abelian gauge sector at low energies.

4.5. Light charged fermions in quantum gravity

The experimental observation of light fermions in our universe motivates us to study the interplay of quantum gravity and chiral symmetry. Chiral symmetry protects fermions from acquiring masses. Accordingly, if chiral symmetry was broken by quantum-gravitational effects, this would result in fermionic bound states with masses of the order of the Planck-scale. Therefore, the observation of light fermions at low energies can be used as a strong consistency test of particular models of quantum gravity. Additionally, it might allow to constrain the parameter-space of quantum gravity [336].

The question whether global symmetries are broken in a given approach to quantum gravity has been answered to different extent in particular models. For the case of a global chiral symmetry, [336] in the context of an effective field theory with finite, trans-Planckian scale of new physics, suggest that quantum gravitational effects do not necessarily break chiral symmetry. In contrast, in the context of string theory, general arguments for the breaking of any global symmetry have been put forward in [344, 357–359]. Similar arguments were made in the context of the AdS/CFT conjecture [360], and related to the weak-gravity conjecture [342], see e.g., [341] for a review.

On regular lattices, the Nielsen-Ninomiya theorem, the formalization of the fermion-doubling problem, states that chiral fermions cannot exist at finite lattice spacing [361, 362]. Furthermore, the continuum limit has to be taken with care in order to recover chiral symmetry in the contin-

uum theory. While discrete approaches to quantum gravity are in general no regular lattices, the theorem could be an indication that chiral fermions are difficult to accommodate. In the context of loop quantum gravity, the presence of chiral fermions has been investigated in [363–365]. In the context of Causal sets, where a departure from manifold-like structures is made, the mere definition of fermions is an open question. In contrast, in EDT a first study of Kähler fermions shows indications that a global $U(1)$ symmetry, which is related to chiral symmetry in the continuum limit, remains unbroken [194], cf. also Section 2.3.

Within the FRG approach to asymptotically safe quantum gravity, the interplay of quantum gravity with chiral symmetry was first investigated in [336], see also [265, 315]. Even though gravity remains attractive at microscopic scales, quantum gravitational fluctuations do not lead to the formation of fermionic bound states. This is in contrast to (non)-Abelian gauge theories, where spontaneous chiral symmetry breaking was studied within the FRG in [366–373]. The difference between both situations lies, on a technical level, in different diagrams contributing to the RG flow of fermionic interactions [336], which has been studied in the broader context of the WGB in [302, 314], see also Section 4.2. Furthermore, FRG studies indicate that operators that explicitly break chiral symmetry at the fixed point are not generated by the RG flow, when starting from the chirally symmetric subspace of theory space [316].

Recently, it has been shown that topological fluctuations can lead to spontaneous chiral symmetry breaking, if they are present within asymptotic safety [374]. Furthermore, classical curvature can act as a source for chiral symmetry breaking, which is known under the name of gravitational catalysis [375–379]. Combining this with the effect of gravitational fluctuations gives rise to an upper bound on the number of fermions for which chiral symmetry remains unbroken in asymptotic safety [349, 380].

In the following sections, we will go beyond the study of quantum gravitational effects on fermionic interactions, and also include the effect of quantum fluctuations of an Abelian gauge field. This study is motivated by indications for a NGFP for the Abelian gauge coupling e, which is induced by metric fluctuations [297, 298, 302], see also [242, 300, 301] and Section 4.4. We aim at answering the question, whether there is a UV-completion at non-vanishing Abelian gauge coupling with intact chiral symmetry. In the absence of gravitational fluctuations a large value of the Abelian gauge coupling can break chiral symmetry [296, 381–385]. Therefore, we expect a competition between quantum fluctuations of the metric and of the Abelian gauge field. Furthermore, the value of the NGFP for the Abelian gauge coupling decreases with increasing number of fermions [297, 298, 302]. We hence expect a lower bound on the number of fermions arising from the gauge-gravity-fermion interplay.

4.5.1. Four-fermion interactions and chiral symmetry breaking

We will firstly review the mechanism of chiral symmetry breaking in the presence of an external field, and how it can be investigated by analyzing the RG flow of the system, see, e.g., [366–373, 386–388]. Therefore, we will consider fermions with a chiral $SU(N_{\mathrm{F}})_{\mathrm{L}} \times SU(N_{\mathrm{F}})_{\mathrm{R}}$ symmetry. In particular, we will study the scale dependence of four-fermion operators. At the lowest canonical mass dimension the two independent tensor-structures read

$$\lambda_+(V+A)\,, \qquad \lambda_-(V-A)\,, \tag{4.41}$$

with

$$V = \left(\bar{\psi}^i \gamma_\mu \psi^i\right)\left(\bar{\psi}^j \gamma^\mu \psi^j\right)\,, \qquad \text{and} \qquad A = -\left(\bar{\psi}^i \gamma_\mu \gamma_5 \psi^i\right)\left(\bar{\psi}^j \gamma^\mu \gamma_5 \psi^j\right)\,, \tag{4.42}$$

where the summation over flavor indices is over $i \in [1, N_{\mathrm{F}}]$. Without taking derivative interactions into account, these two operators, labeled by λ_+ and λ_- respectively, are the only Fierz-independent four-fermion interactions which are Lorentz scalars, see [366].

In the following, we will review the relation of the couplings $\lambda_\pm$ with the spontaneous breaking of chiral symmetry, leading to the generation of non-trivial fermionic bound states. For simplicity, let us focus on the operator labeled by λ_+, which can be Fierz transformed to

$$\lambda_+(V+A) = \lambda_\sigma \left[(\bar{\psi}^i \psi^j)(\bar{\psi}^i \psi^j) - (\bar{\psi}^i \gamma_5 \psi^j)(\bar{\psi}^i \gamma_5 \psi^j) \right] , \tag{4.43}$$

which is an exact Fierz identity if [366, 373]

$$\lambda_\sigma = -\frac{1}{2}\lambda_+ . \tag{4.44}$$

We can now use a Hubbard-Stratonovich transformation, see, e.g., [373, 389, 390], to rewrite the fermionic operator in terms of auxiliary fields. For simplicity of the notation, we will assume the case of a single flavor, but the following arguments generalize to general flavors straightforwardly. The scalar part of the four-fermion operators reads in terms of an auxiliary scalar field σ:

$$-\frac{\lambda_\psi}{4}(\bar{\psi}\psi)(\bar{\psi}\psi) = \left[h(\bar{\psi}\psi)\sigma + m_\varphi^2 \sigma^2 \right]_{\mathrm{EoM}(\sigma)} , \qquad \text{with} \qquad m_\varphi^2 = \frac{h^2}{\lambda_\psi} , \tag{4.45}$$

which holds on the equation of motion for the scalar field σ. Just as in scalar field theories, the spontaneous symmetry-breaking in terms of σ occurs, when the mass term m_φ^2 of the scalar field becomes negative. Therefore, a divergence of the four-fermion interaction λ_ψ indicates the spontaneous breaking of chiral symmetry. While this argument was explicitly shown only for the scalar channel, it holds in a similar way for the other channels. Since the spontaneous breaking of chiral symmetry might occur in one single channel and remain isolated there, it is important to take a Fierz-complete basis of operators into account. Explicit studies of spontaneous chiral-symmetry-breaking in QCD have shown that the RG-scale $k_{\chi SB}$ where the four-fermion interactions diverge is in quantitative agreement with the physical scale of chiral symmetry breaking [367, 391, 392]. This sets the mass scale of fermionic bound states. In the context of quantum gravity, this observation is particularly important, because quantum-gravity induced breaking of chiral symmetry is expected to occur above or around the Planck scale. In analogy to QCD, it would lead to Planck-size masses of fermionic bound states. This would be in conflict with the observation of light fermions below the Planck scale.

Summarizing the previous paragraphs, the spontaneous breaking of chiral symmetry can be investigated by analyzing the RG-flow of the four-fermion interactions $\lambda_\pm$. In particular, the Abelian gauge coupling induces the couplings $\lambda_\pm$, which feature a sGFP for small enough values of the Abelian gauge coupling. In analogy to the mechanism that gives rise to the WGB discussed in Section 4.2, larger values of the Abelian gauge coupling can induce a collision of the sGFP with another fixed point, where it vanishes into the complex plane. The absence of a real fixed point indicates the UV-incompleteness of the system. Conversely, a divergence in one of the four-fermion couplings is unavoidable in this case. We discuss the fixed-point collision in the four-fermion system in more detail in Appendix D.

Setup

For the present investigation, we approximate the dynamics of the gravity-gauge-fermion system by the effective action

$$\Gamma_k = \Gamma_k^{\rm EH} + \Gamma_k^{U(1)} + \Gamma_k^{\rm F}\,, \tag{4.46}$$

where $\Gamma_k^{\rm EH}$ is the Einstein-Hilbert action (3.16) with dimensionless couplings G and Λ, and with gauge fixing action (3.18), specified to $d = 4$, as well as $\beta_h \to \alpha_h \to 0$. Since we are mainly interested in the scale dependence of pure-matter interactions, the Fadeev-Popov ghosts arising due to the gauge fixing do not contribute to the scale dependence of $\lambda_\pm$. The dynamics of the Abelian gauge field is encoded in $\Gamma_k^{U(1)}$, which consists of the standard kinetic term with gauge fixing, and is defined in (4.9). The dynamics of the fermionic system is given by

$$\Gamma_k^{\rm F} = i\, Z_\psi \int \mathrm{d}^4x\sqrt{g}\,\bar\psi^i \not\nabla\, \psi^i + \frac{Z_\psi^2}{2k^2}\int \mathrm{d}^4x\sqrt{g}\,\left[\lambda_-(k)(V-A) + \lambda_+(k)(V+A)\right]\,, \tag{4.47}$$

with the fermion wavefunction renormalization Z_ψ. The minimal coupling of fermions to the Abelian gauge field and to gravity is implemented via the covariant derivative in the fermionic action (4.47). We give more details on the setup, including the choice of regulators in Section D.2.

4.5.2. Light charged fermions in asymptotic safety and beyond

In our approximation, which is discussed in more detail in Section D.2, the scale dependence of the four-fermion interactions reads

$$\begin{aligned}\beta_{\lambda_\pm} =& 2\lambda_\pm + M_\pm \pm \frac{5G^2}{8\pi(1-2\Lambda)^3} - \frac{5\lambda_\pm G}{8\pi(1-2\Lambda)^2} + \frac{5\lambda_\pm G}{4\pi(3-4\Lambda)} + \frac{15\lambda_\pm G}{8\pi(3-4\Lambda)^2}\\ &+ \frac{5e^2 G}{16\pi(1-2\Lambda)} + \frac{5e^2 G}{16\pi(1-2\Lambda)^2} + \frac{9e^2 G}{160\pi(3-4\Lambda)} - \frac{27e^2 G}{160\pi(3-4\Lambda)^2}\,,\end{aligned} \tag{4.48}$$

where the first term captures the scaling due to the canonical mass dimension, while the matter contributions $M_\pm$ arise due to quantum fluctuations of fermions and gauge fields. They are given by [387]

$$\begin{aligned}M_+ =& \frac{8\lambda_+(\lambda_-(N_{\rm F}+1) - 3e^2) + 9e^4 + 12\lambda_+^2}{32\pi^2}\,,\\ M_- =& \frac{4\lambda_-^2(N_{\rm F}-1) + 4\lambda_+^2 N_{\rm F} + 24\lambda_- e^2 - 9e^4}{32\pi^2}\,.\end{aligned} \tag{4.49}$$

The third to sixth term in (4.48) encode the gravitational contributions to the scale dependence of $\lambda_\pm$ [336]. Finally, those terms proportional to e^2G arise due to the gauge-gravity-fermion interplay. The diagrammatic representation of these contributions is shown in Figure 4.12. The full dependence of $\beta_{\lambda_\pm}$ on the gauge parameter β_h, and beyond the perturbative approximation is reported in Appendix D. This set of beta functions $\beta_{\lambda_\pm}$ features four zeros. In the following, we will focus on the sGFP, which is the most predictive fixed point of these zeros, and features two irrelevant directions. Furthermore, in the current setup, and in the presence of quantum gravitational fluctuations, the Abelian gauge coupling features two potentially viable fixed points which read [7, 297, 298, 302], cf. (D.2)

$$e_{*,\,\rm int} = \sqrt{\frac{40\pi G}{N_{\rm F}}\left(\frac{1}{6(1-2\Lambda)^2} - \frac{1}{3(1-2\Lambda)}\right)}\,, \qquad \text{and} \qquad e_{*,\,\rm free} = 0\,. \tag{4.50}$$

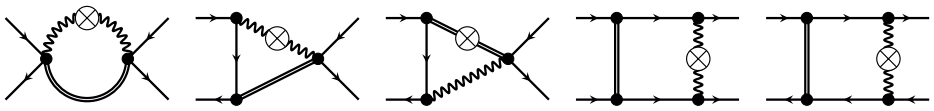

Fig. 4.12.: Diagrams contributing to the scale dependence of the four-fermion interactions $\lambda_\pm$ containing internal gauge boson (curly lines), metric fluctuations (double lines) and fermion lines (solid lines). The regulator insertion is to be understood on each of the different internal lines. These diagrams correspond to the terms $\sim e^2\, G$ in (4.48).

Asymptotic safety and chiral symmetry

In order to investigate the existence of an asymptotically safe fixed point which is chirally symmetric and features a non-vanishing fixed-point value for the Abelian gauge coupling, we supplement the beta functions of the matter sector with those for the gravitational couplings in our system. Specifically, we approximate the scale dependence of G and Λ by the pure-gravity contributions obtained in [262, 316]. To account for the presence of minimally coupled matter, we add the matter contribution obtained in [257]. While the asymptotically safe fixed point is expected to also feature finite non-minimal gravity matter couplings, we neglect those in the present setup. Explicit studies including induced non-minimal couplings show that the fixed-point structure is not changed on a qualitative level [243]. The resulting beta functions for the gravitational couplings read

$$\begin{aligned}\beta_G =& 2G - G^2\,\eta_g\,,\\ \beta_\Lambda =& -2\Lambda - G\,\Lambda\,\eta_g - \frac{G}{2\pi}\left(\frac{5}{4\Lambda-2}+\frac{3}{8\Lambda-6}+2N_{\rm F}+6-8\log\left(\frac{3}{2}\right)\right)\,,\end{aligned} \tag{4.51}$$

where

$$\eta_g = \frac{1}{12\pi}\left(\frac{6}{4\Lambda-3}+\frac{10}{1-2\Lambda}+\frac{20}{(1-2\Lambda)^2}-4N_{\rm F}+19+32\log\left(\frac{3}{2}\right)\right)\,. \tag{4.52}$$

The set of gravitational beta functions (4.51) features a fixed point only for $N_{\rm F}\leq 7$ [257, 316]. This is a limitation of the employed approximation and could change in a setup where background metric and metric fluctuations are distinguished carefully [53, 241, 243]. Since in the present analysis, we will mostly be interested in the limit of small numbers of fermions, we expect the beta functions (4.51) to capture the relevant features on a qualitative level in this limit. Furthermore, the behavior of the effective gravitational coupling $G_{\rm eff}$ (4.7) encoding the effect of quantum gravity on the matter system, evaluated at the fixed point behaves similarly in the background approximation and fluctuation studies as a function of $N_{\rm F}$, see the discussion in [243].

Fixed-point collision for finite fermion number We will now consider the full system of beta functions in the matter sector. Since $\lambda_\pm$ do not contribute to the scale dependence of the Abelian gauge coupling, we evaluate $\beta_{\lambda_\pm}$ at a fixed point for the Abelian gauge coupling. The case for $e_{*,\,\rm free}$ was investigated for small $N_{\rm F}$, indicating that all four fixed-points for $\lambda_\pm$ exist everywhere in the investigated gravitational parameter space [336]. We will focus on the case where $e=e_{*,\,\rm int}$ in the following. Let us start by promoting the gravitational coupling G and Λ to scale dependent couplings. Since, in the present approximation, the matter couplings do not backreact onto the gravitational sector, we can search for a suitable extension of the Reuter fixed point for the gravitational couplings for a given value of $N_{\rm F}$. We then evaluate the remaining beta functions at these fixed-point values. For $2.9\lesssim N_{\rm F}\leq 7$, all four possible fixed points for

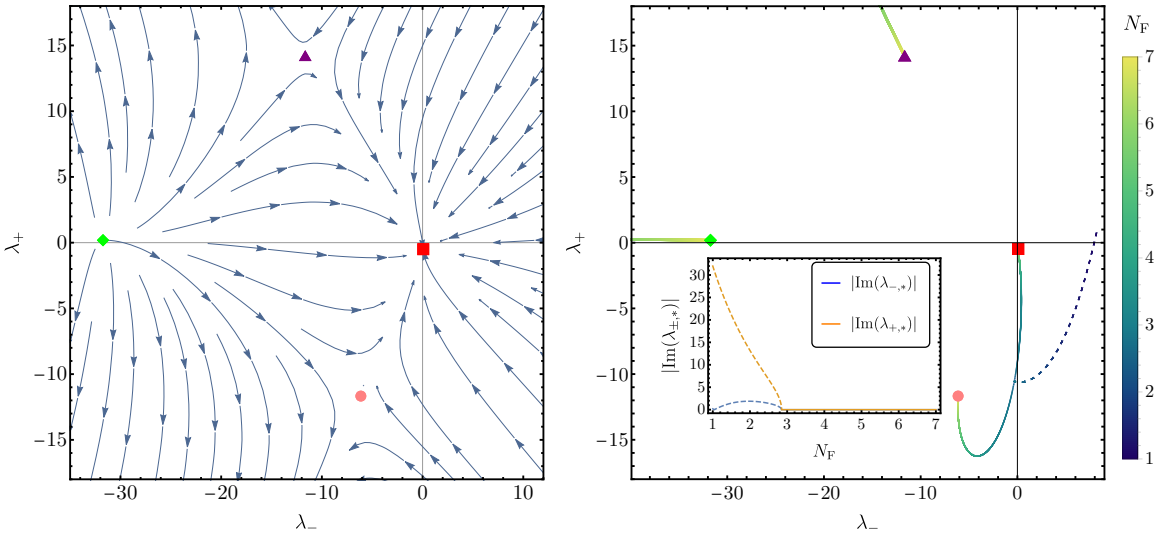

Fig. 4.13.: Left panel: fixed-point structure of the system in the plane spanned by $\lambda_\pm$, evaluated on the NGFP $e_{*,\mathrm{int}}$ (D.2), and on the fixed-point values for G and Λ for $N_F = 7$. The sGFP of $\lambda_\pm$, which is the most predictive one and marked as red box, features two irrelevant directions. Two of the other fixed point (purple triangle and orange circle) feature one relevant and one irrelevant direction, while at the fourth fixed point (green diamond) both directions are relevant. Right panel: we show the evolution of all fixed points of $\lambda_\pm$ as a function of the number N_F of Dirac fermions. While two fixed points (green diamond and purple triangle) move to larger absolute values when decreasing N_F, the sGFP collides with the last fixed point (orange circle) at $N_F \approx 2.9$. Below $N_F = 2.9$, we show the real part of the fixed-point values as dashed line, while the inset shows the absolute value of the imaginary parts.

$\lambda_\pm$ exist, cf. Figure 4.13. Specifically, the most predictive fixed point, where both $\lambda_\pm$ correspond to irrelevant directions, and where the whole matter sector does not add any new relevant directions, only appears out of the complex plane at $N_F \approx 2.9$, see Figure 4.13. Below $N_F \approx 2.9$, the value of the NGFP $e_{*,\mathrm{int}}$ exceeds a critical value e_{crit}, such that the fermionic interactions $\lambda_\pm$ do not feature a real sGFP. Therefore, the realization of the NGFP $e_{*,\mathrm{int}}$ does not only allow for a first principles prediction of the IR value of the Abelian gauge coupling, but might additionally give rise to a lower bound on the number of fermions in our universe. More than $N_F = 3$ fermions are necessary within our approximations to reconcile the observation of light fermions at low energies with asymptotically safe quantum gravity and a predictive UV-completion of the Abelian gauge sector.

In the discussion so far we focused on the question, whether there is a fixed point in the chirally symmetric subspace of theory space, at which the matter sector does not contribute any relevant direction to the system. A similar lower bound also arises if the GFP $e_* = 0$ is realized: Due to the IR-attractive nature of the NGFP, the value of the Abelian gauge coupling $e(k)$ above the Planck scale will be driven away from $e_* = 0$ and pulled towards the predictive trajectory. The exact value of $e(k)$ at the Planck scale is a free parameter, but it cannot exceed the maximum value e_{max}, which is set by the predictive trajectory. In this scenario, chiral symmetry can be spontaneously broken at a finite scale $k \geq M_{\mathrm{Pl}}$, if $e_{\mathrm{max}} > e_{\mathrm{crit}}$. Then, the fixed point value for $\lambda_\pm$ vanishes into the complex plane at a finite scale above the Planck scale, which potentially triggers spontaneous chiral symmetry breaking, which is in analogy to the situation in QCD [367–373, 384, 386, 388, 393]. Since any trajectory emanating from $e_* = 0$ will strictly stay below e_{max}, the value of the lower bound on the number of fermions is strictly smaller

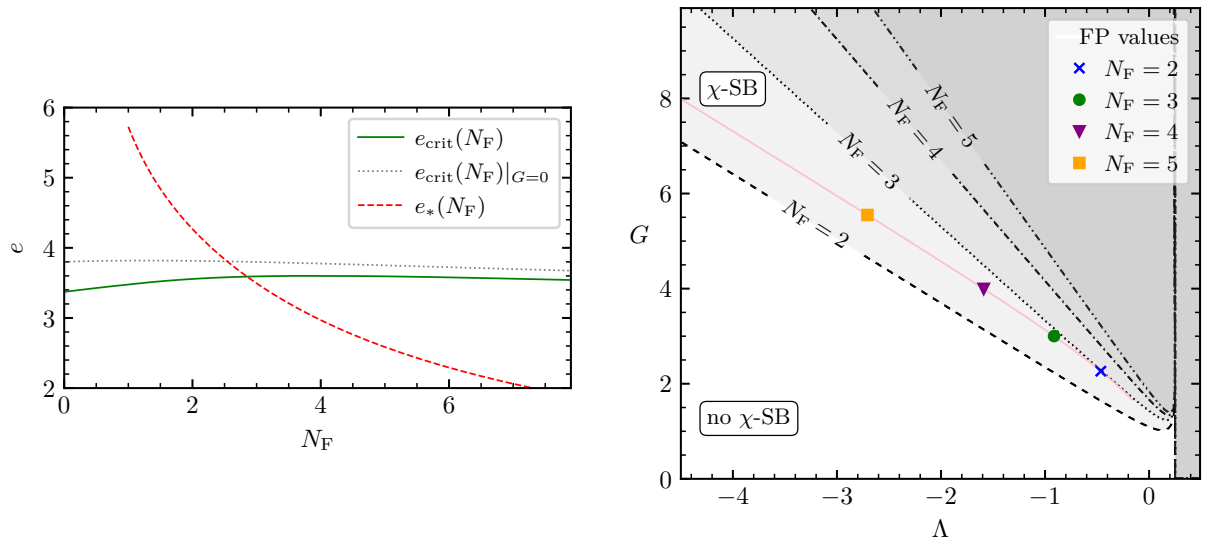

Fig. 4.14.: Left panel: The green solid line shows the value of the critical value $e_{\rm crit}$ for the Abelian gauge coupling e, where the fixed point of the four-fermion interactions $\lambda_\pm$ is shifted into the complex plane, under the impact of asymptotically safe quantum gravity. The grey dotted line shows for comparison the value of $e_{\rm crit}$ without gravity. The red dashed line shows the value of the NGFP $e_{*,\,\rm int}$ (D.2) at the asymptotically safe fixed point for gravity.
Right panel: For a fixed number of fermions, the dashed (dotted, dashdotted, dashdotdotted) line indicates the boundary between spontaneously broken (gray) and intact (white) chiral symmetry. The pink line, together with the markers indicate the asymptotically safe fixed point.

than the bound arising from the NGFP, i.e., ${N_{\rm F}}^{\rm crit}(e_*=0) < {N_{\rm F}}^{\rm crit}(e_*>0)$. In this scenario, the divergence of the four-fermion interaction does not necessarily indicate the onset of chiral symmetry breaking, since other channels than the chiral one might become critical, resulting in a condensate formation related to the breaking of a different symmetry. This is indeed realized in QED$_3$ [394], featuring a phase dominated by broken Lorentz symmetry.

Critical value of the gauge coupling at finite $N_{\rm F}$ To understand the dynamics of the mechanism giving rise to the lower bound on the number of fermions in a more intuitive way, we will now treat the Abelian gauge coupling as an external parameter. We will still solve the remaining beta functions and search for a suitable extension of the Reuter fixed point for a given value of e. In this setup and for a fixed value of $N_{\rm F}$, we will determine the critical value $e_{\rm crit}$ where the fixed-point collision is induced by a strong gauge coupling. The green line in Figure 4.14 shows this value, as a function of the number of fermions. As a comparison, the gray line shows the critical value of the gauge coupling in the absence of gravity. We see that quantum gravitational interactions reduce the critical value, indicating a slight destabilization in the sense that the system is closer to the fixed-point collision with gravity at the extension of the Reuter fixed point. This effect is caused by the gauge-gravity interplay, encoded in the contributions $\sim e^2 G$ in (4.48). The red line in Figure 4.14 indicates the fixed-point value of the system as a function of $N_{\rm F}$. For $N_{\rm F} < 2$, the value of the would-be fixed point is larger than the critical value, such that, within our truncation and approximations, a fixed point at non-vanishing Abelian gauge coupling and light fermions cannot be achieved within asymptotically safe quantum gravity in this case. For $N_{\rm F} > 3$ the fixed-point value lies below the critical value and decreases further for increasing $N_{\rm F}$. Therefore, within our approximations, if sufficiently many fermions exist, the

lightness of fermions can be reconciled with a scenario of asymptotically safe quantum gravity, where the value of the Abelian gauge coupling can be predicted. In Figure 4.14 we show the boundary of the region where a chirally symmetric and UV complete theory is possible and the region where the chirally symmetric theory space remains UV incomplete, if the NGFP for e is realized, in the parameter space spanned by G and Λ. The pink line shows the fixed-point values as a function of N_{F}, resulting in the lower bound on the number of fermions.

The presented results are subject to systematic uncertainties, due to the employed truncation and approximations. However, the NGFP e_* decreases as a function of N_{F}, suggesting that the mechanism remains robust. This dynamics suggests that a UV-complete model with few fermions is more likely to leave the chirally symmetric theory space, than a UV-complete model with many fermionic degrees of freedom. While the exact number of the critical value ${N_{\mathrm{F}}}^{\mathrm{crit}} \approx 3$ should be understood to come with systematic uncertainty, the qualitative mechanism resulting in a lower bound on the number of fermions is expected to persist in less extended approximations.

Effective-field-theory setting for quantum gravity

To interpret our results in a broader context, we will employ the effective-field-theory picture introduced in Subsection 4.3.1. In the present context, the more fundamental theory is not necessarily restricted to string theory. We assume that a quantum-field theoretic description of gravity and matter is possible above the Planck-scale. This description breaks down at a UV-scale k_{UV}, where a fundamental theory takes over, see also [6, 337, 338] and Subsection 4.3.1. This fundamental theory sets the initial conditions for G and Λ. Well below k_{UV} the scale dependence of the matter system is well approximated by the beta functions discussed previously. We will further assume that $e(k_{\mathrm{UV}})$ lies in the basin of attraction of the NGFP. Due to the IR attractive nature of this fixed point, it is approached by $e(k)$, and approximately realized around the Planck scale. In Figure 4.14 we show, as a function of the initial conditions for G and Λ, in which region of the gravitational parameter space a divergence of one of the four-fermion interactions $\lambda_{\pm}$ can be avoided. For an initial condition left of the boundary, chiral symmetry will remain intact when flowing towards the IR. If on the other hand, the more fundamental theory sets initial conditions in the gray area, the sGFP of $\lambda_{\pm}$ will vanish into the complex plane, potentially leading to the formation of massive fermion bound states. Since this would be a quantum gravitational effect, the associated mass scale would be the Planck scale, such that this scenario would not be compatible with the observation of light fermions in the IR. As a function of the number of fermions, the region of initial conditions leading to spontaneous chiral symmetry breaking decreases and shifts into a more strongly coupled regime of gravity. This happens since the NGFP of the Abelian gauge coupling (D.2) can be kept constant by increasing G, when N_{F} is increased at the same time. Therefore, in theories with sufficiently many fermions there is more parameter room available to feature light fermions. Gravitationally induced chiral symmetry breaking shifts into a more strongly coupled regime of quantum gravity, when increasing the number of fermions. Furthermore, when increasing the number of fermions, the upper bound on the initial condition of the Abelian gauge coupling decreases, which might additionally give rise to an *upper* bound on the number of fermions, see also the discussion in Subsection 4.3.2.

4.5.3. Summary and conclusion

We have investigated whether light, charged fermions can be observed within the asymptotic safety scenario for gravity and matter. We find indications that under the impact of quantum gravity, a critical value e_{crit} exists, beyond which the chirally symmetric theory space is not

UV-complete. In particular, we find indications that quantum gravitational fluctuations reduce the critical value e_{crit} compared to a system without gravitational effects, cf. Figure 4.14. We combine this finding with the observation that the NGFP for the Abelian gauge coupling $e_{*,\,\text{int}}$ (D.2) decreases as a function of the number of fermions N_{F}. As a result, light fermions might only be accommodated in the most predictive UV completion of the gauge-gravity system, if the number of fermions exceeds a critical vale $N_{\text{F},\,\text{crit}}$. This critical value is $N_{\text{F},\,\text{crit}} \approx 3$, within our approximations and in the current setup, cf. Figure 4.14.

We highlight that the mechanism of gravitational catalysis in asymptotically safe quantum gravity gives rise to a maximal number of fermions that could be allowed in a chirally symmetric, UV-complete theory space [349, 380]. This mechanism requires a non-trivial background curvature and is therefore absent in the present setup. Nevertheless, the present setup might also give rise to an upper bound on the number of fermions. In the present setup the value of the NGFP $e_{*,\,\text{int}}$ gives rise to an upper bound on the IR value of the Abelian gauge coupling, which can be achieved in a UV-complete theory [298]. Since $e_{*,\,\text{int}}$ decreases with N_{F}, too many fermions might prohibit to reach the observed IR -value of the Abelian gauge coupling. We combine this upper bound on N_{F} with the lower bound due to chiral symmetry breaking. We conclude that light charged fermions might only exist in asymptotically safe quantum within a non-trivial range of N_{F}.

As a technical point, we would like to stress that the performed analysis relies on the scale-dependence of G and Λ extracted using the background field approximation. Qualitatively similar results are obtained when the scale dependence of G and Λ is extracted in a momentum-dependent way and in the fluctuation approach [266], with the extraction of η_A at finite momentum $p^2 = k^2$ [242]. The analysis is presented in Appendix D. In summary, the shared qualitative features are i) the existence of a non-trivial lower bound $N_{\text{F},\,\text{crit}} > 1$, ii) a regime of unbroken chiral symmetry in the weak-gravity regime and iii) the shift of the boundary between broken and intact chiral symmetry towards a more strongly coupled regime, when N_{F} is increased.

As emphasized above, we expect that the mechanism giving rise to the lower bound on N_{F} is qualitatively robust. The quantitatively robust determination of $N_{\text{F},\,\text{crit}}$ is beyond the scope of this work. A more comprehensive investigation of the NGFP $e_{*,\,\text{int}}$ requires the inclusion of induced gauge interactions, e.g., the operator $(F_{\mu\nu}F^{\mu\nu})^2$ [7, 302] also studied in Section 4.2. Investigating the interplay of the WGB arising for these operators [314, 333, 336], with the boundary between broken and intact chiral symmetry, might in the future allow to extract the lower bound on the number of fermions in a more quantitatively robust way.

A different direction to test the robustness of the described mechanism, and to extract $N_{\text{F},\,\text{crit}}$ more accurately would be possible via the extraction of the scale dependence of e from the gauge-fermion three-point vertex. While this way to extract the scale dependence agrees with (D.6) at one loop, this is not necessarily true at the interacting, gravity induced fixed point. However explicit computations show that the extraction of e from different vertices in scalar QED agrees for the gauge choice $\beta_h \to 1$ [298]. Therefore, the concept of effective universality [113, 216, 243, 266], which was discovered for different avatars of extracting the Newton coupling, could also hold for the gauge coupling. This would provide further evidence for a near-perturbative nature of asymptotically safe quantum gravity.

In summary, we have confronted the scenario of asymptotically safe quantum gravity at the NGFP for the gauge coupling with the observation of light fermions at low energies. We find that for a sufficiently high number of fermions, light fermions can be accommodated in the predictive scenario of asymptotically safe quantum gravity. Therefore, the scenario of asymptotically safe quantum gravity and matter, where the gauge coupling can be predicted, passes

an important phenomenological consistency test for a fundamental description of our universe.

4.6. Lorentz invariance violations in the interplay of quantum gravity and matter

Symmetries play a key role in the current understanding of fundamental building blocks of nature. As we push the understanding of nature to higher and higher energies, the fate of symmetries across different energies is crucial. It might allow us to unravel the fundamental structures of our universe.

In particular, there are proposals that Lorentz invariance is an emergent symmetry at low energies, see [395–403]. Experimental tests for these scenarios have been proposed in [404], see also [405, 406] for recent reviews. In the context of quantum gravity, these scenarios are appealing, since the breaking of Lorentz invariance at high energies might allow for a perturbatively renormalizable theory of quantum gravity [401]. In quantum gravity, the existence of Lorentz invariance violations (LIV) implies for example the presence of a preferred frame. In this case, full diffeomorphism invariance breaks down to foliation preserving diffeomorphisms. This implies that the remaining theory is invariant under three-dimensional spatial rotations orthogonal to the direction of the preferred frame. In general, diffeomorphism invariance can be broken further by the presence of LIV. In these cases, the high energy theory does not necessarily feature a residual symmetry [407–412].

From an experimental perspective, most indications for Lorentz invariance are provided by the non-observation of LIV in the matter sector, see, e.g., [413–418] and references therein, and [419] for a summary of experimental bounds. More recently gravitational waves from binary neutron star mergers [420–422] and binary black-hole mergers [11, 12, 423] have been observed. These open a new observational windows in this area, cf. [424, 425] and [426, 427] respectively, specifically with the potential to investigate the status of Lorentz invariance of gravity-matter systems. In fact, we expect that LIV cannot be isolated into one sector only. In contrast, we expect that a potential LIV percolates from one sector into the other. This expectation is based on the simple observation that all matter gravitates. Hence, matter influences the gravitational dynamics, and vice versa. This interplay is expected to also mediate the breaking of symmetries from one sector into the other. More technically, loop-corrections in gravity-matter systems mediate the breaking of symmetries. We have seen in Section 4.4 and Section 4.5 that gravitational quantum fluctuations induce operators that are compatible with the symmetries of the entire system. In the presence of a preferred frame, we would expect the same. Specifically, we would expect that gravitational dynamics which single out a preferred frame also induce operators in the matter sector, which are invariant under foliation preserving diffeomorphisms. As a consequence, gravitational LIV would percolate into the matter sector. This general argument has been made, for example, in [428–434]. Here, we provide an explicit computation supporting this expectation.

Let us now refer to the "amount of LIV" as the strength of the Lorentz-invariance violating interaction. We will show that, under certain approximations and assumptions which we will explain below, the minimal "amount of LIV" in the matter is parametrically set by the "amount of LIV" in the gravitational sector. Generically, and except for very specific gravitational dynamics, LIV couplings in the gravitational sector of the order $\mathcal{O}(10^{-n})$ will result in LIV couplings in the matter sector of at least the same order of magnitude. Therefore, strong experimental constraints on LIV in one sector lead to similarly strong constraints in the other sector. Importantly, the matter sector features marginal LIV couplings. This is in contrast to the gravitational sector,

where all LIV couplings are Planck-scale suppressed. Therefore, matter LIV couplings can be observationally more strongly constrained at low energies.

In the following section, we will study the RG flow of gravitational dynamics that single out a preferred frame, coupled to an Abelian gauge field. Specifically, we will study the RG flow of a LIV coupling in the Abelian gauge sector. This system serves as a simplified toy model for the Abelian gauge sector of the SM coupled to foliation preserving gravity. In our toy model, we neglect the effect of spontaneous symmetry breaking towards low energies, as well as the effect of the other degrees of freedom of the SM. In the SM, the presence of LIV couplings in the Abelian gauge sector, i.e., the photon at low energies, is strongly constrained both by laboratory experiments, as well as by astrophysical observations, see Table 4.1 for an overview.

The following analysis indicates that, within our toy model and its assumptions (which we will spell out in more detail), quantum gravitational dynamics that violate Lorentz invariance by singling out a preferred frame induce LIV in the matter sector. Furthermore, under generic assumptions, these violations of Lorentz invariance in the matter sector will persist in the IR. More specifically, under certain conditions, the "amount of LIV" in the IR is directly correlated with the "amount of LIV" in the gravitational sector in the UV. This correlation relies on the existence of an IR attractive fixed point for the LIV matter coupling. On a qualitative level, small LIV in the UV grow under the RG flow towards the IR. As emphasized in Subsection 4.3.1, an IR attractive fixed point acts akin to an attractor of trajectories towards the IR. The IR attractive fixed points prevents the violations of Lorentz invariance from growing even further. In the toy model, the size of LIV in the matter sector is set by the IR attractive fixed-point for the LIV matter coupling. In turn, potential experimental bounds on LIV in the IR put indirect constraints on the IR attractive fixed point, and thereby on violations of Lorentz invariance in the gravitational sector.

As a second point, we point out that the different terms in the Standard Model Extension (SME) [435, 436], see [412] for a recent review, are not independent when derived from a fundamental theory. In general, a microscopic theory is likely to generate all operators that are compatible with the symmetries of the theory, see also the discussion in Section 4.2. Typically, one expects that all these operators are generated with a coupling whose dimensionless counterpart is of order one. This typical naturalness argument can of course be circumvented by a given fundamental theory, where some operators are predicted to be unnaturally small. We will provide an explicit computation of the inducing part for a higher-order LIV coupling in the matter sector. As we will argue, this inducing part, which depends on the other LIV couplings, sets the size of the higher-order operator coupling around the Planck scale. Under certain conditions, weaker direct constraints on higher-order operators could be supplemented with strong indirect constraints.

In summary, our analysis indicates that, within our toy model, and further assumptions and conditions the following holds:

1. quantum gravitational fluctuations that single out a preferred frame induce LIV in the Abelian gauge sector,

2. except for special points in the parameter-space of gravitational LIV couplings, LIV in the matter sector persist in the IR, and are parametrically set by the LIV couplings in the gravitational sector,

3. the size of one particular higher-order LIV matter operator is not independent of the other LIV operators, leading to potential indirect constraints for this higher-order operator.

We emphasize again that we work in a toy model that does not account for the degrees of freedom of the SM other than the Abelian gauge sector. Specifically, the toy model neglects spontaneous symmetry-breaking in the Abelian gauge sector, and therefore does not distinguish between the Abelian hypercharge at high energies, and the electromagnetic charge at low energies. The mechanism of spontaneous electroweak symmetry breaking has been studied in [435]. We therefore expect that the qualitative features of our results are robust, despite the limitations of the employed model.

The rest of this section is structured as follows: In Subsection 4.6.1 we introduce the gravitational system that is invariant under foliation preserving diffeomorphisms. We discuss the foliation structure of the system, and introduce the minimally coupled Abelian gauge field, together with the Lorentz-invariance violating interaction ζ in the Abelian gauge sector. In Subsection 4.6.2 we investigate the impact of Lorentz invariance violations in gravity on the matter sector. We briefly summarize the ideas of effective asymptotic safety, and generalize them to the system with broken Lorentz invariance. In Subsection 4.6.3 we discuss the regions in the parameter space, where a universal value of ζ at the Planck scale arises in our approximation. We point out, how this universal value might constrain the gravitational LIV parameter space indirectly. To highlight the strength of these indirect constraints, we translate the experimental constraints on LIV in the photon sector into bounds in the Planck-scale value of ζ. The combination of these bounds, together with the universal value of ζ might result in strong, indirect constraints on the gravitational LIV parameter space. We point out in detail the limitations of the analysis and sources for systematic uncertainties. We view the study as a blueprint that exemplifies the potential constraining power of the gravity-matter interplay in the presence of broken symmetries. In Subsection 4.6.4 we show that higher order LIV couplings in the matter sector are also induced in our approximation. Under certain conditions, these couplings also feature a universal value at the Planck scale. This value is not independent of the experimentally strongly constrained marginal couplings. As a result, higher-order LIV couplings might be indirectly constrained. Finally, in Subsection 4.6.5 we summarize our results and conclude.

4.6.1. Impact of quantum gravity with a preferred frame on Abelian gauge fields

For the following investigation of the impact of gravitational dynamics that single out a preferred frame on the matter sector, we will employ an RG study of the scale dependence of LIV matter couplings. For this purpose, we employ the FRG adapted to the presence of a foliation [248] in Euclidean spaces. The analytical continuation to Lorentzian spacetimes is an open challenge of the FRG approach to quantum gravity, see also [238] and the discussion in Subsection 3.1.1. We will assume in the following that the main results carry over to Lorentzian spacetimes on a qualitative level, even in the presence of a preferred frame.

To study the scale dependence of the system, we employ an approximation of the dynamics based on canonical power counting. While this approximation might be insufficient in a very non-perturbative regime of quantum gravity and matter, it is expected to capture the relevant physics in a near-perturbative regime. For diffeomorphism invariant theories, indications have been discovered that the asymptotically safe fixed point for pure quantum gravity, and for gravity-matter systems might be near-perturbative, cf. Section 3.1. For the following discussion, the precise value of the dimensionless counterpart of the Newton coupling, which could be interpreted as a measure of the non-perturbativeness of the system, does not play any role, as we will see in Subsection 4.6.2. Therefore, we expect that an approximation of the gravitational dynamics based on canonical power counting captures the relevant dynamics on a qualitative

level, at least in a near-perturbative regime of quantum gravity.

We approximate the Lorentz invariant part of the gravitational dynamics with the Einstein-Hilbert action (3.16) with G_{N} and Λ as dimensionless and scale dependent counterparts of the Newton coupling and cosmological constant, respectively. This is supplemented with the standard gauge fixing term (3.18), with the choices $\alpha_h = \gamma_h = 0$ and $\beta_h = 1$. The Fadeev-Popov ghosts which arise due to the gauge fixing do not play a role in the following investigation, since we neglect induced ghost-matter interactions. To explore the consequence of a preferred frame, we need to adapt the FRG setup discussed in Section 2.2. To gain access to the foliation structure of the system, we decompose the Euclidean manifold $\mathcal{M} = \Sigma \times \mathbb{R}$ into a Riemannian three-space Σ and a "time" direction $\mathbb{R}$. To achieve this, we decompose the metric g according to [248]

$$g_{\mu\nu} = \sigma_{\mu\nu} + n_\mu n_\nu \,, \tag{4.53}$$

where the tensor σ encodes the three-metric on Σ in a covariant way, and where n is an orthogonal, normalized vector. The tensor σ and the normalized vector n satisfy

$$g^{\mu\nu} n_\mu \sigma_{\nu\rho} = 0 \,, \qquad g^{\mu\nu} n_\mu n_\nu = 1 \,. \tag{4.54}$$

With this decomposition, the metric fluctuations $h_{\mu\nu}$ translate into fluctuations of the foliation tensors σ and n. For details on the relation between $h_{\mu\nu}$ and the foliation fluctuations, we refer to Appendix E. The foliation structure (4.53) is implemented via the inclusion of a suitable constraint in the form of a gauge-fixing term into the effective action, as discussed in Appendix E. The conditions (4.54) are second-class constraints, as opposed to gauge constraints, which are first-class constraints. Therefore, the implementation of the constraints (4.54) might require a modification of the procedure proposed in [248]. We will however continue with this procedure to implement the foliation, see Appendix E. Any difference between these different procedures is counted as part of the systematic uncertainties of our results, which we expect to be dominated by the approximation of the dynamics of the system.

With the decomposition (4.53) we now have direct access to the foliation structure of the metric. This allows us to single out a preferred frame. We achieve this by including the canonically most relevant operators that break full diffeomorphism invariance down to foliation preserving diffeomorphisms into the approximation for the dynamics of the system. Therefore, the Lorentz invariant Einstein-Hilbert action is supplemented with

$$\Gamma_k^{\text{Grav, LIV}} = \frac{k^2}{16\pi G_{\mathrm{N}}} \int \mathrm{d}^4x \sqrt{g} \left(k_2 \, K^{\mu\nu} K_{\mu\nu} + k_0 \, K^2 + a_1 \, \mathcal{A}^\mu \mathcal{A}_\mu \right) \,, \tag{4.55}$$

where k_2, k_0 and a_1 are dimensionless, scale dependent couplings, and where $K^{\mu\nu}$ is the extrinsic curvature on the spatial slices

$$K_{\mu\nu} = \frac{1}{2} \left(n^\alpha D_\alpha \sigma_{\mu\nu} + D_\mu n_\nu + D_\nu n_\mu \right) \,, \qquad K = g^{\mu\nu} K_{\mu\nu} \,, \tag{4.56}$$

and is orthogonal to the normal vector

$$n^\mu K_{\mu\nu} = 0 \,. \tag{4.57}$$

To the lowest order in canonical mass dimension $\Gamma_k^{\text{Grav, LIV}}$ (4.55) contains all independent operators that are invariant under foliation preserving diffeomorphisms, but break full diffeomorphism invariance. All other operators are related via Gauss-Codazzi relations, or are total

derivatives [248]. The symmetry-breaking operators contained in (4.55) single out a preferred frame due to the explicit appearance of n_μ. The existence of this frame is parametrized by the symmetry-breaking gravitational couplings k_2, k_0 and a_1. The dynamics of the system discussed so far corresponds to the IR limit of Horava-Lifshitz gravity [401, 437–442], which is perturbatively renormalizable. The RG treatment which we will employ allows us to broaden the viewpoint and study the theory in terms of an effective field theory above the Planck scale, where some other theory sets in at a far UV scale k_{UV}, cf. Subsection 4.3.1.

The main goal of this section is to investigate the impact of the existence of a dynamical preferred frame on the matter sector. We will focus on the Abelian gauge sector in the following, where the action describing the dynamics is divided into a Lorentz invariant, and a LIV part, i.e.,

$$\Gamma_k^{\text{Abelian}} = \Gamma_k^{\text{Abelian, LI}} + \Gamma_k^{\text{Abelian, LIV}} , \tag{4.58}$$

where $\Gamma_k^{\text{Abelian, LI}}$ is the standard kinetic term of the gauge field (4.9) complemented by gauge fixing for the Abelian gauge field. The most general Lorentz invariance violating term at quadratic order in the gauge field is given by [435]

$$\Gamma_k^{\text{Abelian, LIV}} = \frac{Z_A}{4} \int \mathrm{d}^4x \sqrt{g}\, k_{\mathrm{F}}^{\mu\nu\rho\sigma} F_{\mu\nu} F_{\rho\sigma} , \tag{4.59}$$

where $F_{\mu\nu}$ is the field strength of the Abelian gauge field, and where $k_{\mathrm{F}}^{\mu\nu\rho\sigma}$ is a real, scale dependent tensor. Let us restrict the symmetries of $k_{\mathrm{F}}^{\mu\nu\rho\sigma}$ by demanding that the effective action $\Gamma_k^{\text{Abelian, LIV}}$ satisfies certain symmetries. First, demanding that CPT-symmetry remains intact, the totally anti-symmetric component of $k_{\mathrm{F}}^{\mu\nu\rho\sigma}$ is eliminated. This would lead to contributions proportional to the topological term $F\tilde{F}$ that violates CPT-symmetry. Furthermore, the contraction with two field strength tensors requires that $k_{\mathrm{F}}^{\mu\nu\rho\sigma}$ is symmetric under the exchange of index pairs $\{\mu\nu\} \leftrightarrow \{\rho\sigma\}$. Finally, gauge invariance requires that the field strength is anti-symmetric. The contraction of $k_{\mathrm{F}}^{\mu\nu\rho\sigma}$ with the field strength therefore translates into anti-symmetry under exchanges of $\mu \leftrightarrow \nu$ and $\rho \leftrightarrow \sigma$. In summary, the tensor $k_{\mathrm{F}}^{\mu\nu\rho\sigma}$ has the same symmetries as the Riemann tensor. A potential observational consequence of a non-vanishing tensor $k_{\mathrm{F}}^{\mu\nu\rho\sigma}$ might be vacuum birefringence, see, e.g. [436, 443] for a detailed discussion. In the presence of the tensor $k_{\mathrm{F}}^{\mu\nu\rho\sigma}$, the dispersion relation is still linear in the spatial momentum, i.e. $p_0 = c(k_{\mathrm{F}})|\vec{p}|$, such that there is no wavelength-dependent speed of propagation. However, the two physical polarizations feature different prefactors $c(k_{\mathrm{F}})$, which results in a phase shift between them. This phase difference accumulates with the propagation distance, and might lead to observational consequences, cf. [436, 443].

For a general dynamical preferred frame [396], the only possible tensor k_{F} is

$$k_{\mathrm{F}}^{\mu\nu\rho\sigma} = \frac{\zeta}{4} \left(n^\mu n^\rho g^{\nu\sigma} + n^\nu n^\sigma g^{\mu\rho} - n^\nu n^\rho g^{\mu\sigma} - n^\mu n^\sigma g^{\nu\rho} \right) , \tag{4.60}$$

with the single scale dependent and dimensionless coupling ζ. For an explicit analysis of this system in the context of Horava-Lifshitz gravity, see [449]. In the presence of a dynamical preferred vector n, the coupling ζ is the only coupling that captures the breaking of Lorentz invariance in the Abelian gauge sector, at this order in canonical mass dimension. If Lorentz invariance was broken due to the presence of a preferred tensor, different components of k_{F} would contribute with independent couplings. Experimental constraints usually do not assume a specific origin for the breaking of Lorentz invariance, and hence constrain each of the components of the tensor k_{F} independently. In the present context, the strongest of those constraints would result in the constraint for the LIV matter coupling ζ in (4.60). For a brief overview of various

Bound	Year	Ref.	Method
10^{-37}	2006	[444]	polarization measurement in gamma ray bursts
10^{-9}	2007	[445]	atomic gravimeter
10^{-15}	2004	[446]	comparison of a cryogenic sapphire microwave resonator and a hydrogen maser
10^{-18}	2014	[447]	terrestrial Michelson-Morley experiment
10^{-21}	2018	[414]	Michelson-Morley with trapped ions (assuming no Lorentz-symmetry violation for electrons)
10^{-20}	2016	[448]	light interferometry (LIGO data)

Tab. 4.1.: Various experimental bounds on the Lorentz-symmetry breaking in the photon sector of the SM. The constrained coupling it the analogue of our LIV coupling ζ. We assume that the presence of a preferred frame, caused by the existence of the vector field n_μ is the only source of Lorentz-symmetry violations. Then ζ is the unique non-zero coupling. For each experiment, the strongest bound on the coefficients of $k_{\text{F}}^{\mu\nu\rho\sigma}$, cf. (4.59), are translated into bounds on ζ. All bounds, except for the second line, assume the absence of LIV couplings in the pure gravity sector. Such an assumption is necessary to convert the experimental data into bounds on LIV couplings. We stress the difference between the experimentally constrained photon LIV coupling and the coupling ζ in our toy model. The list of experimental bounds on the photon LIV coupling is intended to provide an overview on the sensitivity of experiments in the photon sector. They do not directly translate into constraints on the LIV coupling ζ in our toy model.

experiments and their constraining power on Lorentz-invariance violations in the photon sector, see Table 4.1. Even though the presence of higher-order operators, which we neglect in our study, will influence the exact value of ζ, their effect is Planck-scale suppressed. Therefore, those operators will only play a negligible role on the low-energy behavior of k_{F}.

4.6.2. Relating Lorentz invariance violations in gravity and matter

As a first step, we will investigate the crucial question, if and under which conditions Lorentz invariance violations percolate from the gravitational into the matter sector. From the theoretical viewpoint, this question is crucial in order to understand the overall symmetry structure. Furthermore, especially in the context of UV-completions that violate Lorentz invariance, it is inevitable to understand how the breaking of symmetries in one sector influences the other sectors of a system. From the phenomenological viewpoint, the question is crucial, since the gravity-matter interplay might allow to translate strong observational constraints on LIV in the matter sector into indirect constraints on LIV in the gravitational sector.

Specifically, we would like to understand, if the Lorentz-invariant subspace of theory space is IR attractive or repulsive. In other words, starting from small violations of Lorentz invariance at high energies, do these violations grow or shrink under the RG flow towards the IR.

To understand this crucial question, we study the system in an effective-field-theoretic setup. The setup we will study is very similar to the scenario described in the context of effective asymptotic safety, see Subsection 4.3.1. Again, we will consider a theory with a quantum-field theoretic description beyond the Planck-scale, and below a high-energy scale k_{UV}. The main difference of the present setup to the scenario discussed in Subsection 4.3.1 is that the more fundamental theory setting the initial conditions at k_{UV} features Lorentz invariance violating couplings. For these initial conditions, the origin of violations of Lorentz invariance, be it explicit or effective, does not play a role, see [428] and [434, 449] for a discussion of both possibilities. The question we aim to answer is, whether quantum gravitational fluctuations that single out a preferred frame drive the LIV matter coupling ζ towards zero, or towards a preferred non-vanishing value.

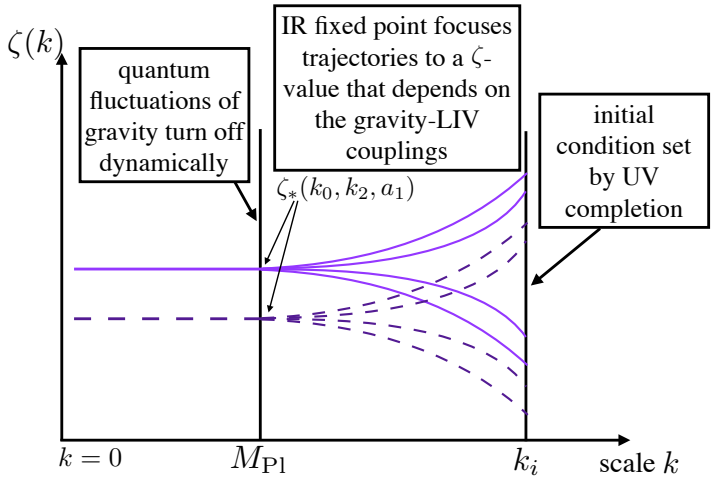

Fig. 4.15.: We illustrate the key idea that underlies our result, if $\zeta(k)$ is situated in the basin of attraction of the IR attractive fixed point.

As a first result, we will show that the LIV matter coupling ζ cannot consistently be set to zero, as long as gravitational dynamics single out a preferred frame. This is a consequence of the absence of a GFP for ζ: the Lorentz-invariance violating matter coupling ζ is induced by Lorentz-invariance violating gravitational couplings k_2, k_0 and a_1. This is in complete analogy to the inducing of additional matter interactions in a diffeomorphism invariant scenario, as discussed in detail in Section 4.2 and Subsection 4.5.1. Therefore, quantum gravitational dynamics that are invariant under foliation preserving diffeomorphisms generate matter couplings invariant under the same transformations.

As a second result, we will find that, in approximations and under additional assumptions, ζ always features an IR attractive, non-trivial fixed point $\zeta_* \neq 0$. Consequently, quantum fluctuations drive $\zeta(k)$ towards a preferred, non-vanishing value in the IR. As discussed in detail in Subsection 4.3.1, a large interval of initial conditions in the UV is mapped onto a small interval around ζ_* at the Planck scale. As a third result, we will show that this preferred value ζ_* is determined by the Planck scale values of the gravitational LIV couplings. Below the Planck scale, the effect of gravitational fluctuations switches off dynamically. Therefore, in our toy model, the scale dependence of ζ vanishes below the Planck scale. Hence, the Planck-scale value of ζ also correspond to its IR value, which, in a more realistic model, could be constrained experimentally. The scenario we will discuss in the following is illustrated in Figure 4.15. Combining these three findings, applied to a more realistic model, potential experimental bounds on ζ can be mapped onto constraints for the Planck scale value $\zeta(M_{\rm Pl})$. The latter is a function of the gravitational LIV couplings k_2, k_0 and a_1. Thus, the constraint on $\zeta(M_{\rm Pl})$ can be translated into regions in the space of gravitational LIV couplings, which are in conflict with experimental bounds on ζ. Therefore, the interplay of quantum gravity and matter might allow to indirectly constrain the fundamental symmetries of the gravitational sector.

We will work in a setup that is very similar to the scenario outlined in Subsection 4.3.1. We will be agnostic about the UV-completion of the theory and assume that the conditions 1.) to 4.) discussed in Subsection 4.3.1 are satisfied. To investigate the fate of Lorentz invariance in the matter sector, we will compute the scale dependence of the LIV matter coupling ζ, cf. (4.60), and take the gravitational LIV couplings as input. In this way, we will study a large class of possible fundamental theories that might feature violations of Lorentz invariance.

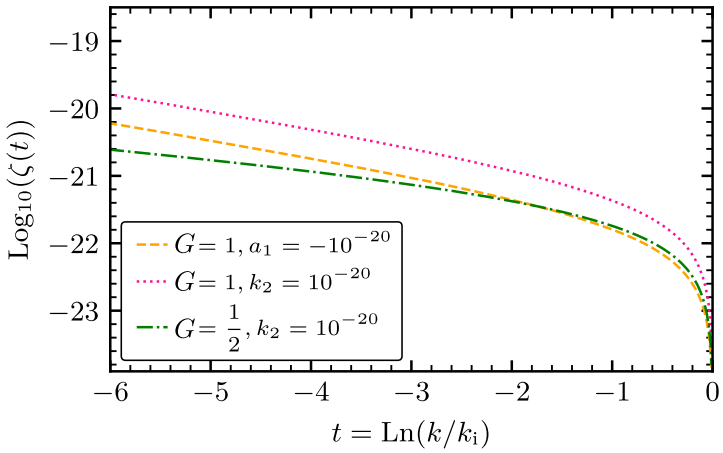

Fig. 4.16.: Starting from initial conditions $\zeta(k_\mathrm{I})=0$, the RG flow towards the IR over a few orders of magnitude generates $\zeta(k)\sim c$, for any non-vanishing gravity LIV coupling of $\mathcal{O}(c)$. The couplings gravitational LIV couplings which are not mentioned in the respective label are set to zero, and we choose $\Lambda=0$ for the illustration.

To obtain an analytic expression for the scale dependence of ζ, we will expand all expressions to linear order in the gravitational LIV couplings, and to quadratic order in ζ. For the study of tiny deviations from the Lorentz-invariant subspace of theory space, this expansion is expected to be sufficient. More details on computational details are provided in Appendix E. As a first result, we report the scale dependence of ζ, which reads

$$\begin{aligned}\beta_\zeta =& G_\mathrm{N}\left(-\frac{10a_1+21k_0+257k_2}{384\pi(1-2\Lambda)^2}+\frac{-6a_1+53k_0+329k_2}{576\pi(1-2\Lambda)^3}\right)\\ &+\zeta\, G_\mathrm{N}\left(\frac{1}{6\pi(1-2\Lambda)}-\frac{183a_1-390k_0-1690k_2+1840}{960\pi(1-2\Lambda)^2}+\frac{2313a_1-5(246k_0+4039k_2)}{1440\pi(1-2\Lambda)^3}\right)\\ &+\zeta^2\, G_\mathrm{N}\left(\frac{79}{60\pi(1-2\Lambda)}-\frac{21a_1+495k_0-920k_2+5072}{960\pi(1-2\Lambda)^2}+\frac{6911a_1-9515k_0-60420k_2}{1440\pi(1-2\Lambda)^3}\right).\end{aligned} \tag{4.61}$$

We will now focus on special cases first, to understand the dynamics described by the scale dependence (4.61). First, for $G_\mathrm{N}=0$, the action just consists of a kinetic term for the Abelian gauge field. The resulting free theory does not contain any interactions, and the scale dependence of any coupling, including that of ζ, therefore vanishes. This result will persist in the presence of additional matter, unless the other, non-gravitational LIV-matter interactions are present.

Let us now generalize to the case of non-vanishing gravitational interactions, i.e., $G_\mathrm{N}\neq 0$. Only the first line in the scale dependence of ζ remains, when setting $\zeta=0$. This line is non-vanishing, except for very specific combinations of the gravitational LIV couplings k_2, k_0 and a_1. Therefore, generically, $\zeta=0$ is not a fixed point for ζ. Even of $\zeta(k_\mathrm{I})=0$ for some trans-Planckian scale k_I, the LIV matter coupling will be re-generated, such that $\zeta(k_\mathrm{I}-\delta k)\neq 0$, see Figure 4.16. The finiteness of the first line of β_ζ (4.61) is in complete analogy with the presence of the coefficient A_0 in the scale dependence of the four-gauge-field interaction (4.4), and the coefficients $c_\pm$ in the scale dependence for the four-fermion interactions (D.1). In all cases, this term indicates, that the corresponding coupling cannot be set to zero consistently, but that the Gaussian fixed point is shifted away from zero. This shift is induced by interactions that respect the same symmetries. In the case of the LIV matter coupling ζ, it is induced by the gravitational LIV couplings. If all gravitational LIV couplings k_2, k_0 and a_1 vanish, then $\zeta=0$ is a fixed point of β_ζ, and violations of Lorentz invariance can be consistently avoided.

We now take the second and third line of β_ζ into account. Generically, $\beta_\zeta \neq 0$ holds, such that any initial condition $\zeta(k_\mathrm{I})$ is driven towards different values towards the IR. Depending on the specific initial conditions for all couplings, $\zeta(k_\mathrm{I})$ can either lie in the basin of attraction of an IR attractive fixed point, or an IR repulsive fixed point. We refer to the discussion in Subsection 4.3.1 for a detailed discussion on the role of fixed points and pseudo fixed-points as attractors or repulsers of RG trajectories, even in the presence of scale dependent gravitational couplings. Figure 4.7 summarizes this role of IR attractive and repulsive fixed points: For initial conditions in the basin of attraction of an IR attractive fixed point, the coupling $\zeta(k)$ approximates the fixed-point value after some RG-time towards the IR. Specifically, $\zeta(M_\mathrm{Pl}) \approx \zeta_*$ will hold, such that the IR value of ζ is an universal prediction of the theory. Conversely, for initial conditions in the basin of attraction of an IR repulsive fixed point, the coupling $\zeta(k)$ is driven away from the fixed-point value during the RG flow towards the IR. In this case, no universal IR value arises, but the coupling is generically driven to large absolute values. Specifically, if $\zeta(k_\mathrm{I}) = 0$ lies in the basin of attraction of an IR repulsive fixed point, this results in a non-vanishing value at lower scales k given by

$$\zeta(k) \approx -\frac{b_0}{b_1}\left(1 - \left(\frac{k_\mathrm{I}}{k}\right)^{b_1}\right) , \tag{4.62}$$

where the coefficients b_0 and b_1 refer to the constant and linear coefficients in ζ contributing to β_ζ. This expression holds for small enough values of ζ, where the quadratic contribution b_2 can be neglected. It shows that the scale dependent LIV matter coupling $\zeta(k)$ is parametrically set by the gravitational LIV couplings contributing to the coefficients b_i. A small value of $\zeta(k)$ can be achieved either by $b_0 \ll 1$, if $b_0 \sim \mathcal{O}(1)$, or by $b_1 \ll 1$. These conditions require either that all gravitational LIV couplings are small, or at least one LIV coupling $\sim \mathcal{O}(1)$. An $\mathcal{O}(1)$ value for a gravitational LIV coupling is however in conflict with direct constraints [424], which were derived under the assumption of a Lorentz-invariant photon sector. We tentatively conclude from this brief qualitative analysis of the scale dependence of the LIV matter coupling, that strong observational constraints on ζ could only be compatible with $\mathcal{O}(1)$ gravitational LIV couplings for very special initial conditions. We will discuss this question in more detail in the following.

4.6.3. Indirect constraints on gravitational LIV couplings

We will now discuss, how the considerations of the previous subsections could lead to strong indirect constraints on the gravitational LIV parameter space. Before continuing however, we emphasize that the scale dependence encoded in β_ζ (4.61) relies on approximations and on truncations of the dynamics of the gravity-matter system. Therefore, it is subject to systematic uncertainties. Additionally, using the FRG to extract β_ζ requires choosing an Euclidean background metric. Furthermore, the system we investigate is a simplified toy model, which neglects the additional degrees of freedom of the SM, as well as electroweak symmetry breaking. These approximations result in clear quantitative limitations of the results we will present in the following. However, we expect that the main qualitative result is robust. The main qualitative result is that the gravitational LIV couplings enter β_ζ with $\mathcal{O}(1)$ prefactors. This implies that a constraint on ζ of $\mathcal{O}(10^n)$ will result in a similarly strong, indirect constraint on the gravitational LIV couplings. The derivation of this result will be the main point of the present section.

Since we will study tiny deviations from the Lorentz invariant subspace of theory space, let us first focus on the absence of violations of Lorentz invariance, i.e. on $k_2 = k_0 = a_1 = 0$. As a result, the first line in the scale dependence of ζ (4.61) vanishes identically. Without this inducing contribution for ζ, β_ζ features one GFP and one NGFP, with corresponding critical

exponents Θ_i:

$$(\zeta_{*,1},\, \zeta_{*,2})\,|_{k_2=k_0=a_1=0} = \left(0,\, -\frac{5(4\Lambda+21)}{158\Lambda+238}\right), \qquad \Theta_{1/2}|_{k_2=k_0=a_1=0} = \pm\frac{G_{\rm N}(4\Lambda+21)}{12\pi(1-2\Lambda)^2}\,. \quad (4.63)$$

For small but non-vanishing gravitational LIV couplings, the ζ-independent contributions to β_ζ do not vanish. Those contributions shift the GFP $\zeta_{*,1}$ away from zero, to a non-vanishing sGFP. This is in direct analogy to the induced four-gauge and four-fermion interactions discussed in Section 4.2 and Section 4.5, where the Newton coupling is the inducing coupling. For small LIV couplings, the sGFP is a continuous deformation of the GFP. Therefore, the existence of the sGFP is controlled and robust in the limit of sufficiently small gravitational LIV couplings. The NGFP $\zeta_{*,2}$ on the other hand cannot be traced back to the GFP. Its existence might therefore be subject to truncation artifacts, which can be tested by extending the truncation.

From the expression (4.63) for the critical exponents, we see that the critical exponent for the sGFP changes sign at $\Lambda_{\rm crit} = -\frac{21}{4}$. For $\Lambda > \Lambda_{\rm crit}$, the sGFP is IR-repulsive, while for $\Lambda < \Lambda_{\rm crit}$, it is IR-attractive. The quantitative value for Λ is subject to systematic uncertainties.

In the following, we investigate both cases, $\Lambda > \Lambda_{\rm crit}$ and $\Lambda < \Lambda_{\rm crit}$. Specifically, we will study the fate of violations of Lorentz invariance in the matter sector, with initial conditions for $\zeta(k_{\rm UV})$ in the basin of attraction of the sGFP and the NGFP. When translating the Planck-scale value $\zeta(M_{\rm Pl})$ into IR values, we assume that the dimensionless version of the Newton coupling follows the canonical scaling $G_{\rm N} \sim k^2$. This follows from the assumption that gravitational fluctuations turn off swiftly below the Planck scale. Since the scale dependence of ζ is only driven by gravitational fluctuations, ζ follows the canonical scaling below the Planck scaling. Since ζ is a canonically marginal coupling, this results in logarithmic scaling below the Planck scale. We account for this scaling in the derivation of the excluded regions in Figure 4.17, and Figures 4.18-4.20, by assuming that $\zeta(M_{\rm Pl})/\zeta(0) \sim 10$. We will combine the indirect constraints on the gravitational LIV parameter space obtained in this way with direct constraints from cosmology and gravitational wave observations. These direct constraints lead to $a_1 < 0$ and $|k_2| < 10^{-15}$ [424]. However, the latter constraint is obtained by the LIGO data on the observation of gravitational waves from a neutron-star merger with electromagnetic counterpart [420–422], under the assumption that Lorentz invariance is intact in the matter sector. Neglecting the difference between the Abelian gauge field and the photon, the photons in the present setup would however propagate with speed $v_\gamma = 1 + C\zeta$, where the constant C arises due to the breaking of Lorentz invariance. Therefore, the observation of gravitational waves with electromagnetic counterpart would result in $|k_2 - C\zeta| < 10^{-15}$. For $k_2 = 0$, this would actually additionally constrain ζ. We will however not use this constraint in the following, to emphasize the toy-model character of the present investigation. Furthermore, despite the presence of LIV in the matter sector, we will use the direct constraints on gravitational LIV as obtained in [424].

Constraints on gravitational LIV couplings for $\Lambda > \Lambda_{\rm crit}$

If $\Lambda > \Lambda_{\rm crit}$, the sGFP $\zeta_{*,1}$ is IR repulsive, and the NGFP$\zeta_{*,2}$ is IR attractive. This situation is illustrated in Figure 4.7. The basin of attraction of $\zeta_{*,2}$ spans all initial conditions with $\zeta(k) < \zeta_{*,1}$. Such an initial condition is attracted by the IR attractive fixed point $\zeta_{*,2}$, the value of which is determined by the gravitational couplings. This fixed point $\zeta_{*,2}$ is therefore approximately realized at the Planck scale, and also constitutes the IR value of ζ. This results in the map $\{k_2, k_0, a_1\} \to \zeta_{*,2} \approx \zeta(M_{\rm Pl}) \to \zeta(0)$, between the gravitational LIV couplings and the IR value of ζ. In turn, this map allows to translate observational constraints in ζ in the IR into indirect

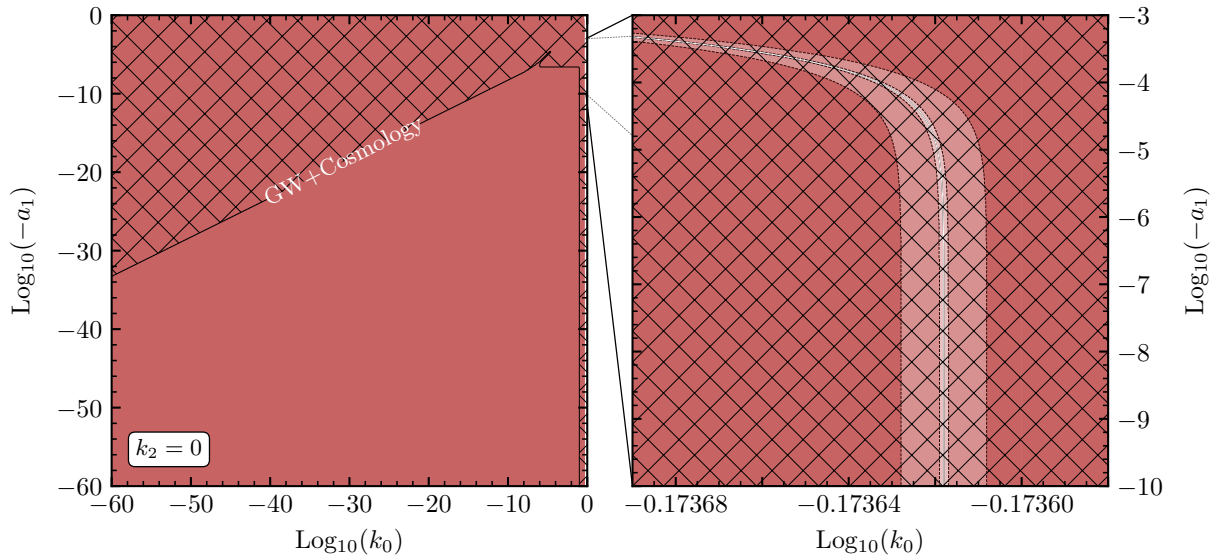

Fig. 4.17.: We show the excluded regions in the gravitational LIV parameter space for $\Lambda > \Lambda_{\mathrm{crit}}$, and with initial conditions in the basin of attraction of the IR attractive NGFP$\zeta_{*,2}$. We show the constraints that result for $k_2 = 0$. Left panel: the red region marks the region which is excluded by demanding that $\zeta_{*,2} < 10^{-4}$. The hatched area indicates the region which is excluded by cosmology and the observation of gravitational waves, as derived in [424]. Right panel: we zoom into a part of the region in the $(k_0 - a_1)$-plane, which allows for $\zeta_{*,2} < 10^{-4}$ (lighter red areas). This region is centered around the line where $\zeta_{*,2} = 0$ (white band), according to (4.64). The entire region shown in the right panel is excluded by cosmology and the observation of gravitational waves [424].

constraints on the gravitational LIV couplings; generic values of the gravitational LIV couplings might result in a fixed-point value $\zeta_{*,2}$ which would be in conflict with experimental constraints on $\zeta(0)$, thereby excluding these values for the gravitational LIV couplings from the viable parameter space.

We will illustrate the strength of the constraints for the specific case $\Lambda = 0$. The IR attractive fixed point $\zeta_{*,2}$ in this case, and to linear order in the gravitational LIV couplings reads

$$\zeta_{*,2} \approx 1.52\, k_2 + 0.66\, k_0 - 0.15\, a_1 - 0.44\,. \tag{4.64}$$

Here, the last term corresponds to the contribution which is non-vanishing for vanishing gravitational LIV couplings, cf. (4.63). This contribution causes that generic choices of k_2, k_0 and a_1 lead to $\zeta_{*,2} \sim \mathcal{O}(1)$, which could be in conflict with experimental constraints on ζ. Specifically, only very specific values of the gravitational LIV couplings could avoid conflict with an observational bound of $|\zeta| < 10^{-10}$, which is shown in Figure 4.17. Due to the last term in (4.64), at least one of the gravitational LIV couplings has to be of order one to lead to $\zeta_{*,2} \sim \mathcal{O}(10^{-10})$. Figure 4.17 also shows that the potentially viable region is already excluded by direct cosmological constraints and the observation of gravitational waves [424]. The constraints shown in Figure 4.17 are not generated by the IR attractive fixed point $\zeta_{*,2}$. Instead, the fixed point $\zeta_{*,2}$ prevents violations of Lorentz invariance to grow even larger towards the IR. Therefore, if the NGFP $\zeta_{*,2}$ turns out to be spurious in more refined approximations, there will not be any attractor of RG trajectories towards the IR. Therefore, any tiny violation of Lorentz invariance in the UV might be in conflict with observational constraints in the IR.

If the initial condition $\zeta(k)$ lies in the basin of attraction of the IR repulsive, sGFP $\zeta_{*,1}$, the

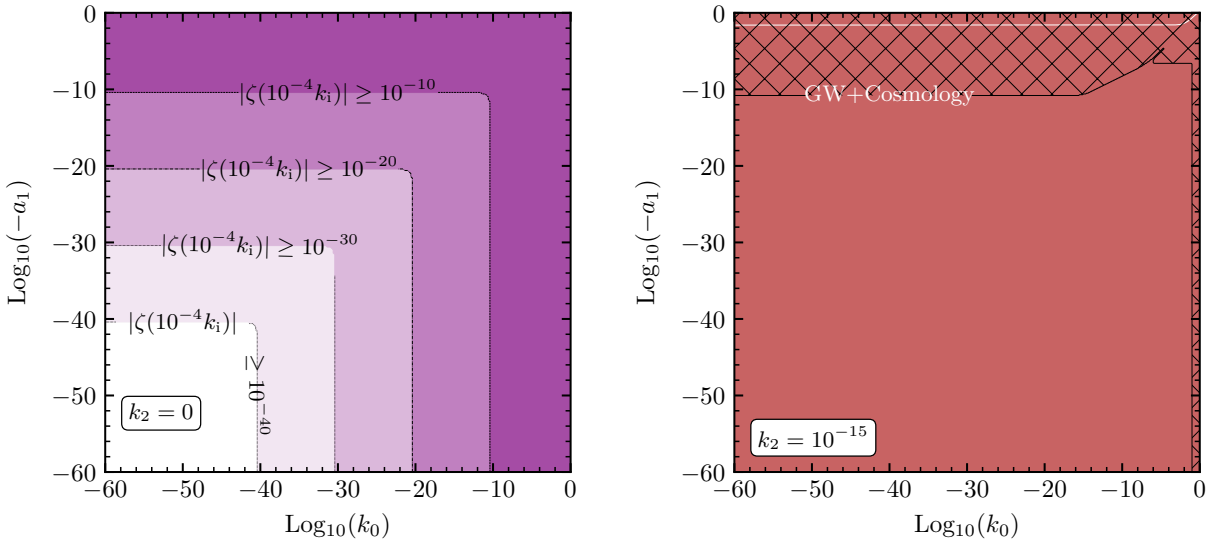

Fig. 4.18.: Left Panel: For $\Lambda > \Lambda_{\rm crit}$ we show the regions where the values for $\zeta(10^{-4}k_{\rm I})$ as generated by RG flow exceed certain bounds, when starting from $\zeta(k_{\rm I}) = 0$. We show these regions for $G_{\rm N} = 1$ and $k_2 = 0$, and $\Lambda = 0$. Under these conditions, $\zeta(k_{\rm I}) = 0$ lies in the basin of attraction of the IR repulsive sGFP $\zeta_{*,1}$ given in (4.65).
Right panel: We show the excluded regions for $\Lambda < \Lambda_{\rm crit}$, and with initial conditions close to the IR repulsive NGFP$\zeta_{*,2}$. The excluded regions are illustrated for $\Lambda = -11/2$, which is generic for the purposes of this argument. The red region indicates where $|\zeta| > 10^{-10}$, and the white band is centered around the line where $\zeta_{*,2} = 0$ (4.66). The condition $\zeta_{*,2} < \zeta_{\rm exp}$ is satisfied in a band of width $2\,\zeta_{\rm exp}$ that is centered around the white line. The black hatched region marks the regions which are excluded by cosmological and gravitational-wave observations [424].

flow towards the IR is governed by its IR -repulsive nature. This defocuses trajectories, and in particular drives $\zeta(k)$ away from $\zeta_{*,1}$. This defocusing avoids a universal value for $\zeta(M_{\rm Pl})$, but typically results in large absolute values of $\zeta(M_{\rm Pl})$. Specifically, if any of the gravitational LIV couplings has a non-vanishing value c, this will result in $\zeta(10^{-5}k_{\rm I}) \sim c$, starting from $\zeta(k_{\rm I}) = 0$, see Figure 4.16. This follows because $\zeta_{*,1}$ depends on the gravitational LIV couplings, and reads

$$\zeta_{*,1} \approx -0.056\,k_2 + 0.021\,k_0 - 0.021\,a_1\,, \tag{4.65}$$

such that only very small, or very specific values for the gravitational LIV couplings are necessary to accommodate a small value of the sGFP. To obtain an impression on how large values of $\zeta(k)$ are generated by the RG flow, we start at $\zeta(k_{\rm I}) = 0$ at different points in the gravitational parameter space. Since this is not a fixed point for ζ, the RG flow will drive $\zeta(k)$ to larger values towards the IR. The regions in the gravitational parameter space, where $\zeta(10^{-4}k_{\rm I})$ exceeds specific bounds are shown as colored regions in the left panel of Figure 4.18. If ζ in the IR was constrained to be smaller than these values, the corresponding region would be excluded from the viable gravitational LIV parameter space.

Constraints on gravitational LIV couplings for $\Lambda < \Lambda_{\rm crit}$

We will now discuss the case, where the UV value of the dimensionless version of the cosmological constant Λ is below the critical value $\Lambda_{\rm crit}$. Here, $\Lambda_{\rm crit}$ refers to the UV value of the dimensionless cosmological constant, which might be driven towards positive values in agreement with observations in the IR by quantum fluctuations of matter [257]. For a specific realization of

a trajectory in the approximation of [257], which holds in the case of Lorentz-invariant gravity, see [6].

For $\Lambda < \Lambda_{\text{crit}}$, the sGFP $\zeta_{*,1}$ is IR attractive, and the NGFP$\zeta_{*,2}$ is IR repulsive. The NGFP $\zeta_{*,2}$ shields all trajectories with $\zeta(k_{\text{I}}) < \zeta_{*,2}$ from a phenomenologically viable region featuring small violations of Lorentz invariance. The IR repulsive nature of $\zeta_{*,2}$ can be avoided by initial conditions exactly on the fixed point, such that a small value of $\zeta(M_{\text{Pl}})$ can still be realized. For the specific choice of $\Lambda = -\frac{11}{2}$, which is generic for the following argument, the fixed-point value to linear order in gravitational LIV couplings reads

$$\zeta_{*,2} \approx -7.518\, k_2 - 0.597\, k_0 - 0.317\, a_1 - 0.00792\,. \tag{4.66}$$

The line where $\zeta_{*,2} = 0$ in the gravitational parameter space is shown as a white line in the right panel of Figure 4.18. Specifically this can only happen if the absolute value of at least one gravitational LIV coupling is of the order of one. The situation for $k_2 = 10^{-15}$, and $k_0 > 0$ is shown in Figure 4.18, which includes also the direct constraints from cosmology and gravitational waves. The region of initial conditions for which an experimental constraint can be satisfied, i.e. $|\zeta_{*,2}| < \zeta_{\text{exp}}$ is located as a band of width $2\zeta_{\text{exp}}$ centered around the white line in Figure 4.18. We therefore conclude that any region where an experimental constraint on ζ can be satisfied is in conflict with direct constraints on the gravitational LIV couplings.

Next, we focus on initial conditions in the basin of attraction of the sGFP $\zeta_{*,1}$, which is IR attractive for $\Lambda < \Lambda_{\text{crit}}$. Therefore, trajectories with $\zeta(k_{\text{I}}) > \zeta_{*,2}$ are focused around $\zeta_{*,1}$ towards the IR, giving rise to a universal value $\zeta(M_{\text{Pl}}) \approx \zeta_{*,1}(M_{\text{Pl}})$. This universal value depends on the gravitational LIV couplings k_2, k_0 and a_1, and in turn allows to translate the IR constraints on ζ into constraints on k_2, k_0 and a_1 in the UV. We will use the observational bounds on $\zeta(0)$ to constrain $\zeta(M_{\text{Pl}})$ with the caveats on the validity of this scenario in mind. The resulting exclusion plots are shown in Figure 4.19 and Figure 4.20. In these figures, we combine the indirect constraints on gravitational LIV couplings from strong observational bounds on ζ with the direct constraints from cosmological and gravitational wave observations [424]. We focus on the $(k_0,\, a_1)$-plane for different values of k_2, since the observation of gravitational waves with electromagnetic counterpart [420–422] leads to $|k_2| < 10^{-15}$. For the generic choice $\Lambda = -\frac{11}{2}$, the IR attractive sGFP $\zeta_{*,1}$ expanded to linear order in gravitational LIV couplings reads

$$\zeta_{*,1} \approx 7.46\, k_2 + 0.56\, k_0 + 0.32 a_1\,. \tag{4.67}$$

Saturating the direct observational bounds, i.e., for $k_2 = \pm 10^{-15}$, the region leading to $|\zeta_{*,1}| < \zeta_{\text{exp}}$ corresponds to a band of width $2\zeta_{\text{exp}}$ centered around ζ_{exp} in the $(k_0,\, a_1)$-plane, which is shown in Figure 4.19 and Figure 4.20, respectively. This highlights the potential constraining power of the gravity-matter interplay in the presented toy model. The IR attractive sGFP $\zeta_{*,1}$ does not generate these strong constraints, but rather prevents small violations of Lorentz invariance to grow larger towards the IR. Furthermore, the sGFP is a continuous deformation of the GFP of the Lorentz-invariant theory. Therefore, for small enough gravitational LIV couplings, the existence of the sGFP is expected to be robust. Thus, we expect the qualitative features induced by the IR attractive nature of $\zeta_{*,1}$ to be robust. In turn the NGFP$\zeta_{*,2}$ cannot be traced back to a GFP. If therefore $\zeta_{*,2}$ is an artifact of the employed truncations and approximations, all values for ζ in the UV are in the basin of attraction of the IR attractive sGFP. In this case, the constraints summarized in Figure 4.19 and Figure 4.20 would be applicable for any initial condition for ζ.

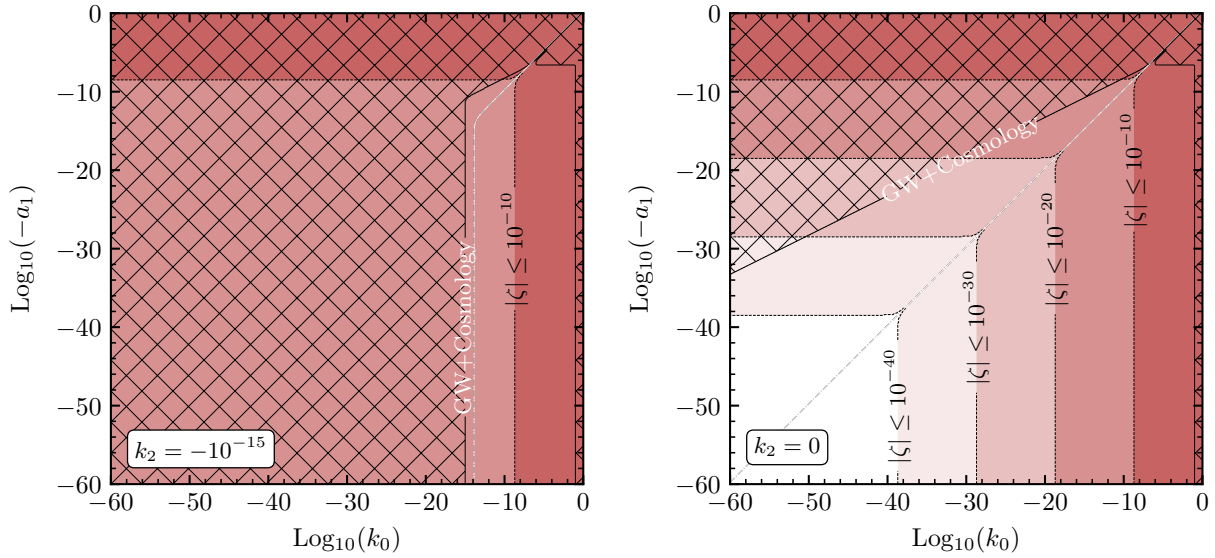

Fig. 4.19.: We show the excluded regions for $\Lambda < \Lambda_{\mathrm{crit}}$ with initial conditions in the basin of attraction of the IR attractive sGFP, cf. (4.67). The white line indicates $\zeta_{*,1} = 0$, and the red regions mark the areas where $\zeta_{*,1}$ exceeds a certain bound, e.g., $|\zeta| \leq 10^{-10}$. The hatched region marks area of exclusion by direct observations [424]. The left panel shows the case $k_2 = -10^{-15}$, while the right panel refers to the case $k_2 = 0$.

4.6.4. Modified dispersion relations

Experimental searches for violations of Lorentz invariance usually constrain each term in the SME independently. These terms are however generically related, at least within a given fundamental description, or within "natural" assumptions on their initial conditions. Specifically, canonically irrelevant couplings are typically not independent from marginal couplings. Marginal couplings are not suppressed with the Planck scale, and therefore easier to constrain with low energy experiments than canonically irrelevant couplings. The consistency relations between these different couplings are also encoded in the scale dependence of the respective couplings.

Specifically, we will consider the higher-order Lorentz-invariance violating gauge interaction described by the dimension six operator

$$\Gamma_k^{\text{Abelian, LIV,6}} \sim \bar{\kappa} \int \mathrm{d}^4x \sqrt{g}\, n_\alpha n_\beta D^\alpha D^\beta g^{\mu\rho} g^{\nu\sigma} F_{\mu\nu} F_{\rho\sigma}\,, \tag{4.68}$$

with the scale-dependent coupling $\bar{\kappa} = \kappa/k^2$, where κ is dimensionless. Such higher-order operators give rise to higher order dependencies on the energy in the dispersion relation, i.e.

$$\vec{p}^2 = E^2 + \frac{\kappa}{M_{\mathrm{Pl}}^2} E^4 \tag{4.69}$$

whose effect is Planck-scale suppressed towards lower energies, due to the canonically irrelevant nature. Such modifications of the dispersion relation have received significant interest in the photon sector, see [450–456].

Schematically, the scale dependence of κ to linear order can be written as

$$\beta_\kappa = b_{0,\kappa} + 2\kappa + b_{1,\kappa} + \mathcal{O}(\kappa^2)\,, \tag{4.70}$$

where the first term is the inducing term, in analogy to b_0 in (4.16), and where the second term

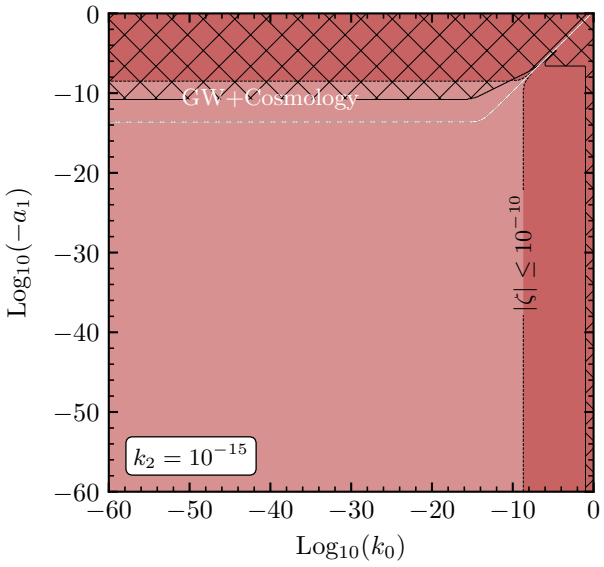

Fig. 4.20.: We show the excluded regions for $\Lambda < \Lambda_{\text{crit}}$ with initial conditions in the basin of attraction of the IR attractive sGFP, cf. (4.67), and for $k_2 = 10^{-15}$. The white line indicates $\zeta_{*,1} = 0$, and the red regions mark the areas where $\zeta_{*,1}$ exceeds a certain bound, e.g., $|\zeta| \leq 10^{-10}$. The hatched region marks area of exclusion by direct observations [424].

indicates the contribution due to the canonical mass dimension of $\bar{\kappa}$. Instead of studying the full scale dependence of κ, we will as a first step study the inducing contribution $b_{0,\kappa}$, which reads

$$\begin{aligned} b_{0,\kappa} =& G_{\mathrm{N}}\left(\frac{815a_1 - 179k_0 - 1847k_2}{1080\pi(1-2\Lambda)^2} + \frac{230a_1 + 262k_0 + 1021k_2}{540\pi(1-2\Lambda)^3}\right) \\ &+ G_{\mathrm{N}}\,\zeta\left(\frac{-4}{3\pi(1-2\Lambda)} - \frac{3167a_1 - 243k_0 + 280k_2 + 5760}{2160\pi(1-2\Lambda)^2} + \frac{1685a_1 - 1905k_0 + 1204k_2}{2160\pi(1-2\Lambda)^3}\right) \\ &+ G_{\mathrm{N}}\,\zeta^2\left(\frac{9}{4\pi(1-2\Lambda)} + \frac{24819a_1 + 3797k_0 - 5109k_2 + 32580}{10800\pi(1-2\Lambda)^2}\right. \\ &\qquad \left. + \frac{-17277a_1 + 6809k_0 + 9807k_2}{5400\pi(1-2\Lambda)^3}\right). \end{aligned} \tag{4.71}$$

The first term in (4.71) shows that the higher-order matter LIV coupling κ is induced by gravitational fluctuations that single out a preferred frame. The second and third term indicate that κ is also induced by the marginal LIV matter coupling ζ. Therefore, on the one hand LIV percolates from gravity into the matter sector, and on the other hand LIV spreads in the matter sector, once Lorentz invariance violating matter interactions are present.

The scale dependence of κ as approximated in (4.71) features a fixed point with critical exponent Θ at

$$\kappa_* \approx \frac{-b_{0,\kappa}}{2 + b_{1,\kappa}}\,, \qquad \text{with} \qquad \Theta \approx -2 - b_{1,\kappa}\,. \tag{4.72}$$

This solution is self consistent as long as $\kappa_* \ll 1$, where higher-order contributions to β_κ can be neglected. The sGFP κ_* is IR attractive in the near-perturbative regime, where $|b_{1,\kappa}| < 1$ should hold.

Due to the constant offset in the denominator of (4.72), κ_* is parametrically set by the inducing term $b_{0,\kappa}$, and hence by the LIV couplings ζ, k_2, k_0 and a_1. The IR attractive fixed point κ_* focuses RG trajectories towards the IR, and therefore is approximated at the Planck scale, which follows the same logic as in the previous section.

Below the Planck scale, gravitational fluctuations dynamically switch off, and the scale dependence of κ is dominated by the canonical scaling. In this simplified picture, the flow of the dimensionfull higher order coupling and its dimensionless counterpart read

$$\bar{\kappa}(k < M_{\rm Pl}) = \frac{\kappa_*}{M_{\rm Pl}^2}\,, \qquad \text{and} \qquad \kappa(k < M_{\rm Pl}) = \kappa_* \left(\frac{k}{M_{\rm Pl}}\right)^2\,. \tag{4.73}$$

Demanding that ζ, k_2, k_0 and a_1 satisfy their individual direct and indirect constraints, but maximize κ_* can result in very strong indirect constraints on κ. Except for very special initial conditions, we expect that strong indirect constraints on κ in the IR arise, by demanding that ζ, k_2, k_0 and a_1 satisfy themselves their individual direct and indirect constraints. These constraints for κ are expected to arise except for very special points in the parameter space, and constrain κ_* to about the same order as ζ_*. Therefore, in a setting described by the present toy model, we do not expect the observation of κ in direct searches, since direct experimental constraint on modified dispersion relations for photons result in $|\kappa_{\rm exp}| < 10^6$ [457], see also [454].

This analysis is only the first step to characterize the scale dependence of higher-order LIV operators. Especially the inclusion of the quadratic contribution to β_κ might alter the constraints on a quantitative level. The inclusion of this term also gives rise to a second fixed point, which is IR -repulsive and therefore shields certain initial conditions from the IR attractive fixed point. The qualitative features, namely the IR attractive nature of κ_*, as well as the parametric dependence of κ_* on ζ, k_2, k_0 and a_1 are expected to persist.

4.6.5. Conclusions and outlook

Probing the fundamental structure of spacetime experimentally in a direct way is difficult due to the typical Planck-scale suppression of gravitational contributions at lower energies. This difficulty might be circumvented with the study of gravity-matter systems. The interplay of quantum gravity and matter could determine fundamental properties of low-energy physics, like symmetries, or the masses of elementary particles. Some of those properties are experimentally accessible and are determined with growing precision. Using matter degrees of freedom in this way to gain insights into the quantum nature of spacetime is at the heart of parts of the Swampland program in string theory, as well as in asymptotically safe quantum gravity.

In this section, we investigated the fate of Lorentz-invariance violations in gravity-matter systems across different energies. The key idea of our study is the following: quantum gravitational fluctuations that single out a preferred frame lead to violations of Lorentz invariance at low energies. In the studied toy model, we parametrize Lorentz invariance violations in the matter sector by a scale-dependent coupling $\zeta(k)$.

Specifically, we have studied a scenario, where the scale dependence of ζ is governed by an IR attractive fixed point, the value of which is determined by the gravitational LIV coupling. Under certain conditions, this IR attractive fixed point focuses RG trajectories and results in a universal value of ζ at the Planck scale. This universality refers to the feature that the Planck-scale $\zeta(M_{\rm Pl})$ value is independent of the exact initial conditions at high energies. $\zeta(M_{\rm Pl})$ does however depend on the gravitational LIV couplings, and can be mapped to low energies by the RG flow without gravitational fluctuations. At low energies, Lorentz-invariance violations in the matter sector are constrained experimentally. Those experimental constraints also put indirect bounds on the LIV matter couplings at Planckian scales. Since the Planck-scale value of ζ depends on the gravitational LIV couplings, constraints on ζ result in indirect constraints on

the gravitational LIV parameter space. These indirect constraints could be significantly stronger than direct experimental bounds, if the observational constraints on ζ are sufficiently strong.

We support this general idea by explicitly computing the scale dependence of the LIV matter coupling ζ within a toy model. This toy model studies how of gravitational dynamics that single out a preferred frame affect the Abelian gauge sector. The study is limited in the following ways: First, we truncate the full dynamics of the gravity matter system and neglect the feedback of higher-order interactions. This results in systematic uncertainties of our computations. Second, we employ a toy model for the photon-gravity system and neglect the difference between an Abelian gauge field and the photon. Furthermore, we neglect the presence of additional degrees of freedom in the SM. Third, we employ a computation in Euclidean spacetimes to extract scale dependences using the FRG.

With these limitations in mind, our study supports the main idea summarized above. Specifically, we have shown that violations of Lorentz invariance percolate from the gravitational sector into the matter sector. This percolation of symmetry breaking is encoded in the scale dependence of ζ, which does not feature a Gaussian fixed point. The Gaussian fixed point $\zeta_* = 0$ is absent in the presence of a preferred frame, due to the ζ independent contribution to β_ζ. Therefore, a non-vanishing value for ζ is automatically generated by the RG flow, even if it is set to zero at some scale.

Furthermore, β_ζ always features an IR attractive fixed point, within the outlined approximations. This fixed point can be reached by a wide range of initial conditions for ζ at high energies, and focuses trajectories towards the IR. The focusing nature of the IR attractive fixed point allows us to remain agnostic about the UV completion of the system. If the initial conditions for ζ are located in the basin of attraction of the IR attractive fixed point, $\zeta(k)$ looses the memory of these initial conditions towards lower scales. This results in a Planck-scale value, which is independent of the initial conditions. In this case, the value of ζ at the Planck scale is given by the fixed-point value and is completely determined by the values of the gravitational LIV couplings k_2, k_0, and a_1, as well as the cosmological constant Λ. In our approximation, the flow below the Planck scale is trivial, which leads to $\zeta(0) \approx \zeta(M_{\rm Pl})$, see also Figure 4.15.

To highlight the constraining power of the gravity matter system in the presence of an IR attractive fixed point, we can translate the strong observational bounds on the photon-LIV coupling into bounds on the gravitational LIV couplings. For this translation we exploit the dependence of $\zeta(M_{\rm Pl})$ on the gravitational LIV couplings. The constraints we obtain are subject to systematic uncertainties. They should hence be confirmed on a quantitative level by computations in extended truncations, also accounting for the presence of additional degrees of freedom. If we nevertheless use the fixed-point relation for ζ to translate the constraints on the photon-LIV coupling into constraints on gravity-LIV couplings, this results in the constraints shown in Figure 4.19 and Figure 4.20. Even the least stringent bound $|\zeta| < 10^{-10}$ would therefore indirectly exclude regions in the gravitational LIV parameter space that are not excluded by cosmological observations.

Therefore, Figure 4.19 and Figure 4.20 highlight the constraining power of an IR attractive fixed point which is related to the breaking of a symmetry. If the symmetry-breaking is strongly constrained in one sector, an IR attractive fixed point might allow to translate these constraints into indirect constraints on the other sector.

Finally, we have performed first steps towards studying the scale dependence of the higher-order LIV coupling κ, which would modify the dispersion relation of the gauge field. We find indications that κ is induced in a similar way as ζ. Due to the canonical mass dimension of

κ, it features an IR attractive fixed point, as long as quantum gravitational fluctuations remain near-perturbative. The value of this fixed-point value is parametrically set by the value of ζ, and focuses RG trajectories such that $\kappa(M_{\rm Pl}) \approx \kappa_*$. Therefore, the parametric dependence of $\kappa(M_{\rm Pl})$ on $\zeta(M_{\rm Pl})$, together with the strong constraints on ζ might result in strong indirect constraints on κ. Due to the Planck-scale suppression of the canonically irrelevant coupling κ, we expect that the indirect constraints might be stronger than direct experimental constraints.

5. Conclusion and outlook

In this thesis we have investigated asymptotic safety for pure gravity and in gravity-matter systems, and have discussed several consistency tests for this scenario. In this chapter, we will summarize our results, and provide an outlook on future tests of asymptotically safe quantum gravity.

5.1. Conclusion

Due to the large separation of the Planck scale from scales that are experimentally accessible, it is crucial to confront any theory of quantum gravity with consistency tests. These consistency tests can either be theoretical, in the sense that one demands internal consistency and stability of the theory. They can also be phenomenologically motivated, in the sense that any theory that describes nature should be compatible with the phenomena we observe at low energies. The observation of matter, such as light fermions at low energies, is an example for these phenomena that a theory of quantum gravity should be compatible with. In this spirit, we have confronted the scenario of asymptotically safe quantum gravity with several theoretical and phenomenological consistency tests in this thesis.

Let us add as a note of caution that all results were obtained within approximations and are therefore subject to systematic uncertainties. Specifically, all computations are performed in the Euclidean space. The analytic continuation to Lorentzian spacetimes is an open challenge in the FRG approach to asymptotically safe quantum gravity. Similarly, the relation of numerical simulations in EDT with high-energy observables in a Lorentzian spacetime is an open question.

In Chapter 3 we have focused on theoretical consistency tests, where we investigated if and under which conditions asymptotically safe quantum gravity might be internally consistent.

Specifically, we have studied the full non-perturbative momentum dependence of the graviton and ghost propagator in asymptotic safety in Section 3.2. As our key result, we found that the propagators of different graviton modes behave qualitatively different. While the spin-two mode approaches a constant value at large momenta, the spin-zero mode does not. We find that this conclusion is independent of the chosen gauge, which indicates that, even in small truncations, the FRG gives rise to reliable and stable results. We have also reconstructed the form factors of both graviton modes according to (3.52). The evaluation of these form factors indicates no non-trivial poles in the propagator, at least at the investigated point. In turn, if the form factors are expanded in a derivative expansion, the expansion alternates in signs, indicating possible additional *fake* poles in the propagator [251]. This highlights the importance of extracting the full momentum dependence to address the question of unitarity in asymptotically safe quantum gravity.

In Section 3.3 we have performed consistency test of asymptotically safe quantum gravity on the lattice. We investigated two independent classical limits of EDT, where we have tested, whether the simulated geometries give rise to the expected behavior. On the one hand, we have investigated the gravitational binding energy of two scalar particles as a function of the mass of a single scalar. We found that in the appropriate classical and non-relativistic limit, the potential

between two scalar particles is well described by the Newton potential in four dimensions. This result, which only holds in the continuum, infinite volume extrapolation, indicates that indeed EDT reproduces classical gravity at low energies. On the other hand, we have studied the finite-volume dependence of the bare cosmological constant. In a saddle-point approximation of the EDT partition function, we found that the finite-volume scaling agrees with the $1/\sqrt{V}$ scaling, which is expected from a saddle-point approximation in the continuum.

Furthermore, both of these studies allowed us to extract a value of the Newton coupling in units of the lattice spacing. For the system with scalar particles, the Newton coupling can be extracted from the binding energy of the two-particle bound state. From the saddle-point approximation of the EDT partition function, the Newton coupling can be extracted by comparison with the corresponding expansion in the continuum, given by the Hawking-Moss instanton solution. Intriguingly, we found that the Newton coupling extracted in both ways agree within 1σ. This agreement is highly non-trivial, and indicates that EDT is indeed a theory of gravity, and not just of random geometries.

In Chapter 4 we have discussed several phenomenologically motivated consistency tests of asymptotic safety, based on FRG methods. In Section 4.4 we have investigated conditions for a UV-complete Abelian gauge sector in $d \geq 4$. We find two competing effects when increasing the dimensionality. On the one hand, we find indications that metric fluctuations have to be strong enough to induce asymptotic freedom for the Abelian gauge coupling. On the other hand, we find indications that metric fluctuations have to be weak enough to avoid new divergences in higher-order operators, due to the *weak gravity bound*. Combining these two conditions, we find that $d = 4$ and $d = 5$ appear to be special in asymptotic safety, as they are the only dimensionalities that might allow for a UV-complete Abelian gauge sector.

In Section 4.5 we have confronted the interacting fixed point for the Abelian gauge coupling with an observational consistency test. We have studied, if this interacting fixed point is compatible with the observations of light fermions in the IR, or whether it might induce chiral symmetry breaking. In the latter case fermions would necessarily become very heavy, conflicting with the observation of light fermions in our universe. We find that the fixed point is only compatible with chiral symmetry beyond a minimal number of fermions. Below this minimal number, the chirally symmetric subspace is not UV-complete at the interacting fixed point for the Abelian gauge coupling.

We have introduced and discussed the scenario of *effective asymptotic safety* in Subsection 4.3.1. In this scenario, a field-theoretic description emerges from a more fundamental theory at a finite UV scale, which is above the Planck scale. We have discussed conditions under which the predictive power of the asymptotically safe fixed point carries over to this non-fundamental realization of approximate scale invariance.

Working in this scenario, we have derived further conditions that this scenario might be realized with string theory as the more fundamental description of nature. Specifically, we have found that the weak-gravity conjecture, which should be fulfilled by any field theory emerging from string theory, imposes non-trivial conditions on the asymptotically safe fixed point. These conditions can be checked explicitly within a given model.

In the scenario of effective asymptotic safety, we have investigated how Lorentz-invariance violations (LIV) in the gravitational sector affect the matter sector, see Section 4.6. We found indications that, if the gravitational sector violates Lorentz invariance, LIV matter couplings are driven towards preferred non-vanishing values in the IR. There, they are subject to strong observational constraints. We find that the interplay of quantum gravity and matter might allow

to translate these strong constraints on LIV in the matter sector into strong indirect bounds on LIV in the gravitational sector. This highlights the constraining power of the gravity-matter interplay in the presence of an asymptotically safe fixed point.

5.2. Outlook

Based on the results presented in this thesis, we identify the following directions as promising possibilities to perform further consistency tests for asymptotically safe quantum gravity, which we will briefly discuss below: i) the phenomenology of the interacting fixed point for the Abelian gauge coupling; ii) the inclusion of dynamical matter in EDT simulations; iii) the connection between EDT and colored tensor models in the large N limit; and iv) common observables with the FRG and EDT.

i) Phenomenology of the interacting fixed point

Quantum fluctuations of the metric might render the free fixed point of the Abelian gauge coupling UV attractive, inducing a UV completion of the Abelian gauge sector [242, 297, 298, 300–302]. In this scenario, metric fluctuations would give rise to a second, interacting fixed point for the Abelian gauge coupling $g_{Y*,\text{int}}$. If $g_{Y*,\text{int}}$ is realized, the IR value for the gauge coupling is a prediction of the theory [297, 298, 300]. In principle, the viability of this fixed point could be tested by performing very precise computations, which is notoriously difficult. The resulting prediction with the experimentally determined value. The current status of this comparison is that, within an estimate on the error-bars of the FRG computations, the prediction is compatible with the experimentally measured value [298].

To test the viability of $g_{Y*,\text{int}}$, it can instead be confronted with consistency tests. The discussion of Section 4.6 provides one example of such consistency tests, since the realization of $g_{Y*,\text{int}}$ is only compatible with the observation of light fermions under certain conditions. In this spirit, the realization of $g_{Y*,\text{int}}$ can be tested by additional consistency tests. Specifically, the WGB for the $w_2\,F^4$ operator, see Figure 4.3 might be significantly stronger at $g_Y \neq 0$. Furthermore, the WGB will depend on the number of charged scalars and fermions, such that the interacting fixed point might only be a viable candidate for a UV completion for specific matter contents. In turn, w_2 will shift the value of $g_{Y*,\text{int}}$ and therefore modify the predicted IR value. An investigation of the interplay of $g_{Y*,\text{int}}$ with higher-order operators might therefore provide crucial insights into the viability of this predictive scenario of asymptotically safe quantum gravity and matter.

ii) Dynamical scalars and vectors in EDT

Including matter in EDT can be motivated at least in two ways. First, with the inclusion of dynamical matter, see [187, 194, 279] for first steps, the classical regime of EDT can be tested with a plethora of consistency tests, similar to those performed with FRG methods, see Section 4.1. Specifically, dynamical matter would allow to extract the gravitational effect on the marginal matter couplings, the f_{g_i} in (4.1). In this way, EDT itself could be confronted with phenomenological consistency tests.

Second, recent results in CDT indicate that the inclusion of matter might result in drastic changes in the phase diagram [167]. It would be interesting to investigate, whether the inclusion of matter fields in EDT has a similar effect, and could potentially create new phase transitions.

iii) EDT and colored tensor models

The EDT results discussed in this thesis are based on the partition function for random geometries (2.39), that includes a non-trivial measure term. The same partition function, including the measure term, has been studied in dually weighted colored tensor models [177], where a continuous phase transition is found analytically in a $1/N$ expansion in the $N \to \infty$ limit.

In EDT, the existence of the phase transition is postulated, but not proven. Connecting the EDT simulations to the tensor model of [177] would provide strong evidence for a higher-order phase transition in EDT. Intriguingly, the limit $N \to \infty$ limit in tensor models corresponds to the $\kappa_2 \to \infty$ limit in EDT, which seems to be the limit where the EDT lattices become finer.

The regime of large κ_2 however is numerically difficult to investigate, since the acceptance rate of the Metropolis algorithm is very low. Employing the rejection-free algorithm discussed in Subsection 3.3.3 will allow us to perform simulations in this region. Following the first-order phase transition line to larger values of κ_2 might be a first step towards establishing a connection between the numerical simulations in EDT, and the higher-order phase transition discovered in [177].

iv) Common observables from the FRG and EDT

As already highlighted above, connecting several methods to investigate the high-energy behavior of gravity-matter systems might be crucial. Since all methods employ approximations and assumptions, discovering qualitatively similar features with different methods provides a strong cross-check for the validity of the result. For methods with complementary systematic uncertainties, it is unlikely to discover the same approximation-induced effect.

One specific example for an observable that could be studied in EDT [279], which is already studied with the FRG [87, 89, 256, 312, 313, 319] is the critical exponent of the scalar mass. On the lattice, it can be extracted in the quenched approximation, comparing the renormalized and the bare mass, see, e.g., Figure 3.6. FRG studies suggest that the mass remains a relevant parameter, which allows to reproduce the observed vacuum expectation value of the scalar field. Extracting the critical exponent of the scalar mass from the lattice following [279], comparing it with FRG results, and discussing both results in a common context, might be one step towards using the FRG and EDT in a concerted way to investigate asymptotically safe gravity-matter models.

The highlighted directions are examples for strong consistency tests, which asymptotically safe quantum gravity might be confronted with in the future. The confluence of different methods addressing a variety of consistency tests could establish the phenomenological significance of a scale invariant regime of quantum gravity and matter.

6. Acknowledgements

First and foremost, I would like to thank my supervisor Astrid Eichhorn for the amazing opportunity to be part of her research group. I thank Astrid for her very conscientious and careful supervision, for her guidance and mentorship and for her enthusiasm towards discussing ideas and projects. Thank you also for providing a stimulating, interactive and respectful atmosphere in the entire research group, even when it was extended through various countries and home-offices. It is hard to imagine a better research environment than your group.

I would also like to thank Razvan Gurau for agreeing to be the second examiner of this thesis.

My appreciation extends to all former and current group members of the quantum gravity groups in Heidelberg and in Odense for many thought-provoking discussions, lunch walks, and fun activities. I would like to thank Aaron, Alessia, Andreas, Antonio, Arslan, Fleur, Gustavo, Jan, Joao, Johannes, Manuel, Masatoshi, Stefan, Tobias, and Rafael for a very friendly, inspiring and stimulating atmosphere in the group.

I would like to thank Aaron Held, Alessia Platania, Antonio Pereira, Gustavo de Brito, Johannes Lumma, and Melina Filzinger constructive feedback on this thesis.

Furthermore, I would like to thank all my collaborators for inspiring, fruitful and pleasant collaborations, for respectful discussions, as well as detailed and patient explanations whenever I had issues following an argument. Specifically, I thank Aaron Held, Alessia Platania, Benjamin Knorr, Fleur Versteegen, Gustavo de Brito, Jan Kwapisz, Jan Pawlowski, Manuel Reichert, Senarath de Alwis, and Stefan Lippoldt for collaboration on the FRG-projects that are in parts presented in this thesis.

Part of the work presented in this thesis was initiated during a research stay at Syracuse University. I would like to thank Jack Laiho for hosting me, and for providing a warm welcome in the high-energy physics group at Syracuse University. I would like to thank Jack for introducing me to lattice quantum gravity, and for proof-reading parts of this thesis.

I would also like to thank Aaron Trowbridge, Jack Laiho, Judah Unmuth-Yockey, Mingwei Dai, Scott Bassler, and Walter Freeman for collaborations on Euclidean dynamical triangulations, for welcoming me in the collaboration and for providing detailed explanations on lattice methods and subtleties.

I would like to thank the Studienstiftung for supporting my PhD proposal, and for enabling research stays in Odense and in Syracuse. Furthermore, I would like to thank Syracuse University and the CP3-Origins institute for extended hospitality.

Last but certainly not least, I would like to thank Martin Pauly for being a great office partner in the last years. Thank you for always welcoming me with an enthusiastic and big smile, even on rainy days. Most importantly, sharing the office with you made the time of my PhD even more enjoyable, and helped me to overcome difficult and challenging phases. Thank you very much.

Appendices

A. Non-perturbative propagators in quantum gravity: Supplementary material

In the following we will provide supplementary material for the discussion in Section 3.2. In particular, we will provide the explicit expressions for the projectors, and discuss several analytical properties of the anomalous dimensions.

A.1. Projectors

The transverse traceless projector, defined by the properties (3.24), in momentum space reads

$$\begin{aligned}\Pi^{\mathrm{TT}}{}_{\mu\nu}{}^{\rho\sigma} = \delta_{(\mu}{}^{\rho}\delta_{\nu)}{}^{\sigma} - \frac{1}{d-1}\bar{g}_{\mu\nu}\bar{g}^{\rho\sigma} - \frac{2}{p^2}\delta_{(\mu}{}^{(\rho}p_{\nu)}p^{\sigma)} \\ + \frac{1}{d-1}\frac{1}{p^2}\left(\bar{g}_{\mu\nu}p^{\rho}p^{\sigma} + p_{\mu}p_{\nu}\bar{g}^{\rho\sigma}\right) + \frac{d-2}{d-1}\frac{1}{p^4}p_{\mu}p_{\nu}p^{\rho}p^{\sigma}\,,\end{aligned} \tag{A.1}$$

where the round brackets indicate normalized symmetrization. The projector on the scalar mode h_0 of the graviton, is defined in (3.25). The form of the projector is entirely determined by demanding orthogonality to the transverse-traceless projector, and to the gauge-fixing action, see (3.26). Explicitly, the projector reads

$$\Pi^{0}{}_{\mu\nu}{}^{\rho\sigma} = \frac{B^2}{C}\left(\bar{g}_{\mu\nu} + \frac{A}{B}\frac{p_{\mu}p_{\nu}}{p^2}\right)\left(\bar{g}^{\rho\sigma} + \frac{A}{B}\frac{p^{\rho}p^{\sigma}}{p^2}\right)\,, \tag{A.2}$$

with

$$A = (d\beta_h - \gamma_h)\,, \tag{A.3}$$

$$B = (d - \beta_h - 1 + \gamma_h)\,, \tag{A.4}$$

$$C = (d-1)\left(\gamma_h(-2\beta_h + \gamma_h - 2) + d^2 + d\left({\beta_h}^2 + 2\gamma_h - 1\right)\right)\,. \tag{A.5}$$

The coefficients B, and C also explicitly enter the graviton propagator (3.34), and the regularized graviton propagator (3.39), while the coefficient C does not.

The trace projector Π^{Tr} and the traceless projector Π^{TL} are used to introduce the individual graviton mass parameters μ_{TL} and μ_0 for the two graviton modes, on the level of the two-point function, see (3.27). They are explicitly given by

$$\Pi^{\mathrm{Tr}}{}_{\mu\nu}{}^{\rho\sigma} = \frac{1}{d}\bar{g}_{\mu\nu}\bar{g}^{\rho\sigma}\,, \qquad \Pi^{\mathrm{TL}}{}_{\mu\nu}{}^{\rho\sigma} = \delta_{(\mu}{}^{\rho}\delta_{\nu)}{}^{\sigma} - \Pi^{\mathrm{Tr}}{}_{\mu\nu}{}^{\rho\sigma}\,. \tag{A.6}$$

The rescaling of μ_{TL} and μ_0 as in (3.28) relates both dimensionless mass parameters to the cosmological constant $\bar{\Lambda}$ in the seed action (3.16).

The two mass parameters μ_{TL} and μ_0 of the individual modes of the graviton are introduced in (3.27). On the level of a classical two-point function, (3.27) is just a convenient rewriting of the graviton two-point function including gauge fixing. On the level of the classical action,

and neglecting the breaking of gauge invariance due to the gauge fixing and the regulator, the two mass parameters are related to the single cosmological constant appearing in the Einstein-Hilbert action (3.16) via

$$\mu_{\mathrm{TL}} \to -2k^{-2}\bar{\Lambda}\,, \qquad \mu_0 \to -2k^{-2}\alpha\bar{\Lambda}\,, \tag{A.7}$$

where

$$\alpha = \frac{\left(d\left(-2{\beta_h}^2 + (\gamma_h - 6)\gamma_h + 2\right) + \gamma_h(4\beta_h - 3\gamma_h + 4) + d^2(2\gamma_h - 3) + d^3\right)}{2(d-2)(-\beta_h + d + \gamma_h - 1)^2}\,. \tag{A.8}$$

With this rescaling, the equation (3.28), which relates the two-point function in terms of μ_{TL} and μ_0 to the second functional derivative of the Einstein-Hilbert action with gauge-fixing.

The ghost propagator features two modes, the longitudinal and the transverse mode, cf. (3.36). The corresponding longitudinal and transverse projectors are defined in the usual way,

$$\Pi^{\mathrm{L}}{}_{\mu}{}^{\nu} = \frac{p_\mu p^\nu}{p^2}\,, \qquad \Pi^{\mathrm{T}}{}_{\mu}{}^{\nu} = \delta_\mu{}^\nu - \Pi^{\mathrm{L}}{}_{\mu}{}^{\nu}\,. \tag{A.9}$$

A.2. Relating anomalous dimensions ans form factors

In this section we will give more detail on the derivation of (3.52), which relates the fixed-point fluctuation form factors to the anomalous dimension. The starting point is the fixed-point condition for the anomalous dimension in terms of dimensionless wavefunction renormalizations (3.50):

$$\eta_*(y) = \eta_*(0) + 2y\frac{z_*'(y)}{z_*(y)}\,. \tag{A.10}$$

The differential equation can be solved for the dimensionless wavefunction renormalization, resulting in

$$z_*(y) = z_*(0)e^{\int_0^y \mathrm{d}s\, \frac{\eta_*(s)-\eta_*(0)}{2s}} = z_*(0)e^{\int_0^1 \mathrm{d}\omega\, \frac{\eta_*(\omega\, y)-\eta_*(0)}{2\omega}}\,. \tag{A.11}$$

If we assume that the momentum-dependent anomalous dimension is bounded, the scaling for large y of the wavefunction renormalization reads

$$z_*(y) \propto y^{\frac{\eta_*(\infty)-\eta_*(0)}{2}}\,, \qquad \text{as } y \to \infty\,. \tag{A.12}$$

Only if the anomalous dimension vanished asymptotically, the standard fall-off behavior of the propagator, which depends on the anomalous dimension at $y = 0$ follows, see (3.34). This is the case, if the anomalous dimension is *momentum local* [213], which means that the ratio of its flow and the correlator itself vanishes asymptotically at large momenta. In this case, the propagator for large momenta reads

$$G(y) \propto \frac{1}{y^{1-\frac{\eta(0)}{2}}}\,, \qquad \text{as } y \to \infty\,. \qquad \text{(momentum locality)} \tag{A.13}$$

If momentum locality is not fulfilled, i.e., if the anomalous dimension does not vanish at large momenta, we need non-local information on the momentum dependence, and the formula reads

$$G(y) \propto \frac{1}{y^{1+\frac{\eta(\infty)-\eta(0)}{2}}}\,, \qquad \text{as } y \to \infty\,. \qquad \text{(no momentum locality)} \tag{A.14}$$

With the direct access to the fixed-point wavefunction renormalization in (A.11), the fixed-

point form factor follows from the corresponding anomalous dimension by inverting (A.11). It reads

$$f_*(y) = \frac{e^{\int_0^y \mathrm{d}s\, \frac{\eta_*(s)-\eta_*(0)}{2s}} - 1}{y}\,. \tag{A.15}$$

Consequently, at large momentum the form factor is given by

$$f_*(y) \sim \begin{cases} cy^{\frac{\eta_*(\infty)-\eta_*(0)}{2}-1}\,, & \eta_*(\infty)-\eta_*(0) > 0\,, \\ -\frac{1}{y} + cy^{\frac{\eta_*(\infty)-\eta_*(0)}{2}-1}\,, & \eta_*(\infty)-\eta_*(0) \leq 0\,, \end{cases} \qquad \text{as } y \to \infty\,, \tag{A.16}$$

where c is given by

$$c = e^{\int_0^\infty \mathrm{d}s \left[\frac{\eta_*(s)-\eta_*(0)}{2s} - \frac{\eta_*(\infty)-\eta_*(0)}{2(1+s)}\right]}\,. \tag{A.17}$$

For a detailed derivation of this, see [1] (appendix A).

This concludes the proof of (3.52), which will be used to construct the fluctuation form factors.

A.3. Analytical structure of the fluctuation RG flow

In the following, we will analyze several analytical properties of the momentum dependent flow equations. These properties mainly serve as a cross-check for the numerical integration presented in Subsection 3.2.4. For a simpler notation, we will work with dimensionless momenta p^2 in the following, i.e., we make the identification $p^2/k^2 \to p^2$.

Behavior at small momenta

We have already discussed the appearance of the terms given in (3.53). Their origin lies in the projectors that appear in the propagators. Besides the discussed issue for the numerical integration, those terms also cause technical difficulties at small momenta p, in particular for the derivative expansion at $p = 0$. Expanding these terms in p is actually an expansion in p^2/q^2. Therefore, higher-orders in the external momentum p introduce higher negative powers in the loop momentum q. At a critical order in the expansion in p, the negative powers cancel the factor q^{d-1} from the integral measure, and potential powers in q from the vertices. For higher orders in the derivative expansion, these integrals do not converge, but feature IR divergences. This problem has been encountered in [458], where momentum-independent vertices had to be neglected to obtain a finite, but inconsistent result. This problem illustrates that the derivative expansion does not commute with performing the loop integral. Once the integral over the loop momentum has been performed, the flow is smooth.

To provide quantitative cross-checks for the numerical integration, we can investigate relations between different flows at vanishing momenta. In the graviton sector, we find

$$\beta_h \to -\infty: \qquad \left.\frac{\mathrm{flow}_{\mathrm{TT}}}{\mathrm{flow}_0}\right|_{p^2=0} = \frac{2}{d} - 1 < 0\,, \tag{A.18}$$

which is formally singular, in parts as a consequence how we introduce the graviton mass parameter μ_0 in (3.27). In this limit, our ansatz for the two-point function formally diverges, indicating that we are introducing a mass parameter for the spin zero gauge mode.

In the ghost sector, we find that

$$\left.\frac{\mathrm{flow}_{\mathrm{c}^\mathrm{T}}}{\mathrm{flow}_{\mathrm{c}^\mathrm{L}}}\right|_{p^2=0} = \frac{d-1-\beta_h}{d-1} > 0\,. \tag{A.19}$$

The divergence for $\beta_h \to -\infty$ indicates that the longitudinal flow vanishes at $p = 0$ for this gauge choice. Since $\beta_h < d - 1$ is a necessary condition for an invertible ghost operator, the flows, and thus the ghost anomalous dimensions, have the same sign at vanishing momentum.

Behavior at large momentum

We will now discuss the opposite limit, namely the limit of large momenta. We emphasize at this point that the three-and four-point functions are not computed in the present work. Therefore, the following conclusions only apply in our truncation. A dynamical implementation of the scale-dependence of higher-order n-point functions could change these results. We will assume that the regulator falls off exponentially. Some of the aspects that we will discuss have been studied previously in [53, 459].

In the large momentum limit, the self-energy diagrams simplify, due to the exponentially fall-off of the regulators. Due to this feature, we can neglect the regulator in the propagator that carries the external and the loop momentum. As a consequence, the remaining therms are of the form

$$\int_{-1}^{1} \mathrm{d}x \left(1-x^2\right)^{\frac{d-3}{2}} \left(p^2+2pqx+q^2\right)^k \left(p^2+2pqx+q^2+\mu\right)^{-1} , \qquad k \in \{-2,\dots,6\} , \tag{A.20}$$

where we can perform the angular integration exactly, leading to hypergeometric functions. We will now focus on each of the modes separately in this limit.

In $d = 4$, and when identifying the three- and four-graviton couplings, the spin two two-point function is momentum local [212, 213, 216]. This means that the flow of the two-point function approaches a constant value at large momentum. This is in contrast to the naive expectation that the two-point function would grow quadratically with p. Momentum locality is realized as a consequence of a cancellation of the self-energy and the tadpole diagrams.

In the present investigation, we confirm that this cancellation only happens in $d = 4$, and that in higher dimensions the expectation of a power-law behavior of the two-point function is realized. This qualitative behavior is independent of the choice for β_h.

There are three terms contributing to the flow of the spin tw two-point function, namely the graviton tadpole, the graviton self-energy and the ghost self-energy diagram, see Figure 3.2. Since there is no momentum transfer in the tadpole diagram, the integration over the loop momentum can be performed. Therefore, the tadpole diagram has the form

$$\mathrm{flow}^{\mathrm{tadpole}}_{\mathrm{TT}}(p^2,\mu_{\mathrm{TL}},\mu_0) = g_4 \left(A^{\mathrm{tadpole}}_{\mathrm{TT},0}[\eta_{h^{\mathrm{TT}}},\eta_{h^0}](\mu_{\mathrm{TL}},\mu_0) + A^{\mathrm{tadpole}}_{\mathrm{TT},2}[\eta_{h^{\mathrm{TT}}},\eta_{h^0}](\mu_{\mathrm{TL}},\mu_0) p^2 \right) , \tag{A.21}$$

where the coefficients $A^{\mathrm{tadpole}}_{\mathrm{TT,i}}$ functionally depend on the graviton anomalous dimensions, the regulators, as well as on the gaps, gauge parameters and the dimension. Since one of the propagators in the self-energy diagram depends on the external momentum and on the loop momentum, the structure is move involved. In the limit of large external momenta, we can neglect the regulator depending on the external momentum. In this limit, we find

$$\begin{aligned} \mathrm{flow}^{\mathrm{hSE}}_{\mathrm{TT}}(p^2,\mu_{\mathrm{TL}},\mu_0) \sim g_3 \int \frac{\mathrm{d}^d q}{(2\pi)^d} \sum_{i=-2}^{6} \Bigg[& A^{\mathrm{hSE}}_{\mathrm{TT,i}}[\eta_{h^0}](p^2,q^2) \frac{\left(p^2+2pqx+q^2\right)^i}{p^2+2pqx+q^2+\mu_0} \\ & + B^{\mathrm{hSE}}_{\mathrm{TT,i}}[\eta_{h^{\mathrm{TT}}}](p^2,q^2) \frac{\left(p^2+2pqx+q^2\right)^i}{p^2+2pqx+q^2+\mu_{\mathrm{TL}}} \Bigg] , \qquad \text{as } p \to \infty , \end{aligned} \tag{A.22}$$

for the graviton self-energy diagram, and

$$\text{flow}^{\text{cSE}}_{\text{TT}}(p^2) \sim g_c \int \frac{\mathrm{d}^d q}{(2\pi)^d} \sum_{i=-2}^{4} A^{\text{cSE}}_{\text{TT},i}[\eta_{c^{\text{T}}}, \eta_{c^{\text{L}}}](p^2, q^2) \left(p^2 + 2pqx + q^2\right)^i , \qquad \text{as } p \to \infty . \tag{A.23}$$

for the ghost self-energy diagram. These integrals can be performed, which results in

$$\begin{aligned} \text{flow}_{\text{TT}}(p^2, \mu_{\text{TL}}, \mu_0) \sim p^2 \Big[& (d-4) g_3 \mathcal{I}^1_{\text{TT}}[\eta_{h^{\text{TT}}}, \eta_{h^0}](\mu_{\text{TL}}, \mu_0) \\ & + (g_4 - g_3) \mathcal{I}^2_{\text{TT}}[\eta_{h^{\text{TT}}}, \eta_{h^0}](\mu_{\text{TL}}, \mu_0) \Big] , \text{ as } p \to \infty , \end{aligned} \tag{A.24}$$

where the $\mathcal{I}^i_{\text{TT}}$ are gauge- and dimension-dependent functions. We see that only for $g_3 = g_4$, and in $d = 4$, the flow vanishes at large momenta. The ghost diagram does not contribute to the leading order behavior in this limit.

More generally, we find that the only integer dimension, where a choice $g_4 = c\, g_3$ leads to momentum locality is

$$d = 6 , \qquad \text{and} \qquad g_4 = \frac{7}{4} g_3 . \tag{A.25}$$

The spin zero sector shares the same structure as the spin two sector. In particular, the asymptotic expansions as in (A.21), (A.22) and (A.23) also hold for the spin zero mode. However, the main qualitative difference is, that we do not find momentum locality for the spin zero two-point function in $d = 4$. The only combination of an integer dimension and a constant relation between g_3 and g_4 that leads to momentum locality in the spin-zero mode is

$$d = 6 , \qquad \text{and} \qquad g_4 = -2 g_3 . \tag{A.26}$$

Therefore, in our approximation, there is no situation where both sectors can be momentum local. This might however change, if higher-order operators are taken into account.

Let us now assume that $g_4 = g_3$. In this case, there are only three cases in $d \neq 4$, where there is a specific relation between the behavior at large external momentum. In general such a relation does not exist, since the contributions from the spin zero and the spin two mode to each diagram generically differ. Two of the exceptions exceptions are independent of the gauge parameter β_h:

$$\begin{aligned} d = 3 : \qquad & \frac{\text{flow}_{\text{TT}}}{\text{flow}_0}(p^2, \mu_{\text{TL}}, \mu_0) \sim 1 , \qquad \text{as } p \to \infty , \\ d = 6 : \qquad & \frac{\text{flow}_{\text{TT}}}{\text{flow}_0}(p^2, \mu_{\text{TL}}, \mu_0) \sim -\frac{1}{4} , \qquad \text{as } p \to \infty , \end{aligned} \tag{A.27}$$

and the third exception is the gauge choice $\beta_h \to -\infty$, so that

$$\beta_h \to -\infty : \quad \frac{\text{flow}_{\text{TT}}}{\text{flow}_0}(p^2, \mu_{\text{TL}}, \mu_0) \sim -\frac{(d-4)(d^3 - d^2 + 8d - 12)}{(d-2)(d+2)(3d^2 - 11d + 12)} , \quad \text{as } p \to \infty . \tag{A.28}$$

In the ghost sector, the tadpole vanishes identically in the linear parameterization of metric fluctuations [460]. In this parameterization, the ghost action is only linear in $h_{\mu\nu}$. Therefore, the flow in the ghost sector is structurally different from the flow in the graviton sector. Neither of the ghost modes shows momentum locality in our setup. This holds for any choice of the

dimension d, and the gauge. However, the two flows agree asymptotically

$$\frac{\text{flow}_{\text{c}^{\text{T}}}}{\text{flow}_{\text{c}^{\text{L}}}}(p^2, \mu_{\text{TL}}, \mu_0) \sim 1\,, \qquad \text{as } p \to \infty\,, \tag{A.29}$$

independent of dimension and gauge choice. In this limit, only one of the two self-energy diagrams contribute, namely the first one in Figure 3.2, where the regulator insertion acts on the graviton line. This feature, together with the fixed relation at $p^2 = 0$, cf. (A.19) gives an estimate on the difference between the two ghost modes.

B. Evidence for asymptotic safety from the lattice: Supplementary material

In this appendix we collect the data of all generated and analyzed ensembles. Furthermore, following [3] and [2], we will give details on the fitting procedure, which was only mentioned briefly in the main part of the thesis.

B.1. Newtonian Binding energy

B.1.1. Correlation functions

The correlators defined in (3.65) are obtained from exact inversions of the matrix L_{xy} calculated on a given lattice configuration for a given bare mass value. We do not consider every simplex on the lattice as a possible source. Instead, we vary the number of sources on each configuration from one, five, 20, and 60 in order to assess the effect the number of source simplices used has on the statistical error. We find that for a large number of sources, say 60, the systematic errors associated with modeling the deviations of the data from the model fit function are dominant. These deviations could be due to excited states, and finite-size and discretization effects. In order to avoid this difficulty of modeling the systematics, we use a single source per configuration in our main analysis. All source simplices are selected randomly from the largest three-volume cross-section of the entire lattice. This is done by first shelling a configuration starting from a source chosen at random, and then only selecting sources for the propagator from the largest slice in the shelling. We find that restricting our sources to come from the largest three-slice minimizes finite lattice spacing effects, and it is the same procedure that we have used in previous work on the spectral dimension [172] and for our studies of Kähler-Dirac fermions [194].

An example of correlator data is shown in the left panel of Figure B.1, and an example of the ratio F defined in (3.67) is shown in the right panel of Figure B.1. Both plots use log-linear coordinates and show results for several masses. These figures display a feature that appears across all ensembles, to varying degrees. We see around $r \approx 10$ lattice spacings a bend in the correlator, and a peak where the derivative of $\log[F]$ changes sign. We also see this feature is a function of the bare mass, and as the bare mass is increased, this bend is pushed out further to larger distances. The same thing happens as the volume of the system is increased. In Figure B.2 we see the peak is pushed to larger distances as the system volume is increased. This indicates that the turn-over in the data is most likely due to long-distance lattice artifacts. As noted in Ref. [172], there are baby universes that branch off of the mother universe, where the baby universes can be quite long, although their cross-section is of order the lattice spacing. This effect is most pronounced on our coarsest lattices, where it can significantly modify long-distance physics, although the effect appears to vanish in the continuum limit. It is useful to keep this in mind when choosing a fit window to extract masses from our correlation functions, since it sets an upper bound on how far in the Euclidean time extent we can fit and still expect our model fit function to describe the data. This bend in the data that we see is most likely due to baby-universe effects at long distances. At short distance scales we expect the usual discretization

ℓ_{rel}	a/ℓ	β	κ_2	N_4	Number of configs
1.59(10)	3.4(3)	1.5	0.5886	4000	367
1.28(9)	3.9(2)	0.8	1.032	4000	524
1	5.2(1)	0	1.605	2000	248
1	5.2(1)	0	1.669	4000	575
1	5.2(1)	0	1.7024	8000	489
1	5.2(1)	0	1.7325	16000	501
1	5.2(1)	0	1.75665	32000	1218
0.80(4)	7.2(7)	-0.6	2.45	4000	414
0.70(4)	8.6(9)	-0.8	3.0	8000	1486
0.70(4)	8.6(9)	-0.776	3.0	16000	2341

Tab. B.1.: The different ensembles that were used to analyze the Newtonian binding energy with their parameters, see Subsection 3.3.1. The first column shows the relative lattice spacing, normalized to the lattice spacing of the $\beta = 0$ ensembles. The errors on the relative lattice spacing are systematic errors associated with finite-volume effects [2]. The second column shows the conversion factors between link distance a and simplex distance ℓ on a given ensemble, which we will use in Subsection 3.3.2. The systematic error is associated with the matching procedure, see [2]. All a/ℓ have been corrected for finite size effects. The second column The third and fourth column are the parameters β and κ_2, which span the phase-diagram of EDT. The fifth column is the number of four-simplices in the simulation, which determines the lattice volume. The last column is the number of configurations that were analyzed.

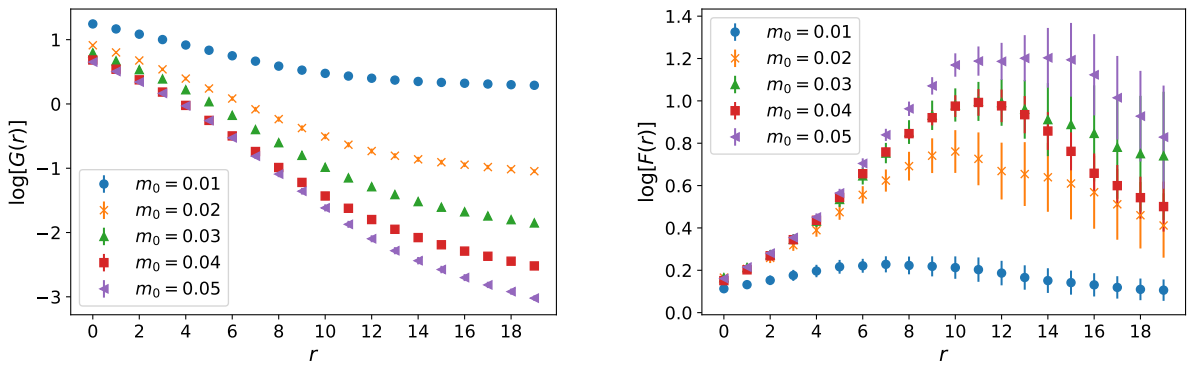

Fig. B.1.: Left panel: The logarithm of the two-point correlator, $G(r)$, for five masses on the $N_4 = 8000$, $\beta = 0$ ensemble. We see a bend in the data which is pushed progressively out to larger r values as the bare mass is increased. The distances displayed on the horizontal axis are in units of the distance between the centers of adjacent four-simplices, *i.e.* a dual edge length.
Right panel: The logarithm of the ratio between the two-particle, two-point correlator, and the square of the one-particle, two-point correlator, $F(r)$. Five different bare masses are shown on the $N_4 = 8000$, $\beta = 0$ ensemble. We see a peak in the data, separating a positively sloped region and a negatively sloped region, which is pushed to larger r values for larger bare mass values. The distances displayed on the horizontal axis are in units of the distance between the centers of adjacent four-simplices, *i.e.* a dual edge length.

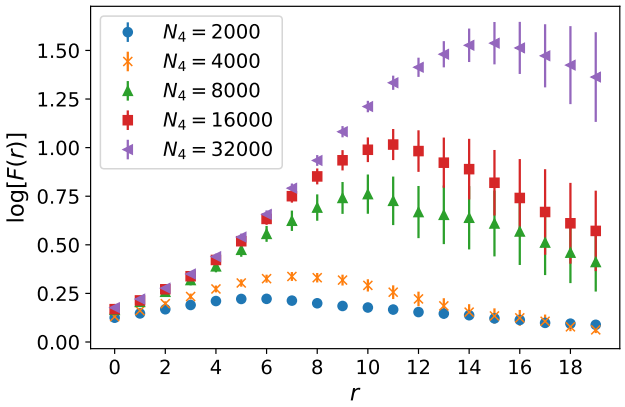

Fig. B.2.: The logarithm of the ratio of the two-particle correlator to the square of the one-particle correlator as a function of distance for multiple volumes at $\beta = 0$, and $m_0 = 0.02$. We see as the volume is increased the peak is pushed to larger values of r indicating the turn-over in the data is most likely a long-distance lattice artifact. The distances displayed on the horizontal axis are in units of the distance between the centers of adjacent four-simplices, *i.e.* a dual edge length.

effects, as well as excited state contamination. Thus, the fit window to the correlation function is rather constrained in our current approach.

The peak in $\log[F]$ is one of the first clues on how to extract a physically motivated answer for the binding energy. From the definition of E_b in (3.68) the coefficient of r should be positive if the two-particle state is bound. We see this is only possible between $r = 0$ and the peak around $r \approx 10$ lattice spacings (for the specific ensemble in Figure B.1). In fact, the existence of such a region is already encouraging, since it implies there exists an attractive force between scalar masses inside the dynamical triangulations framework. This was noticed already in Ref. [278].

Additionally, looking at the right panel in Figure B.1 we can see a change in concavity for the larger masses around a value of $r \approx 5$. This inflection point marks the change of the concavity from a region that is concave up, to a region where the data turns over *i.e.* the peak. This inflection point denotes the end of the valid fitting region according to (3.69), since after this point the long-distance effects begin to dominate the shape of the function. Across all bare masses and ensembles, we fit to a region that begins at $r = 1$ and ends around the inflection point of $\log[F]$. We fit this same range in the one-particle correlator, and the F function.

The choice of fit function is decided by the expressions in (3.69). Thus, we use a function of the form,

$$f(r) = Xr + Y + Z \log r \tag{B.1}$$

for both the $\log[F]$ and $\log[G]$ data, with X, Y, and Z as fit parameters. By fitting the $\log[F]$ and $\log[G]$ data to the functional form in (B.1) we can extract the binding energy, the renormalized mass, and the exponents p and γ as a function of the bare mass.

The fits are done with non-linear least squares fitting including the correlations of the dependent data. The errors are estimated using single-elimination jackknife resampling, including the off-diagonal terms in the correlation matrix. The size of autocorrelation errors is estimated using a blocking procedure; the data is blocked until the errors no longer increase. In order to retain enough information to resolve the correlation matrix when performing fits, the data is not blocked, but the errors are inflated to reflect the increased error due to autocorrelations. The fits are performed under a jackknife, and the correlation matrix is reconstructed for each individual

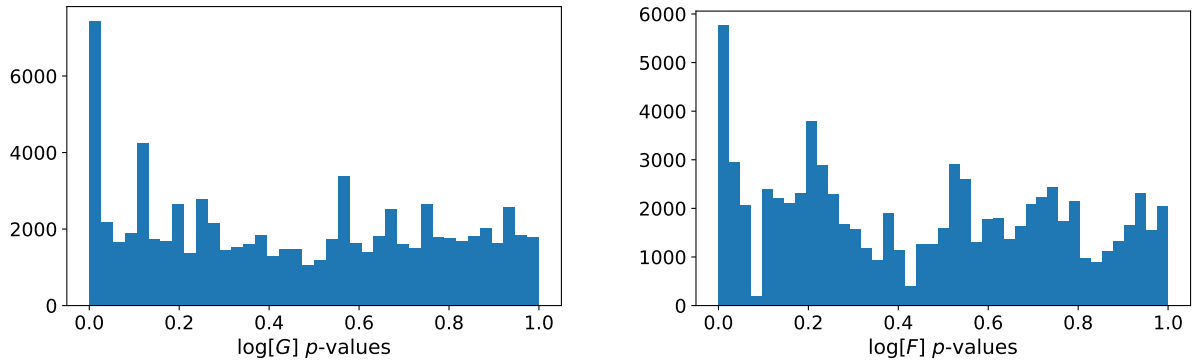

Fig. B.3.: Left panel: A histogram of the p-values extracted from fits to $\log[G]$. This histogram contains the p-values from the individual jackknife fits for all ensembles and mass values used downstream in the analysis, combined into a single data set.
Right panel: A histogram of the p-values extracted from fits to $\log[F]$. This histogram contains the p-values from the individual jackknife fits for all ensembles and mass values used downstream in the analysis, combined into a single data set.

fit under the jackknife from the data on each jackknife sub-ensemble. By including correlations in the fit, the χ^2 per degree of freedom is expected to be a reliable measure of goodness of fit. We compute from the χ^2 and the number of degrees of freedom a confidence interval (a p-value) for the fit, correcting for finite sample size. We make a histogram of p-values from the fits for which the fit parameters are propagated through to the rest of the analysis. This includes fits from all ensembles. The resulting histogram of p-values is relatively uniform, and is shown in Figure B.3 for the correlator fits, and F fits, respectively. Only the lowest bin possesses a small spike. Since the fits in this bin are scattered throughout the parameter values of the analysis more or less at random, we do not ascribe an additional error to this slight deviation from a flat distribution. An example of the fit for the $N_4 = 16,000$ simplex ensemble with $\beta = -0.776$ to the $\log[F]$ and $\log[G]$ data can be seen in Figure 3.5. Given the results for the binding energy and the renormalized mass for a wide range of bare mass values on many different ensembles, we are able to test the theory presented in Subsection 3.3.1. This is done in the following subsections.

B.1.2. Mass dependence of the binding energy

The dependence of the renormalized mass on bare mass is shown in Figure B.4 for four different volumes at fixed lattice spacing ($\beta = 0$). It is clear from this plot that the renormalized mass goes to zero as the bare mass also approaches zero, which is a consequence of the shift symmetry of the lattice action. This provides a useful check of our calculation.

The dependence of the binding energy on the renormalized mass is shown in Figs. B.5, and B.6 for four different ensembles. In order to make contact with Newtonian gravity, we must look for a power-law dependence for the binding energy as a function of renormalized mass, as given in Eq. ((3.72)). As a first step, in order to eventually be able to compare results across lattice spacings, we put the results in the same lattice spacing units. Before performing the fits we re-scale all the binding energies and renormalized masses to that of the fiducial lattice spacing at $\beta = 0$ using the relative lattice spacings given in table B.1.

To study the power-law behavior, we must also determine a fit window for the masses m, to which we fit the data. To find the beginning of a fit range, we search for the smallest bare mass for which the expected physical inflection *exists* in the quantity $\log F$ (*e.g.* in Figure B.1, $\geq m_0 = 0.02$). This identifies the minimal bare mass at which physical behavior appears in the

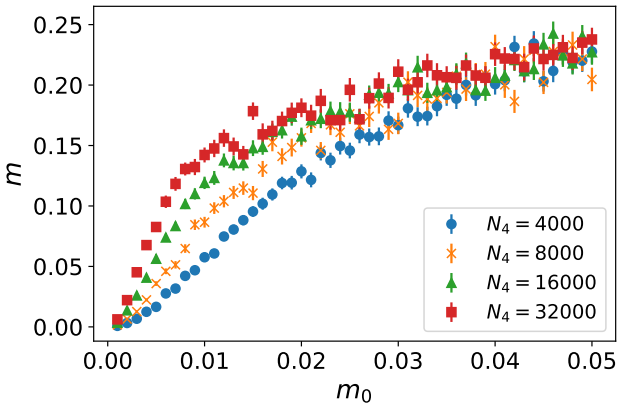

Fig. B.4.: The renormalized mass plotted against the bare mass for four volumes with $\beta = 0$. Here we see the renormalized mass is multiplicatively renormalized for sufficiently small bare masses.

correlation function. The renormalized mass m corresponding to this bare mass is the beginning of the fit window. The end of the fit window is determined by a change of inflection in the plots of binding energy versus renormalized mass. This point is where the nonrelativistic power-law behavior has been overtaken by effects due to strong coupling at larger mass values.

For our power-law fits, we assume the functional form

$$E_b = Am^\alpha \tag{B.2}$$

where A and α are fit parameters, which in the continuum, nonrelativistic limit are expected to be $A = G^2/4$, and $\alpha = 5$, as given in (3.72). We find that this simple fit function is a good description of the data on all of our ensembles, with two exceptions: our two coarsest ensembles ($\beta = 1.5$ and $\beta = 0.8$). For these ensembles we notice negative (in our convention) binding energy at small masses indicating the absence of an attractive force, which can be seen in Figs. B.6 and B.7. We do not have a good model for how discretization effects modify the expected behavior of the binding energy at very coarse lattice spacings, but it is at least encouraging that this unphysical behavior is absent on our three finest lattice spacings. We have the option of dropping these coarse lattices in our continuum extrapolation, and this is something we do as a cross-check, since we have to model the unphysical behavior of the binding energy on these two ensembles. In order to describe this data, we choose a model with two additional fit parameters beyond the simple power law of Eq. ((B.2)). The motivation for the fit function to the coarser ensembles is data driven; this is the simplest ansatz that describes the data that also reduces to the expected fit form when the new parameters are taken to zero. Thus, for our two coarsest ensembles we use the fit function

$$E_b = A|x - B|^\alpha + C \tag{B.3}$$

with A, B, α, and C the fit parameters. As before, A and α can be identified with their continuum, infinite-volume counterparts in (3.72). For these two ensembles the criteria for selecting the starting mass value of the fit is never satisfied *i.e.* the correct inflection in $\log[F]$ is not observed for any bare mass. This is most likely due to large discretization errors on these coarse lattices masking the physical behavior. Therefore the start of the fit window is somewhat arbitrary on these ensembles. We choose a fit range that begins in the region where the binding energy trends negative and ends before the inflection in the E_b versus m plot at larger masses.

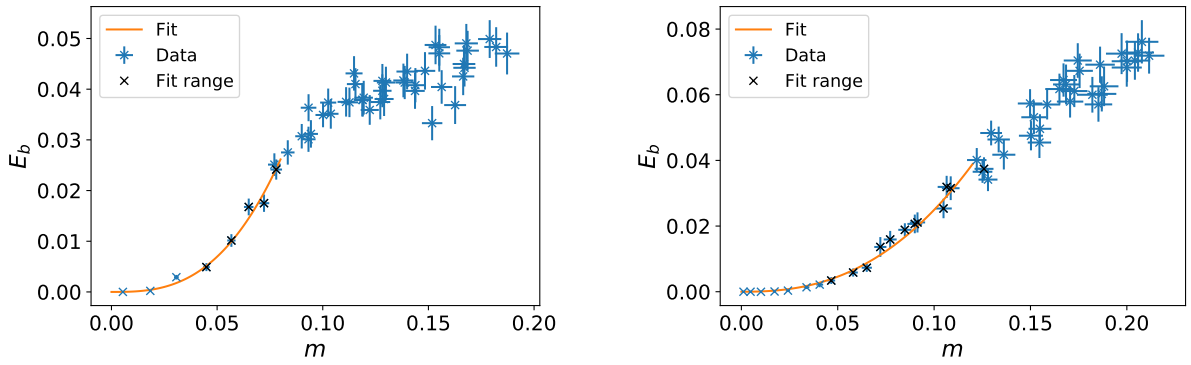

Fig. B.5.: Left panel: The power-law fit to the binding energy plotted against the renormalized mass for the $N_4 = 16,000$, $\beta = -0.776$ ensemble. The fit range is shown in black, and the solid line is the fit to the data. The fit corresponds to a χ^2/d.o.f. $= 0.59$, with a p-value of 0.62.
Right Panel: The power-law fit to the binding energy plotted against the renormalized mass for the $N_4 = 4,000$, $\beta = -0.6$ ensemble. The fit range is shown in black, and the solid line is the fit to the data. The fit corresponds to a χ^2/d.o.f. $= 0.64$, with a p-value of 0.79.

We vary this fit range to include a systematic error due to this choice.

The form in (B.2)—even at finite lattice spacing—is reinforced by the existence of the shift symmetry, which ensures that the bare mass is only multiplicatively renormalized, and hence, the binding energy is strictly proportional to some power of the renormalized mass.

In Figs. B.5, and B.6 we show examples of the binding energy plotted against the renormalized mass, along with a best fit line and the fit range used (in black), for three different lattice spacings. These are the finer lattices at $\ell_{rel} = 0.7$ and $\ell_{rel} = 0.8$, and one of the coarser ensembles at $\ell_{rel} = 1$, respectively. In Figs. B.6 and B.7 we show the same quantities for the extra coarse, $\ell_{rel} = 1.59$ ensemble, and $\ell_{\text{rel}} = 1.28$ ensemble. We see good agreement between the fit functions (B.2) and (B.3), and the data.

These fits are done by taking the correlations in the data into account. We use weighted orthogonal distance regression [461, 462] to incorporate correlations in the renormalized mass and in the binding energy data sets simultaneously. For the weights we use the inverse covariances in both data sets to obtain the best fit to the data points using χ^2 minimization. A detailed discussion of this procedure can be found in [3].

To assess a systematic error associated with the choice of fit range, we vary the start and end points of a fit range over a reasonable set of values guided by the quality of fit and tabulate the results. We then calculate the standard deviation of those results and include it as a systematic error, adding it in quadrature to the statistical error of the result from the central fit to give a total error.

We perform this power-law fit across all of our ensembles, extracting a power α and a coefficient A. From that coefficient A we calculate $\sqrt{4A}$, which we associate with a value for G at fixed volume and lattice spacing. While this association with G at finite lattice spacing or volume may suffer from systematic errors, in the continuum, infinite volume limit the quantity $\sqrt{4A}$ should extrapolate to G. With these results for α and G across ensembles, we are able to obtain their continuum, infinite-volume values.

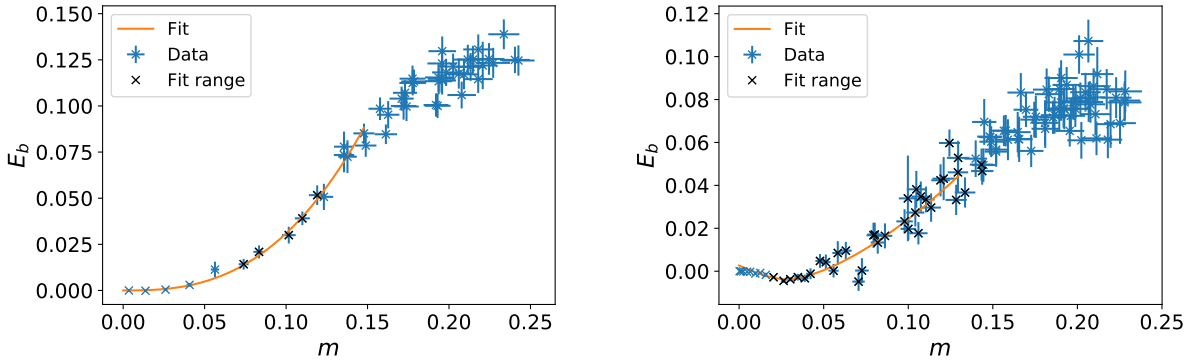

Fig. B.6.: Left panel: The power-law fit to the binding energy plotted against the renormalized mass for the $N_4 = 16,000$, $\beta = 0$ ensemble. The fit range is shown in black, and the solid line is the fit to the data. The fit corresponds to a χ^2/d.o.f. $= 0.15$, with a p-value of 0.93.
Right panel: The power-law fit to the binding energy plotted against the renormalized mass for the $N_4 = 4,000$, $\beta = 1.5$ ensemble. The fit range is shown in black, and the solid line is the fit to the data. The fit corresponds to a χ^2/d.o.f. $= 1.16$, with a p-value of 0.31.

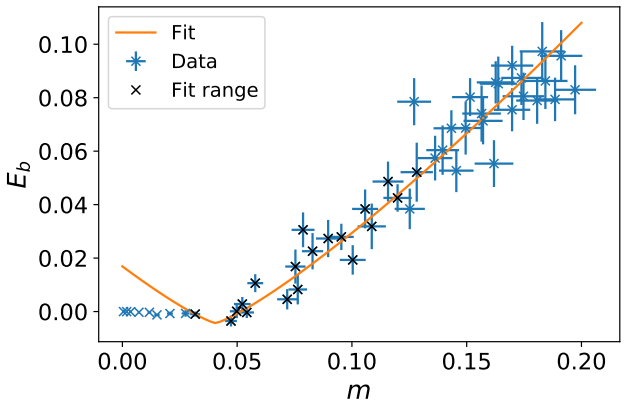

Fig. B.7.: The power-law fit to the binding energy plotted against the renormalized mass for the $N_4 = 4,000$, $\beta = 0.8$ ensemble. The fit range is shown in black, and the solid line is the fit to the data. The fit corresponds to a χ^2/d.o.f. $= 1.24$, with a p-value of 0.26.

B.2. The de Sitter instanton

B.2.1. Relating lattice distance measurements

We present the calculation of the conversion factors between link units a and simplex units ℓ on our EDT ensembles. First, we review the calculation of the return probability $P(\sigma)$, with diffusion time σ, on the dual lattice. This quantity has been used to set the relative lattice spacing in previous works [3, 172]. Before starting the random walk of the diffusion process on the dual lattice, the lattice is first shelled, with a starting four-simplex chosen at random as the source; the next shell consists of the nearest neighbors of the source simplex. The next shell consists of all of their nearest neighbors, without replacement, and so on until all of the four-simplices of the lattice configuration have been counted. The starting simplex for the diffusion process is then chosen from the shell with the maximum number of four-simplices. We find that restricting our sources to come from the largest three-slice minimizes finite lattice spacing effects, and it is the same procedure that has been used throughout the recent EDT work involving the present authors, including the study of Kähler-Dirac fermions [194] and the study of scalar interactions [3].

The diffusion process on the dual lattice uses a random walk where the next jump is chosen from the neighbors of a given simplex. Because degenerate triangulations are used, some of the five neighbors of a four-simplex are not unique, that is, sometimes the same four-simplex shares multiple tetrahedra with a neighboring four-simplex. Even so, each of the five neighbors of a given four-simplex is given equal weight when choosing the next step of the random walk. One source is used per configuration, and many random walks starting from that source are run in order to sample the probability of returning to the starting four-simplex. One peculiarity of degenerate triangulations is that for the dual lattice return probability, all of the odd time steps have zero probability, at least for time steps sufficiently early in the diffusion process. In order to compute the return probability, and the corresponding spectral dimension, we take only the even time steps, so that each step σ is actually two lattice hops in the diffusion process. This procedure of omitting the odd steps in the return probability was shown to work in the branched polymer phase, where it correctly reproduces the known spectral dimension of $4/3$ [188]. This procedure was also used to compute the return probability and spectral dimension in the subsequent work on the tuned semi-classical geometries [172].

In order to get the ratio of the link distance and the simplex distance, we compare the return probability on the direct lattice with that on the dual lattice. The implementation of the diffusion process on the direct lattice is new to the present work. Since the hops are now between vertices, and each vertex is separated by link length a, this allows us to convert simplex distance to link distance. The random walk used to compute the return probability is once again chosen from the shell with the maximal volume, but this time the shelling is performed on the vertices. In the diffusion process, a given vertex does not have a fixed number of neighbors. In fact, the number of neighbors can occasionally grow to be quite large. For this reason it is helpful to use dynamical memory allocation while computing the diffusion process. For this work, an array of linked lists was used to store all of the neighboring vertices to any particular vertex on a given configuration. Because the triangulations are degenerate, there can exist multiple links connecting the same two vertices. All such links are given equal weight when computing the probability of a hop to a nearest neighbor. In the case of the return probability on the direct lattice, both even and odd diffusion time steps are non-zero and are used in the calculation. There is an oscillation visible between the even and odd steps at early times due to discretization effects; this oscillation dies out after a sufficiently large number of time steps. This effect is

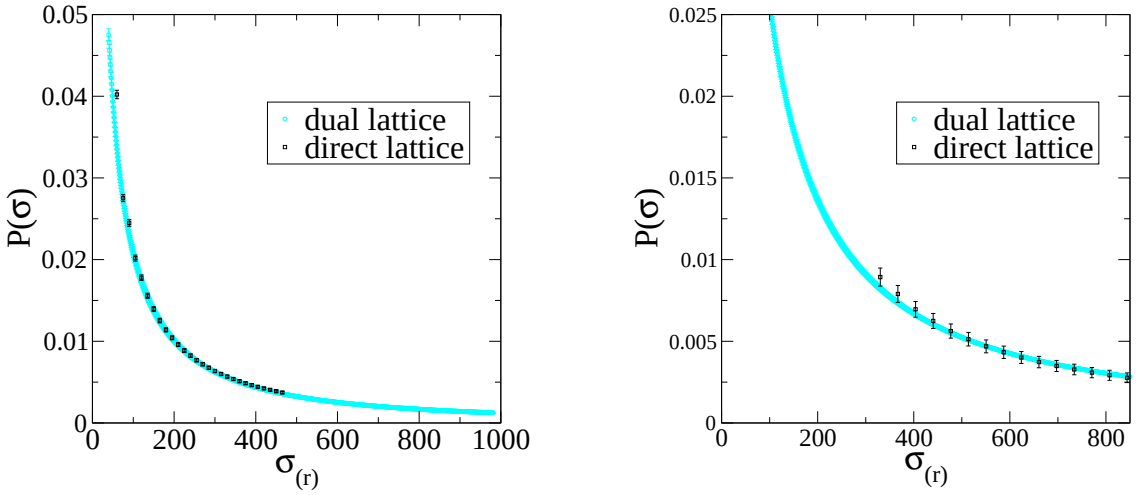

Fig. B.8.: Left panel:The return probability $P(\sigma)$ as a function of the diffusion step size σ for both the dual lattice and the direct lattice at a volume of $N_4 = 32,000$ and $\beta = 0$. The return probability for the direct lattice has a rescaled σ_r so that it overlaps with the return probability of the dual lattice.
Right panel: The return probability $P(\sigma)$ as a function of the diffusion step size σ for both the dual lattice and the direct lattice at a volume of $N_4 = 4000$ and $\beta = -0.6$. The return probability for the direct lattice has a rescaled σ_r so that it overlaps with the return probability of the dual lattice.

common in computations involving the return probability or spectral dimension on random lattices [463].

Figure B.8 shows the return probabilities for both the dual and direct lattice diffusion processes on the 32k, $\beta = 0$ ensemble. The return probability on the direct lattice has been rescaled along the σ axis so that the two curves overlap. This rescaling factor is used to determine the ratio a/ℓ. Recalling that the diffusion step is proportional to distance squared, calling σ_{dual} the diffusion time step on the dual lattice, and σ_{direct} the diffusion time step on the direct lattice, we find

$$\frac{a}{\ell} = \sqrt{\frac{2\sigma_{\text{dual}}}{\sigma_{\text{direct}}}} \tag{B.4}$$

where it is assumed that the σs are at matching points on the return probability curve. The factor of 2 accounts for the fact that each step of the diffusion process on the dual lattice is actually two lattice hops. As can be seen in the left panel of Figure B.8, the agreement between the rescaled curves is very good. The right panel in Figure B.8 shows this same matching on the finer ensemble at $\beta = -0.6$. Again, the rescaled curves line up nicely.

Table B.2 presents our values for a/ℓ extracted from each of our ensembles. For our Newton's constant analysis we quote a single number for a/ℓ at a given lattice spacing. These values are corrected for finite-volume effects. In the case of the $\beta = 0$ ensembles, where we have multiple lattice volumes, we do a direct extrapolation to infinite volume. This extrapolation is shown in Figure B.9. In order to correct all of the values of a/ℓ at other lattice spacings for finite-volume effects, we assume that the finite volume dependence is the same as that of the $\beta = 0$ ensembles, and we use that dependence to determine a correction factor for a/ℓ. This is done by matching the physical volume of the ensembles at other lattice spacings against those at $\beta = 0$, and computing the percentage difference between where that physical volume lines up with

ℓ_{rel}	N_4	a/ℓ
1.59(10)	4000	3.6(3)
1.28(9)	4000	4.3(2)
1	2000	6.2(3)
1	4000	6.3(2)
1	8000	6.1(2)
1	16000	5.7(2)
1	32000	5.43(16)
0.80(4)	4000	8.6(2)
0.70(4)	8000	10.6(6)
0.70(4)	16000	10.4(5)

Tab. B.2.: The values of a/ℓ for the different ensembles in our analysis. The first two columns identify the ensemble, the first by its relative lattice spacing in units of simplex distance, with the ensembles at $\beta = 0$ serving as the fiducial lattice spacing. The second column identifies the ensemble by the lattice volume. The third column is the value of a/ℓ on that ensemble, with an error associated with matching the return probability curves.

ℓ_{rel}	a/ℓ
1.59(10)	3.4(3)
1.28(9)	3.9(2)
1	5.2(1)
0.80(4)	7.2(7)
0.70(4)	8.6(9)

Tab. B.3.: The values of a/ℓ for different lattice spacings. The first column identifies the ensemble by its relative lattice spacing in units of simplex distance. The second column is the value of a/ℓ at that lattice spacing in the infinite volume limit, including the total error.

the curve in Figure B.9 and the infinite volume limit.

The errors in the values of a/ℓ are estimated as follows. First, the statistical errors are taken into account by varying the matching factor according to the 1σ statistical errors in the data points for the return probabilities. Second, we account for the errors associated with extrapolating a/ℓ at a given lattice spacing to its value in the infinite volume limit. At $\beta = 0$, where the extrapolation to infinite volume can be done explicitly, we vary the fit form and the number of data points included in the fit in order to estimate a systematic error associated with the infinite-volume extrapolation. Figure B.9 shows a quadratic fit to all five volumes at $\beta = 0$ and a linear fit to the largest three volumes. We also consider a quadratic fit to the four largest volumes. Based on the spread in these results, we quote an infinite volume result of $a/\ell = 5.2(1)$ at $\beta = 0$. The errors in the infinite-volume results for a/ℓ at other lattice spacings are obtained by combining the error in the finite volume correction with the error in a/ℓ at a given lattice spacing; the central values with their errors are quoted in Tab. B.3.

Data

β	κ_2	N_4	# of configs	κ_4
1.5	0.5886	4000	414	7.989973(93)
		8000	327	7.99258(18)
		16000	801	7.99530(27)
		32000	584	7.996832(49)
		64000	494	7.997903(77)
0.8	1.032	4000	262	7.00464(11)
		8000	495	7.00800(18)
		16000	91	7.01003(15)
		32000	369	7.011645(77)
		64000	869	7.012781(43)
0	1.605	2000	1712	6.147791(67)
		4000	414	6.152958(79)
		6000	579	6.154980(81)
		8000	327	6.15600(12)
		12000	244	6.15733(12)
		16000	28	6.15800(31)
0	1.669	4000	476	6.32841(18)
		8000	2849	6.330489(58)
		16000	1216	6.332214(59)
		32000	1208	6.333493(49)
		64000	903	6.33420(11)
0	1.7024	8000	489	6.42259(18)
		12000	1056	6.424000(58)
		16000	1145	6.424592(59)
		32000	1529	6.425800(49)
		64000	295	6.42652(11)
0	1.7325	16000	402	6.50854(20)
		24000	430	6.509460(96)
		32000	1369	6.509929(58)
		64000	95	6.510592(73)
-0.6	2.45	4000	414	6.78342(25)
		8000	298	6.78545(15)
		12000	807	6.786175(94)
		16000	973	6.786636(98)
		24000	1057	6.787203(78)
		32000	343	6.78758(15)

Tab. B.4.: The parameters of the ensembles used to extract the volume scaling of κ_4. The first three columns label the ensembles. The first column is β, the second is κ_2, and the third is the lattice volume N_4. The fourth column is the number of configurations used to determine κ_4, and the fifth column is the value of κ_4 determined on that ensemble, along with its statistical error.

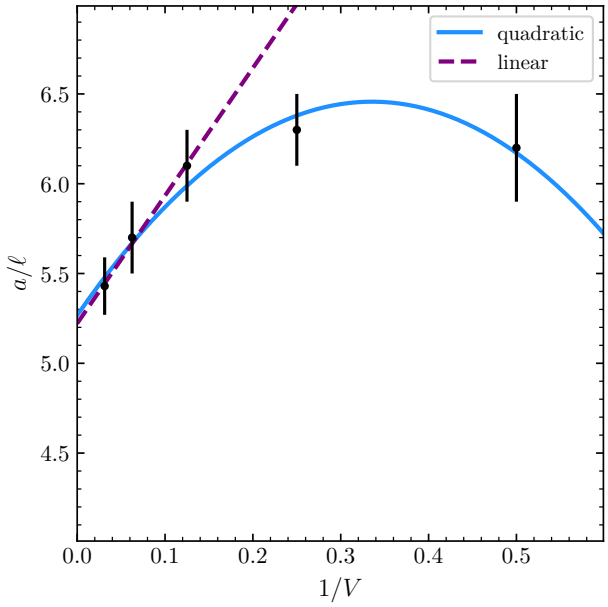

Fig. B.9.: The ratio of direct to dual lattice spacings a/ℓ as a function of $1/V$ at $\beta = 0$ for multiple volumes, and two sample fits extrapolating this quantity to the infinite volume limit.

ℓ_{rel}	V	β	κ_2	$\lvert s\rvert$	χ^2/d.o.f.	p-value
1.59(10)	25.6(6.4)	1.5	0.5886	0.724(32)	1.4	0.24
1.28(9)	10.7(3.0)	0.8	1.032	0.6840(55)	0.35	0.79
1	2.0(0)	0	1.605	0.652(14)	0.60	0.62
1	4.0(0)	0	1.669	0.521(11)	1.4	0.24
1	8.0(0)	0	1.7024	0.502(12)	0.43	0.65
1	16.0(0)	0	1.7325	0.436(39)	0.76	0.38
0.80(4)	1.64(32)	-0.6	2.45	0.393(22)	0.15	0.96

Tab. B.5.: We summarize the slopes extracted from the finite-volume scaling of κ_4, following a fit of the data in Table B.4 to the fit function (3.93). The first column is the relative lattice spacing in simplex units, and the second column is the relative physical volume $V = N_4\,\ell_{\text{rel}}^4$, in units of 1000 four-simplices. The third and fourth column are the relevant parameters of our simulations. The fifth column is the fit parameter $|s|$ in (3.93), and the two last columns give the χ^2/d.o.f and the p-value of the fit, respectively.

C. The weak gravity regime of asymptotic safety: Supplementary material

C.1. Beta functions for w_2

To simplify the notation, we label the propagator of the scalar mode with a cosmological constant Λ_0, cf. Subsection 3.2.1. This relates to the dimensionless counterpart of the cosmological constant Λ appearing in the Einstein Hilbert action via (A.8). For $d = 4$, this can be simplified to

$$\Lambda_0 = \frac{2\Lambda\left(3-{\beta_h}^2\right)}{(\beta_h-3)^2}\,. \tag{C.1}$$

For $\beta_h = 0$, the scale dependence of w_2 reads

$$\begin{aligned}\beta_{w_2} =&2(2+\eta_A)w_2 - \frac{19(\eta_A-10)w_2^2}{240\pi^2} - \frac{2(279\eta_{h^{\mathrm{TT}}}-1430)G^2}{405(1-2\Lambda)^3}\\ &+\frac{G(8\pi(61\eta_A-80)G+3(363\eta_{h^{\mathrm{TT}}}-1930)w_2)}{1620\pi(1-2\Lambda)^2} - \frac{(31\eta_A-110)w_2G}{135\pi(1-2\Lambda)}\\ &-\frac{(\eta_{h^{\mathrm{TT}}}-6)w_2G}{6\pi(1-2\Lambda_0)^2} + \frac{20(\eta_{h^{\mathrm{TT}}}-6)G^2}{81(1-2\Lambda)(1-2\Lambda_0)^2}\\ &+\frac{20(\eta_{h^{\mathrm{TT}}}-6)G^2}{81(1-2\Lambda)^2(1-2\Lambda_0)}\,.\end{aligned} \tag{C.2}$$

For $\beta_h = d/2-1$, it reads

$$\begin{aligned}\beta_{w_2} =&(d+2\eta_A)w_2\\ &+G^2\Bigg(\frac{2^{7-d}\pi^{2-\frac{d}{2}}}{(d-2)^2(1-2\Lambda)^2\Gamma\left[3+\frac{d}{2}\right]}\Bigg((4-d)(4-10d+d^3)\\ &\quad+\frac{d^7+d^6-30d^5+36d^4+136d^3-544d^2+1152d-512}{2^3d(1-2\Lambda)}\Bigg)\Bigg)\\ &+G\,w_2\Bigg(\frac{2^{8-d}\pi^{1-\frac{d}{2}}}{(d-2)(1-2\Lambda)\Gamma\left[3+\frac{d}{2}\right]}\Bigg((3+d(d-5))\\ &\quad+\frac{d^6-13d^5-48d^4+276d^3+112d^2-256d-256}{2^7d(1-2\Lambda)}\Bigg)\Bigg)\\ &+w_2^2\frac{2^{1-d}(48+d(6+d+d^2))}{\pi^{d/2}\Gamma\left[3+\frac{d}{2}\right]}.\end{aligned} \tag{C.3}$$

D. Light charged fermions in quantum gravity: Supplementary material

D.1. Fixed-point collisions in four-fermion interactions

We discuss in detail the mechanism of fixed-point collisions in the four-fermion system discussed in Section 4.5. The mechanism is in analogy with the mechanism that gives rise to the WGB, see Section 4.2. The only differences are: First, we discuss the fixed-point collision in a two-dimensional system explicitly, and second, the external coupling that drives the collision in the four-fermion system is the Abelian gauge coupling, and not gravity, as discussed in Section 4.2.

For the purpose of the following discussion, we schematically write the RG-scale dependence of the four-fermion interactions $\lambda_\pm$ as

$$\beta_{\lambda_\pm} = 2\lambda_\pm + \sum_{i=0}^{2} a_i^\pm \lambda_+^i \, \lambda_-^{2-i} + b_\pm \lambda_\pm h_{\text{ext}} + c_\pm h_{\text{ext}}^2 \,, \tag{D.1}$$

where $a_i^\pm$, $b_\pm$ and $c_\pm$ are numerical coefficients, and where h_{ext} is an external coupling encoding the interaction of fermions with other fields.

In the absence of the external coupling, i.e., $h_{\text{ext}} = 0$, the system of beta functions (D.1) has four real-valued fixed points, as shown in Figure D.1. At the GFP, where $\lambda_{+,*} = \lambda_{-,*} = 0$, the critical exponent of both couplings is their canonical mass dimension. Thus, the fixed point has two irrelevant directions. Two of the other three fixed points are (partially) interacting, with one relevant and one irrelevant direction. The fourth fixed point is fully interacting and features two relevant directions. Therefore, any initial conditions for the couplings $\lambda_\pm$outside the green region in Figure D.1 does not lie within the basin of attraction of an IR-attractive fixed point. Accordingly, the couplings will be driven further away from the green region towards lower energies, resulting in a divergence in one of the four-fermion interactions at some RG-scale $k_{\chi SB}$. Therefore, any initial condition outside the green region leads to spontaneous chiral-symmetry breaking.

A qualitatively similar picture holds for small values of the external field, i.e., $|h_{\text{ext}}| < |h_{\text{ext,crit}}|$. The RG-flow is still dominated by the h_{ext}-independent terms. However, due to the finite contribution $c_\pm$, a non-vanishing $\lambda_{\pm,*} \neq 0$ is unavoidable. In this case, the Gaussian fixed point, which exists at $h_{\text{ext}} = 0$ is shifted to a non-vanishing fixed-point value for small h_{ext}. This sGFP still features two irrelevant directions, such that the situation shown in Figure D.1 qualitatively carries over to non-vanishing values of the external coupling. Specifically, for small enough values of h_{ext}, all four fixed-points will be real-valued, and the basin of attraction of the sGFP will only be slightly deformed. As discussed in Section 4.2 in the context of the WGB, it depends on the sign of the coefficients $c_\pm$ if there is a critical value $h_{\text{ext,crit}}$ such that the sGFP collides with one of the other fixed points. If this is the case, for $|h_{\text{ext}}| > |h_{\text{ext,crit}}|$ the sGFP lies off the real axis. Accordingly, any initial condition for $\lambda_\pm$ will give rise to a divergence in one of the induced interactions, and therefore lead to the spontaneous breaking of chiral symmetry. This

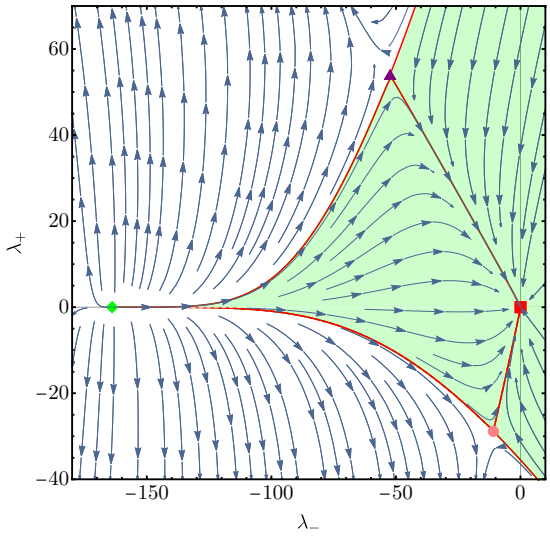

Fig. D.1.: We show the fixed-point structure of the four fermion interactions $\lambda_\pm$. The green region indicates the region of initial conditions $\lambda_{\pm,\,\text{in}}$ which does not give rise to spontaneous breaking of chiral symmetry. Initial conditions outside the green region will result in the divergence of one of the four-fermion interactions, indicating the onset of spontaneous chiral-symmetry breaking. For the illustration we choose N_F=2, $G = \Lambda = 0$, and $e = 1$.

mechanism is very similar to the mechanism giving rise to the WGB discussed in Section 4.2, the only difference being that in the present discussion the external coupling h_ext does not need to be the gravitational coupling.

Indeed, if the external coupling is gravitational, the coefficients $c_\pm$ have the appropriate sign to potentially trigger the collision of fixed points [336]. However, this effect is compensated by the linear coefficients $b_\pm$. Therefore, in the absence of additional external couplings, quantum gravitational fluctuations stabilize the system and drive the fixed points away from each other [336]. If on the other hand h_ext is the non-Abelian gauge coupling, the described mechanism determines the IR spectrum of bound states in QCD. There, the four-fermion interactions are driven towards criticality in the IR, driven by the strong non-Abelian gauge coupling [367–373, 384, 386, 388, 393]. A similar mechanism is found in QED in three and four dimensions, where the Abelian gauge coupling e becomes strong in the UV [294, 394, 464].

In the following, we include two external couplings, and investigate the four-fermion system in the presence of an Abelian gauge field; we include quantum gravitational fluctuations. As discussed in Section 4.4, a screening nature of metric fluctuations might induce a predictive UV-completion of the Abelian gauge coupling in $d = 4$, featuring a non-vanishing fixed-point value e_* for the Abelian gauge field [297, 298, 302]. We will investigate whether the generation of a non-vanishing Abelian gauge coupling in the UV triggers a fixed-point collision for $\lambda_\pm$, or whether the stabilizing effect of metric fluctuations dominates [336], which would result in no chiral symmetry breaking in the fermion-gauge-gravity system.

Specifically, the value of the NGFP for the gauge coupling depends on the number of fermions. In our approximation it reads

$$e_{*,\,\text{int}} = \sqrt{\frac{24\pi^2 f_g}{N_\text{F}}}\,, \tag{D.2}$$

where the gravitational contribution f_g also implicitly depends on the number of fermions, and where $f_g \geq 0$ was found within the FRG [7, 242, 297, 298, 300–302, 465]. We will therefore

investigate, for which value of $N_{\rm F}$ the predictive fixed point for the gauge coupling lies in a strong coupling regime. Specifically, we will study, whether there exists a critical number of fermions, for which $e_{*,\,\rm int}$ induces a fixed-point collision for $\lambda_\pm$.

D.2. Details on the setup

For investigation in Section 4.5, we approximate the dynamics of the gravity-gauge-fermion system by the effective action

$$\Gamma_k = \Gamma_k^{\rm EH} + \Gamma_k^{U(1)} + \Gamma_k^{\rm F}\,, \tag{D.3}$$

where $\Gamma_k^{\rm EH}$ is the Einstein-Hilbert action (3.16), and where the dynamics of the Abelian gauge field is encoded in $\Gamma_k^{U(1)}$, see (4.9).

The minimal coupling of fermions to the Abelian gauge field and to gravity is implemented via the covariant derivative in the fermionic action (4.47) and reads

$$\nabla_\mu = \partial_\mu + i\,eA_\mu + \frac{1}{8}\left[\gamma^a,\gamma^b\right]\omega_\mu^{ab}\,, \tag{D.4}$$

where we have introduced the Abelian gauge coupling e. The spin connection ω_μ^{ab} is not treated as an independent variable in the present formalism. In this case, it can be determined in terms of the Christoffel connection in the Vielbein formalism or can equivalently be expressed via the the spin-base invariance formalism [466–468]. Studies going beyond the minimal coupling of fermions to gravity have been put forward in [243, 263, 316]. The wavefunction renormalizations for fermions and gauge fields give rise to respective anomalous dimensions via

$$\eta_A = -k\partial_k\, Z_A\,, \qquad \text{and} \qquad \eta_\psi = -k\partial_k\, Z_\psi\,. \tag{D.5}$$

As in the previous section, we use the anomalous dimension of the Abelian gauge field to extract the scale dependence of the Abelian gauge coupling by making use of perturbative Ward identities. Accordingly, the scale dependence of the Abelian gauge coupling reads

$$\beta_e = \frac{e}{2}\,\eta_A\,. \tag{D.6}$$

For the present investigation, we choose a regulator $\mathcal{R}_k$ in (2.21) which inherits the tensor structure from the two-point vertex $\Gamma_k^{(2)}$ [71, 88, 270, 469], such that it is diagonal in field space and reads

$$\mathcal{R}_k(p^2) = \Gamma_k^{(2)}(p^2)\, r_k(p^2/k^2)\big|_{\Lambda=\lambda_+=\lambda_-=0}\,. \tag{D.7}$$

Here $\Gamma_k^{(2)}$ refers to the second functional derivative of the effective action (4.46) with respect to one of the fields. For the shape functions r_k we choose Litim-type cutoffs [470], i.e.

$$r_k^h(x) = r_k^A(x) = \left(\frac{1}{x}-1\right)\Theta(1-x)\,, \quad \text{and} \quad r_k^\psi(x) = \left(\frac{1}{\sqrt{x}}-1\right)\Theta(1-x)\,. \tag{D.8}$$

Evaluating $\Gamma_k^{(2)}$ in (D.7) at $\Lambda=\lambda_+=\lambda_-=0$ ensures that no momentum-independent contributions enter the regulator, such that the regulator properties (2.20) are always ensured. Choosing the regulator proportional to the tensor structure of the two-point vertex also ensures that the $\mathcal{R}_k$ does not break chiral symmetry. Since the aim of this study is to investigate the spontaneous breaking of chiral symmetry via quantum fluctuations of vector bosons and gravity, this

is a crucial prerequisite. Specifically, the regulator for the fermions reads

$$\mathcal{R}_k(p^2) = Z_\psi \not{p} \left(\sqrt{\frac{k^2}{p^2}} - 1 \right) \Theta \left(1 - \frac{p^2}{k^2} \right) , \tag{D.9}$$

which can be generalized in terms of $\not{\nabla}$ for the fermionic contributions to the gravitational beta functions.

We employ a perturbative approximation when evaluating the scale dependence of all couplings, where the anomalous dimensions stemming from the scale derivative of the regulator $k\partial_k \mathcal{R}_k$ are neglected.

D.3. Beta-functions

For completeness, we give the general β_h-dependent beta-functions for the four-fermion interactions $\lambda_\pm$ in $d = 4$ dimensions. To simplify the notation, we label the propagator of the scalar mode with a cosmological constant Λ_0, cf. Subsection 3.2.1. This relates to the dimensionless counterpart of the cosmological constant Λ appearing in the Einstein Hilbert action via (A.8). For $d = 4$, this can be simplified to

$$\Lambda_0 = \frac{2\Lambda \left(3 - {\beta_h}^2\right)}{(\beta_h - 3)^2} . \tag{D.10}$$

With this, the scale dependence of $\lambda_\pm$ read

$$\begin{aligned}
\beta_{\lambda_+} =& (2 + 2\eta_\psi)\lambda_+ \\
&+ \frac{2e^2\lambda_+(5\eta_A + 6\eta_\psi - 60) + e^4(-5\eta_A - 3\eta_\psi + 45) - 4(\eta_\psi - 5)\lambda_+(3\lambda_+ + 2\lambda_-(N_{\rm F} + 1))}{160\pi^2} \\
&- \frac{5(\eta_A - 6)Ge^2}{96\pi(1 - 2\Lambda)} - \frac{5(\eta_{h^{\rm TT}} - 6)G\left(e^2 + 8\lambda_+\right)}{96\pi(1 - 2\Lambda)^2} - \frac{5(\eta_{h^{\rm TT}} - 8)G^2}{64(1 - 2\Lambda)^3} \\
&+ \frac{G\left(e^2(673\eta_A + 528\eta_\psi - 8484) - 1440(\eta_\psi - 7)\lambda_+\right)}{13440\pi(1 - 2\Lambda_0)} \\
&+ \frac{G\left(e^2(107\eta_A + 42(\eta_\psi - 23)) - 112(\eta_\psi - 6)\lambda_+\right)}{280\pi(1 - 2\Lambda_0)(\beta_h - 3)} + \frac{3(\eta_A - 6)Ge^2}{4\pi(1 - 2\Lambda_0)(\beta_h - 3)^2} \\
&+ \frac{G\left((673\eta_{h^{\rm TT}} - 4956)e^2 + 140(7\eta_{h^{\rm TT}} - 24)\lambda_+\right)}{13440\pi(1 - 2\Lambda_0)^2} \\
&+ \frac{G\left((107\eta_{h^{\rm TT}} - 714)e^2 + 8(11\eta_{h^{\rm TT}} - 42)\lambda_+\right)}{280\pi(1 - 2\Lambda_0)^2(\beta_h - 3)} + \frac{(\eta_{h^{\rm TT}} - 6)G\left(3e^2 + 4\lambda_+\right)}{4\pi(1 - 2\Lambda_0)^2(\beta_h - 3)^2} ,
\end{aligned} \tag{D.11}$$

and

$$\begin{aligned}\beta_{\lambda_-} =&(2+2\eta_\psi)\lambda_- \\ &+\frac{-2e^2\lambda_-(5\eta_A+6\eta_\psi-60)+e^4(5\eta_A+3\eta_\psi-45)-4(\eta_\psi-5)\left(\lambda_-^2(N_{\rm F}-1)+\lambda_+^2N_{\rm F}\right)}{160\pi^2} \\ &-\frac{5(\eta_A-6)Ge^2}{96\pi(1-2\Lambda)}-\frac{5(\eta_{h^{\rm TT}}-6)G\left(e^2+8\lambda_-\right)}{96\pi(1-2\Lambda)^2}+\frac{5(\eta_{h^{\rm TT}}-8)G^2}{64(1-2\Lambda)^3} \\ &+\frac{G\left(e^2(673\eta_A+528\eta_\psi-8484)-1440(\eta_\psi-7)\lambda_-\right)}{13440\pi(1-2\Lambda_0)} \\ &+\frac{G\left(e^2(107\eta_A+42(\eta_\psi-23))-112(\eta_\psi-6)\lambda_-\right)}{280\pi(1-2\Lambda_0)(\beta_h-3)}+\frac{3(\eta_A-6)Ge^2}{4\pi(1-2\Lambda_0)(\beta_h-3)^2} \\ &+\frac{G\left((673\eta_{h^{\rm TT}}-4956)e^2+140(7\eta_{h^{\rm TT}}-24)\lambda_-\right)}{13440\pi(1-2\Lambda_0)^2} \\ &+\frac{G\left((107\eta_{h^{\rm TT}}-714)e^2+8(11\eta_{h^{\rm TT}}-42)\lambda_-\right)}{280\pi(1-2\Lambda_0)^2(\beta_h-3)}+\frac{(\eta_{h^{\rm TT}}-6)\left(3e^2+4\lambda_-\right)}{4\pi(1-2\Lambda_0)^2(\beta_h-3)^2}\,,\end{aligned} \tag{D.12}$$

where the first lines constitute the canonical contribution, respectively. We have explicitly written the anomalous dimensions, both the one appearing in the canonical term, as well as the anomalous dimensions from the regulator insertion. The fermion and gauge anomalous dimension extracted in a derivative expansion reads

$$\begin{aligned}\eta_\psi =&\frac{25(\eta_{h^{\rm TT}}-6)G}{96\pi(1-2\Lambda)^2}+\frac{(\eta_\psi-6)G}{40\pi(1-2\Lambda_0)}+\frac{3(\eta_\psi-6)G}{20\pi(1-2\Lambda_0)(\beta_h-3)} \\ &+\frac{(861-148\eta_{h^{\rm TT}})G}{1680\pi(1-2\Lambda_0)^2}+\frac{(546-103\eta_{h^{\rm TT}})G}{280\pi(1-2\Lambda_0)^2(\beta_h-3)} \\ &-\frac{3(\eta_{h^{\rm TT}}-6)G}{4\pi(1-2\Lambda_0)^2(\beta_h-3)^2}\,.\end{aligned} \tag{D.13}$$

The anomalous dimension of the gauge field is given in (4.40), from which the scale dependence of the Abelian gauge coupling follows in our approximation, see (D.6).

D.4. Comparison of background and fluctuation computations

Besides the gauge dependence, we will now additionally test the robustness of the system investigated in Section 4.5. Specifically, we will show that the main qualitative features investigated in Section 4.5 are also realized in a fluctuation setup. In summary, the shared qualitative features are i) the existence of a non-trivial lower bound $N_{\rm F\,crit} > 1$, ii) a regime of unbroken chiral symmetry in the weak-gravity regime and iii) the shift of the boundary between broken and intact chiral symmetry towards a more strongly coupled regime, when $N_{\rm F}$ is increased.

We will refer to the approximation described in Section 4.5 as the background results. In this approximation background diffeomorphism invariance remains intact, but the propagator driving the scale-dependence of the gravitational couplings is approximated as the propagator of the background field, instead of the fluctuation field. To allow a direct comparison, we employ the gauge $\beta_h = 1$ in the following, which constitutes a difference to the investigations of Section 4.5. We will refer to the fluctuation approximation as the results reported in [266], with $N_{\rm s} = 0$ and $N_{\rm v} = 1$. In this approximation, the scale dependence of fluctuation couplings g, λ_2 and λ_3 is computed, which is driven by the propagator of metric fluctuations, see also the discussion in Subsection 3.2.1. In addition to the distinction of fluctuation field and background

field, the fluctuation approximation performed in [266] also takes the momentum dependence of correlation functions into account. This was found to be crucial for the feature of *effective universality* [113, 243, 266], which provides indications for the effective restoration of diffeomorphism invariance. For consistency, we extract the scale dependence of the Abelian gauge coupling e from the momentum-dependent anomalous dimension of the gauge field, evaluated at $p^2 = k^2$. As discussed in [242], in contrast to $\eta_A(0)$, which is part of the background approximation, $\eta_A(k^2)$ does not feature a sign-flip as a function of λ_2, which is found to be a truncation and regulator artefact. Additionally, the anomalous dimension $\eta_A(k^2)$ provides a more accurate approximation to the global momentum dependence of $\eta_A(p^2)$ [242].

In the following, we will compare both approximations, each of them in a perturbative approximation for the anomalous dimension. In this approximation, the anomalous dimension resulting from the regulator insertion is neglected. This approximation is valid, as long as the anomalous dimensions remain small.

The main focus of this comparison is to determine, whether and to what extend the qualitative features of the scenario described in [4] remain unchanged in both approximations. In the light of the disagreement on the level of fixed-point values, as well as on the existence of bounds on the matter content between both approximations, it is intriguing to understand, whether more physical features of a system, such as the status of chiral symmetry, remains qualitatively similar between different approximations.

Our comparison constitutes two parts. In the first part, we compare both approximations on the asymptotically safe fixed point for the gravity-mater system. In the second part, we compare the regions of intact and spontaneously broken chiral symmetry in the plane spanned by gravitational couplings G and Λ for the background approximation, and by g and λ_2 in the fluctuation approximation.

D.4.1. Asymptotic safety and chiral symmetry

In both approximations the scale dependence of the gravitational couplings in independent of the Abelian gauge coupling e. Therefore, we investigate the compatibility of light fermions with an asymptotically safe fixed point for the gravity-matter system, by comparing the critical value e_{crit} of the Abelian gauge coupling, at which the four-fermion interactions $\lambda_\pm$ are driven to criticality. From Fig. D.2 we observe that the difference between background and fluctuation approximation is of quantitative nature only. Despite rather different gravitational fixed-point values, the qualitative behavior of $e_*(\mathrm{F})$ is similar in both approximation. In similar fashion, the behavior of the critical value $e_{\text{crit}}(N_{\mathrm{F}})$ is similar. The latter can be understood by realizing that the scale dependence of $\lambda_\pm$ remains unchanged in both approximations. Therefore, the effect of quantum gravity on the four-fermion interactions is parameterized by effective gravitational couplings

$$G_{\text{eff},\,n} = \frac{G}{(1-2\Lambda)^n} \quad \text{and} \quad g_{\text{eff},\,n} = \frac{g}{(1-2\lambda_2)^n}\,. \tag{D.14}$$

However, despite different dynamics of the fixed-point values $(G_*(N_{\mathrm{F}}),\, \Lambda_*(N_{\mathrm{F}}))$ as well as $(g_*(N_{\mathrm{F}}),\, \lambda_{2*}(N_{\mathrm{F}}))$, these effective gravitational couplings evolve in a qualitatively similar behavior for increasing N_{F}, cf. [243]. In summary, the effective gravitational couplings in both approximations decrease with increasing number of fermions, explaining the similar qualitative behavior of the green lines in Fig. D.2. The different absolute value of the effective gravitational coupling in both approximations, as well as the quantitative differences in the fixed point value for the Abelian gauge coupling, lead to quantitatively different value of the critical value $N_{\mathrm{F\,crit}}$. However, both approximations feature a non-trivial lower bound on the number of fermions

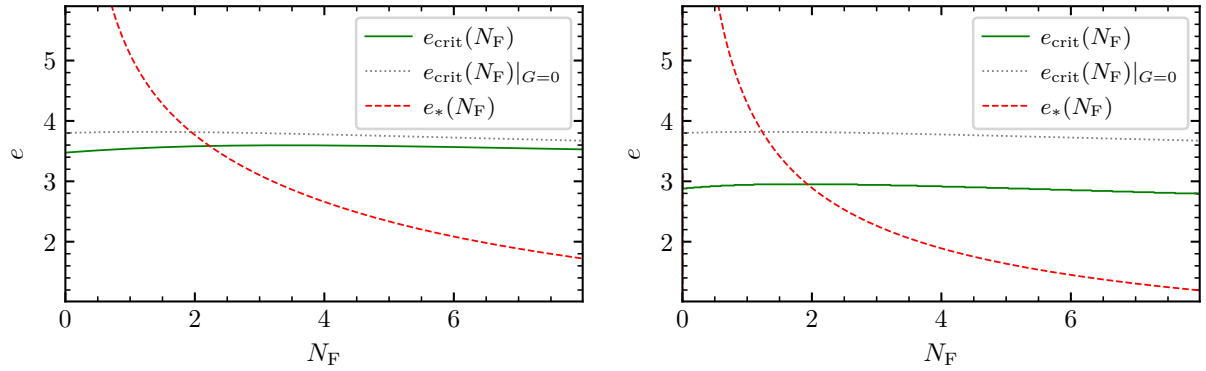

Fig. D.2.: The green solid line shows the critical value of the Abelian gauge coupling at which the system is driven to criticality, including the impact of asymptotically safe quantum gravity, as a function of the number of Dirac fermions N_{F}. The red dashed line shows the fixed point value e_* of the interacting fixed point. The gray dotted line shows the critical value without gravity. Left panel: background approximation, as reported in [4]. Right panel: fluctuation approximation, with the scale dependence of gravitational couplings from [266], and the anomalous dimension of the gauge field from [242].

$N_{\mathrm{F\,crit}} > 1$. Furthermore, the behavior towards larger numbers of fermions is similar, since in both cases, more fermions stabilize the system in the sense that the four-fermion couplings are driven away from a fixed-point collision.

D.4.2. Effective-field-theoretic setting for quantum gravity

In the broader EFT-perspective of the analysis, the difference between both approximations presented above lies in the evaluation of the anomalous dimension of the Abelian gauge field. While the background approximation relies on a derivative expansion, leading to an evaluation of the anomalous dimension at $p^2 = 0$, the fluctuation approximation as described above involves the extraction of the scale dependence of the Abelian gauge coupling via $\eta_A(k^2)$.
Also in this perspective there is qualitative agreement between both approximations. The common qualitative feature is that chiral symmetry remains intact in a weak-gravity regime, while it is spontaneously broken in a strongly interacting regime. However, due to the difference in the scale dependence of the Abelian gauge coupling, leading to differences in the value of the interacting fixed point e_*, the boundary between broken and intact chiral symmetry lies at different values in the $G - \Lambda$ and the $g - \lambda_2$ plane, respectively. Another feature that both approximations share, is that the boundary of chiral-symmetry-breaking shift to larger values of the Newton coupling, for a fixed value of the cosmological constant.

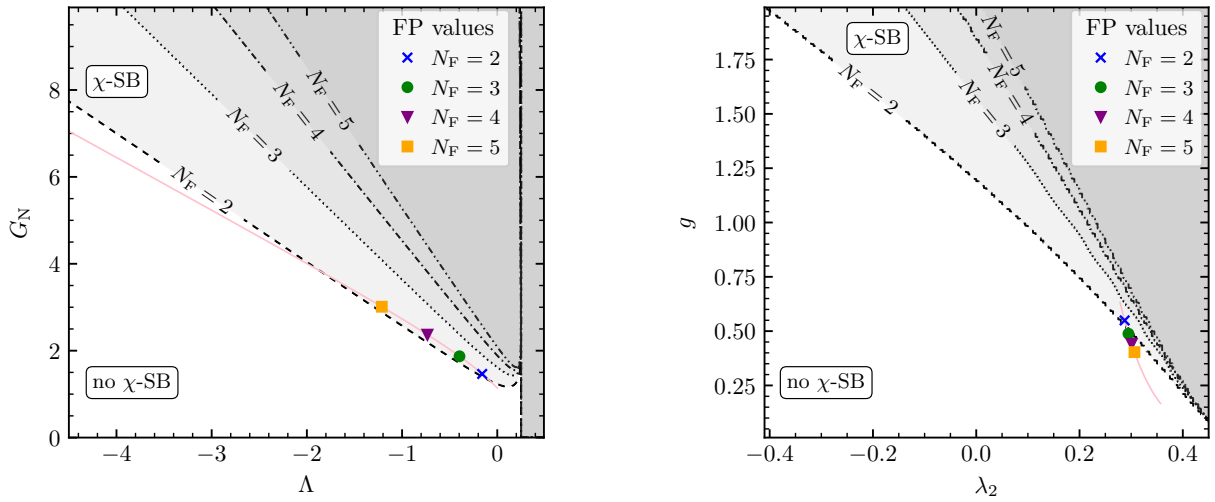

Fig. D.3.: For a fixed number of fermions, the dashed (dotted, dashdotted, dashdotdotted) line represents the boundary between the region of intact chiral symmetry (white area) and spontaneously broken chiral symmetry (shaded area). The gray solid line, together with the cross, circle, triangle and square, indicate the gravitational fixed point as a function of the number of fermions. Left panel: background approximation. Right panel: momentum dependent evaluation of the anomalous dimension of the Abelian gauge field.

E. Lorentz invariance violations in the interplay of quantum gravity with matter: Supplementary material

We provide technical details of the computations in Section 4.6, specifically on the implementation of the foliation structure, and on the projection procedure for the matter LIV coupling ζ.

We aim at studying the effect of operators which are invariant under foliation preserving diffeomorphisms. As a prerequisite, we need to implement a foliation structure on the four dimensional Euclidean space. With the access to the foliation structure, we can then single out a preferred frame and study operators that are invariant under foliation preserving diffeomorphisms only.

To implement the foliation structure, and to restrict the integration over all metrics in the gravitational path integral to globally hyperbolic spacetimes, we need to employ a suitable parameterization for the full metric, and the fluctuations.

The most common choice to parameterize the metric in the context of foliated spacetimes and Lorentz-symmetry-breaking theories is the ADM setup [471, 472]. In asymptotically safe quantum gravity, each of the ADM fields is decomposed linearly into background and fluctuation quantities, see [245–247, 258, 473, 474]. The advantage of this procedure is that the ADM variables automatically implement the foliation structure of the full metric. However, the relation between metric fluctuations $h_{\mu\nu}$ and the fluctuations of the ADM variables is non-linear.

Due to this non-linearity however, using the flow equation (2.21) is not straightforward: The one-loop structure of the flow equation relies on introducing the mass-like term ΔS_k in (2.19), which is quadratic in the fluctuation fields. If we assume that the path integral of quantum gravity is defined in terms of metric fluctuations $h_{\mu\nu}$ with appropriate mass-like term ΔS_k, transitioning to ADM fields is problematic: due to the non-linearity of $h_{\mu\nu}$ in the fluctuations of the ADM fields, the term term ΔS_k would not be quadratic in those fields. Since they are the integration variables of the foliated path integral, this would break the one-loop structure of the flow equation.

Preserving the one-loop structure of the flow equation whole using ADM variables requires to define ΔS_k in terms ov ADM fields. However, for a diffeomorphism invariant theory, we also require that the regulator terms is invariant under background gauge invariance. However, in a diffeomorphism invariant setup, the fluctuation fields of the ADM variables transform non-linearly under gauge invariance. Therefore, the only way to preserve the one-loop structure of the flow equation, namely to define the regulator with respect to the ADM fields, would break full background diffeomorphism invariance. The remaining theory would only be invariant under foliation preserving diffeomorphisms. In other words, when using the ADM variables together with the FRG it appears to be impossible to construct a ΔS_k-term that is quadratic in the ADM fields, while arising from a linear parameterization of metric fluctuations $h_{\mu\nu}$, as emphasized in [246].

Our goal is to study whether and how LIV interactions in the gravitational sector influence

the matter sector. Therefore it is crucial to work in a system that features a diffeomorphism invariant gravitational subsector. In this way we can be sure that it is the gravitational LIV couplings that induce LIVin the matter sector.

To implement the foliation in a way that preserves the one-loop structure of the flow equation, while at the same time preserving full diffeomorphism invariance, we employ the formalism proposed in [248]. In this formalism, the metric $g_{\mu\nu}$ is decomposed in a covariant was into a spatial metric $\sigma_{\mu\nu}$ and a normalized time-like vector n_μ, according to (4.53). The linear split of the metric $g_{\mu\nu}$ into background $\bar{g}_{\mu\nu}$ and fluctuation $h_{\mu\nu}$ translates into the following decomposition of the foliation fields:

$$n_\mu = \bar{n}_\mu + \hat{n}_\mu\,, \qquad \text{and} \qquad \sigma_{\mu\nu} = \bar{\sigma}_{\mu\nu} + \hat{\sigma}_{\mu\nu} - \hat{n}_\mu\hat{n}_\nu\,. \tag{E.1}$$

The non-linearity in the decomposition of σ results in a linear parameterization of the metric fluctuations $h_{\mu\nu}$ in terms of $\hat{\sigma}$ and $\hat{n}$, namely

$$h_{\mu\nu} = \hat{\sigma}_{\mu\nu} + \bar{n}_\mu\hat{n}_\nu + \hat{n}_\mu\bar{n}_\nu\,. \tag{E.2}$$

The linearity of $h_{\mu\nu}$ in each of the foliation fluctuations $\hat{n}_\mu$ and $\hat{\sigma}_{\mu\nu}$ is crucial for the construction of a background-diffeomorphism-invariant flow equation on foliated spacetimes that preserves the one-loop structure of the flow equation (2.21).

The decomposition of $h_{\mu\nu}$ into $\hat{n}_\mu$ and $\hat{\sigma}_{\mu\nu}$ has also introduced additional degrees of freedom. To remove these, and to restrict the path integral to foliated spacetimes, the conditions (4.54) are translated into conditions for $\hat{n}_\mu$ and $\hat{\sigma}_{\mu\nu}$. Both conditions are satisfied if

$$\mathcal{F}_\mu = \bar{n}^\nu\hat{\sigma}_{\mu\nu} - \bar{n}^\nu\hat{n}_\mu\hat{n}_\nu = 0\,. \tag{E.3}$$

We will implement this constraint into the path integral like a gauge-fixing term, i.e., by exponentiating a delta-distribution that enforces this condition. This results in an additional contribution to the action,

$$\Gamma_k^{\text{Fol}} = \frac{1}{32\pi G_{\text{N}}\,\alpha_{\text{Fol}}}\int \mathrm{d}^4x\sqrt{g}\,\bar{g}^{\mu\nu}\mathcal{F}_\mu\mathcal{F}_\nu\,, \qquad \text{and} \qquad \alpha_{\text{Fol}}\to 0\,. \tag{E.4}$$

The conditions (4.54) are second-class constraints, and, as opposed to first-class constraints, second-class constraints cannot be implemented via the Fadeev-Popov trick. To implement second-class constraints, a Hamiltonian analysis is necessary to understand, if additional secondary constraints need to be imposed.

In the present work, we assume that the implementation of the second class constraints (4.54) via the additional term (E.4) is sufficient to capture the relevant dynamics on a qualitative level.

Let us also add some comments on the projection procedure on the LIV matter coupling ζ. To extract the scale dependence of ζ, we need to project the flow equation (2.21) with our ansatz for Γ_k onto the matter LIV coupling itself, and on the wavefunction renormalization of the gauge field. We can project on the wavefunction renormalization by projecting on the $F_{\mu\nu}F^{\mu\nu}$ tensor structure, i.e., by taking two derivatives with respect to the Abelian gauge field, closing the open indices with a transverse projector, selecting the terms quadratic in external momenta, and taking the 0th order term in n_μ. We follow the same steps to project on ζ, except that we take all terms containing the vector field n_μ, or its norm, into account. Only after this procedure we set $n^2 = 1$.

This projection procedure is not unique, and, within truncations the different projection schemes

might lead to quantitatively different results for the scale dependence of the LIV matter coupling ζ.

References

[1] Benjamin Knorr and Marc Schiffer. "Non-Perturbative Propagators in Quantum Gravity". In: *Universe* 7.7 (2021), p. 216. DOI: 10.3390/universe7070216. arXiv: 2105.04566 [hep-th].

[2] Scott Bassler, Jack Laiho, Marc Schiffer, and Judah Unmuth-Yockey. "The de Sitter Instanton from Euclidean Dynamical Triangulations". In: *Phys. Rev. D* 103 (2021), p. 114504. DOI: 10.1103/PhysRevD.103.114504. arXiv: 2103.06973 [hep-lat].

[3] Mingwei Dai, Jack Laiho, Marc Schiffer, and Judah Unmuth-Yockey. "Newtonian binding from lattice quantum gravity". In: *Phys. Rev. D* 103.11 (2021), p. 114511. DOI: 10.1103/PhysRevD.103.114511. arXiv: 2102.04492 [hep-lat].

[4] Gustavo P. de Brito, Astrid Eichhorn, and Marc Schiffer. "Light charged fermions in quantum gravity". In: *Phys. Lett. B* 815 (2021), p. 136128. DOI: 10.1016/j.physletb.2021.136128. arXiv: 2010.00605 [hep-th].

[5] Astrid Eichhorn, Alessia Platania, and Marc Schiffer. "Lorentz invariance violations in the interplay of quantum gravity with matter". In: *Phys. Rev. D* 102.2 (2020), p. 026007. DOI: 10.1103/PhysRevD.102.026007. arXiv: 1911.10066 [hep-th].

[6] Senarath de Alwis, Astrid Eichhorn, Aaron Held, Jan M. Pawlowski, Marc Schiffer, and Fleur Versteegen. "Asymptotic safety, string theory and the weak gravity conjecture". In: *Phys. Lett. B* 798 (2019), p. 134991. DOI: 10.1016/j.physletb.2019.134991. arXiv: 1907.07894 [hep-th].

[7] Astrid Eichhorn and Marc Schiffer. "$d = 4$ as the critical dimensionality of asymptotically safe interactions". In: *Phys. Lett. B* 793 (2019), pp. 383–389. DOI: 10.1016/j.physletb.2019.05.005. arXiv: 1902.06479 [hep-th].

[8] Kazunori Akiyama et al. "First M87 Event Horizon Telescope Results. I. The Shadow of the Supermassive Black Hole". In: *Astrophys. J. Lett.* 875 (2019), p. L1. DOI: 10.3847/2041-8213/ab0ec7. arXiv: 1906.11238 [astro-ph.GA].

[9] Kazunori Akiyama et al. "First M87 Event Horizon Telescope Results. II. Array and Instrumentation". In: *Astrophys. J. Lett.* 875.1 (2019), p. L2. DOI: 10.3847/2041-8213/ab0c96. arXiv: 1906.11239 [astro-ph.IM].

[10] Kazunori Akiyama et al. "First M87 Event Horizon Telescope Results. VI. The Shadow and Mass of the Central Black Hole". In: *Astrophys. J. Lett.* 875.1 (2019), p. L6. DOI: 10.3847/2041-8213/ab1141. arXiv: 1906.11243 [astro-ph.GA].

[11] B. P. Abbott et al. "Observation of Gravitational Waves from a Binary Black Hole Merger". In: *Phys. Rev. Lett.* 116.6 (2016), p. 061102. DOI: 10.1103/PhysRevLett.116.061102. arXiv: 1602.03837 [gr-qc].

[12] B. P. Abbott et al. "GW151226: Observation of Gravitational Waves from a 22-Solar-Mass Binary Black Hole Coalescence". In: *Phys. Rev. Lett.* 116.24 (2016), p. 241103. DOI: 10.1103/PhysRevLett.116.241103. arXiv: 1606.04855 [gr-qc].

[13] R. Abbott et al. "Tests of general relativity with binary black holes from the second LIGO-Virgo gravitational-wave transient catalog". In: *Phys. Rev. D* 103.12 (2021), p. 122002. DOI: 10.1103/PhysRevD.103.122002. arXiv: 2010.14529 [gr-qc].

[14] Georges Aad et al. "Observation of a new particle in the search for the Standard Model Higgs boson with the ATLAS detector at the LHC". In: *Phys. Lett. B* 716 (2012), pp. 1–29. DOI: 10.1016/j.physletb.2012.08.020. arXiv: 1207.7214 [hep-ex].

[15] Serguei Chatrchyan et al. "Observation of a New Boson at a Mass of 125 GeV with the CMS Experiment at the LHC". In: *Phys. Lett. B* 716 (2012), pp. 30–61. DOI: 10.1016/j.physletb.2012.08.021. arXiv: 1207.7235 [hep-ex].

[16] Fedor Bezrukov, Mikhail Yu. Kalmykov, Bernd A. Kniehl, and Mikhail Shaposhnikov. "Higgs Boson Mass and New Physics". In: *JHEP* 10 (2012). Ed. by Gudrid Moortgat-Pick, p. 140. DOI: 10.1007/JHEP10(2012)140. arXiv: 1205.2893 [hep-ph].

[17] Dario Buttazzo, Giuseppe Degrassi, Pier Paolo Giardino, Gian F. Giudice, Filippo Sala, Alberto Salvio, and Alessandro Strumia. "Investigating the near-criticality of the Higgs boson". In: *JHEP* 12 (2013), p. 089. DOI: 10.1007/JHEP12(2013)089. arXiv: 1307.3536 [hep-ph].

[18] Steven Weinberg. "ULTRAVIOLET DIVERGENCES IN QUANTUM THEORIES OF GRAVITATION". In: *General Relativity: An Einstein Centenary Survey*. 1980.

[19] Gerard 't Hooft and M. J. G. Veltman. "One loop divergencies in the theory of gravitation". In: *Ann. Inst. H. Poincare Phys. Theor. A* 20 (1974), pp. 69–94.

[20] Stanley Deser and P. Van Nieuwenhuizen. "Nonrenormalizability of quantized fermion-gravitation interactions". In: *Lett. Nuovo Cim.* 11S2 (1974), pp. 218–220.

[21] S. Deser and P. van Nieuwenhuizen. "Nonrenormalizability of the Quantized Einstein-Maxwell System". In: *Phys. Rev. Lett.* 32 (1974), pp. 245–247. DOI: 10.1103/PhysRevLett.32.245.

[22] Marc H. Goroff and Augusto Sagnotti. "The Ultraviolet Behavior of Einstein Gravity". In: *Nucl. Phys. B* 266 (1986), pp. 709–736. DOI: 10.1016/0550-3213(86)90193-8.

[23] Bryce S. DeWitt. "Quantum Theory of Gravity. 3. Applications of the Covariant Theory". In: *Phys. Rev.* 162 (1967). Ed. by Jong-Ping Hsu and D. Fine, pp. 1239–1256. DOI: 10.1103/PhysRev.162.1239.

[24] J. Honerkamp. "The Question of invariant renormalizability of the massless Yang-Mills theory in a manifest covariant approach". In: *Nucl. Phys. B* 48 (1972), pp. 269–287. DOI: 10.1016/0550-3213(72)90063-6.

[25] G. 't Hooft. "Perturbative quantum gravity". In: *Subnucl. Ser.* 40 (2003). Ed. by A. Zichichi, pp. 249–269. DOI: 10.1142/9789812796653_0007.

[26] A. E. M. van de Ven. "Two loop quantum gravity". In: *Nucl. Phys. B* 378 (1992), pp. 309–366. DOI: 10.1016/0550-3213(92)90011-Y.

[27] K. S. Stelle. "Renormalization of Higher Derivative Quantum Gravity". In: *Phys. Rev. D* 16 (1977), pp. 953–969. DOI: 10.1103/PhysRevD.16.953.

[28] E. S. Fradkin and Arkady A. Tseytlin. "Renormalizable Asymptotically Free Quantum Theory of Gravity". In: *Phys. Lett. B* 104 (1981), pp. 377–381. DOI: 10.1016/0370-2693(81)90702-4.

[29] E. S. Fradkin and Arkady A. Tseytlin. "Renormalizable asymptotically free quantum theory of gravity". In: *Nucl. Phys. B* 201 (1982), pp. 469–491. DOI: 10.1016/0550-3213(82)90444-8.

[30] M. Ostrogradsky. "Mémoires sur les équations différentielles, relatives au problème des isopérimètres". In: *Mem. Acad. St. Petersbourg* 6.4 (1850), pp. 385–517.

[31] John F. Donoghue and Gabriel Menezes. "Arrow of Causality and Quantum Gravity". In: *Phys. Rev. Lett.* 123.17 (2019), p. 171601. DOI: 10.1103/PhysRevLett.123.171601. arXiv: 1908.04170 [hep-th].

[32] Fulvio Sbisà. "Classical and quantum ghosts". In: *Eur. J. Phys.* 36 (2015), p. 015009. DOI: 10.1088/0143-0807/36/1/015009. arXiv: 1406.4550 [hep-th].

[33] T. D. Lee and G. C. Wick. "Negative Metric and the Unitarity of the S Matrix". In: *Nucl. Phys. B* 9 (1969). Ed. by G. Feinberg, pp. 209–243. DOI: 10.1016/0550-3213(69)90098-4.

[34] S. W. Hawking and Thomas Hertog. "Living with ghosts". In: *Phys. Rev. D* 65 (2002), p. 103515. DOI: 10.1103/PhysRevD.65.103515. arXiv: hep-th/0107088.

[35] Alberto Salvio and Alessandro Strumia. "Agravity". In: *JHEP* 06 (2014), p. 080. DOI: 10.1007/JHEP06(2014)080. arXiv: 1403.4226 [hep-ph].

[36] John F. Donoghue. "Quartic propagators, negative norms and the physical spectrum". In: *Phys. Rev. D* 96.4 (2017), p. 044007. DOI: 10.1103/PhysRevD.96.044007. arXiv: 1704.01533 [hep-th].

[37] John F. Donoghue. "Leading quantum correction to the Newtonian potential". In: *Phys. Rev. Lett.* 72 (1994), pp. 2996–2999. DOI: 10.1103/PhysRevLett.72.2996. arXiv: gr-qc/9310024.

[38] John F. Donoghue. "Introduction to the effective field theory description of gravity". In: *Advanced School on Effective Theories*. June 1995. arXiv: gr-qc/9512024.

[39] John F. Donoghue. "The effective field theory treatment of quantum gravity". In: *AIP Conf. Proc.* 1483.1 (2012). Ed. by Waldyr Alves Rodrigues, Richard Kerner, Gentil Pires, and Carols Pinheiro, pp. 73–94. DOI: 10.1063/1.4756964. arXiv: 1209.3511 [gr-qc].

[40] John F. Donoghue. "General relativity as an effective field theory: The leading quantum corrections". In: *Phys. Rev. D* 50 (1994), pp. 3874–3888. DOI: 10.1103/PhysRevD.50.3874. arXiv: gr-qc/9405057.

[41] J. Polchinski. *String theory. Vol. 1: An introduction to the bosonic string*. Cambridge Monographs on Mathematical Physics. Cambridge University Press, Dec. 2007. ISBN: 978-0-511-25227-3, 978-0-521-67227-6, 978-0-521-63303-1. DOI: 10.1017/CBO9780511816079.

[42] J. Polchinski. *String theory. Vol. 2: Superstring theory and beyond*. Cambridge Monographs on Mathematical Physics. Cambridge University Press, Dec. 2007. ISBN: 978-0-511-25228-0, 978-0-521-63304-8, 978-0-521-67228-3. DOI: 10.1017/CBO9780511618123.

[43] Sumati Surya. "The causal set approach to quantum gravity". In: *Living Rev. Rel.* 22.1 (2019), p. 5. DOI: 10.1007/s41114-019-0023-1. arXiv: 1903.11544 [gr-qc].

[44] Abhay Ashtekar and Eugenio Bianchi. "A short review of loop quantum gravity". In: *Rept. Prog. Phys.* 84.4 (2021), p. 042001. DOI: 10.1088/1361-6633/abed91. arXiv: 2104.04394 [gr-qc].

[45] David J. Gross and Frank Wilczek. "Ultraviolet Behavior of Nonabelian Gauge Theories". In: *Phys. Rev. Lett.* 30 (1973). Ed. by J. C. Taylor, pp. 1343–1346. DOI: 10.1103/PhysRevLett.30.1343.

[46] H. David Politzer. "Reliable Perturbative Results for Strong Interactions?" In: *Phys. Rev. Lett.* 30 (1973). Ed. by J. C. Taylor, pp. 1346–1349. DOI: 10.1103/PhysRevLett.30.1346.

[47] M. Niedermaier. "The Asymptotic safety scenario in quantum gravity: An Introduction". In: *Class. Quant. Grav.* 24 (2007), R171–230. DOI: 10.1088/0264-9381/24/18/R01. arXiv: gr-qc/0610018.

[48] Daniel F. Litim. "Fixed Points of Quantum Gravity and the Renormalisation Group". In: *PoS* QG-Ph (2007), p. 024. DOI: 10.22323/1.043.0024. arXiv: 0810.3675 [hep-th].

[49] Roberto Percacci. "A Short introduction to asymptotic safety". In: *Time and Matter*. Oct. 2011. arXiv: 1110.6389 [hep-th].

[50] Martin Reuter and Frank Saueressig. "Quantum Einstein Gravity". In: *New J. Phys.* 14 (2012), p. 055022. DOI: 10.1088/1367-2630/14/5/055022. arXiv: 1202.2274 [hep-th].

[51] Astrid Eichhorn. "Status of the asymptotic safety paradigm for quantum gravity and matter". In: *Found. Phys.* 48.10 (2018), pp. 1407–1429. DOI: 10.1007/s10701-018-0196-6. arXiv: 1709.03696 [gr-qc].

[52] Astrid Eichhorn. "An asymptotically safe guide to quantum gravity and matter". In: *Front. Astron. Space Sci.* 5 (2019), p. 47. DOI: 10.3389/fspas.2018.00047. arXiv: 1810.07615 [hep-th].

[53] Jan M. Pawlowski and Manuel Reichert. "Quantum gravity: a fluctuating point of view". In: (July 2020). arXiv: 2007.10353 [hep-th].

[54] C. Wetterich. "Quantum scale symmetry". In: (Jan. 2019). arXiv: 1901.04741 [hep-th].

[55] Michael E. Peskin. "CRITICAL POINT BEHAVIOR OF THE WILSON LOOP". In: *Phys. Lett. B* 94 (1980), pp. 161–165. DOI: 10.1016/0370-2693(80)90848-5.

[56] William A. Bardeen, Benjamin W. Lee, and Robert E. Shrock. "Phase Transition in the Nonlinear σ Model in $2+\epsilon$ Dimensional Continuum". In: *Phys. Rev. D* 14 (1976), p. 985. DOI: 10.1103/PhysRevD.14.985.

[57] D. Friedan. "Nonlinear Models in Two Epsilon Dimensions". In: *Phys. Rev. Lett.* 45 (1980), p. 1057. DOI: 10.1103/PhysRevLett.45.1057.

[58] Kiyoshi Higashijima and Etsuko Itou. "Three-dimensional nonlinear sigma models in the Wilsonian renormalization method". In: *Prog. Theor. Phys.* 110 (2003), pp. 563–578. DOI: 10.1143/PTP.110.563. arXiv: hep-th/0304194.

[59] Alessandro Codello and Roberto Percacci. "Fixed Points of Nonlinear Sigma Models in d>2". In: *Phys. Lett. B* 672 (2009), pp. 280–283. DOI: 10.1016/j.physletb.2009.01.032. arXiv: 0810.0715 [hep-th].

[60] K. Gawedzki and A. Kupiainen. "RENORMALIZING THE NONRENORMALIZABLE". In: *Phys. Rev. Lett.* 55 (1985), pp. 363–365. DOI: 10.1103/PhysRevLett.55.363.

[61] Hong-Jian He, Yu-Ping Kuang, Qing Wang, and Yu-Ping Yi. "Effective potential, renormalization, and nontrivial ultraviolet fixed point in D-dimensional four fermion theories ($2 < D < 4$) to order 1/N in 1/N expansion". In: *Phys. Rev. D* 45 (1992), pp. 4610–4620. DOI: 10.1103/PhysRevD.45.4610.

[62] Simon Hands, Aleksandar Kocic, and John B. Kogut. "Four Fermi theories in fewer than four-dimensions". In: *Annals Phys.* 224 (1993), pp. 29–89. DOI: 10.1006/aphy.1993.1039. arXiv: hep-lat/9208022.

[63] Jens Braun, Holger Gies, and Daniel D. Scherer. "Asymptotic safety: a simple example". In: *Phys. Rev. D* 83 (2011), p. 085012. DOI: 10.1103/PhysRevD.83.085012. arXiv: 1011.1456 [hep-th].

[64] A. Palanques-Mestre and P. Pascual. "The $1/N^-$f Expansion of the γ and Beta Functions in QED". In: *Commun. Math. Phys.* 95 (1984), p. 277. DOI: 10.1007/BF01212398.

[65] J. A. Gracey. "The QCD Beta function at O(1/N(f))". In: *Phys. Lett. B* 373 (1996), pp. 178–184. DOI: 10.1016/0370-2693(96)00105-0. arXiv: hep-ph/9602214.

[66] B. Holdom. "Large N flavor beta-functions: a recap". In: *Phys. Lett. B* 694 (2011), pp. 74–79. DOI: 10.1016/j.physletb.2010.09.037. arXiv: 1006.2119 [hep-ph].

[67] Daniel F. Litim and Francesco Sannino. "Asymptotic safety guaranteed". In: *JHEP* 12 (2014), p. 178. DOI: 10.1007/JHEP12(2014)178. arXiv: 1406.2337 [hep-th].

[68] Oleg Antipin and Francesco Sannino. "Conformal Window 2.0: The large N_f safe story". In: *Phys. Rev. D* 97.11 (2018), p. 116007. DOI: 10.1103/PhysRevD.97.116007. arXiv: 1709.02354 [hep-ph].

[69] Juergen Berges, Nikolaos Tetradis, and Christof Wetterich. "Nonperturbative renormalization flow in quantum field theory and statistical physics". In: *Phys. Rept.* 363 (2002), pp. 223–386. DOI: 10.1016/S0370-1573(01)00098-9. arXiv: hep-ph/0005122.

[70] Janos Polonyi. "Lectures on the functional renormalization group method". In: *Central Eur. J. Phys.* 1 (2003), pp. 1–71. DOI: 10.2478/BF02475552. arXiv: hep-th/0110026.

[71] Jan M. Pawlowski. "Aspects of the functional renormalisation group". In: *Annals Phys.* 322 (2007), pp. 2831–2915. DOI: 10.1016/j.aop.2007.01.007. arXiv: hep-th/0512261.

[72] Holger Gies. "Introduction to the functional RG and applications to gauge theories". In: *Lect. Notes Phys.* 852 (2012), pp. 287–348. DOI: 10.1007/978-3-642-27320-9_6. arXiv: hep-ph/0611146.

[73] N. Dupuis, L. Canet, A. Eichhorn, W. Metzner, J. M. Pawlowski, M. Tissier, and N. Wschebor. "The nonperturbative functional renormalization group and its applications". In: *Phys. Rept.* 910 (2021), pp. 1–114. DOI: 10.1016/j.physrep.2021.01.001. arXiv: 2006.04853 [cond-mat.stat-mech].

[74] Christof Wetterich. "Exact evolution equation for the effective potential". In: *Phys. Lett. B* 301 (1993), pp. 90–94. DOI: 10.1016/0370-2693(93)90726-X. arXiv: 1710.05815 [hep-th].

[75] Ulrich Ellwanger. "FLow equations for N point functions and bound states". In: *Z. Phys. C* 62 (1994). Ed. by B. Geyer and E. M. Ilgenfritz, pp. 503–510. DOI: 10.1007/BF01555911. arXiv: hep-ph/9308260.

[76] Tim R. Morris. "The Exact renormalization group and approximate solutions". In: *Int. J. Mod. Phys. A* 9 (1994), pp. 2411–2450. DOI: 10.1142/S0217751X94000972. arXiv: hep-ph/9308265.

[77] Stefan Bornholdt and Christof Wetterich. "Average action for models with fermions". In: *Z. Phys. C* 58 (1993), pp. 585–594. DOI: 10.1007/BF01553018.

[78] M. Reuter and C. Wetterich. "Average action for the Higgs model with Abelian gauge symmetry". In: *Nucl. Phys. B* 391 (1993), pp. 147–175. DOI: 10.1016/0550-3213(93)90145-F.

[79] M. Reuter. "Nonperturbative evolution equation for quantum gravity". In: *Phys. Rev. D* 57 (1998), pp. 971–985. DOI: 10.1103/PhysRevD.57.971. arXiv: hep-th/9605030.

[80] Kenneth G. Wilson. "Renormalization group and critical phenomena. 1. Renormalization group and the Kadanoff scaling picture". In: *Phys. Rev. B* 4 (1971), pp. 3174–3183. DOI: 10.1103/PhysRevB.4.3174.

[81] K. G. Wilson and John B. Kogut. "The Renormalization group and the epsilon expansion". In: *Phys. Rept.* 12 (1974), pp. 75–199. DOI: 10.1016/0370-1573(74)90023-4.

[82] Bryce S. DeWitt. "Quantum Theory of Gravity. 2. The Manifestly Covariant Theory". In: *Phys. Rev.* 162 (1967). Ed. by Jong-Ping Hsu and D. Fine, pp. 1195–1239. DOI: 10.1103/PhysRev.162.1195.

[83] Hikaru Kawai, Yoshihisa Kitazawa, and Masao Ninomiya. "Scaling exponents in quantum gravity near two-dimensions". In: *Nucl. Phys. B* 393 (1993), pp. 280–300. DOI: 10.1016/0550-3213(93)90246-L. arXiv: hep-th/9206081.

[84] Toshiaki Aida, Yoshihisa Kitazawa, Jun Nishimura, and Asato Tsuchiya. "Two loop renormalization in quantum gravity near two-dimensions". In: *Nucl. Phys. B* 444 (1995), pp. 353–380. DOI: 10.1016/0550-3213(95)00071-Y. arXiv: hep-th/9501056.

[85] Andreas Nink. "Field Parametrization Dependence in Asymptotically Safe Quantum Gravity". In: *Phys. Rev. D* 91.4 (2015), p. 044030. DOI: 10.1103/PhysRevD.91.044030. arXiv: 1410.7816 [hep-th].

[86] Maximilian Demmel and Andreas Nink. "Connections and geodesics in the space of metrics". In: *Phys. Rev. D* 92.10 (2015), p. 104013. DOI: 10.1103/PhysRevD.92.104013. arXiv: 1506.03809 [gr-qc].

[87] Roberto Percacci and Gian Paolo Vacca. "Search of scaling solutions in scalar-tensor gravity". In: *Eur. Phys. J. C* 75.5 (2015), p. 188. DOI: 10.1140/epjc/s10052-015-3410-0. arXiv: 1501.00888 [hep-th].

[88] Holger Gies, Benjamin Knorr, and Stefan Lippoldt. "Generalized Parametrization Dependence in Quantum Gravity". In: *Phys. Rev. D* 92.8 (2015), p. 084020. DOI: 10.1103/PhysRevD.92.084020. arXiv: 1507.08859 [hep-th].

[89] Peter Labus, Roberto Percacci, and Gian Paolo Vacca. "Asymptotic safety in $O(N)$ scalar models coupled to gravity". In: *Phys. Lett. B* 753 (2016), pp. 274–281. DOI: 10.1016/j.physletb.2015.12.022. arXiv: 1505.05393 [hep-th].

[90] Nobuyoshi Ohta and Roberto Percacci. "Ultraviolet Fixed Points in Conformal Gravity and General Quadratic Theories". In: *Class. Quant. Grav.* 33 (2016), p. 035001. DOI: 10.1088/0264-9381/33/3/035001. arXiv: 1506.05526 [hep-th].

[91] Nobuyoshi Ohta, Roberto Percacci, and Gian Paolo Vacca. "Flow equation for $f(R)$ gravity and some of its exact solutions". In: *Phys. Rev. D* 92.6 (2015), p. 061501. DOI: 10.1103/PhysRevD.92.061501. arXiv: 1507.00968 [hep-th].

[92] Kevin Falls. "Renormalization of Newton's constant". In: *Phys. Rev. D* 92.12 (2015), p. 124057. DOI: 10.1103/PhysRevD.92.124057. arXiv: 1501.05331 [hep-th].

[93] Nobuyoshi Ohta, Roberto Percacci, and Gian Paolo Vacca. "Renormalization Group Equation and scaling solutions for f(R) gravity in exponential parametrization". In: *Eur. Phys. J. C* 76.2 (2016), p. 46. DOI: 10.1140/epjc/s10052-016-3895-1. arXiv: 1511.09393 [hep-th].

[94] Pietro Donà, Astrid Eichhorn, Peter Labus, and Roberto Percacci. "Asymptotic safety in an interacting system of gravity and scalar matter". In: *Phys. Rev. D* 93.4 (2016). [Erratum: Phys.Rev.D 93, 129904 (2016)], p. 044049. DOI: 10.1103/PhysRevD.93.129904. arXiv: 1512.01589 [gr-qc].

[95] N. Ohta, R. Percacci, and A. D. Pereira. "Gauges and functional measures in quantum gravity I: Einstein theory". In: *JHEP* 06 (2016), p. 115. DOI: 10.1007/JHEP06(2016)115. arXiv: 1605.00454 [hep-th].

[96] Kevin Falls and Nobuyoshi Ohta. "Renormalization Group Equation for $f(R)$ gravity on hyperbolic spaces". In: *Phys. Rev. D* 94.8 (2016), p. 084005. DOI: 10.1103/PhysRevD.94.084005. arXiv: 1607.08460 [hep-th].

[97] Roberto Percacci and Gian Paolo Vacca. "The background scale Ward identity in quantum gravity". In: *Eur. Phys. J. C* 77.1 (2017), p. 52. DOI: 10.1140/epjc/s10052-017-4619-x. arXiv: 1611.07005 [hep-th].

[98] Benjamin Knorr. "Infinite order quantum-gravitational correlations". In: *Class. Quant. Grav.* 35.11 (2018), p. 115005. DOI: 10.1088/1361-6382/aabaa0. arXiv: 1710.07055 [hep-th].

[99] Natália Alkofer and Frank Saueressig. "Asymptotically safe $f(R)$-gravity coupled to matter I: the polynomial case". In: *Annals Phys.* 396 (2018), pp. 173–201. DOI: 10.1016/j.aop.2018.07.017. arXiv: 1802.00498 [hep-th].

[100] Elisa Manrique and Martin Reuter. "Bimetric Truncations for Quantum Einstein Gravity and Asymptotic Safety". In: *Annals Phys.* 325 (2010), pp. 785–815. DOI: 10.1016/j.aop.2009.11.009. arXiv: 0907.2617 [gr-qc].

[101] M. Reuter and C. Wetterich. "Gluon condensation in nonperturbative flow equations". In: *Phys. Rev. D* 56 (1997), pp. 7893–7916. DOI: 10.1103/PhysRevD.56.7893. arXiv: hep-th/9708051.

[102] Daniel F. Litim and Jan M. Pawlowski. "Renormalization group flows for gauge theories in axial gauges". In: *JHEP* 09 (2002), p. 049. DOI: 10.1088/1126-6708/2002/09/049. arXiv: hep-th/0203005.

[103] Tim R. Morris. "Large curvature and background scale independence in single-metric approximations to asymptotic safety". In: *JHEP* 11 (2016), p. 160. DOI: 10.1007/JHEP11(2016)160. arXiv: 1610.03081 [hep-th].

[104] Peter Labus, Tim R. Morris, and Zoë H. Slade. "Background independence in a background dependent renormalization group". In: *Phys. Rev. D* 94.2 (2016), p. 024007. DOI: 10.1103/PhysRevD.94.024007. arXiv: 1603.04772 [hep-th].

[105] Nobuyoshi Ohta. "Background Scale Independence in Quantum Gravity". In: *PTEP* 2017.3 (2017), 033E02. DOI: 10.1093/ptep/ptx020. arXiv: 1701.01506 [hep-th].

[106] Ulrich Ellwanger. "Flow equations and BRS invariance for Yang-Mills theories". In: *Phys. Lett. B* 335 (1994), pp. 364–370. DOI: 10.1016/0370-2693(94)90365-4. arXiv: hep-th/9402077.

[107] Tim R. Morris. "A Gauge invariant exact renormalization group. 1." In: *Nucl. Phys. B* 573 (2000), pp. 97–126. DOI: 10.1016/S0550-3213(99)00821-4. arXiv: hep-th/9910058.

[108] Yuji Igarashi, Katsumi Itoh, and Hiroto So. "Exact BRS symmetry realized on the renormalization group flow". In: *Prog. Theor. Phys.* 104 (2000), pp. 1053–1066. DOI: 10.1143/PTP.104.1053. arXiv: hep-th/0006180.

[109] Tim R. Morris and Oliver J. Rosten. "Manifestly gauge invariant QCD". In: *J. Phys. A* 39 (2006), pp. 11657–11681. DOI: 10.1088/0305-4470/39/37/020. arXiv: hep-th/0606189.

[110] Kevin Falls and Tim R. Morris. "Conformal anomaly from gauge fields without gauge fixing". In: *Phys. Rev. D* 97.6 (2018), p. 065013. DOI: 10.1103/PhysRevD.97.065013. arXiv: 1712.05011 [hep-th].

[111] C. Wetterich. "Gauge invariant flow equation". In: *Nucl. Phys. B* 931 (2018), pp. 262–282. DOI: 10.1016/j.nuclphysb.2018.04.020. arXiv: 1607.02989 [hep-th].

[112] Shimasadat Asnafi, Holger Gies, and Luca Zambelli. "BRST invariant RG flows". In: *Phys. Rev. D* 99.8 (2019), p. 085009. DOI: 10.1103/PhysRevD.99.085009. arXiv: 1811.03615 [hep-th].

[113] Astrid Eichhorn, Peter Labus, Jan M. Pawlowski, and Manuel Reichert. "Effective universality in quantum gravity". In: *SciPost Phys.* 5.4 (2018), p. 031. DOI: 10.21468/SciPostPhys.5.4.031. arXiv: 1804.00012 [hep-th].

[114] M. Reuter. "Effective average actions and nonperturbative evolution equations". In: *5th Hellenic School and Workshops on Elementary Particle Physics*. Feb. 1996. arXiv: hep-th/9602012.

[115] I. Hamzaan Bridle, Juergen A. Dietz, and Tim R. Morris. "The local potential approximation in the background field formalism". In: *JHEP* 03 (2014), p. 093. DOI: 10.1007/JHEP03(2014)093. arXiv: 1312.2846 [hep-th].

[116] Daniel F. Litim and Jan M. Pawlowski. "Wilsonian flows and background fields". In: *Phys. Lett. B* 546 (2002), pp. 279–286. DOI: 10.1016/S0370-2693(02)02693-X. arXiv: hep-th/0208216.

[117] David Brizuela, Jose M. Martin-Garcia, and Guillermo A. Mena Marugan. "xPert: Computer algebra for metric perturbation theory". In: *Gen. Rel. Grav.* 41 (2009), pp. 2415–2431. DOI: 10.1007/s10714-009-0773-2. arXiv: 0807.0824 [gr-qc].

[118] Jose M. Martin-Garcia, Renato Portugal, and Leon R. U. Manssur. "The Invar Tensor Package". In: *Comput. Phys. Commun.* 177 (2007), pp. 640–648. DOI: 10.1016/j.cpc.2007.05.015. arXiv: 0704.1756 [cs.SC].

[119] Jose M. Martin-Garcia, David Yllanes, and Renato Portugal. "The Invar tensor package: Differential invariants of Riemann". In: *Comput. Phys. Commun.* 179 (2008), pp. 586–590. DOI: 10.1016/j.cpc.2008.04.018. arXiv: 0802.1274 [cs.SC].

[120] J. M. Martín-García. "xPerm: fast index canonicalization for tensor computer algebra". In: *Computer Physics Communications* 179 (2008), pp. 597–603. DOI: 10.1016/j.cpc.2008.05.009. arXiv: 0803.0862 [cs.SC].

[121] T. Nutma. "xTras: A field-theory inspired xAct package for mathematica". In: *Computer Physics Communications* 185 (2014), pp. 1719–1738. DOI: 10.1016/j.cpc.2014.02.006. arXiv: 1308.3493 [cs.SC].

[122] Markus Q. Huber and Jens Braun. "Algorithmic derivation of functional renormalization group equations and Dyson-Schwinger equations". In: *Comput. Phys. Commun.* 183 (2012), pp. 1290–1320. DOI: 10.1016/j.cpc.2012.01.014. arXiv: 1102.5307 [hep-th].

[123] Markus Q. Huber, Anton K. Cyrol, and Jan M. Pawlowski. "DoFun 3.0: Functional equations in Mathematica". In: *Comput. Phys. Commun.* 248 (2020), p. 107058. DOI: 10.1016/j.cpc.2019.107058. arXiv: 1908.02760 [hep-ph].

[124] Anton K. Cyrol, Mario Mitter, and Nils Strodthoff. "FormTracer - A Mathematica Tracing Package Using FORM". In: *Comput. Phys. Commun.* 219 (2017), pp. 346–352. DOI: 10.1016/j.cpc.2017.05.024. arXiv: 1610.09331 [hep-ph].

[125] Jan Ambjorn and Jerzy Jurkiewicz. "Four-dimensional simplicial quantum gravity". In: *Phys. Lett. B* 278 (1992), pp. 42–50. DOI: 10.1016/0370-2693(92)90709-D.

[126] M. E. Agishtein and Alexander A. Migdal. "Simulations of four-dimensional simplicial quantum gravity". In: *Mod. Phys. Lett. A* 7 (1992), pp. 1039–1062. DOI: 10.1142/S0217732392000938.

[127] S. Catterall. "Lattice quantum gravity: review and recent developments". In: *Nucl. Phys. B Proc. Suppl.* 47 (1996), p. 59. DOI: 10.1016/0920-5632(96)00032-1. arXiv: hep-lat/9510008.

[128] T. Regge. "GENERAL RELATIVITY WITHOUT COORDINATES". In: *Nuovo Cim.* 19 (1961), pp. 558–571. DOI: 10.1007/BF02733251.

[129] Jeff Cheeger, Werner Muller, and Robert Schrader. "On the Curvature of Piecewise Flat Spaces". In: *Commun. Math. Phys.* 92 (1984), p. 405. DOI: 10.1007/BF01210729.

[130] Herbert W. Hamber and Ruth M. Williams. "HIGHER DERIVATIVE QUANTUM GRAVITY ON A SIMPLICIAL LATTICE". In: *Nucl. Phys. B* 248 (1984). [Erratum: Nucl.Phys.B 260, 747–747 (1985)], pp. 392–414. DOI: 10.1016/0550-3213(84)90603-5.

[131] V. G. Knizhnik, Alexander M. Polyakov, and A. B. Zamolodchikov. "Fractal Structure of 2D Quantum Gravity". In: *Mod. Phys. Lett. A* 3 (1988). Ed. by I. M. Khalatnikov and V. P. Mineev, p. 819. DOI: 10.1142/S0217732388000982.

[132] F. David. "Conformal Field Theories Coupled to 2D Gravity in the Conformal Gauge". In: *Mod. Phys. Lett. A* 3 (1988), p. 1651. DOI: 10.1142/S0217732388001975.

[133] Jacques Distler and Hikaru Kawai. "Conformal Field Theory and 2D Quantum Gravity". In: *Nucl. Phys. B* 321 (1989), pp. 509–527. DOI: 10.1016/0550-3213(89)90354-4.

[134] Herbert W. Hamber. "Critical behavior in simplicial quantum gravity". In: *Nucl. Phys. B Proc. Suppl.* 20 (1991), pp. 728–732. DOI: 10.1016/0920-5632(91)91009-9.

[135] Herbert W. Hamber. "Phases of simplicial quantum gravity in four-dimensions: Estimates for the critical exponents". In: *Nucl. Phys. B* 400 (1993), pp. 347–389. DOI: 10.1016/0550-3213(93)90409-I.

[136] Jan Ambjorn, Jakob L. Nielsen, Juri Rolf, and George K. Savvidy. "Spikes in quantum Regge calculus". In: *Class. Quant. Grav.* 14 (1997), pp. 3225–3241. DOI: 10.1088/0264-9381/14/12/009. arXiv: gr-qc/9704079.

[137] Benjamin Bahr and Bianca Dittrich. "(Broken) Gauge Symmetries and Constraints in Regge Calculus". In: *Class. Quant. Grav.* 26 (2009), p. 225011. DOI: 10.1088/0264-9381/26/22/225011. arXiv: 0905.1670 [gr-qc].

[138] Benjamin Bahr and Bianca Dittrich. "Regge calculus from a new angle". In: *New J. Phys.* 12 (2010), p. 033010. DOI: 10.1088/1367-2630/12/3/033010. arXiv: 0907.4325 [gr-qc].

[139] Herbert W. Hamber. "Phases of simplicial quantum gravity". In: *Nucl. Phys. B Proc. Suppl.* 25 (1992), pp. 150–175. DOI: 10.1016/S0920-5632(05)80016-7.

[140] Herbert W. Hamber. "Quantum Gravity on the Lattice". In: *Gen. Rel. Grav.* 41 (2009), pp. 817–876. DOI: 10.1007/s10714-009-0769-y. arXiv: 0901.0964 [gr-qc].

[141] Herbert W. Hamber. "Scaling Exponents for Lattice Quantum Gravity in Four Dimensions". In: *Phys. Rev. D* 92.6 (2015), p. 064017. DOI: 10.1103/PhysRevD.92.064017. arXiv: 1506.07795 [hep-th].

[142] F. David. "Planar Diagrams, Two-Dimensional Lattice Gravity and Surface Models". In: *Nucl. Phys. B* 257 (1985). Ed. by E. Brezin and S. R. Wadia, p. 45. DOI: 10.1016/0550-3213(85)90335-9.

[143] F. David. "A Model of Random Surfaces with Nontrivial Critical Behavior". In: *Nucl. Phys. B* 257 (1985), pp. 543–576. DOI: 10.1016/0550-3213(85)90363-3.

[144] Jan Ambjørn, Bergfinnur Jøgvan Durhuus, and J. Frohlich. "Diseases of triangulated random surface models, and possible cures". English. In: *Nuclear Physics, Section B* 257.3 (Jan. 1985), pp. 433–449. ISSN: 0550-3213. DOI: 10.1016/0550-3213(85)90356-6.

[145] V. A. Kazakov, Alexander A. Migdal, and I. K. Kostov. "Critical Properties of Randomly Triangulated Planar Random Surfaces". In: *Phys. Lett. B* 157 (1985), pp. 295–300. DOI: 10.1016/0370-2693(85)90669-0.

[146] W. T. Tutte. "A Census of Planar Triangulations". In: *Canadian Journal of Mathematics* 14 (1962), pp. 21–38. DOI: 10.4153/CJM-1962-002-9.

[147] Jan Ambjorn and Steen Varsted. "Entropy estimate in three-dimensional simplicial quantum gravity". In: *Phys. Lett. B* 266 (1991), pp. 285–290. DOI: 10.1016/0370-2693(91)91041-S.

[148] Jan Ambjorn and J. Jurkiewicz. "On the exponential bound in four-dimensional simplicial gravity". In: *Phys. Lett. B* 335 (1994), pp. 355–358. DOI: 10.1016/0370-2693(94)90363-8. arXiv: hep-lat/9405010.

[149] J. Jurkiewicz, A. Krzywicki, and B. Petersson. "A Numerical Study of Discrete Euclidean Polyakov Surfaces". In: *Phys. Lett. B* 168 (1986), pp. 273–278. DOI: 10.1016/0370-2693(86)90978-0.

[150] J. Jurkiewicz, A. Krzywicki, and B. Petersson. "A Grand Canonical Ensemble of Randomly Triangulated Surfaces". In: *Phys. Lett. B* 177 (1986), pp. 89–92. DOI: 10.1016/0370-2693(86)90021-3.

[151] Jan Ambjorn, B. Durhuus, J. Frohlich, and P. Orland. "The Appearance of Critical Dimensions in Regulated String Theories". In: *Nucl. Phys. B* 270 (1986), pp. 457–482. DOI: 10.1016/0550-3213(86)90563-8.

[152] Jan Ambjorn, B. Durhuus, and J. Frohlich. "The Appearance of Critical Dimensions in Regulated String Theories. 2." In: *Nucl. Phys. B* 275 (1986), pp. 161–184. DOI: 10.1016/0550-3213(86)90594-8.

[153] Alexander M. Polyakov. "Quantum Geometry of Bosonic Strings". In: *Phys. Lett. B* 103 (1981). Ed. by I. M. Khalatnikov and V. P. Mineev, pp. 207–210. DOI: 10.1016/0370-2693(81)90743-7.

[154] P. Di Francesco, Paul H. Ginsparg, and Jean Zinn-Justin. "2-D Gravity and random matrices". In: *Phys. Rept.* 254 (1995), pp. 1–133. DOI: 10.1016/0370-1573(94)00084-G. arXiv: hep-th/9306153.

[155] E. Brezin, C. Itzykson, G. Parisi, and J. B. Zuber. "Planar Diagrams". In: *Commun. Math. Phys.* 59 (1978), p. 35. DOI: 10.1007/BF01614153.

[156] Jan Ambjorn, S. Jain, J. Jurkiewicz, and C. F. Kristjansen. "Observing 4-d baby universes in quantum gravity". In: *Phys. Lett. B* 305 (1993), pp. 208–213. DOI: 10.1016/0370-2693(93)90109-U. arXiv: hep-th/9303041.

[157] S. Catterall, John B. Kogut, R. Renken, and G. Thorleifsson. "Baby universes in 4-D dynamical triangulation". In: *Phys. Lett. B* 366 (1996), pp. 72–76. DOI: 10.1016/0370-2693(95)01372-5. arXiv: hep-lat/9509004.

[158] Bas V. de Bakker and Jan Smit. "Curvature and scaling in 4-d dynamical triangulation". In: *Nucl. Phys. B* 439 (1995), pp. 239–258. DOI: 10.1016/0550-3213(95)00026-O. arXiv: hep-lat/9407014.

[159] Jan Ambjorn and J. Jurkiewicz. "Scaling in four-dimensional quantum gravity". In: *Nucl. Phys. B* 451 (1995), pp. 643–676. DOI: 10.1016/0550-3213(95)00303-A. arXiv: hep-th/9503006.

[160] H. S. Egawa, T. Hotta, T. Izubuchi, N. Tsuda, and T. Yukawa. "Scaling behavior in 4-D simplicial quantum gravity". In: *Prog. Theor. Phys.* 97 (1997), pp. 539–552. DOI: 10.1143/PTP.97.539. arXiv: hep-lat/9611028.

[161] P. Bialas, Z. Burda, A. Krzywicki, and B. Petersson. "Focusing on the fixed point of 4-D simplicial gravity". In: *Nucl. Phys. B* 472 (1996), pp. 293–308. DOI: 10.1016/0550-3213(96)00214-3. arXiv: hep-lat/9601024.

[162] S. Catterall, R. Renken, and John B. Kogut. "Singular structure in 4-D simplicial gravity". In: *Phys. Lett. B* 416 (1998), pp. 274–280. DOI: 10.1016/S0370-2693(97)01349-X. arXiv: hep-lat/9709007.

[163] Jan Ambjorn and R. Loll. "Nonperturbative Lorentzian quantum gravity, causality and topology change". In: *Nucl. Phys. B* 536 (1998), pp. 407–434. DOI: 10.1016/S0550-3213(98)00692-0. arXiv: hep-th/9805108.

[164] Jan Ambjørn, J. Jurkiewicz, and R. Loll. "Lorentzian and Euclidean Quantum Gravity — Analytical and Numerical Results". In: *NATO Sci. Ser. C* 556 (2000). Ed. by Lárus Thorlacius and Thordur Jonsson, pp. 381–450. DOI: 10.1007/978-94-011-4303-5_9. arXiv: hep-th/0001124.

[165] Jan Ambjorn, J. Jurkiewicz, and R. Loll. "Dynamically triangulating Lorentzian quantum gravity". In: *Nucl. Phys. B* 610 (2001), pp. 347–382. DOI: 10.1016/S0550-3213(01)00297-8. arXiv: hep-th/0105267.

[166] R. Loll. "Quantum Gravity from Causal Dynamical Triangulations: A Review". In: *Class. Quant. Grav.* 37.1 (2020), p. 013002. DOI: 10.1088/1361-6382/ab57c7. arXiv: 1905.08669 [hep-th].

[167] J. Ambjørn, Z. Drogosz, J. Gizbert-Studnicki, A. Görlich, J. Jurkiewicz, and D. Németh. "Matter-driven phase transition in lattice quantum gravity". In: (Feb. 2021). arXiv: 2103.00198 [hep-th].

[168] Bernd Bruegmann and Enzo Marinari. "4-d simplicial quantum gravity with a nontrivial measure". In: *Phys. Rev. Lett.* 70 (1993), pp. 1908–1911. DOI: 10.1103/PhysRevLett.70.1908. arXiv: hep-lat/9210002.

[169] S. Bilke, Z. Burda, A. Krzywicki, B. Petersson, J. Tabaczek, and G. Thorleifsson. "4-D simplicial quantum gravity: Matter fields and the corresponding effective action". In: *Phys. Lett. B* 432 (1998), pp. 279–286. DOI: 10.1016/S0370-2693(98)00675-3. arXiv: hep-lat/9804011.

[170] J. Laiho and D. Coumbe. "Evidence for Asymptotic Safety from Lattice Quantum Gravity". In: *Phys. Rev. Lett.* 107 (2011), p. 161301. DOI: 10.1103/PhysRevLett.107.161301. arXiv: 1104.5505 [hep-lat].

[171] J. Ambjorn, L. Glaser, A. Goerlich, and J. Jurkiewicz. "Euclidian 4d quantum gravity with a non-trivial measure term". In: *JHEP* 10 (2013), p. 100. DOI: 10.1007/JHEP10(2013)100. arXiv: 1307.2270 [hep-lat].

[172] J. Laiho, S. Bassler, D. Coumbe, D. Du, and J. T. Neelakanta. "Lattice Quantum Gravity and Asymptotic Safety". In: *Phys. Rev. D* 96.6 (2017), p. 064015. DOI: 10.1103/PhysRevD.96.064015. arXiv: 1604.02745 [hep-th].

[173] Kenneth G. Wilson. "Quarks and Strings on a Lattice". In: *13th International School of Subnuclear Physics: New Phenomena in Subnuclear Physics*. Nov. 1975.

[174] K. G. Wilson. "Quarks: From Paradox to Myth". In: *Subnucl. Ser.* 13 (1977), pp. 13–32.

[175] Kazuo Fujikawa. "Path Integral Measure for Gravitational Interactions". In: *Nucl. Phys. B* 226 (1983), pp. 437–443. DOI: 10.1016/0550-3213(83)90202-X.

[176] Jan Ambjorn, Jerzy Jurkiewicz, and Charlotte F. Kristjansen. "Quantum gravity, dynamical triangulations and higher derivative regularization". In: *Nucl. Phys. B* 393 (1993), pp. 601–632. DOI: 10.1016/0550-3213(93)90075-Z. arXiv: hep-th/9208032.

[177] Dario Benedetti and Razvan Gurau. "Phase Transition in Dually Weighted Colored Tensor Models". In: *Nucl. Phys. B* 855 (2012), pp. 420–437. DOI: 10.1016/j.nuclphysb.2011.10.015. arXiv: 1108.5389 [hep-th].

[178] Razvan Gurau. "The 1/N expansion of colored tensor models". In: *Annales Henri Poincare* 12 (2011), pp. 829–847. DOI: 10.1007/s00023-011-0101-8. arXiv: 1011.2726 [gr-qc].

[179] Razvan Gurau. "The complete 1/N expansion of colored tensor models in arbitrary dimension". In: *Annales Henri Poincare* 13 (2012), pp. 399–423. DOI: 10.1007/s00023-011-0118-z. arXiv: 1102.5759 [gr-qc].

[180] Razvan Gurau and Vincent Rivasseau. "The 1/N expansion of colored tensor models in arbitrary dimension". In: *EPL* 95.5 (2011), p. 50004. DOI: 10.1209/0295-5075/95/50004. arXiv: 1101.4182 [gr-qc].

[181] Razvan Gurau and James P. Ryan. "Colored Tensor Models - a review". In: *SIGMA* 8 (2012), p. 020. DOI: 10.3842/SIGMA.2012.020. arXiv: 1109.4812 [hep-th].

[182] Sven Bilke and Gudmar Thorleifsson. "Simulating four-dimensional simplicial gravity using degenerate triangulations". In: *Phys. Rev. D* 59 (1999), p. 124008. DOI: 10.1103/PhysRevD.59.124008. arXiv: hep-lat/9810049.

[183] Jan Ambjørn, Bergfinnur Durhuus, and Thordur Jonsson. *Quantum Geometry: A Statistical Field Theory Approach*. Cambridge Monographs on Mathematical Physics. Cambridge, UK: Cambridge Univ. Press, Dec. 2005. ISBN: 978-0-521-01736-7, 978-0-521-46167-2, 978-0-511-88535-8. DOI: 10.1017/CBO9780511524417.

[184] Udo Pachner. "P.L. Homeomorphic Manifolds are Equivalent by Elementary Shellings". In: *European Journal of Combinatorics* 12.2 (1991), pp. 129–145. ISSN: 0195-6698. DOI: https://doi.org/10.1016/S0195-6698(13)80080-7. URL: https://www.sciencedirect.com/science/article/pii/S0195669813800807.

[185] Mark Gross and Steen Varsted. "Elementary moves and ergodicity in D-dimensional simplicial quantum gravity". In: *Nucl. Phys. B* 378 (1992), pp. 367–380. DOI: 10.1016/0550-3213(92)90012-Z.

[186] S. Catterall. "Simulations of dynamically triangulated gravity: An Algorithm for arbitrary dimension". In: *Comput. Phys. Commun.* 87 (1995), pp. 409–415. DOI: 10.1016/0010-4655(94)00117-K. arXiv: hep-lat/9405026.

[187] Fleur Versteegen. "Quantum Gravity: From continuous to discrete." PhD thesis. U. Heidelberg (main), 2019. DOI: 10.11588/heidok.00027383.

[188] Daniel Coumbe and John Laiho. "Exploring Euclidean Dynamical Triangulations with a Nontrivial Measure Term". In: *JHEP* 04 (2015), p. 028. DOI: 10.1007/JHEP04(2015)028. arXiv: 1401.3299 [hep-th].

[189] J. Ambjorn, J. Jurkiewicz, and R. Loll. "Spectral dimension of the universe". In: *Phys. Rev. Lett.* 95 (2005), p. 171301. DOI: 10.1103/PhysRevLett.95.171301. arXiv: hep-th/0505113.

[190] O. Lauscher and M. Reuter. "Fractal spacetime structure in asymptotically safe gravity". In: *JHEP* 10 (2005), p. 050. DOI: 10.1088/1126-6708/2005/10/050. arXiv: hep-th/0508202.

[191] S. Carlip. "Dimension and Dimensional Reduction in Quantum Gravity". In: *Class. Quant. Grav.* 34.19 (2017), p. 193001. DOI: 10.1088/1361-6382/aa8535. arXiv: 1705.05417 [gr-qc].

[192] J. Ambjørn, J. Gizbert-Studnicki, A. Görlich, J. Jurkiewicz, N. Klitgaard, and R. Loll. "Characteristics of the new phase in CDT". In: *Eur. Phys. J. C* 77.3 (2017), p. 152. DOI: 10.1140/epjc/s10052-017-4710-3. arXiv: 1610.05245 [hep-th].

[193] Erich Kahler. In: *Rend. Math* 3-4, 21 (1962), p. 425.

[194] Simon Catterall, Jack Laiho, and Judah Unmuth-Yockey. "Kähler-Dirac fermions on Euclidean dynamical triangulations". In: *Phys. Rev. D* 98.11 (2018), p. 114503. DOI: 10.1103/PhysRevD.98.114503. arXiv: 1810.10626 [hep-lat].

[195] Holger Gies. "Renormalizability of gauge theories in extra dimensions". In: *Phys. Rev. D* 68 (2003), p. 085015. DOI: 10.1103/PhysRevD.68.085015. arXiv: hep-th/0305208.

[196] Tim R. Morris. "Renormalizable extra-dimensional models". In: *JHEP* 01 (2005), p. 002. DOI: 10.1088/1126-6708/2005/01/002. arXiv: hep-ph/0410142.

[197] Francesco Knechtli and Enrico Rinaldi. "Extra-dimensional models on the lattice". In: *Int. J. Mod. Phys. A* 31.22 (2016), p. 1643002. DOI: 10.1142/S0217751X16430028. arXiv: 1605.04341 [hep-lat].

[198] R. Gastmans, R. Kallosh, and C. Truffin. "Quantum Gravity Near Two-Dimensions". In: *Nucl. Phys. B* 133 (1978), pp. 417–434. DOI: 10.1016/0550-3213(78)90234-1.

[199] S. M. Christensen and M. J. Duff. "Quantum Gravity in Two + ϵ Dimensions". In: *Phys. Lett. B* 79 (1978), pp. 213–216. DOI: 10.1016/0370-2693(78)90225-3.

[200] Hikaru Kawai and Masao Ninomiya. "Renormalization Group and Quantum Gravity". In: *Nucl. Phys. B* 336 (1990), pp. 115–145. DOI: 10.1016/0550-3213(90)90345-E.

[201] Kevin Falls. "Physical renormalization schemes and asymptotic safety in quantum gravity". In: *Phys. Rev. D* 96.12 (2017), p. 126016. DOI: 10.1103/PhysRevD.96.126016. arXiv: 1702.03577 [hep-th].

[202] Andreas Nink and Martin Reuter. "On the physical mechanism underlying Asymptotic Safety". In: *JHEP* 01 (2013), p. 062. DOI: 10.1007/JHEP01(2013)062. arXiv: 1208.0031 [hep-th].

[203] M. Reuter and Frank Saueressig. "Renormalization group flow of quantum gravity in the Einstein-Hilbert truncation". In: *Phys. Rev. D* 65 (2002), p. 065016. DOI: 10.1103/PhysRevD.65.065016. arXiv: hep-th/0110054.

[204] O. Lauscher and M. Reuter. "Ultraviolet fixed point and generalized flow equation of quantum gravity". In: *Phys. Rev. D* 65 (2002), p. 025013. DOI: 10.1103/PhysRevD.65.025013. arXiv: hep-th/0108040.

[205] Daniel F. Litim. "Fixed points of quantum gravity". In: *Phys. Rev. Lett.* 92 (2004), p. 201301. DOI: 10.1103/PhysRevLett.92.201301. arXiv: hep-th/0312114.

[206] Max Niedermaier and Martin Reuter. "The Asymptotic Safety Scenario in Quantum Gravity". In: *Living Rev. Rel.* 9 (2006), pp. 5–173. DOI: 10.12942/lrr-2006-5.

[207] Alessandro Codello, Roberto Percacci, and Christoph Rahmede. "Investigating the Ultraviolet Properties of Gravity with a Wilsonian Renormalization Group Equation". In: *Annals Phys.* 324 (2009), pp. 414–469. DOI: 10.1016/j.aop.2008.08.008. arXiv: 0805.2909 [hep-th].

[208] Elisa Manrique, Martin Reuter, and Frank Saueressig. "Bimetric Renormalization Group Flows in Quantum Einstein Gravity". In: *Annals Phys.* 326 (2011), pp. 463–485. DOI: 10.1016/j.aop.2010.11.006. arXiv: 1006.0099 [hep-th].

[209] Daniel Becker and Martin Reuter. "En route to Background Independence: Broken split-symmetry, and how to restore it with bi-metric average actions". In: *Annals Phys.* 350 (2014), pp. 225–301. DOI: 10.1016/j.aop.2014.07.023. arXiv: 1404.4537 [hep-th].

[210] Ivan Donkin and Jan M. Pawlowski. "The phase diagram of quantum gravity from diffeomorphism-invariant RG-flows". In: (Mar. 2012). arXiv: 1203.4207 [hep-th].

[211] Nicolai Christiansen, Daniel F. Litim, Jan M. Pawlowski, and Andreas Rodigast. "Fixed points and infrared completion of quantum gravity". In: *Phys. Lett. B* 728 (2014), pp. 114–117. DOI: 10.1016/j.physletb.2013.11.025. arXiv: 1209.4038 [hep-th].

[212] Nicolai Christiansen, Benjamin Knorr, Jan M. Pawlowski, and Andreas Rodigast. "Global Flows in Quantum Gravity". In: *Phys. Rev. D* 93.4 (2016), p. 044036. DOI: 10.1103/PhysRevD.93.044036. arXiv: 1403.1232 [hep-th].

[213] Nicolai Christiansen, Benjamin Knorr, Jan Meibohm, Jan M. Pawlowski, and Manuel Reichert. "Local Quantum Gravity". In: *Phys. Rev. D* 92.12 (2015), p. 121501. DOI: 10.1103/PhysRevD.92.121501. arXiv: 1506.07016 [hep-th].

[214] Nicolai Christiansen, Kevin Falls, Jan M. Pawlowski, and Manuel Reichert. "Curvature dependence of quantum gravity". In: *Phys. Rev. D* 97.4 (2018), p. 046007. DOI: 10.1103/PhysRevD.97.046007. arXiv: 1711.09259 [hep-th].

[215] Benjamin Knorr and Stefan Lippoldt. "Correlation functions on a curved background". In: *Phys. Rev. D* 96.6 (2017), p. 065020. DOI: 10.1103/PhysRevD.96.065020. arXiv: 1707.01397 [hep-th].

[216] Tobias Denz, Jan M. Pawlowski, and Manuel Reichert. "Towards apparent convergence in asymptotically safe quantum gravity". In: *Eur. Phys. J. C* 78.4 (2018), p. 336. DOI: 10.1140/epjc/s10052-018-5806-0. arXiv: 1612.07315 [hep-th].

[217] O. Lauscher and M. Reuter. "Flow equation of quantum Einstein gravity in a higher derivative truncation". In: *Phys. Rev. D* 66 (2002), p. 025026. DOI: 10.1103/PhysRevD.66.025026. arXiv: hep-th/0205062.

[218] Stefan Rechenberger and Frank Saueressig. "The R^2 phase-diagram of QEG and its spectral dimension". In: *Phys. Rev. D* 86 (2012), p. 024018. DOI: 10.1103/PhysRevD.86.024018. arXiv: 1206.0657 [hep-th].

[219] Dario Benedetti, Pedro F. Machado, and Frank Saueressig. "Asymptotic safety in higher-derivative gravity". In: *Mod. Phys. Lett. A* 24 (2009), pp. 2233–2241. DOI: 10.1142/S0217732309031521. arXiv: 0901.2984 [hep-th].

[220] Dario Benedetti, Pedro F. Machado, and Frank Saueressig. "Four-derivative interactions in asymptotically safe gravity". In: *AIP Conf. Proc.* 1196.1 (2009). Ed. by Jerzy Kowalski-Glikman, R. Durka, and M. Szczachor, p. 44. DOI: 10.1063/1.3284399. arXiv: 0909.3265 [hep-th].

[221] Kai Groh, Stefan Rechenberger, Frank Saueressig, and Omar Zanusso. "Higher Derivative Gravity from the Universal Renormalization Group Machine". In: *PoS* EPS-HEP2011 (2011), p. 124. DOI: 10.22323/1.134.0124. arXiv: 1111.1743 [hep-th].

[222] Kevin Falls, Nobuyoshi Ohta, and Roberto Percacci. "Towards the determination of the dimension of the critical surface in asymptotically safe gravity". In: *Phys. Lett. B* 810 (2020), p. 135773. DOI: 10.1016/j.physletb.2020.135773. arXiv: 2004.04126 [hep-th].

[223] Benjamin Knorr. "The derivative expansion in asymptotically safe quantum gravity: general setup and quartic order". In: (Apr. 2021). arXiv: 2104.11336 [hep-th].

[224] Holger Gies, Benjamin Knorr, Stefan Lippoldt, and Frank Saueressig. "Gravitational Two-Loop Counterterm Is Asymptotically Safe". In: *Phys. Rev. Lett.* 116.21 (2016), p. 211302. DOI: 10.1103/PhysRevLett.116.211302. arXiv: 1601.01800 [hep-th].

[225] Yannick Kluth and Daniel F. Litim. "Fixed Points of Quantum Gravity and the Dimensionality of the UV Critical Surface". In: (Aug. 2020). arXiv: 2008.09181 [hep-th].

[226] Gustavo P. De Brito, Nobuyoshi Ohta, Antonio D. Pereira, Anderson A. Tomaz, and Masatoshi Yamada. "Asymptotic safety and field parametrization dependence in the $f(R)$ truncation". In: *Phys. Rev. D* 98.2 (2018), p. 026027. DOI: 10.1103/PhysRevD.98.026027. arXiv: 1805.09656 [hep-th].

[227] K. Falls, D. F. Litim, K. Nikolakopoulos, and C. Rahmede. "A bootstrap towards asymptotic safety". In: (Jan. 2013). arXiv: 1301.4191 [hep-th].

[228] Kevin Falls, Daniel F. Litim, Konstantinos Nikolakopoulos, and Christoph Rahmede. "Further evidence for asymptotic safety of quantum gravity". In: *Phys. Rev. D* 93.10 (2016), p. 104022. DOI: 10.1103/PhysRevD.93.104022. arXiv: 1410.4815 [hep-th].

[229] Kevin G. Falls, Daniel F. Litim, and Jan Schröder. "Aspects of asymptotic safety for quantum gravity". In: *Phys. Rev. D* 99.12 (2019), p. 126015. DOI: 10.1103/PhysRevD.99.126015. arXiv: 1810.08550 [gr-qc].

[230] Dario Benedetti and Francesco Caravelli. "The Local potential approximation in quantum gravity". In: *JHEP* 06 (2012). [Erratum: JHEP 10, 157 (2012)], p. 017. DOI: 10.1007/JHEP06(2012)017. arXiv: 1204.3541 [hep-th].

[231] Juergen A. Dietz and Tim R. Morris. "Asymptotic safety in the f(R) approximation". In: *JHEP* 01 (2013), p. 108. DOI: 10.1007/JHEP01(2013)108. arXiv: 1211.0955 [hep-th].

[232] Maximilian Demmel, Frank Saueressig, and Omar Zanusso. "A proper fixed functional for four-dimensional Quantum Einstein Gravity". In: *JHEP* 08 (2015), p. 113. DOI: 10.1007/JHEP08(2015)113. arXiv: 1504.07656 [hep-th].

[233] Sergio Gonzalez-Martin, Tim R. Morris, and Zoë H. Slade. "Asymptotic solutions in asymptotic safety". In: *Phys. Rev. D* 95.10 (2017), p. 106010. DOI: 10.1103/PhysRevD.95.106010. arXiv: 1704.08873 [hep-th].

[234] Kevin Falls, Callum R. King, Daniel F. Litim, Kostas Nikolakopoulos, and Christoph Rahmede. "Asymptotic safety of quantum gravity beyond Ricci scalars". In: *Phys. Rev. D* 97.8 (2018), p. 086006. DOI: 10.1103/PhysRevD.97.086006. arXiv: 1801.00162 [hep-th].

[235] Lando Bosma, Benjamin Knorr, and Frank Saueressig. "Resolving Spacetime Singularities within Asymptotic Safety". In: *Phys. Rev. Lett.* 123.10 (2019), p. 101301. DOI: 10.1103/PhysRevLett.123.101301. arXiv: 1904.04845 [hep-th].

[236] Benjamin Knorr, Chris Ripken, and Frank Saueressig. "Form Factors in Asymptotic Safety: conceptual ideas and computational toolbox". In: *Class. Quant. Grav.* 36.23 (2019), p. 234001. DOI: 10.1088/1361-6382/ab4a53. arXiv: 1907.02903 [hep-th].

[237] John F. Donoghue. "A Critique of the Asymptotic Safety Program". In: *Front. in Phys.* 8 (2020), p. 56. DOI: 10.3389/fphy.2020.00056. arXiv: 1911.02967 [hep-th].

[238] Alfio Bonanno, Astrid Eichhorn, Holger Gies, Jan M. Pawlowski, Roberto Percacci, Martin Reuter, Frank Saueressig, and Gian Paolo Vacca. "Critical reflections on asymptotically safe gravity". In: *Front. in Phys.* 8 (2020), p. 269. DOI: 10.3389/fphy.2020.00269. arXiv: 2004.06810 [gr-qc].

[239] Tom Draper, Benjamin Knorr, Chris Ripken, and Frank Saueressig. "Finite Quantum Gravity Amplitudes: No Strings Attached". In: *Phys. Rev. Lett.* 125.18 (2020), p. 181301. DOI: 10.1103/PhysRevLett.125.181301. arXiv: 2007.00733 [hep-th].

[240] Tom Draper, Benjamin Knorr, Chris Ripken, and Frank Saueressig. "Graviton-Mediated Scattering Amplitudes from the Quantum Effective Action". In: *JHEP* 11 (2020), p. 136. DOI: 10.1007/JHEP11(2020)136. arXiv: 2007.04396 [hep-th].

[241] Jan Meibohm, Jan M. Pawlowski, and Manuel Reichert. "Asymptotic safety of gravity-matter systems". In: *Phys. Rev. D* 93.8 (2016), p. 084035. DOI: 10.1103/PhysRevD.93.084035. arXiv: 1510.07018 [hep-th].

[242] Nicolai Christiansen, Daniel F. Litim, Jan M. Pawlowski, and Manuel Reichert. "Asymptotic safety of gravity with matter". In: *Phys. Rev. D* 97.10 (2018), p. 106012. DOI: 10.1103/PhysRevD.97.106012. arXiv: 1710.04669 [hep-th].

[243] Astrid Eichhorn, Stefan Lippoldt, and Marc Schiffer. "Zooming in on fermions and quantum gravity". In: *Phys. Rev. D* 99.8 (2019), p. 086002. DOI: 10.1103/PhysRevD.99.086002. arXiv: 1812.08782 [hep-th].

[244] Alfio Bonanno, Tobias Denz, Jan M. Pawlowski, and Manuel Reichert. "Reconstructing the graviton". In: (Feb. 2021). arXiv: 2102.02217 [hep-th].

[245] Elisa Manrique, Stefan Rechenberger, and Frank Saueressig. "Asymptotically Safe Lorentzian Gravity". In: *Phys. Rev. Lett.* 106 (2011), p. 251302. DOI: 10.1103/PhysRevLett.106.251302. arXiv: 1102.5012 [hep-th].

[246] Stefan Rechenberger and Frank Saueressig. "A functional renormalization group equation for foliated spacetimes". In: *JHEP* 03 (2013), p. 010. DOI: 10.1007/JHEP03(2013)010. arXiv: 1212.5114 [hep-th].

[247] Jorn Biemans, Alessia Platania, and Frank Saueressig. "Quantum gravity on foliated spacetimes: Asymptotically safe and sound". In: *Phys. Rev. D* 95.8 (2017), p. 086013. DOI: 10.1103/PhysRevD.95.086013. arXiv: 1609.04813 [hep-th].

[248] Benjamin Knorr. "Lorentz symmetry is relevant". In: *Phys. Lett. B* 792 (2019), pp. 142–148. DOI: 10.1016/j.physletb.2019.01.070. arXiv: 1810.07971 [hep-th].

[249] Francesca Arici, Daniel Becker, Chris Ripken, Frank Saueressig, and Walter D. van Suijlekom. "Reflection positivity in higher derivative scalar theories". In: *J. Math. Phys.* 59.8 (2018), p. 082302. DOI: 10.1063/1.5027231. arXiv: 1712.04308 [hep-th].

[250] Richard P. Woodard. "Ostrogradsky's theorem on Hamiltonian instability". In: *Scholarpedia* 10.8 (2015), p. 32243. DOI: 10.4249/scholarpedia.32243. arXiv: 1506.02210 [hep-th].

[251] Alessia Platania and Christof Wetterich. "Non-perturbative unitarity and fictitious ghosts in quantum gravity". In: *Phys. Lett. B* 811 (2020), p. 135911. DOI: 10.1016/j.physletb.2020.135911. arXiv: 2009.06637 [hep-th].

[252] Alfio Bonanno and Martin Reuter. "Modulated Ground State of Gravity Theories with Stabilized Conformal Factor". In: *Phys. Rev. D* 87.8 (2013), p. 084019. DOI: 10.1103/PhysRevD.87.084019. arXiv: 1302.2928 [hep-th].

[253] Th. Kaluza. "Zum Unitätsproblem der Physik". In: *Sitzungsber. Preuss. Akad. Wiss. Berlin (Math. Phys.)* 1921 (1921), pp. 966–972. DOI: 10.1142/S0218271818700017. arXiv: 1803.08616.

[254] Oskar Klein. "Quantum Theory and Five-Dimensional Theory of Relativity. (In German and English)". In: *Z. Phys.* 37 (1926). Ed. by J. C. Taylor, pp. 895–906. DOI: 10.1007/BF01397481.

[255] O. Klein. "The Atomicity of Electricity as a Quantum Theory Law". In: *Nature* 118 (1926), p. 516. DOI: 10.1038/118516a0.

[256] Gaurav Narain and Roberto Percacci. "Renormalization Group Flow in Scalar-Tensor Theories. I". In: *Class. Quant. Grav.* 27 (2010), p. 075001. DOI: 10.1088/0264-9381/27/7/075001. arXiv: 0911.0386 [hep-th].

[257] Pietro Donà, Astrid Eichhorn, and Roberto Percacci. "Matter matters in asymptotically safe quantum gravity". In: *Phys. Rev. D* 89.8 (2014), p. 084035. DOI: 10.1103/PhysRevD.89.084035. arXiv: 1311.2898 [hep-th].

[258] Jorn Biemans, Alessia Platania, and Frank Saueressig. "Renormalization group fixed points of foliated gravity-matter systems". In: *JHEP* 05 (2017), p. 093. DOI: 10.1007/JHEP05(2017)093. arXiv: 1702.06539 [hep-th].

[259] Benjamin Bürger, Jan M. Pawlowski, Manuel Reichert, and Bernd-Jochen Schaefer. "Curvature dependence of quantum gravity with scalars". In: (Dec. 2019). arXiv: 1912.01624 [hep-th].

[260] Daniel N. Kabat. "Black hole entropy and entropy of entanglement". In: *Nucl. Phys. B* 453 (1995), pp. 281–299. DOI: 10.1016/0550-3213(95)00443-V. arXiv: hep-th/9503016.

[261] Finn Larsen and Frank Wilczek. "Renormalization of black hole entropy and of the gravitational coupling constant". In: *Nucl. Phys. B* 458 (1996), pp. 249–266. DOI: 10.1016/0550-3213(95)00548-X. arXiv: hep-th/9506066.

[262] Pietro Dona and Roberto Percacci. "Functional renormalization with fermions and tetrads". In: *Phys. Rev. D* 87.4 (2013), p. 045002. DOI: 10.1103/PhysRevD.87.045002. arXiv: 1209.3649 [hep-th].

[263] Jesse Daas, Wouter Oosters, Frank Saueressig, and Jian Wang. "Asymptotically safe gravity with fermions". In: *Phys. Lett. B* 809 (2020), p. 135775. DOI: 10.1016/j.physletb.2020.135775. arXiv: 2005.12356 [hep-th].

[264] Jesse Daas, Wouter Oosters, Frank Saueressig, and Jian Wang. "Asymptotically Safe Gravity-Fermion systems on curved backgrounds". In: (July 2021). arXiv: 2107.01071 [hep-th].

[265] Jan Meibohm and Jan M. Pawlowski. "Chiral fermions in asymptotically safe quantum gravity". In: *Eur. Phys. J. C* 76.5 (2016), p. 285. DOI: 10.1140/epjc/s10052-016-4132-7. arXiv: 1601.04597 [hep-th].

[266] Astrid Eichhorn, Stefan Lippoldt, Jan M. Pawlowski, Manuel Reichert, and Marc Schiffer. "How perturbative is quantum gravity?" In: *Phys. Lett. B* 792 (2019), pp. 310–314. DOI: 10.1016/j.physletb.2019.01.071. arXiv: 1810.02828 [hep-th].

[267] Astrid Eichhorn, Stefan Lippoldt, and Vedran Skrinjar. "Nonminimal hints for asymptotic safety". In: *Phys. Rev. D* 97.2 (2018), p. 026002. DOI: 10.1103/PhysRevD.97.026002. arXiv: 1710.03005 [hep-th].

[268] Astrid Eichhorn and Martin Pauly. "Safety in darkness: Higgs portal to simple Yukawa systems". In: *Phys. Lett. B* 819 (2021), p. 136455. DOI: 10.1016/j.physletb.2021.136455. arXiv: 2005.03661 [hep-ph].

[269] Astrid Eichhorn and Martin Pauly. "Constraining power of asymptotic safety for scalar fields". In: *Phys. Rev. D* 103.2 (2021), p. 026006. DOI: 10.1103/PhysRevD.103.026006. arXiv: 2009.13543 [hep-th].

[270] Holger Gies. "Running coupling in Yang-Mills theory: A flow equation study". In: *Phys. Rev. D* 66 (2002), p. 025006. DOI: 10.1103/PhysRevD.66.025006. arXiv: hep-th/0202207.

[271] Dario Benedetti, Kai Groh, Pedro F. Machado, and Frank Saueressig. "The Universal RG Machine". In: *JHEP* 06 (2011), p. 079. DOI: 10.1007/JHEP06(2011)079. arXiv: 1012.3081 [hep-th].

[272] J.P. Boyd. "Orthogonal rational functions on a semi-infinite interval". In: *J.Comp.Phys.* 70 (1987), pp. 63–88.

[273] John P. Boyd. *Chebyshev and Fourier Spectral Methods*. 2nd. Dover Publications, 2000.

[274] Julia Borchardt and Benjamin Knorr. "Global solutions of functional fixed point equations via pseudospectral methods". In: *Phys. Rev. D* 91.10 (2015). [Erratum: Phys.Rev.D 93, 089904 (2016)], p. 105011. DOI: 10.1103/PhysRevD.91.105011. arXiv: 1502.07511 [hep-th].

[275] Julia Borchardt and Benjamin Knorr. "Solving functional flow equations with pseudo-spectral methods". In: *Phys. Rev. D* 94 (2016), p. 025027. DOI: 10.1103/PhysRevD.94.025027. arXiv: 1603.06726 [hep-th].

[276] Eduardo Grossi and Nicolas Wink. "Resolving phase transitions with Discontinuous Galerkin methods". In: (Mar. 2019). arXiv: 1903.09503 [hep-th].

[277] Daniel Becker, Chris Ripken, and Frank Saueressig. "On avoiding Ostrogradski instabilities within Asymptotic Safety". In: *JHEP* 12 (2017), p. 121. DOI: 10.1007/JHEP12(2017)121. arXiv: 1709.09098 [hep-th].

[278] Bas V. de Bakker and Jan Smit. "Gravitational binding in 4-D dynamical triangulation". In: *Nucl. Phys. B* 484 (1997), pp. 476–494. DOI: 10.1016/S0550-3213(96)00616-5. arXiv: hep-lat/9604023.

[279] Raghav G. Jha, Jack Laiho, and Judah Unmuth-Yockey. "Lattice quantum gravity with scalar fields". In: *PoS* LATTICE2018 (2018), p. 043. DOI: 10.22323/1.334.0043. arXiv: 1810.09946 [hep-lat].

[280] Simon Catterall, Jack Laiho, and Judah Unmuth-Yockey. "Topological fermion condensates from anomalies". In: *JHEP* 10 (2018), p. 013. DOI: 10.1007/JHEP10(2018)013. arXiv: 1806.07845 [hep-lat].

[281] J. Ambjorn, A. Goerlich, J. Jurkiewicz, and R. Loll. "Nonperturbative Quantum Gravity". In: *Phys. Rept.* 519 (2012), pp. 127–210. DOI: 10.1016/j.physrep.2012.03.007. arXiv: 1203.3591 [hep-th].

[282] S. W. Hawking and I. G. Moss. "Supercooled Phase Transitions in the Very Early Universe". In: *Phys. Lett. B* 110 (1982), pp. 35–38. DOI: 10.1016/0370-2693(82)90946-7.

[283] N. Metropolis, A. W. Rosenbluth, M. N. Rosenbluth, A. H. Teller, and E. Teller. "Equation of state calculations by fast computing machines". In: *J. Chem. Phys.* 21 (1953), pp. 1087–1092. DOI: 10.1063/1.1699114.

[284] J.E. Norman and L.E. Cannon. "A Computer Program for the Generation of Random Variables from any Discrete Distribution". In: *Journal of Statistical Computation and Simulation* 1.4 (1972). cited By 9, pp. 331–348. DOI: 10.1080/00949657208810026.

[285] A.B. Bortz, M.H. Kalos, and J.L. Lebowitz. "A new algorithm for Monte Carlo simulation of Ising spin systems". In: *Journal of Computational Physics* 17.1 (1975). cited By 1756, pp. 10–18. DOI: 10.1016/0021-9991(75)90060-1.

[286] Daniel T Gillespie. "A general method for numerically simulating the stochastic time evolution of coupled chemical reactions". In: *Journal of computational physics* 22.4 (1976), pp. 403–434.

[287] D.T. Gillespie. "Exact stochastic simulation of coupled chemical reactions". In: *Journal of Physical Chemistry* 81.25 (1977). cited By 6526, pp. 2340–2361. DOI: 10.1021/j100540a008.

[288] James E Gentle. *Random number generation and Monte Carlo methods*. Vol. 381. Springer, 2003.

[289] Tim P Schulze. "A hybrid scheme for simulating epitaxial growth". In: *Journal of crystal growth* 263.1-4 (2004), pp. 605–615.

[290] TP Schulze. "Kinetic Monte-Carlo with minimal searching". In: *Phys. Rev. E* 65 (2002).

[291] Tim P. Schulze. "Efficient kinetic Monte Carlo simulation". In: *Journal of Computational Physics* 227.4 (2008), pp. 2455–2462. ISSN: 0021-9991. DOI: https://doi.org/10.1016/j.jcp.2007.10.021. URL: https://www.sciencedirect.com/science/article/pii/S0021999107004755.

[292] Joachim Oxenius. "Thermal Equilibrium and Detailed Balance". In: *Kinetic Theory of Particles and Photons: Theoretical Foundations of Non-LTE Plasma Spectroscopy*. Berlin, Heidelberg: Springer Berlin Heidelberg, 1986, pp. 1–34. ISBN: 978-3-642-70728-5. DOI: 10.1007/978-3-642-70728-5_1. URL: https://doi.org/10.1007/978-3-642-70728-5_1.

[293] Murray Gell-Mann and F. E. Low. "Quantum electrodynamics at small distances". In: *Phys. Rev.* 95 (1954), pp. 1300–1312. DOI: 10.1103/PhysRev.95.1300.

[294] M. Gockeler, R. Horsley, V. Linke, Paul E. L. Rakow, G. Schierholz, and H. Stuben. "Is there a Landau pole problem in QED?" In: *Phys. Rev. Lett.* 80 (1998), pp. 4119–4122. DOI: 10.1103/PhysRevLett.80.4119. arXiv: hep-th/9712244.

[295] M. Gockeler, R. Horsley, V. Linke, Paul E. L. Rakow, G. Schierholz, and H. Stuben. "Resolution of the Landau pole problem in QED". In: *Nucl. Phys. B Proc. Suppl.* 63 (1998). Ed. by C. T. H. Davies, I. M. Barbour, K. C. Bowler, R. D. Kenway, B. J. Pendleton, and D. G. Richards, pp. 694–696. DOI: 10.1016/S0920-5632(97)00875-X. arXiv: hep-lat/9801004.

[296] Holger Gies and Joerg Jaeckel. "Renormalization flow of QED". In: *Phys. Rev. Lett.* 93 (2004), p. 110405. DOI: 10.1103/PhysRevLett.93.110405. arXiv: hep-ph/0405183.

[297] U. Harst and M. Reuter. "QED coupled to QEG". In: *JHEP* 05 (2011), p. 119. DOI: 10.1007/JHEP05(2011)119. arXiv: 1101.6007 [hep-th].

[298] Astrid Eichhorn and Fleur Versteegen. "Upper bound on the Abelian gauge coupling from asymptotic safety". In: *JHEP* 01 (2018), p. 030. DOI: 10.1007/JHEP01(2018)030. arXiv: 1709.07252 [hep-th].

[299] Astrid Eichhorn and Aaron Held. "Mass difference for charged quarks from asymptotically safe quantum gravity". In: *Phys. Rev. Lett.* 121.15 (2018), p. 151302. DOI: 10.1103/PhysRevLett.121.151302. arXiv: 1803.04027 [hep-th].

[300] Jan-Eric Daum, Ulrich Harst, and Martin Reuter. "Running Gauge Coupling in Asymptotically Safe Quantum Gravity". In: *JHEP* 01 (2010), p. 084. DOI: 10.1007/JHEP01(2010)084. arXiv: 0910.4938 [hep-th].

[301] Sarah Folkerts, Daniel F. Litim, and Jan M. Pawlowski. "Asymptotic freedom of Yang-Mills theory with gravity". In: *Phys. Lett. B* 709 (2012), pp. 234–241. DOI: 10.1016/j.physletb.2012.02.002. arXiv: 1101.5552 [hep-th].

[302] Nicolai Christiansen and Astrid Eichhorn. "An asymptotically safe solution to the U(1) triviality problem". In: *Phys. Lett. B* 770 (2017), pp. 154–160. DOI: 10.1016/j.physletb.2017.04.047. arXiv: 1702.07724 [hep-th].

[303] Artur R. Pietrykowski. "Gauge dependence of gravitational correction to running of gauge couplings". In: *Phys. Rev. Lett.* 98 (2007), p. 061801. DOI: 10.1103/PhysRevLett.98.061801. arXiv: hep-th/0606208.

[304] David J. Toms. "Quantum gravity and charge renormalization". In: *Phys. Rev. D* 76 (2007), p. 045015. DOI: 10.1103/PhysRevD.76.045015. arXiv: 0708.2990 [hep-th].

[305] Dietmar Ebert, Jan Plefka, and Andreas Rodigast. "Absence of gravitational contributions to the running Yang-Mills coupling". In: *Phys. Lett. B* 660 (2008), pp. 579–582. DOI: 10.1016/j.physletb.2008.01.037. arXiv: 0710.1002 [hep-th].

[306] David J. Toms. "Quantum gravitational contributions to quantum electrodynamics". In: *Nature* 468 (2010), pp. 56–59. DOI: 10.1038/nature09506. arXiv: 1010.0793 [hep-th].

[307] Mohamed M. Anber, John F. Donoghue, and Mohamed El-Houssieny. "Running couplings and operator mixing in the gravitational corrections to coupling constants". In: *Phys. Rev. D* 83 (2011), p. 124003. DOI: 10.1103/PhysRevD.83.124003. arXiv: 1011.3229 [hep-th].

[308] Sean P. Robinson and Frank Wilczek. "Gravitational correction to running of gauge couplings". In: *Phys. Rev. Lett.* 96 (2006), p. 231601. DOI: 10.1103/PhysRevLett.96.231601. arXiv: hep-th/0509050.

[309] Astrid Eichhorn, Aaron Held, and Christof Wetterich. "Quantum-gravity predictions for the fine-structure constant". In: *Phys. Lett. B* 782 (2018), pp. 198–201. DOI: 10.1016/j.physletb.2018.05.016. arXiv: 1711.02949 [hep-th].

[310] O. Zanusso, L. Zambelli, G. P. Vacca, and R. Percacci. "Gravitational corrections to Yukawa systems". In: *Phys. Lett. B* 689 (2010), pp. 90–94. DOI: 10.1016/j.physletb.2010.04.043. arXiv: 0904.0938 [hep-th].

[311] G. P. Vacca and O. Zanusso. "Asymptotic Safety in Einstein Gravity and Scalar-Fermion Matter". In: *Phys. Rev. Lett.* 105 (2010), p. 231601. DOI: 10.1103/PhysRevLett.105.231601. arXiv: 1009.1735 [hep-th].

[312] Kin-ya Oda and Masatoshi Yamada. "Non-minimal coupling in Higgs–Yukawa model with asymptotically safe gravity". In: *Class. Quant. Grav.* 33.12 (2016), p. 125011. DOI: 10.1088/0264-9381/33/12/125011. arXiv: 1510.03734 [hep-th].

[313] Yuta Hamada and Masatoshi Yamada. "Asymptotic safety of higher derivative quantum gravity non-minimally coupled with a matter system". In: *JHEP* 08 (2017), p. 070. DOI: 10.1007/JHEP08(2017)070. arXiv: 1703.09033 [hep-th].

[314] Astrid Eichhorn, Aaron Held, and Jan M. Pawlowski. "Quantum-gravity effects on a Higgs-Yukawa model". In: *Phys. Rev. D* 94.10 (2016), p. 104027. DOI: 10.1103/PhysRevD.94.104027. arXiv: 1604.02041 [hep-th].

[315] Astrid Eichhorn and Aaron Held. "Viability of quantum-gravity induced ultraviolet completions for matter". In: *Phys. Rev. D* 96.8 (2017), p. 086025. DOI: 10.1103/PhysRevD.96.086025. arXiv: 1705.02342 [gr-qc].

[316] Astrid Eichhorn and Stefan Lippoldt. "Quantum gravity and Standard-Model-like fermions". In: *Phys. Lett. B* 767 (2017), pp. 142–146. DOI: 10.1016/j.physletb.2017.01.064. arXiv: 1611.05878 [gr-qc].

[317] Astrid Eichhorn and Aaron Held. "Top mass from asymptotic safety". In: *Phys. Lett. B* 777 (2018), pp. 217–221. DOI: 10.1016/j.physletb.2017.12.040. arXiv: 1707.01107 [hep-th].

[318] Reinhard Alkofer, Astrid Eichhorn, Aaron Held, Carlos M. Nieto, Roberto Percacci, and Markus Schröfl. "Quark masses and mixings in minimally parameterized UV completions of the Standard Model". In: *Annals Phys.* 421 (2020), p. 168282. DOI: 10.1016/j.aop.2020.168282. arXiv: 2003.08401 [hep-ph].

[319] Astrid Eichhorn, Yuta Hamada, Johannes Lumma, and Masatoshi Yamada. "Quantum gravity fluctuations flatten the Planck-scale Higgs potential". In: *Phys. Rev. D* 97.8 (2018), p. 086004. DOI: 10.1103/PhysRevD.97.086004. arXiv: 1712.00319 [hep-th].

[320] Mikhail Shaposhnikov and Christof Wetterich. "Asymptotic safety of gravity and the Higgs boson mass". In: *Phys. Lett. B* 683 (2010), pp. 196–200. DOI: 10.1016/j.physletb.2009.12.022. arXiv: 0912.0208 [hep-th].

[321] Gaurav Narain and Christoph Rahmede. "Renormalization Group Flow in Scalar-Tensor Theories. II". In: *Class. Quant. Grav.* 27 (2010), p. 075002. DOI: 10.1088/0264-9381/27/7/075002. arXiv: 0911.0394 [hep-th].

[322] Jan M. Pawlowski, Manuel Reichert, Christof Wetterich, and Masatoshi Yamada. "Higgs scalar potential in asymptotically safe quantum gravity". In: *Phys. Rev. D* 99.8 (2019), p. 086010. DOI: 10.1103/PhysRevD.99.086010. arXiv: 1811.11706 [hep-th].

[323] F. Zwicky. "Die Rotverschiebung von extragalaktischen Nebeln". In: *Helv. Phys. Acta* 6 (1933), pp. 110–127. DOI: 10.1007/s10714-008-0707-4.

[324] Vera C. Rubin, W. Kent Ford Jr., and Norbert Thonnard. "Extended rotation curves of high-luminosity spiral galaxies. IV. Systematic dynamical properties, Sa through Sc". In: *Astrophys. J. Lett.* 225 (1978), pp. L107–L111. DOI: 10.1086/182804.

[325] N. Aghanim et al. "Planck 2018 results. VI. Cosmological parameters". In: *Astron. Astrophys.* 641 (2020), A6. DOI: 10.1051/0004-6361/201833910. arXiv: 1807.06209 [astro-ph.CO].

[326] P. A. Zyla et al. "Review of Particle Physics". In: *PTEP* 2020.8 (2020), p. 083C01. DOI: 10.1093/ptep/ptaa104.

[327] Teresa Marrodán Undagoitia and Ludwig Rauch. "Dark matter direct-detection experiments". In: *J. Phys. G* 43.1 (2016), p. 013001. DOI: 10.1088/0954-3899/43/1/013001. arXiv: 1509.08767 [physics.ins-det].

[328] Manuel Reichert and Juri Smirnov. "Dark Matter meets Quantum Gravity". In: *Phys. Rev. D* 101.6 (2020), p. 063015. DOI: 10.1103/PhysRevD.101.063015. arXiv: 1911.00012 [hep-ph].

[329] Yu Hamada, Koji Tsumura, and Masatoshi Yamada. "Scalegenesis and fermionic dark matters in the flatland scenario". In: *Eur. Phys. J. C* 80.5 (2020), p. 368. DOI: 10.1140/epjc/s10052-020-7929-3. arXiv: 2002.03666 [hep-ph].

[330] Astrid Eichhorn, Martin Pauly, and Shouryya Ray. "Towards a Higgs mass determination in asymptotically safe gravity with a dark portal". In: (July 2021). arXiv: 2107.07949 [hep-ph].

[331] Max R. Niedermaier. "Gravitational Fixed Points from Perturbation Theory". In: *Phys. Rev. Lett.* 103 (2009), p. 101303. DOI: 10.1103/PhysRevLett.103.101303.

[332] M. Niedermaier. "Gravitational fixed points and asymptotic safety from perturbation theory". In: *Nucl. Phys. B* 833 (2010), pp. 226–270. DOI: 10.1016/j.nuclphysb.2010.01.016.

[333] Astrid Eichhorn. "Quantum-gravity-induced matter self-interactions in the asymptotic-safety scenario". In: *Phys. Rev. D* 86 (2012), p. 105021. DOI: 10.1103/PhysRevD.86.105021. arXiv: 1204.0965 [gr-qc].

[334] Gustavo P. de Brito, Astrid Eichhorn, and Rafael Robson Lino dos Santos. "The weak-gravity bound and the need for spin in asymptotically safe matter-gravity models". In: (July 2021). arXiv: 2107.03839 [gr-qc].

[335] Passant Ali, Astrid Eichhorn, Martin Pauly, and Michael M. Scherer. "Constraints on discrete global symmetries in quantum gravity". In: *JHEP* 05 (2021), p. 036. DOI: 10.1007/JHEP05(2021)036. arXiv: 2012.07868 [gr-qc].

[336] Astrid Eichhorn and Holger Gies. "Light fermions in quantum gravity". In: *New J. Phys.* 13 (2011), p. 125012. DOI: 10.1088/1367-2630/13/12/125012. arXiv: 1104.5366 [hep-th].

[337] Roberto Percacci and Gian Paolo Vacca. "Asymptotic Safety, Emergence and Minimal Length". In: *Class. Quant. Grav.* 27 (2010), p. 245026. DOI: 10.1088/0264-9381/27/24/245026. arXiv: 1008.3621 [hep-th].

[338] Aaron Held. "Effective asymptotic safety and its predictive power: Gauge-Yukawa theories". In: *Front. in Phys.* 8 (2020), p. 341. DOI: 10.3389/fphy.2020.00341. arXiv: 2003.13642 [hep-th].

[339] Cumrun Vafa. "The String landscape and the swampland". In: (Sept. 2005). arXiv: hep-th/0509212.

[340] Ivano Basile and Alessia Platania. "Asymptotic Safety: Swampland or Wonderland?" In: (July 2021). arXiv: 2107.06897 [hep-th].

[341] Eran Palti. "The Swampland: Introduction and Review". In: *Fortsch. Phys.* 67.6 (2019), p. 1900037. DOI: 10.1002/prop.201900037. arXiv: 1903.06239 [hep-th].

[342] Nima Arkani-Hamed, Lubos Motl, Alberto Nicolis, and Cumrun Vafa. "The String landscape, black holes and gravity as the weakest force". In: *JHEP* 06 (2007), p. 060. DOI: 10.1088/1126-6708/2007/06/060. arXiv: hep-th/0601001.

[343] Leonard Susskind. "Trouble for remnants". In: (Jan. 1995). arXiv: hep-th/9501106.

[344] Renata Kallosh, Andrei D. Linde, Dmitri A. Linde, and Leonard Susskind. "Gravity and global symmetries". In: *Phys. Rev. D* 52 (1995), pp. 912–935. DOI: 10.1103/PhysRevD.52.912. arXiv: hep-th/9502069.

[345] Tom Banks, Matt Johnson, and Assaf Shomer. "A Note on Gauge Theories Coupled to Gravity". In: *JHEP* 09 (2006), p. 049. DOI: 10.1088/1126-6708/2006/09/049. arXiv: hep-th/0606277.

[346] Daniel Harlow and Hirosi Ooguri. "Symmetries in quantum field theory and quantum gravity". In: *Commun. Math. Phys.* 383.3 (2021), pp. 1669–1804. DOI: 10.1007/s00220-021-04040-y. arXiv: 1810.05338 [hep-th].

[347] David J. Toms. "Cosmological constant and quantum gravitational corrections to the running fine structure constant". In: *Phys. Rev. Lett.* 101 (2008), p. 131301. DOI: 10.1103/PhysRevLett.101.131301. arXiv: 0809.3897 [hep-th].

[348] John Ellis and Nick E. Mavromatos. "On the Interpretation of Gravitational Corrections to Gauge Couplings". In: *Phys. Lett. B* 711 (2012), pp. 139–142. DOI: 10.1016/j.physletb.2012.04.005. arXiv: 1012.4353 [hep-th].

[349] Holger Gies and Riccardo Martini. "Curvature bound from gravitational catalysis". In: *Phys. Rev. D* 97.8 (2018), p. 085017. DOI: 10.1103/PhysRevD.97.085017. arXiv: 1802.02865 [hep-th].

[350] C. D. Hoyle, D. J. Kapner, Blayne R. Heckel, E. G. Adelberger, J. H. Gundlach, U. Schmidt, and H. E. Swanson. "Sub-millimeter tests of the gravitational inverse-square law". In: *Phys. Rev. D* 70 (2004), p. 042004. DOI: 10.1103/PhysRevD.70.042004. arXiv: hep-ph/0405262.

[351] D. J. Kapner, T. S. Cook, E. G. Adelberger, J. H. Gundlach, Blayne R. Heckel, C. D. Hoyle, and H. E. Swanson. "Tests of the gravitational inverse-square law below the dark-energy length scale". In: *Phys. Rev. Lett.* 98 (2007), p. 021101. DOI: 10.1103/PhysRevLett.98.021101. arXiv: hep-ph/0611184.

[352] E. G. Adelberger, J. H. Gundlach, B. R. Heckel, S. Hoedl, and S. Schlamminger. "Torsion balance experiments: A low-energy frontier of particle physics". In: *Prog. Part. Nucl. Phys.* 62 (2009), pp. 102–134. DOI: 10.1016/j.ppnp.2008.08.002.

[353] Jiro Murata and Saki Tanaka. "A review of short-range gravity experiments in the LHC era". In: *Class. Quant. Grav.* 32.3 (2015), p. 033001. DOI: 10.1088/0264-9381/32/3/033001. arXiv: 1408.3588 [hep-ex].

[354] Morad Aaboud et al. "Search for TeV-scale gravity signatures in high-mass final states with leptons and jets with the ATLAS detector at $\sqrt{s} = 13$ TeV". In: *Phys. Lett. B* 760 (2016), pp. 520–537. DOI: 10.1016/j.physletb.2016.07.030. arXiv: 1606.02265 [hep-ex].

[355] Albert M Sirunyan et al. "Search for contact interactions and large extra dimensions in the dilepton mass spectra from proton-proton collisions at $\sqrt{s} = 13$ TeV". In: *JHEP* 04 (2019), p. 114. DOI: 10.1007/JHEP04(2019)114. arXiv: 1812.10443 [hep-ex].

[356] Stefano Bertolini, Luca Di Luzio, and Michal Malinsky. "Intermediate mass scales in the non-supersymmetric SO(10) grand unification: A Reappraisal". In: *Phys. Rev. D* 80 (2009), p. 015013. DOI: 10.1103/PhysRevD.80.015013. arXiv: 0903.4049 [hep-ph].

[357] Tom Banks and Lance J. Dixon. "Constraints on String Vacua with Space-Time Supersymmetry". In: *Nucl. Phys. B* 307 (1988), pp. 93–108. DOI: 10.1016/0550-3213(88)90523-8.

[358] Marc Kamionkowski and John March-Russell. "Planck scale physics and the Peccei-Quinn mechanism". In: *Phys. Lett. B* 282 (1992), pp. 137–141. DOI: 10.1016/0370-2693(92)90492-M. arXiv: hep-th/9202003.

[359] Tom Banks and Nathan Seiberg. "Symmetries and Strings in Field Theory and Gravity". In: *Phys. Rev. D* 83 (2011), p. 084019. DOI: 10.1103/PhysRevD.83.084019. arXiv: 1011.5120 [hep-th].

[360] Daniel Harlow and Hirosi Ooguri. "Constraints on Symmetries from Holography". In: *Phys. Rev. Lett.* 122.19 (2019), p. 191601. DOI: 10.1103/PhysRevLett.122.191601. arXiv: 1810.05337 [hep-th].

[361] Holger Bech Nielsen and M. Ninomiya. "Absence of Neutrinos on a Lattice. 1. Proof by Homotopy Theory". In: *Nucl. Phys. B* 185 (1981). Ed. by J. Julve and M. Ramón-Medrano. [Erratum: Nucl.Phys.B 195, 541 (1982)], p. 20. DOI: 10.1016/0550-3213(82)90011-6.

[362] Holger Bech Nielsen and M. Ninomiya. "Absence of Neutrinos on a Lattice. 2. Intuitive Topological Proof". In: *Nucl. Phys. B* 193 (1981), pp. 173–194. DOI: 10.1016/0550-3213(81)90524-1.

[363] Merced Montesinos-Velasquez, Hugo A. Morales-Tecotl, and Tonatiuh Matos. "Fermion mass gap in the loop representation of quantum gravity". In: *Class. Quant. Grav.* 14 (1997), pp. L135–L142. DOI: 10.1088/0264-9381/14/7/002. arXiv: gr-qc/9704066.

[364] Jacob Barnett and Lee Smolin. "Fermion Doubling in Loop Quantum Gravity". In: (July 2015). arXiv: 1507.01232 [gr-qc].

[365] Rodolfo Gambini and Jorge Pullin. "No fermion doubling in quantum geometry". In: *Phys. Lett. B* 749 (2015), pp. 374–375. DOI: 10.1016/j.physletb.2015.08.022. arXiv: 1506.08794 [gr-qc].

[366] Holger Gies and Christof Wetterich. "Renormalization flow of bound states". In: *Phys. Rev. D* 65 (2002), p. 065001. DOI: 10.1103/PhysRevD.65.065001. arXiv: hep-th/0107221.

[367] Jens Braun and Holger Gies. "Running coupling at finite temperature and chiral symmetry restoration in QCD". In: *Phys. Lett. B* 645 (2007), pp. 53–58. DOI: 10.1016/j.physletb.2006.11.059. arXiv: hep-ph/0512085.

[368] Jens Braun and Holger Gies. "Chiral phase boundary of QCD at finite temperature". In: *JHEP* 06 (2006), p. 024. DOI: 10.1088/1126-6708/2006/06/024. arXiv: hep-ph/0602226.

[369] Jens Braun. "Functional renormalization group methods in quantum chromodynamics". Other thesis. Dec. 2006.

[370] Jens Braun. "The QCD Phase Boundary from Quark-Gluon Dynamics". In: *Eur. Phys. J. C* 64 (2009), pp. 459–482. DOI: 10.1140/epjc/s10052-009-1136-6. arXiv: 0810.1727 [hep-ph].

[371] Lisa M. Haas, Jens Braun, and Jan M. Pawlowski. "On the QCD phase diagram at finite chemical potential". In: *AIP Conf. Proc.* 1343 (2011). Ed. by F. J. Llanes-Estrada and J. R. Peláez, pp. 459–461. DOI: 10.1063/1.3575061. arXiv: 1012.4735 [hep-ph].

[372] Jens Braun, Bertram Klein, and Piotr Piasecki. "On the scaling behavior of the chiral phase transition in QCD in finite and infinite volume". In: *Eur. Phys. J. C* 71 (2011), p. 1576. DOI: 10.1140/epjc/s10052-011-1576-7. arXiv: 1008.2155 [hep-ph].

[373] Jens Braun. "Fermion Interactions and Universal Behavior in Strongly Interacting Theories". In: *J. Phys. G* 39 (2012), p. 033001. DOI: 10.1088/0954-3899/39/3/033001. arXiv: 1108.4449 [hep-ph].

[374] Yu Hamada, Jan M. Pawlowski, and Masatoshi Yamada. "Gravitational instantons and anomalous chiral symmetry breaking". In: *Phys. Rev. D* 103.10 (2021), p. 106016. DOI: 10.1103/PhysRevD.103.106016. arXiv: 2009.08728 [hep-th].

[375] I. L. Buchbinder and E. N. Kirillova. "Phase transitions induced by curvature in the Gross-Neveu model". In: *Sov. Phys. J.* 32 (1989), pp. 446–450. DOI: 10.1007/BF00898628.

[376] I. L. Buchbinder and E. N. Kirillova. "Gross-Neveu Model in Curved Space-time: The Effective Potential and Curvature Induced Phase Transition". In: *Int. J. Mod. Phys. A* 4 (1989), pp. 143–149. DOI: 10.1142/S0217751X89000054.

[377] T. Inagaki, T. Muta, and S. D. Odintsov. "Nambu-Jona-Lasinio model in curved space-time". In: *Mod. Phys. Lett. A* 8 (1993), pp. 2117–2124. DOI: 10.1142/S0217732393001835. arXiv: hep-th/9306023.

[378] I. Sachs and A. Wipf. "Temperature and curvature dependence of the chiral symmetry breaking in 2-D gauge theories". In: *Phys. Lett. B* 326 (1994), pp. 105–110. DOI: 10.1016/0370-2693(94)91200-9. arXiv: hep-th/9310085.

[379] Holger Gies and Stefan Lippoldt. "Renormalization flow towards gravitational catalysis in the 3d Gross-Neveu model". In: *Phys. Rev. D* 87 (2013), p. 104026. DOI: 10.1103/PhysRevD.87.104026. arXiv: 1303.4253 [hep-th].

[380] Holger Gies and Abdol Sabor Salek. "Curvature bound from gravitational catalysis in thermal backgrounds". In: *Phys. Rev. D* 103.12 (2021), p. 125027. DOI: 10.1103/PhysRevD.103.125027. arXiv: 2103.05542 [hep-th].

[381] V. A. Miransky. "Dynamics of Spontaneous Chiral Symmetry Breaking and Continuum Limit in Quantum Electrodynamics". In: *Nuovo Cim. A* 90 (1985), pp. 149–170. DOI: 10.1007/BF02724229.

[382] Craig D. Roberts and Anthony G. Williams. "Dyson-Schwinger equations and their application to hadronic physics". In: *Prog. Part. Nucl. Phys.* 33 (1994), pp. 477–575. DOI: 10.1016/0146-6410(94)90049-3. arXiv: hep-ph/9403224.

[383] Ken-Ichi Aoki, Kei-ichi Morikawa, Jun-Ichi Sumi, Haruhiko Terao, and Masashi Tomoyose. "Non-perturbative renormalization group analysis of the chiral critical behaviors in QED". In: *Prog. Theor. Phys.* 97 (1997), pp. 479–490. DOI: 10.1143/PTP.97.479. arXiv: hep-ph/9612459.

[384] Reinhard Alkofer and Lorenz von Smekal. "The Infrared behavior of QCD Green's functions: Confinement dynamical symmetry breaking, and hadrons as relativistic bound states". In: *Phys. Rept.* 353 (2001), p. 281. DOI: 10.1016/S0370-1573(01)00010-2. arXiv: hep-ph/0007355.

[385] S. Kim, John B. Kogut, and Maria-Paola Lombardo. "On the triviality of textbook quantum electrodynamics". In: *Phys. Lett. B* 502 (2001), pp. 345–349. DOI: 10.1016/S0370-2693(01)00201-5. arXiv: hep-lat/0009029.

[386] Holger Gies and Christof Wetterich. "Universality of spontaneous chiral symmetry breaking in gauge theories". In: *Phys. Rev. D* 69 (2004), p. 025001. DOI: 10.1103/PhysRevD.69.025001. arXiv: hep-th/0209183.

[387] Holger Gies, Joerg Jaeckel, and Christof Wetterich. "Towards a renormalizable standard model without fundamental Higgs scalar". In: *Phys. Rev. D* 69 (2004), p. 105008. DOI: 10.1103/PhysRevD.69.105008. arXiv: hep-ph/0312034.

[388] Jens Braun and Alexander Janot. "Dynamical Locking of the Chiral and the Deconfinement Phase Transition in QCD". In: *Phys. Rev. D* 84 (2011), p. 114022. DOI: 10.1103/PhysRevD.84.114022. arXiv: 1102.4841 [hep-ph].

[389] S. P. Klevansky. "The Nambu-Jona-Lasinio model of quantum chromodynamics". In: *Rev. Mod. Phys.* 64 (1992), pp. 649–708. DOI: 10.1103/RevModPhys.64.649.

[390] Michael Buballa. "NJL model analysis of quark matter at large density". In: *Phys. Rept.* 407 (2005), pp. 205–376. DOI: 10.1016/j.physrep.2004.11.004. arXiv: hep-ph/0402234.

[391] U. Ellwanger and C. Wetterich. "Evolution equations for the quark - meson transition". In: *Nucl. Phys. B* 423 (1994), pp. 137–170. DOI: 10.1016/0550-3213(94)90568-1. arXiv: hep-ph/9402221.

[392] Joerg Jaeckel. "Effective actions for strongly interacting fermionic systems". Other thesis. Sept. 2003. arXiv: hep-ph/0309090.

[393] Holger Gies and Joerg Jaeckel. "Chiral phase structure of QCD with many flavors". In: *Eur. Phys. J. C* 46 (2006), pp. 433–438. DOI: 10.1140/epjc/s2006-02475-0. arXiv: hep-ph/0507171.

[394] Jens Braun, Holger Gies, Lukas Janssen, and Dietrich Roscher. "Phase structure of many-flavor QED_3". In: *Phys. Rev. D* 90.3 (2014), p. 036002. DOI: 10.1103/PhysRevD.90.036002. arXiv: 1404.1362 [hep-ph].

[395] Rodolfo Gambini and Jorge Pullin. "Nonstandard optics from quantum space-time". In: *Phys. Rev. D* 59 (1999), p. 124021. DOI: 10.1103/PhysRevD.59.124021. arXiv: gr-qc/9809038.

[396] Ted Jacobson and David Mattingly. "Gravity with a dynamical preferred frame". In: *Phys. Rev. D* 64 (2001), p. 024028. DOI: 10.1103/PhysRevD.64.024028. arXiv: gr-qc/0007031.

[397] Sean M. Carroll, Jeffrey A. Harvey, V. Alan Kostelecky, Charles D. Lane, and Takemi Okamoto. "Noncommutative field theory and Lorentz violation". In: *Phys. Rev. Lett.* 87 (2001), p. 141601. DOI: 10.1103/PhysRevLett.87.141601. arXiv: hep-th/0105082.

[398] Joao Magueijo and Lee Smolin. "Lorentz invariance with an invariant energy scale". In: *Phys. Rev. Lett.* 88 (2002), p. 190403. DOI: 10.1103/PhysRevLett.88.190403. arXiv: hep-th/0112090.

[399] Joao Magueijo and Lee Smolin. "Generalized Lorentz invariance with an invariant energy scale". In: *Phys. Rev. D* 67 (2003), p. 044017. DOI: 10.1103/PhysRevD.67.044017. arXiv: gr-qc/0207085.

[400] Stefan Groot Nibbelink and Maxim Pospelov. "Lorentz violation in supersymmetric field theories". In: *Phys. Rev. Lett.* 94 (2005), p. 081601. DOI: 10.1103/PhysRevLett.94.081601. arXiv: hep-ph/0404271.

[401] Petr Horava. "Quantum Gravity at a Lifshitz Point". In: *Phys. Rev. D* 79 (2009), p. 084008. DOI: 10.1103/PhysRevD.79.084008. arXiv: 0901.3775 [hep-th].

[402] Stefano Liberati and Luca Maccione. "Lorentz Violation: Motivation and new constraints". In: *Ann. Rev. Nucl. Part. Sci.* 59 (2009), pp. 245–267. DOI: 10.1146/annurev.nucl.010909.083640. arXiv: 0906.0681 [astro-ph.HE].

[403] Ivan Kharuk and S. M. Sibiryakov. "Emergent Lorentz invariance with chiral fermions". In: *Theor. Math. Phys.* 189.3 (2016), pp. 1755–1774. DOI: 10.1134/S0040577916120084. arXiv: 1505.04130 [hep-th].

[404] G. Amelino-Camelia, John R. Ellis, N. E. Mavromatos, Dimitri V. Nanopoulos, and Subir Sarkar. "Tests of quantum gravity from observations of gamma-ray bursts". In: *Nature* 393 (1998), pp. 763–765. DOI: 10.1038/31647. arXiv: astro-ph/9712103.

[405] Sabine Hossenfelder. "Minimal Length Scale Scenarios for Quantum Gravity". In: *Living Rev. Rel.* 16 (2013), p. 2. DOI: 10.12942/lrr-2013-2. arXiv: 1203.6191 [gr-qc].

[406] Stefano Liberati. "Tests of Lorentz invariance: a 2013 update". In: *Class. Quant. Grav.* 30 (2013), p. 133001. DOI: 10.1088/0264-9381/30/13/133001. arXiv: 1304.5795 [gr-qc].

[407] D. Sudarsky and J. A. Caicedo. "On the proposals of Lorentz invariance violation resulting from a quantum-gravitational granularity of space-time". In: *J. Phys. Conf. Ser.* 24 (2005). Ed. by Miguel Alcubierre, Jorge L. Cervantes-Cota, and Merced Montesinos, pp. 69–76. DOI: 10.1088/1742-6596/24/1/009.

[408] Andrew G. Cohen and Sheldon L. Glashow. "Very special relativity". In: *Phys. Rev. Lett.* 97 (2006), p. 021601. DOI: 10.1103/PhysRevLett.97.021601. arXiv: hep-ph/0601236.

[409] Quentin G. Bailey and V. Alan Kostelecky. "Signals for Lorentz violation in post-Newtonian gravity". In: *Phys. Rev. D* 74 (2006), p. 045001. DOI: 10.1103/PhysRevD.74.045001. arXiv: gr-qc/0603030.

[410] Alex E. Bernardini and Roldao da Rocha. "Lorentz-violating dilatations in the momentum space and some extensions on non-linear actions of Lorentz algebra-preserving systems". In: *Phys. Rev. D* 75 (2007), p. 065014. DOI: 10.1103/PhysRevD.75.065014. arXiv: hep-th/0701094.

[411] Lotty Ackerman, Sean M. Carroll, and Mark B. Wise. "Imprints of a Primordial Preferred Direction on the Microwave Background". In: *Phys. Rev. D* 75 (2007). [Erratum: Phys.Rev.D 80, 069901 (2009)], p. 083502. DOI: 10.1103/PhysRevD.75.083502. arXiv: astro-ph/0701357.

[412] Jay D. Tasson. "What Do We Know About Lorentz Invariance?" In: *Rept. Prog. Phys.* 77 (2014), p. 062901. DOI: 10.1088/0034-4885/77/6/062901. arXiv: 1403.7785 [hep-ph].

[413] Ralf Lehnert. "Constraining Lorentz Violation in Electroweak Physics". In: *J. Phys. Conf. Ser.* 952.1 (2018), p. 012008. DOI: 10.1088/1742-6596/952/1/012008.

[414] Christian Sanner, Nils Huntemann, Richard Lange, Christian Tamm, Ekkehard Peik, Marianna S. Safronova, and Sergey G. Porsev. "Optical clock comparison for Lorentz symmetry testing". In: *Nature* 567.7747 (2019), pp. 204–208. DOI: 10.1038/s41586-019-0972-2. arXiv: 1809.10742 [physics.atom-ph].

[415] Maxim Goryachev, Zeyu Kuang, Eugene N. Ivanov, Philipp Haslinger, Holger Muller, and Michael E. Tobar. "Next Generation of Phonon Tests of Lorentz Invariance using Quartz BAW Resonators". In: (Apr. 2018). DOI: 10.1109/TUFFC.2018.2824845. arXiv: 1804.02615 [physics.ins-det].

[416] Eli Megidish, Joseph Broz, Nicole Greene, and Hartmut Häffner. "Improved Test of Local Lorentz Invariance from a Deterministic Preparation of Entangled States". In: *Phys. Rev. Lett.* 122.12 (2019), p. 123605. DOI: 10.1103/PhysRevLett.122.123605. arXiv: 1809.09807 [quant-ph].

[417] Jarod George Kelly and Sanjeev S. Seahra. "Velocity-dependent deformations of the energy spectrum of a quantum cavity from Lorentz symmetry violations". In: *Phys. Rev. D* 100.6 (2019), p. 064002. DOI: 10.1103/PhysRevD.100.064002. arXiv: 1812.06047 [gr-qc].

[418] Yunhua Ding. "Lorentz and CPT Tests using Penning Traps". In: *Symmetry* 11.10 (2019), p. 1220. DOI: 10.3390/sym11101220. arXiv: 1910.00456 [hep-ph].

[419] V. Alan Kostelecky and Neil Russell. "Data Tables for Lorentz and CPT Violation". In: (Jan. 2008). arXiv: 0801.0287 [hep-ph].

[420] B. P. Abbott et al. "GW170817: Observation of Gravitational Waves from a Binary Neutron Star Inspiral". In: *Phys. Rev. Lett.* 119.16 (2017), p. 161101. DOI: 10.1103/PhysRevLett.119.161101. arXiv: 1710.05832 [gr-qc].

[421] B. P. Abbott et al. "Multi-messenger Observations of a Binary Neutron Star Merger". In: *Astrophys. J. Lett.* 848.2 (2017), p. L12. DOI: 10.3847/2041-8213/aa91c9. arXiv: 1710.05833 [astro-ph.HE].

[422] B. P. Abbott et al. "Gravitational Waves and Gamma-rays from a Binary Neutron Star Merger: GW170817 and GRB 170817A". In: *Astrophys. J. Lett.* 848.2 (2017), p. L13. DOI: 10.3847/2041-8213/aa920c. arXiv: 1710.05834 [astro-ph.HE].

[423] B. P. Abbott et al. "Tests of General Relativity with GW170817". In: *Phys. Rev. Lett.* 123.1 (2019), p. 011102. DOI: 10.1103/PhysRevLett.123.011102. arXiv: 1811.00364 [gr-qc].

[424] A. Emir Gümrükçüoğlu, Mehdi Saravani, and Thomas P. Sotiriou. "Hořava gravity after GW170817". In: *Phys. Rev. D* 97.2 (2018), p. 024032. DOI: 10.1103/PhysRevD.97.024032. arXiv: 1711.08845 [gr-qc].

[425] Matthew Mewes. "Signals for Lorentz violation in gravitational waves". In: *Phys. Rev. D* 99.10 (2019), p. 104062. DOI: 10.1103/PhysRevD.99.104062. arXiv: 1905.00409 [gr-qc].

[426] Nicolas Yunes, Kent Yagi, and Frans Pretorius. "Theoretical Physics Implications of the Binary Black-Hole Mergers GW150914 and GW151226". In: *Phys. Rev. D* 94.8 (2016), p. 084002. DOI: 10.1103/PhysRevD.94.084002. arXiv: 1603.08955 [gr-qc].

[427] Oscar Ramos and Enrico Barausse. "Constraints on Hořava gravity from binary black hole observations". In: *Phys. Rev. D* 99.2 (2019), p. 024034. DOI: 10.1103/PhysRevD.99.024034. arXiv: 1811.07786 [gr-qc].

[428] V. Alan Kostelecky. "Gravity, Lorentz violation, and the standard model". In: *Phys. Rev. D* 69 (2004), p. 105009. DOI: 10.1103/PhysRevD.69.105009. arXiv: hep-th/0312310.

[429] John Collins, Alejandro Perez, Daniel Sudarsky, Luis Urrutia, and Hector Vucetich. "Lorentz invariance and quantum gravity: an additional fine-tuning problem?" In: *Phys. Rev. Lett.* 93 (2004), p. 191301. DOI: 10.1103/PhysRevLett.93.191301. arXiv: gr-qc/0403053.

[430] Alan V. Kostelecky and Jay D. Tasson. "Matter-gravity couplings and Lorentz violation". In: *Phys. Rev. D* 83 (2011), p. 016013. DOI: 10.1103/PhysRevD.83.016013. arXiv: 1006.4106 [gr-qc].

[431] Maxim Pospelov and Yanwen Shang. "On Lorentz violation in Horava-Lifshitz type theories". In: *Phys. Rev. D* 85 (2012), p. 105001. DOI: 10.1103/PhysRevD.85.105001. arXiv: 1010.5249 [hep-th].

[432] Stefano Liberati, Luca Maccione, and Thomas P. Sotiriou. "Scale hierarchy in Horava-Lifshitz gravity: a strong constraint from synchrotron radiation in the Crab nebula". In: *Phys. Rev. Lett.* 109 (2012), p. 151602. DOI: 10.1103/PhysRevLett.109.151602. arXiv: 1207.0670 [gr-qc].

[433] Alessio Belenchia, Andrea Gambassi, and Stefano Liberati. "Lorentz violation naturalness revisited". In: *JHEP* 06 (2016), p. 049. DOI: 10.1007/JHEP06(2016)049. arXiv: 1601.06700 [hep-th].

[434] Robert Bluhm. "The SME with gravity and explicit diffeomorphism breaking". In: *8th Meeting on CPT and Lorentz Symmetry*. Nov. 2019. DOI: 10.1142/9789811213984_0031. arXiv: 1911.02517 [gr-qc].

[435] Don Colladay and V. Alan Kostelecky. "Lorentz violating extension of the standard model". In: *Phys. Rev. D* 58 (1998), p. 116002. DOI: 10.1103/PhysRevD.58.116002. arXiv: hep-ph/9809521.

[436] V. Alan Kostelecky and Matthew Mewes. "Signals for Lorentz violation in electrodynamics". In: *Phys. Rev. D* 66 (2002), p. 056005. DOI: 10.1103/PhysRevD.66.056005. arXiv: hep-ph/0205211.

[437] Adriano Contillo, Stefan Rechenberger, and Frank Saueressig. "Renormalization group flow of Hořava-Lifshitz gravity at low energies". In: *JHEP* 12 (2013), p. 017. DOI: 10.1007/JHEP12(2013)017. arXiv: 1309.7273 [hep-th].

[438] Giulio D'Odorico, Frank Saueressig, and Marrit Schutten. "Asymptotic Freedom in Hořava-Lifshitz Gravity". In: *Phys. Rev. Lett.* 113.17 (2014), p. 171101. DOI: 10.1103/PhysRevLett.113.171101. arXiv: 1406.4366 [gr-qc].

[439] Giulio D'Odorico, Jan-Willem Goossens, and Frank Saueressig. "Covariant computation of effective actions in Hořava-Lifshitz gravity". In: *JHEP* 10 (2015), p. 126. DOI: 10.1007/JHEP10(2015)126. arXiv: 1508.00590 [hep-th].

[440] Andrei O. Barvinsky, Diego Blas, Mario Herrero-Valea, Sergey M. Sibiryakov, and Christian F. Steinwachs. "Renormalization of Hořava gravity". In: *Phys. Rev. D* 93.6 (2016), p. 064022. DOI: 10.1103/PhysRevD.93.064022. arXiv: 1512.02250 [hep-th].

[441] Andrei O. Barvinsky, Diego Blas, Mario Herrero-Valea, Sergey M. Sibiryakov, and Christian F. Steinwachs. "Hořava Gravity is Asymptotically Free in 2 + 1 Dimensions". In: *Phys. Rev. Lett.* 119.21 (2017), p. 211301. DOI: 10.1103/PhysRevLett.119.211301. arXiv: 1706.06809 [hep-th].

[442] Andrei O. Barvinsky, Mario Herrero-Valea, and Sergey M. Sibiryakov. "Towards the renormalization group flow of Horava gravity in $(3 + 1)$ dimensions". In: *Phys. Rev. D* 100.2 (2019), p. 026012. DOI: 10.1103/PhysRevD.100.026012. arXiv: 1905.03798 [hep-th].

[443] V. Alan Kostelecky and Matthew Mewes. "Cosmological constraints on Lorentz violation in electrodynamics". In: *Phys. Rev. Lett.* 87 (2001), p. 251304. DOI: 10.1103/PhysRevLett.87.251304. arXiv: hep-ph/0111026.

[444] V. Alan Kostelecky and Matthew Mewes. "Sensitive polarimetric search for relativity violations in gamma-ray bursts". In: *Phys. Rev. Lett.* 97 (2006), p. 140401. DOI: 10.1103/PhysRevLett.97.140401. arXiv: hep-ph/0607084.

[445] Holger Muller, Sheng-wey Chiow, Sven Herrmann, Steven Chu, and Keng-Yeow Chung. "Atom Interferometry tests of the isotropy of post-Newtonian gravity". In: *Phys. Rev. Lett.* 100 (2008), p. 031101. DOI: 10.1103/PhysRevLett.100.031101. arXiv: 0710.3768 [gr-qc].

[446] Peter Wolf, Sebastien Bize, Andre Clairon, Giorgio Santarelli, Michael E. Tobar, and Andre N. Luiten. "Improved test of Lorentz invariance in electrodynamics". In: *Phys. Rev. D* 70 (2004), p. 051902. DOI: 10.1103/PhysRevD.70.051902. arXiv: hep-ph/0407232.

[447] Moritz Nagel, Stephen R. Parker, Evgeny V. Kovalchuk, Paul L. Stanwix, John G. Hartnett, Eugene N. Ivanov, Achim Peters, and Michael E. Tobar. "Direct Terrestrial Test of Lorentz Symmetry in Electrodynamics to 10^{-18}". In: *Nature Commun.* 6 (2015), p. 8174. DOI: 10.1038/ncomms9174. arXiv: 1412.6954 [hep-ph].

[448] V. Alan Kostelecký, Adrian C. Melissinos, and Matthew Mewes. "Searching for photon-sector Lorentz violation using gravitational-wave detectors". In: *Phys. Lett. B* 761 (2016), pp. 1–7. DOI: 10.1016/j.physletb.2016.08.001. arXiv: 1608.02592 [gr-qc].

[449] Robert Bluhm, Hannah Bossi, and Yuewei Wen. "Gravity with explicit spacetime symmetry breaking and the Standard-Model Extension". In: *Phys. Rev. D* 100.8 (2019), p. 084022. DOI: 10.1103/PhysRevD.100.084022. arXiv: 1907.13209 [gr-qc].

[450] Ted Jacobson, Stefano Liberati, and David Mattingly. "TeV astrophysics constraints on Planck scale Lorentz violation". In: *Phys. Rev. D* 66 (2002), p. 081302. DOI: 10.1103/PhysRevD.66.081302. arXiv: hep-ph/0112207.

[451] T. Jacobson, Stefano Liberati, and D. Mattingly. "A Strong astrophysical constraint on the violation of special relativity by quantum gravity". In: *Nature* 424 (2003), pp. 1019–1021. DOI: 10.1038/nature01882. arXiv: astro-ph/0212190.

[452] J. Bolmont, A. Jacholkowska, J. L. Atteia, F. Piron, and G. Pizzichini. "Study of time lags in HETE-2 Gamma-Ray Bursts with redshift: search for astrophysical effects and Quantum Gravity signature". In: *Astrophys. J.* 676 (2008), pp. 532–544. DOI: 10.1086/527524. arXiv: astro-ph/0603725.

[453] M. Ackermann et al. "A limit on the variation of the speed of light arising from quantum gravity effects". In: *Nature* 462 (2009), pp. 331–334. DOI: 10.1038/nature08574. arXiv: 0908.1832 [astro-ph.HE].

[454] V. Vasileiou, A. Jacholkowska, F. Piron, J. Bolmont, C. Couturier, J. Granot, F. W. Stecker, J. Cohen-Tanugi, and F. Longo. "Constraints on Lorentz Invariance Violation from Fermi-Large Area Telescope Observations of Gamma-Ray Bursts". In: *Phys. Rev. D* 87.12 (2013), p. 122001. DOI: 10.1103/PhysRevD.87.122001. arXiv: 1305.3463 [astro-ph.HE].

[455] John Ellis, Rostislav Konoplich, Nikolaos E. Mavromatos, Linh Nguyen, Alexander S. Sakharov, and Edward K. Sarkisyan-Grinbaum. "Robust Constraint on Lorentz Violation Using Fermi-LAT Gamma-Ray Burst Data". In: *Phys. Rev. D* 99.8 (2019), p. 083009. DOI: 10.1103/PhysRevD.99.083009. arXiv: 1807.00189 [astro-ph.HE].

[456] H. Abdalla et al. "The 2014 TeV γ-Ray Flare of Mrk 501 Seen with H.E.S.S.: Temporal and Spectral Constraints on Lorentz Invariance Violation". In: *Astrophys. J.* 870.2 (2019), p. 93. DOI: 10.3847/1538-4357/aaf1c4. arXiv: 1901.05209 [astro-ph.HE].

[457] V. Alan Kostelecký and Matthew Mewes. "Constraints on relativity violations from gamma-ray bursts". In: *Phys. Rev. Lett.* 110.20 (2013), p. 201601. DOI: 10.1103/PhysRevLett.110.201601. arXiv: 1301.5367 [astro-ph.HE].

[458] Nicolai Christiansen. "Four-Derivative Quantum Gravity Beyond Perturbation Theory". In: (Dec. 2016). arXiv: 1612.06223 [hep-th].

[459] Manuel Reichert. "Towards a UV-complete Standard Model: From baryogenesis to asymptotic safety". PhD thesis. Heidelberg U., 2018. DOI: 10.11588/heidok.00024469.

[460] Astrid Eichhorn and Holger Gies. "Ghost anomalous dimension in asymptotically safe quantum gravity". In: *Phys. Rev. D* 81 (2010), p. 104010. DOI: 10.1103/PhysRevD.81.104010. arXiv: 1001.5033 [hep-th].

[461] P. T. Boggs and J. E. Rogers. ""Orthogonal Distance Regression" in "Statistical analysis of measurement error models and applications"". In: *Contemporary Mathematics* 112 (Proceedings of the AMS-IMS-SIAM joint summer research conference 1990), p. 186.

[462] Paul T. Boggs, Richard H. Byrd, Janet E. Rogers, and Robert B. Schnabel. *User's Reference Guide for ODRPACK Version 2.01 Software for Weighted Orthogonal Distance Regression*. 1992. URL: https://docs.scipy.org/doc/external/odrpack_guide.pdf.

[463] J. Ambjorn, J. Jurkiewicz, and R. Loll. "Reconstructing the universe". In: *Phys. Rev. D* 72 (2005), p. 064014. DOI: 10.1103/PhysRevD.72.064014. arXiv: hep-th/0505154.

[464] Thomas W. Appelquist, Mark J. Bowick, Dimitra Karabali, and L. C. R. Wijewardhana. "Spontaneous Chiral Symmetry Breaking in Three-Dimensional QED". In: *Phys. Rev. D* 33 (1986), p. 3704. DOI: 10.1103/PhysRevD.33.3704.

[465] Gustavo P. De Brito, Astrid Eichhorn, and Antonio D. Pereira. "A link that matters: Towards phenomenological tests of unimodular asymptotic safety". In: *JHEP* 09 (2019), p. 100. DOI: 10.1007/JHEP09(2019)100. arXiv: 1907.11173 [hep-th].

[466] Holger Gies and Stefan Lippoldt. "Fermions in gravity with local spin-base invariance". In: *Phys. Rev. D* 89.6 (2014), p. 064040. DOI: 10.1103/PhysRevD.89.064040. arXiv: 1310.2509 [hep-th].

[467] Holger Gies and Stefan Lippoldt. "Global surpluses of spin-base invariant fermions". In: *Phys. Lett. B* 743 (2015), pp. 415–419. DOI: 10.1016/j.physletb.2015.03.014. arXiv: 1502.00918 [hep-th].

[468] Stefan Lippoldt. "Spin-base invariance of Fermions in arbitrary dimensions". In: *Phys. Rev. D* 91.10 (2015), p. 104006. DOI: 10.1103/PhysRevD.91.104006. arXiv: 1502.05607 [hep-th].

[469] Jan M. Pawlowski. "On Wilsonian flows in gauge theories". In: *Int. J. Mod. Phys. A* 16 (2001), pp. 2105–2110. DOI: 10.1142/S0217751X01004785.

[470] Daniel F. Litim. "Optimized renormalization group flows". In: *Phys. Rev. D* 64 (2001), p. 105007. DOI: 10.1103/PhysRevD.64.105007. arXiv: hep-th/0103195.

[471] Richard L. Arnowitt, Stanley Deser, and Charles W. Misner. "Dynamical Structure and Definition of Energy in General Relativity". In: *Phys. Rev.* 116 (1959), pp. 1322–1330. DOI: 10.1103/PhysRev.116.1322.

[472] Richard L. Arnowitt, Stanley Deser, and Charles W. Misner. "The Dynamics of general relativity". In: *Gen. Rel. Grav.* 40 (2008), pp. 1997–2027. DOI: 10.1007/s10714-008-0661-1. arXiv: gr-qc/0405109.

[473] Alessia Platania and Frank Saueressig. "Functional Renormalization Group Flows on Friedman-Lemaître-Robertson-Walker backgrounds". In: *Found. Phys.* 48.10 (2018), pp. 1291–1304. DOI: 10.1007/s10701-018-0181-0. arXiv: 1710.01972 [hep-th].

[474] W. B. Houthoff, A. Kurov, and F. Saueressig. "Impact of topology in foliated Quantum Einstein Gravity". In: *Eur. Phys. J. C* 77 (2017), p. 491. DOI: 10.1140/epjc/s10052-017-5046-8. arXiv: 1705.01848 [hep-th].